Neuronal nicotinic receptors: the role of the β3 and α5 subunits

James Philip Boorman

The School of Pharmacy

PhD Pharmacology

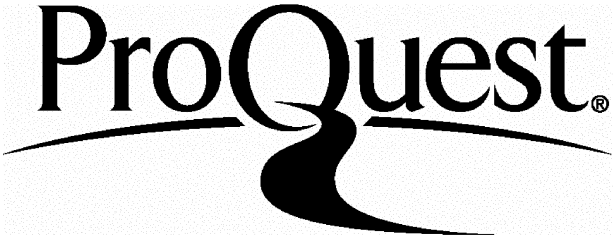

Foreword

Please note that the data in chapters 3, 4 and 5 of this thesis has been published in the following two papers:

1. **Boorman, J. P.**, Groot-Kormelink, P. J., & Sivilotti, L. G. (2000). Stoichiometry of human recombinant neuronal nicotinic receptors containing the β3 subunit expressed in *Xenopus* oocytes. *J.Physiol* 529 Pt 3, 565-577.

2. Groot-Kormelink, P. J., **Boorman, J. P.**, & Sivilotti, L. G. (2001). Formation of functional α3β4α5 human neuronal nicotinic receptors in *Xenopus* oocytes: a reporter mutation approach. *Br.J.Pharmacol.* 134, 789-796.

Additionally, the data presented in chapter 6 has recently been submitted for publication.

Boorman, J. P., Beato, M, Groot-Kormelink, P. J., & Sivilotti, L. G. (2002). The β3 subunit increases channel conductance but has only subtle effects on other properties of human recombinant neuronal nicotinic α3β4 receptors.

Abstract

Using a reporter mutation approach and the two-electrode voltage clamp technique, Groot-Kormelink *et al* (1998) have shown that the 'orphan' β3 subunit can be incorporated into a functional 'triplet' α3β4β3 neuronal nicotinic acetylcholine receptor, when expressed in *Xenopus* oocytes.

Based on the observation that in α3β4 receptors the EC_{50} value decreases with the number of 9'T mutations, we used the same reporter mutation approach to determine the stoichiometry of 'triplet' receptors. When either α3 or β4 carried the 9'T mutation in 'triplet' α3β4β3 or α3β4α5 receptors, the observed decreases in EC_{50} values were similar and larger than if only β3 or α5 were mutated. This suggests α3 and β4 are present in equal copy number, greater than that of β3 or α5, namely: 2 copies of α, 2 copies of β and 1 copy of β3 or α5.

Potency ratio data for α3β4 and α3β4β3 receptors demonstrated that the incorporation of β3 reduced the potency of lobeline (relative to ACh) from 23.0 to 7.14 (p 0.01). However, the rank order of the seven nicotinic agonists tested was unchanged.

Schild analysis showed that the *Kd* for the competitive antagonist trimetaphan was not affected by β3 incorporation (75.5 and 66.0 nM for α3β4 and α3β4β3, respectively), suggesting that β3 may not contribute to the properties of the agonist binding site.

Calcium permeability data failed to detect differences in calcium permeability for α3β4 and α3β4β3 receptors, with mean shifts in reversal potential of 7.68 mV for α3β4 and 5.20 mV for α3β4β3 (for a 10 times increase in external calcium concentration).

Acknowledgements

First of all, I would like to thank Lucia Sivilotti for giving me the chance to learn classical pharmacology and electrophysiology, and for ongoing support and advice. The last three or so years have been interesting and enjoyable. It is good to work for and learn from someone who has a passion for what they do and I hope Lucia that your passion will continue. Starting from a Biochemistry and computing background, I have had a lot to learn and I hope I have learnt well.

Secondly, I would like to thank Trevor Smart and the School of Pharmacy for funding this PhD with a studentship from the Millennium Fund.

Additionally, I would like to thank the members of the exponentially (almost) expanding Sivilotti lab, for being great fun to work with and their contributions to my PhD. The group has moved a long way since beginning with one room containing Lucia's office, my rig and Paul's Molecular Biology corner ! Specifically, I would like to thank Paul Groot-Kormelink for providing this 'pessimist' with the nicotinic clones and RNA every Friday (without which this thesis would not have been possible). Thanks also to Marco Beato for providing the single channel data, for his patient help, general advice and good taste in music.

Further, I would like to thank David Colquhoun for his advice, sharing his opinions on our data, generous loan of equipment and supply of CVfit. I would also like to thank John Wood for the loan of the Axoclamp, Philippe Béhé for his advice and Chris Hatton, Chris Shelley and Stephanie Schorge for their support and continuous supply of

PDFs. Thanks to Chris Courtice, John and Lionel for making essential parts for my rig at a moments notice and lending me their tools when required. Thanks to Carles Canti, Helena DeSilva and George Peters for generously providing oocytes every Thursday. Thanks to my family, friends and all at FTH for reminding me that there is more to life than science. Last, but not least, I would like to thank my wife Nicole for putting up with my manic days of writing and not poisoning my tuna pasta.

Table of contents

List of figures

List of abbreviations

Å	= angstrom
α-Bgt	= alpha-bungarotoxin
5-HT	= serotonin
ACh	= acetylcholine
AChBP	= the snail ACh binding protein
CCh	= carbachol
Cyt	= cytisine
DMPP	= dimethylphenylpiperazinium
+-tubo	= +-tubocurarine
Epi	= epibatidine
GABA	= γ-aminobutyric acid
HEK293	= human embryonic kidney cell line 293
Lob	= lobeline
M_x	= muscarinic acetylcholine receptor type x (x = 1, 2, 3, or 4)
m_5	= muscarinic acetylcholine receptor type 5
mAChR	= muscarinic acetylcholine receptor
MLA	= methyllycaconitine
n'	= the n^{th} residues in the second transmembrane domain, downstream of the N-terminus
nAChR	= nicotinic acetylcholine receptor
Nic	= nicotine
PCR	= polymerase chain reaction
RNAase	= ribonuclease
T_m	= melting temperature
TM	= transmembrane domain
U.V.	= ultraviolet

Chapter 1: Introduction

1.1. Receptors: A brief history

In the study of pharmacology the term receptor is used to describe a class of cellular macromolecules which are specifically and directly involved in transmitting information between and within cells by way of specific chemical messengers, resulting in a change in cellular activity.

It was Du Bois Reymond who first proposed in 1877 that the transmission of nervous stimuli could be of a chemical or electrical nature:

"*Of known natural processes that might pass on excitation, only two are, in my opinion, worth talking about; either there exists at the boundary of the contractile substance a stimulatory secretion....; or the phenomenon is electrical in nature.*" (Cited in H. P. Rang and M. M. Dale: Pharmacology, 2nd edition, p125).

The concept of a receptor was introduced around the same time by Paul Ehrlich and John Newport Langley.

Ehrlich, working together with the organic chemist A. Bertheim, studied the relationship between chemical structure and biological action of a series of organometallic compounds. Ehrlich proposed that chemicals that have a biological action must become bound to become effective (cited in H. P. Rang and M. M. Dale: Pharmacology, 2nd edition, p125).

Langley studied the salivation stimulating action of pilocarpine and the block of this action by atropine on the salivary gland of the dog.

"*the pilocarpine secretion that has been stopped by atropine can be removed by pilocarpine and again stopped by atropine... there is some substance or substances in the nerve ending or gland cell with which both atropine and pilocarpine are capable of forming compounds.*" (Langley, 1878).

Thus Langley had introduced the concept of receptors into pharmacology, demonstrating that both pilocarpine and atropine were working on the same receptor (now known as the muscarinic receptor).

In 1904 T R Elliot re-affirmed the idea that chemical transmission could be involved in mediating nervous stimuli, suggesting that adrenaline could act as a chemical transmitter in the sympathetic nervous system (H. P. Rang and M. M. Dale: Pharmacology, 2nd edition, p125). However, Elliot's hypothesis was not taken very seriously until a year later when Langley found more compelling evidence for the existence of receptors, while working on the action of nicotine (Nic) and the Nic blocking action of curare on the skeletal muscle of chickens. Langley hypothesised that the muscle possessed a "*receptive substance*" that specifically interacted with Nic and curare (Langley, 1905).

"*Since, in the normal state, both nicotine and curari abolish the effect of nerve stimulation, but do not prevent contraction from being obtained by direct stimulation of the muscle or by a further adequate injection of nicotine, it may be inferred that neither the poisons nor the nervous impulse act directly on the contractile substance of the muscle but on some accessory substance.*

Since this accessory substance is the recipient of stimuli which it transfers to the contractile material, we may speak of it as the ***receptive substance*** *of the muscle.*" (Langley, 1905).

While the concept of receptors had started to become accepted by pharmacologists, more experimental evidence was required to validate the chemical transmission hypothesis of Du Bois Reymond. Dixon was the first person to attempt to experimentally verify the hypothesis of chemical transmission in 1907. Dixon's idea was to electrically stimulate the vagus nerve of a dog's heart, stopping the heart from beating. Dixon proposed that if chemical transmission did indeed occur, then the stimulation of the vagus nerve would release a chemical into the blood that would be capable of inhibiting the heart. Thus applying a sample of this blood to a second heart would stop it from beating. However, his experiment failed and he abandoned the idea with some embarrassment (H. P. Rang and M. M. Dale: Pharmacology, 2nd edition, p126).

It wasn't until 1921 that Otto Loewi picked up where Dixon left off, to provide the first convincing experimental evidence of chemical transmission. Loewi this time using two frog hearts, showed that when the vagus nerve of the first heart was stimulated, the nerve terminals secreted a chemical substance. When Loewi applied this unknown chemical substance to the second heart, it stopped beating (Loewi, 1921). He termed the chemical substance '*Vagusstoff*' (vagus substance), which was later identified as acetylcholine (ACh).

Thus Loewi demonstrated the action of ACh on the heart, adding to the known action of ACh on the adrenal medulla previously described by Reid Hunt in 1900 (Hunt, 1900).

However, it was Sir Henry Dale who first classified the activity of ACh into two pharmacologically distinct groups in 1914. Dale distinguished the different actions of ACh on the heart (released from the vagus nerve) and the adrenal medulla as muscarinic and nicotinic, with muscarinic actions defined as those that are reproduced by injection of muscarine (one of the active compounds of the poisonous mushroom *Amanita muscaria*), and abolished by small doses of atropine. After the muscarinic effects have been blocked by atropine, higher doses of ACh are required to produce another set of effects, reproduced by the injection of Nic (see Dale *et al.*, 1914; Dale *et al.*, 1936). At the time Dale did not realise that the muscarinic and nicotinic effects of ACh were caused by the action of two different ACh receptors.

1.2. Acetylcholine receptors

It is now well established that synaptic transmission mediated by ACh involves two major classes of ACh receptors, muscarinic and nicotinic. The muscarinic acetylcholine receptor (mAChR) mediate the majority of inhibitory and excitatory effects of ACh on central neurons and the periphery (Caulfield, 1993). The muscarinic class consists of at least five distinct types, named M_1, M_2, M_3, M_4, and M_5. All mAChRs are G-protein-coupled receptors, which upon the binding of an agonist can cause a variety of effects, including activation of phospholipase C, inhibition of adenylate cyclase, activation of potassium channels or inhibition of calcium channels (Nathanson, 1987; Bonner, 1989; Wess, 1996).

The nicotinic acetylcholine receptors (nAChRs) are members of a gene family of ligand-gated ion channels that mediate fast signal transmission at synapses. The nicotinic family of ligand-gated ion channels also includes the glycine, γ-aminobutyric

acid ($GABA_A$ & $GABA_C$), and the serotonin $5HT_3$ receptors (for reviews, see Stroud *et al.*, 1990 and Karlin & Akabas, 1995). All subunits in this family are of similar size and demonstrate considerable sequence identity, with four hydrophobic membrane-crossing segments (usually termed transmembrane domains or TM), a large extracellular N-terminal domain, and a variable cytoplasmic domain between TM3 and TM4. These receptors can either be excitatory (the cation-conducting channels; nAChR and 5-HT_3) or inhibitory (the anion-conducting channels; Glycine, $GABA_A$, and $GABA_C$) at the synapse. Another characteristic of this family of receptors is the presence of two cysteine residues at positions 128 and 142 (numbering of the *Torpedo* α1 subunit without the signal peptide), forming a cysteine loop in the N-terminal domain.

1.3. The muscle nicotinic acetylcholine receptors

1.3.1. Structure of the muscle nicotinic acetylcholine receptors

The muscle type nAChR at the neuromuscular junction (NMJ), and in the electroplaque membranes of *Torpedo* rays, is the best-characterised member of the ligand-gated ion channel family (Hille, 1992; Karlin, 1993; Sivilotti *et al.*, 2000). Unwin has resolved much of the *Torpedo* nAChR structure to 4.6 Å resolution and new light comes from the recent discovery and structure solution of the ACh binding protein of *Lymnaea stagnalis* (AChBP), a pentameric protein highly homologous to the extracellular nAChR domain. Additionally, a wealth of single channel data from muscle nAChRs has led to a greater understanding of the mechanism of activation. Hence it is useful to review this data, as much of it is relevant to the study of neuronal nAChRs.

The receptor is a membrane spanning hetero-oligomer of approximately 300,000 Da, composed of a ring of five membrane-spanning subunits (α, γ, α, δ, β in *Torpedo* and

embryonic muscle or α, ε, α, δ, β in adult muscle) arranged as a pentamer around a narrow central, cation-conducting pore (Unwin, 1993 & 2000).

Electron microscope data from tubular crystal structures of the *Torpedo* ray nAChR at 9 Å resolution (Unwin, 1993) show that the receptor is approximately 120 Å in length, protruding approximately 65 Å into the extracellular domain and 20 Å into the intracellular domain. The pore is flanked on either side by 20 Å wide vestibules, whose inner walls are lined with negatively charged residues. The charged residues on the vestibule wall are thought to selectively attract cations (repelling anions) to the pore (Imoto *et al.*, 1988; Konno *et al.*, 1991; Unwin, 2000). The pore is shaped by the contribution of 5 kinked α helical rods, one from each of the subunits in the pentamer (Unwin, 1993; Unwin, 1998; see figure 1.3.1.a).

More recent 4.6 Å resolution data of the *Torpedo* nAChR from the same group (Miyazawa *et al.*, 1999) describes an 'inverted pentagonal cone' at the cytoplasmic end of the pore that extends approximately 40 Å away from the cytoplasmic membrane, where it is associated with what is proposed to be the anchoring protein rapsyn. The cone structure is thought to restrict the flow of ions through the pore and is formed by α helical rods of approximately 30 Å in length contributed by the loop between TM3 and TM4 from each of the subunits in the pentamer (Miyazawa *et al.*, 1999). Unwin proposes that two narrow (approximately 8 Å in diameter and 15 Å in length), transverse tunnels at the bottom of the inverted cone structure (one in each of the α subunits; see figure 1.3.1.a), are negatively charged and provide dedicated channels for the flow of cations into (and K^+ out of) the cell. The negative charges on the tunnel would restrict the flow only to cations, by repelling the cytoplasmic anions away from the conducting pore (Miyazawa *et al.*, 1999).

Figure 1.3.1.a. The three dimensional structure of the *Torpedo* nicotinic receptor

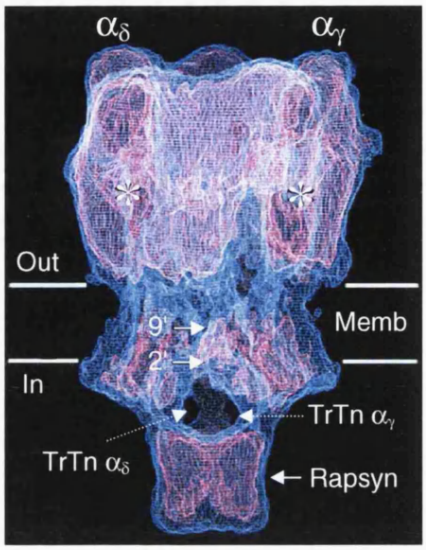

Figure 1.3.1.a. Shows a computer generated model of the three-dimensional structure of the *Torpedo* nAChR, based on electron microscope data (Unwin, 2001). The positions of the α_γ and α_δ subunits are indicated, with the ligand binding pockets within each α subunit (asterisks). The proposed locations of the gate of the closed channel (9') and the narrowest constricting of channel in the open state (2') are indicated. The transverse tunnels at the bottom of the inverted cone structure, one in each of the α subunits (TrTn α_δ and TrTn α_γ) and the anchoring protein rapsyn are indicated (adapted from Unwin, 2001).

Muscle nAChR subunits are encoded by different but related genes, and consequently have similar amino acid sequences. The subunit polypeptides vary in length between 437 (α) and 501 (δ) amino acid residues. Each subunit contains: (1) a long, highly conserved extracellular N-terminal domain, exposed to the synaptic cleft; (2) four conserved hydrophobic transmembrane domains (TM 1 - 4); (3) a long cytoplasmic loop between TM 3 and TM 4, varying in amino acid sequence between the subunits; (4) an extracellular C-terminal domain (see figure 1.3.1.b; for a review, see Galzi & Changeux, 1995).

Segments of the first extracellular domain are important in forming the ligand-binding domain (discussed below). The subunits are classed as either α or non-α (β, γ, δ or ε) if

they posses or lack a pair of adjacent cysteine residues at positions 192 and 193 (Cys 192 and Cys 193, numbering of the *Torpedo* α1 subunit without the signal peptide), in the N-terminal domain.

The TM2 domain of each subunit contributes to the formation of a cation-conducting pore in the membrane (Unwin, 1993; Unwin, 1995; Unwin, 1998; Miyazawa *et al.*, 1999; for a review, see Hucho *et al.*, 1996; see also figure.1.3.1.b). The TM2 domain is thought to have a dominant α-helical conformation (with slight elongation for the middle portion) on the basis of photolabelling and cysteine mutation scanning data (Hille, 1992; Karlin, 1993; Karlin & Akabas, 1995).

The long cytoplasmic loop between TM3 and TM4 has been shown by Williams *et al.* (1998) to be involved in targeting neuronal nAChRs to specific subdomains of the subsynaptic membrane. The cytoplasmic loop also contains a number of consensus segments for phosphorylation, the function of which is ill-understood (see Moss *et al.*, 1996).

Figure 1.3.1.b. The membrane topology of a nicotinic receptor subunit

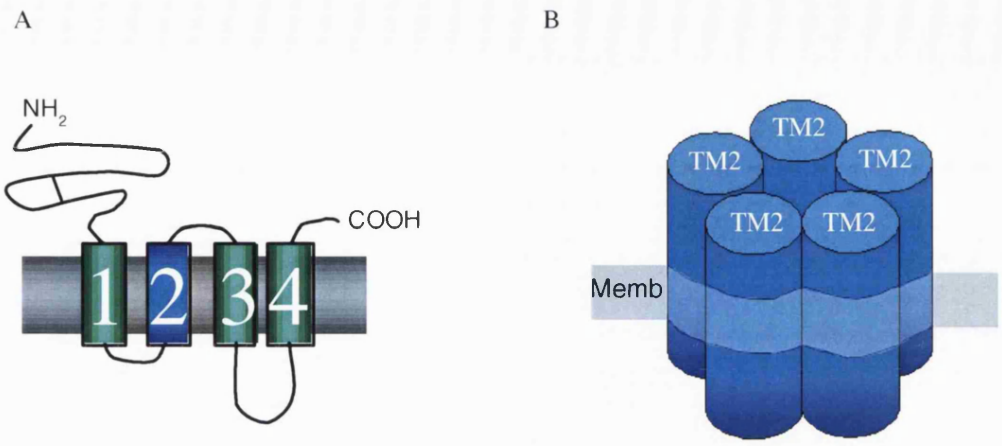

Figure 1.3.1.b. Shows the four transmembrane domains of one subunit, including the extracellular ligand binding N-terminal (NH_2) domain. Note the pore lining TM2 domain is highlighted in blue. B shows a representation of the pore-lining region, formed by the five TM2 domains (one from each subunit) highlighted in blue. The membrane is represented by the grey band surrounding the TM2 domains (memb).

1.3.2. The ACh binding site

There are two ACh binding sites located in the extracellular N-terminal portion of the receptor. Single channel data has shown that two molecules of ACh are required to bind in order to produce a high probability of opening. Mono-liganded openings do occur in the muscle nAChR, but are rare events unless very low ACh concentrations are used (Colquhoun & Sakmann, 1985).

Expression studies of mouse muscle subunits expressed in fibroblasts have shown that the α subunit on its own can form complexes with δ or γ, but not β (Blount & Merlie, 1989). While αγ and αδ complexes also bind carbachol (CCh) and the competitive antagonist +-tubocurarine (+-tubo), α on its own cannot bind either (Blount & Merlie, 1989; Blount *et al.*, 1990; Gu *et al.*, 1991b; Pedersen & Cohen, 1990; Sine & Claudio,

1991a). Thus αγ and αδ complexes are required for the formation of the ligand binding site. αδ pairs have also been shown to have high affinity for ACh and low affinity for +-tubo, whereas αγ has comparatively low affinity for ACh and high affinity for +-tubo (Blount & Merlie, 1989). Single channel data has also established that the two binding sites display different binding affinities for ACh (Jackson, 1988; Sine *et al.*, 1990; Zhang *et al.*, 1995).

However, the nature of the binding sites and the molecular basis for their disparate affinities is still controversial. There are currently two main proposals:

1.3.3. The α-δ, α-γ subunit interface:

It is proposed on the basis of affinity binding, photoaffinity labelling, mutational analysis, cross linking and amino acid sequence analysis of *Torpedo* and muscle nAChR that ACh binds at the interface between α-δ and α-γ subunits (Pedersen *et al.*, 1990; Sine & Claudio, 1991b; Czajkowski *et al.*, 1993; for a review see Arias, 1997). More recent data in support of this model comes from the solving of the crystal structure of the snail ACh binding protein at 2.7 Å (Brejc *et al.*, 2001; discussed below). In the muscle model of the binding site, the interface consists of an α specific principal binding domain and a complementary site on the neighbouring δ or γ subunit (Arias, 1997). Thus the two sites differ because different residues from the contributing subunits form them.

The principal binding domain is formed within the tertiary structure of the α1 subunit, by interactions between three separate segments of predominantly aromatic residues and the α subunit specific pair of adjacent cysteines (Cys 192 and Cys 193; *Torpedo* α1

numbering), contributed by the extracellular N-terminal domain and highly conserved throughout the nicotinic α subunits. The three segments (termed loops A, B and C, reviewed by Galzi & Changeux 1995) of residues are conserved throughout all α nAChR subunits, except in the triplet forming α5, which is most similar in terms of amino acid sequence to β3 and is only termed α on the basis that it has the adjacent cysteine residues 192 and 193 (see table 1.3.5.d).

In the human muscle nAChR the main conserved residues for each loop are Tyrosine (Tyr) 93 (Loop A; numbering of the *Torpedo* α1); Tryptophan (Trp) 149 (loop B); and Tyr 190, Cys 192, Cys193 and Tyr198 (loop C, see figure 1.3.3.a). It is thought that these residues form a binding pocket that interacts with the ester moiety of the ACh molecule (Karlin & Akabas, 1995).

The complementary binding domain, contributed by the δ or γ (ε in adult muscle) subunit, is formed by another three separate segments of the extracellular N-terminal domain (termed loops D, E and F, see Galzi & Changeux, 1995). In the δ and ε subunits, the first section downstream of the N-terminus is formed by the residue Trp 55 (Loop D; *Torpedo* α1 numbering). The second section is formed by residue Tyrosine (Tyr) 117 (loop E) and the third is formed by residues Aspartic acid (Asp) 166 and Glutamic acid (Glu) 175 (loop F, see figure 1.3.3.a). In the γ subunit loop E is formed by Threonine (Thr) 117. This part of the binding site is negatively charged, due to the Asp and Glu residues and may interact with the quaternary ammonium moiety of the ACh molecule (Karlin & Akabas, 1995).

The high affinity +-tubo binding site is thought to be formed at the α-γ interface (and the low affinity at the α-δ interface) as revealed by expressing pairs of αγ or αδ mouse

muscle subunits in fibroblasts (Blount & Merlie, 1989). Here +-tubo inhibited the initial rate of radiolabelled bungarotoxin binding most potently when only αγ were expressed, with an IC_{50} of 19 nM compared to 280 nM for αδ (Blount & Merlie, 1989).

Sine (1993) went on to identify residues 116, 117 and 159 (*Torpedo* α1 numbering) on the γ and δ subunits as being responsible for determining the different affinities for +-tubo at the α-γ and α-δ interfaces, as revealed by mutating single residues in chimeras of mouse γ and δ subunits expressed in HEK293 cells. Here mutating Val 116, Thr 117 and Ser 159 on the δ subunit to the corresponding Ile 116, Tyr 117 and Lys 159 of the γ subunit confers αγ-like +-tubo affinity to the αδ mutant (Sine 1993).

Figure 1.3.3.a. The α-δ, α-γ interface

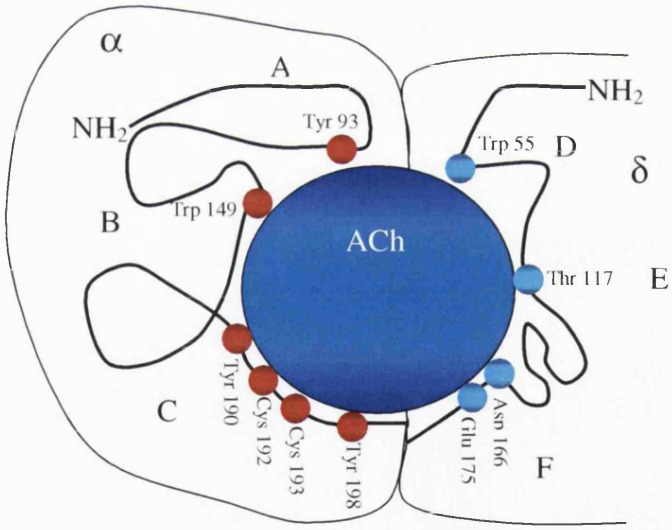

Figure 1.3.3.a. Adapted from Galzi & Changeux, 1995 and Arias, 1997. Shown here is a diagram of the α-δ binding interface model of the muscle nAChR binding site. ACh (blue circle) is represented in all possible orientations, binding at the interface between α and δ subunits, interacting with the principal binding domain (loops A-C) on the α subunit and the complementary binding domain (loops D – F) on the δ subunit. Red circles indicate the residues of loops A-C and light blue circles indicate the residues of loops D-F. Each residue is labelled with the three-letter amino acid code and its numbering as in *Torpedo* α1.

1.3.4. The α subunit binding pocket

On the basis of electron microscope data from tubular crystal structures of the *Torpedo* ray nAChR, Unwin suggested that ACh binds to cavities (pockets) entirely within the α subunits (as opposed to at the interface between α-δ and α-γ subunits; Unwin, 1993). These cavities are formed by three α helical rods from each α1 subunit (see figure 1.3.4.a), but have different conformations in the absence of ACh binding.

At 4.6 Å resolution, narrow 'tunnels' of approximately 10 to 15 Å in length can be resolved in the walls of the extracellular portion of the receptor (Miyazawa *et al.*, 1999). These tunnels lead from the pore, through the walls of the vestibules and into the ACh binding pockets in the α subunits. A further tunnel can be resolved in the α_γ subunit, closer to the membrane and leading from the binding pocket to the extracellular space, away from the pore (Unwin, 2000). This second tunnel cannot be resolved in the α_δ subunit in the absence of ACh. However, upon ACh binding both α subunits assume a similar conformation. Unwin proposes that this second tunnel may act as an exit tunnel for ACh into the extracellular space, only appearing in the α_δ subunit upon ACh binding (Unwin, 2000). Miyazawa *et al.*, (1999) draw parallels with structures described in the enzyme acetylcholinesterase (Sussman *et al.*, 1991) and propose that these tunnels provide a specific route of access for ACh to the binding pockets in both α subunits. Here ACh would initially be conducted through the pore of the channel with other cations, until it reaches the narrow tunnels in the vestibule walls, travelling along the tunnels to the binding pocket.

In this model, it is proposed that the non-equivalent affinities of the two α binding sites are a result of different neighbouring subunits (δ or γ). Here the δ and γ subunits would

contribute different charged or aromatic side chains not to the binding pocket, but to the tunnels leading to binding pockets, unequally distorting the tunnels and interacting with the quaternary ammonium group in ACh (Unwin, 2000).

Figure 1.3.4.a. An electron micrograph of the ACh binding pockets

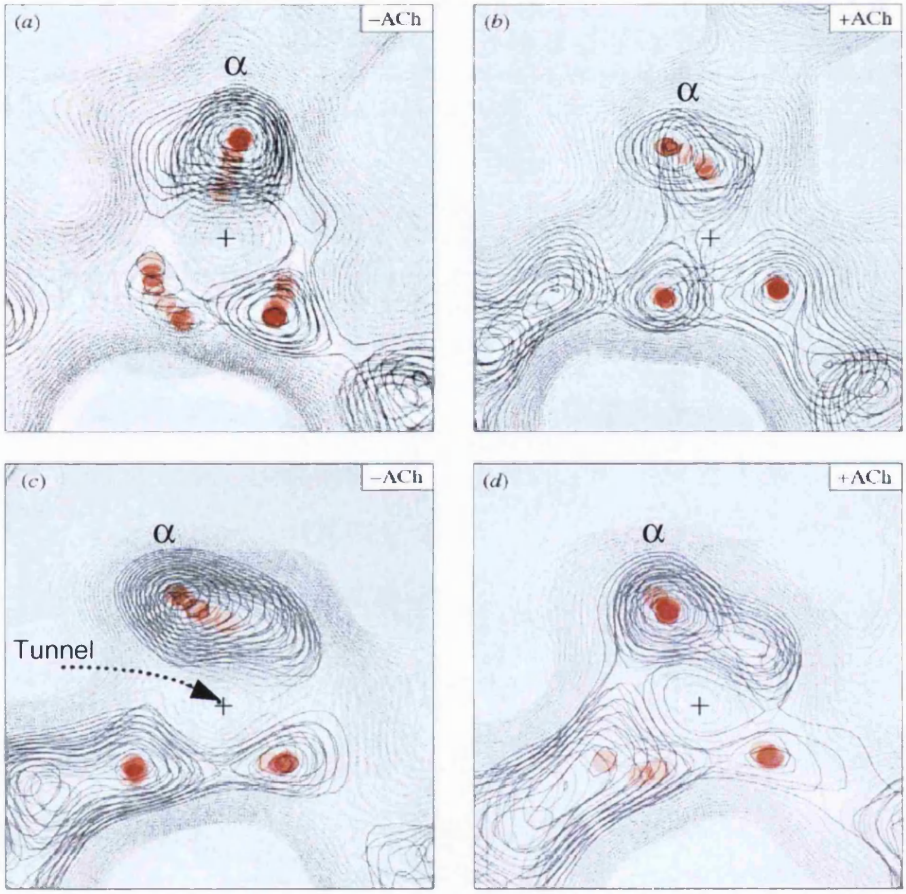

Figure 1.3.4.a. Shows electron microscope data (9Å) of the ligand binding pockets in the two α-subunits before (- ACh) and after brief exposure to ACh (+ ACh). Panels A and B show the data for the α_δ-subunits and panels C and D the α_γ-subunits. The three α helical rods, which are thought to form the ligand binding pocket in each of the α subunit, are highlighted in orange. Upon ACh binding, the three α-helical rods of the αδ subunit appear to twist around the centre of the binding pocket (+), causing the αδ subunit to establish a new configuration. However, in the absence of ACh the three α-helical rods of the α_γ subunit resemble the ACh bound configuration of αδ. Further, the configuration of the α–helical rods of the α_γ subunit does not appear to significantly change upon binding ACh. The dotted line shown in panel C follows a tunnel in the α_γ subunit, leading from the binding pocket to the extracellular space (Adapted from Unwin, 2001).

1.3.5. Insights from a snail acetylcholine binding protein

The recent discovery of an ACh binding protein (AChBP) in the snail and the solving of its crystal structure has thrown new light on our understanding of the binding site (Smit *et al.*, 2001; Brejc *et al.*, 2001). Whole cell recordings from glial cells have shown that the AChBP is released into the synaptic cleft of snail synapses from perisynaptic glial cells in response to the activation of an α-bungarotoxin (α-Bgt) sensitive nAChR by presynaptically released ACh (Smit *et al.*, 2001). Smit *et al.* (2001) propose that once in the synaptic cleft of the snail cholinergic synapses, the protein binds presynaptically released ACh and suppresses cholinergic transmission.

The AChBP binds radiolabelled α-Bgt, with a *Kd* of 3.5 nM (Smit *et al.*, 2001). Competitive binding experiments have shown that radiolabelled α-Bgt binding is inhibited by known nicotinic agonists and antagonists in a concentration dependent manner (Smit *et al.*, 2001). The agonists ACh and Nic produced IC_{50} values of 4.2 μM and 98 nM respectively (Smit *et al.*, 2001).

In terms of amino acid sequence, the AChBP aligns with the subunits of the nAChR family, but lacks the transmembrane domains. The N-terminal domain of the AChBP does contain a cysteine loop analogous to the loop formed by cysteine 128 and 142 in the nicotinic AChR subunits, although it is not fully conserved in the AChBP, being separated by 12 residues as opposed to 15. The AChBP shares most sequence similarity with nAChR α subunits (and especially with α7, see below), as it contains the adjacent cysteine residues (Cys 192 and Cys 193). The majority of the residues involved in forming the loops in the subunit interface model of the binding site are also conserved:

Tyr 93, Trp 149, Tyr 190, Tyr 198 and Trp 55 (numbering of *Torpedo* α1; see table 1.3.5.a).

The crystal structure of the AChBP has been solved to a resolution of 2.7 Å (Brejc *et al.*, 2001): it can be seen that 5 identical AChBP 'protomers' (or subunits) form a pentameric cylinder 62 Å high, with a diameter of 80 Å and a central hole of approximately 18 Å (Brejc *et al.*, 2001). Each protomer has both a positive and negative side, thus protomers form dimer interfaces with their neighbour, with the first protomer interfacing its positive side with its neighbour's negative side. The dimensions of the AChBP pentamer are in good agreement with the 4.6 Å data from Unwin's group (Miyazawa *et al.*, 1999) on the *Torpedo* nAChR. The orientation of the AChBP pentamer is also analogous to the nAChR, with the N-terminal domain at the top (extracellular face of the nAChR) and the C-terminal at the bottom (cytoplasmic face of the nAChR).

Brejc *et al.* (2001) report that each AChBP protomer contains a large uncharged, hydrophobic pocket framed by β-strands and analogous to the ACh binding pocket of *Torpedo* (Miyazawa *et al.*, 1999). Brejc *et al.* (2001) also describe a distinct second cavity and propose that this second cavity, which is occupied by a HEPES molecule in the crystal, is the location of the ligand binding site.

The second cavity is lined with the residues conserved from the presumed ACh binding site of the muscle nAChR, located close to the outer edge of the pentamer, at the interface between the protomers. Brejc *et al.* (2001) describe additional residues lining this cavity that are not assigned to the formation of the binding site in the muscle nAChR subunit interface model described above.

Table 1.3.5.a. Residues in the second cavity of the AChBP

Loop	Torpedo	AChBP
A	Y93	Y93
B	W149	W149, H151
C	Y190, C192, C193 Y198	Y190, C192, C193 Y198
D	W55	W55, Q57
E	Y/T117	R109, V111, L117, M119
F	D166, E175	Y169

Table 1.3.5.a. The residues contributing to the ligand binding domain loops are indicated with the single amino acid code and the corresponding residue number, aligned with the *Torpedo* α1 subunit.

The primary plus side of the interface (A) consists of loops A, B & C. The minus side of the interface is formed by β–strands in the neighbouring protomer (B), contributed by loops D, E & F. Together all 6 loops form and line the cavity as summarised in table 1.3.5.b.

Table 1.3.5.b. Residues lining the second cavity of the AChBP

Region of Cavity	Residues from Protomer A	Residues from Protomer B
Bottom	Loop A, Tyr 190 from loop C	Trp 55 from loop D and Loop F
Walls	Trp 149, main chain of His 151 from loop B; Tyr 198, Cys 192, Cys 193 from loop C	side chain of Gln 57 from loop D and side chain of Met 119 from loop E
Top		hydrophobic parts of: Arg 109,Val 111 and Leu 117 from loop E

Table 1.3.5.b. The residues lining the second cavity of the AChBP contributed by neighbouring protomers A and B are indicated with the three letter amino acid code and residue number, using the numbering of the *Torpedo* α1 subunit.

Interestingly, Brejc *et al.* (2001) report that HEPES, a buffer with a quaternary ammonium group like ACh, binds to Trp 149 in loop B, but the precise orientation of the molecule could not be resolved.

Brejc *et al.* (2001) propose that this interface that they see in the AChBP is analogous to the nAChR binding site. Aligning the amino acid sequence of the nAChR subunits to the AChBP reveals that many of the binding site loops of the AChBP are conserved in the nAChR subunits (see tables 1.3.5.c. and 1.3.5.d.). In this alignment Brejc *et al.* (2001) propose that the observed variability of AChBP loop F in the *Torpedo* and muscle nAChR γ and δ subunits, may account for disparate binding affinities at the two binding sites in the nAChR.

Table 1.3.5.c. An alignment of the *Torpedo* and human muscle nAChR subunits with the residues of the AChBP model of the ligand binding site

Loop	D		A	E				B		F	C			
No.	53	55	89	104	106	112	114	143	145	164	185	187	188	192
AChBP	W	Q	Y	R	V	L	M	W	W	Y	Y	C	C	Y
α1 Torpedo	-	-	Y	-	-	-	-	W	Y	-	Y	C	C	Y
α1 Human	-	-	Y	-	-	-	-	W	Y	-	Y	C	C	Y
γ Torpedo	W	E	-	L	Y	Y	L	-	-	D	-	-	-	-
γ Human	W	E	-	L	S	Y	L	-	-	A	-	-	-	-
ε Human	W	G	-	L	Y	T	L	-	-	A	-	-	-	-
δ Torpedo	W	D	-	L	R	T	L	-	-	A	-	-	-	-
δ Human	W	E	-	L	Y	Y	L	-	-	G	-	-	-	-

Table 1.3.5.c. Shows a sequence alignment of *Torpedo* and human muscle nAChR subunits to the amino acid residues (single letter code) involved in the AChBP model of the ligand binding site (loops indicated with numbering of the AChBP). The subunit type and species are indicated. Note the variability in loop F between δ and γ or ε subunits.

Table 1.3.5.d. An alignment of the neuronal nicotinic subunits with the residues of the AChBP model of the ligand binding site

Loop	D		A	E				B		F	C			
No.	53	55	89	104	106	112	114	143	145	164	185	187	188	192
AChBP	W	Q	Y	R	V	L	M	W	W	Y	Y	C	C	Y
α2 Human	W	K	Y	H	F	H	V	W	Y	D	Y	C	C	Y
α3 Human	W	K	Y	L	K	T	I	W	Y	D	Y	C	C	Y
α4 Human	W	K	Y	H	F	Q	T	W	Y	D	Y	C	C	Y
α6 Human	W	R	Y	L	K	T	T	W	Y	D	Y	C	C	Y
α7 Human	W	Q	Y	L	N	Q	L	W	Y	G	Y	C	C	Y
α8 Chick	W	Q	Y	L	N	Q	I	W	H	N	Y	C	C	Y
α9 Human	W	R	Y	V	R	T	D	W	Y	D	Y	C	C	Y
α10 Human	W	R	Y	V	R	R	D	W	H	D	Y	C	C	Y
β2 Human	W	T	Y	V	S	F	L	W	Y	D	P	D	S	Y
β4 Human	W	K	Y	I	R	L	L	W	Y	D	P	D	P	Y
α5 Human	W	K	F	V	R	T	T	W	Y	D	D	C	C	Y
β3 Human	W	K	F	I	K	V	T	W	Y	D	D	V	Y	Y

Table 1.3.5.d. Shows a sequence alignment of human (except α8) neuronal nAChR subunits to the amino acid residues (single letter code) involved in the AChBP model of the ligand binding site (loops indicated with numbering of the AChBP). The subunit type is indicated.

1.3.6. Subunit arrangement

The subunit arrangement of the functional muscle nAChR has been extensively investigated, mainly by expressing *Torpedo* nAChRs. It is generally accepted that one of the α subunits pairs with a δ subunit and that the other α subunit pairs with the γ subunit in embryonic muscle or *Torpedo* nAChR (ε for the adult muscle nAChR) in order to form the ligand binding site (discussed above). However, there is still some controversy over the position of the β subunit in the functional receptor complex.

On the basis of cross-linking studies coupled with immunoprecipitation data using a toxin specific antibody, Chatrenet *et al.* (1990) propose that the β subunit is located in-between the two α subunits and the low and high affinity ACh binding sites are located close to γ (or ε) and δ respectively. Interpretation of electron microscopy data of tubular crystals of *Torpedo* nAChRs at 9 Å resolution, led Unwin to suggest that the β subunit is located between the two α subunits leading to the clockwise arrangement of αβαγδ (and αβαεδ consequently for the adult form, Unwin, 1998).

Photoaffinity labelling data using +-tubo on *Torpedo* nAChRs (Pedersen & Cohen, 1990) demonstrates that +-tubo binds between α–γ and α–δ subunits, but not between α–β or α on its own. In the subunit interface model of the binding site, both α subunits must maintain the same orientation in order to contribute the same subunit face to interface with neighbouring δ or γ subunits. In this model the β subunit cannot be located in-between the α subunits. Further, toxin cross-linking experiments (see Blount & Merlie, 1989; Karlin, 1993; reviewed by Karlin & Akabas, 1995) support this view, leading to a clockwise arrangement of αγαβδ.

More recently Brejc *et al.* (2001) solved the crystal structure of the snail AChBP, leading them to propose an anticlockwise orientation for the principal vs. the complementary binding site. Brejc *et al.* (2001) propose that in the adult muscle nAChR, this results in an anticlockwise αεαδβ subunit arrangement.

1.3.7. Receptor assembly

We have seen the proposed models for the subunit arrangement of the muscle nAChRs, but what determines this precise assembly? We know that muscle nAChRs are assembled in the secretory pathway and that specialised mechanisms assist in the folding and assembly of proteins produced in this pathway.

Initially the mRNAs are specifically targeted to the rough endoplasmic reticulum membrane where the ribosome simultaneously translates and translocates each subunit protein chain into the endoplasmic reticulum, where assembly of the complex begins. The first assembly events occur simultaneously with translation, starting from the emerging N-terminal end, and are described as 'co-translational'. Co-translational events include: membrane insertion of subunits, the attachment of the core N-linked glycan, the cleavage of the N-terminal signal peptide, and initial rapid folding. Slower folding reactions proceed at the end of translation, involving various chaperone proteins. These slower folding reactions allow separate subunit domains to interact and other types of editing or quality control to occur, including disulphide bond formation and proline isomerisation. Incorrectly assembled subunits are retained within the endoplasmic reticulum and degraded (Green, 1999). Although the initial assembly of muscle nAChR subunits shares many of the general features for proteins produced in

the secretory pathway, important differences have been described (Green & Millar, 1995; Green, 1999).

The main difference between other membrane proteins and the muscle nAChR, is that the muscle nAChR (in common with other ion channels) is a large heteromeric protein, which in order to form functional channels requires a precise subunit composition, stoichiometry and arrangement. Due to the large complex structure of the assembled receptor and the requirement for precision, assembly is likely to be more demanding and less efficient than for other proteins in the secretory pathway. Merlie & Lindstrom (1983) report that the assembly of nAChRs is a long and inefficient process (mouse muscle nAChRs expressed in BC3H-1 cells), taking 2-3 hours and yielding only 20-30 % of correctly assembled nAChR complexes. In order to avoid rapid degradation, each subunit is required to interact with chaperone proteins in order to correctly fold and associate with other subunits, stabilising the intermediate step towards the formation of the nAChR complex (Keller *et al.*, 1996; Keller *et al.*, 1998). Pulse-chase data from α, γ, δ and β subunits expressed individually in mouse fibroblasts demonstrates that unassembled or incorrectly folded subunits are rapidly degraded, with maximum half lives of approximately 40 mins (Claudio *et al.*, 1989; Blount & Merlie, 1990). Gu *et al.* (1991a) report that assembly and arrangement of the subunits into the specific structure of the pentamer is required within the endoplasmic reticulum before export of the subunits to the Golgi complex, *en route* to the membrane. Specific residues in the N-terminal domain are thought to control the precise assembly and arrangement of the subunits around the pentamer (Gu *et al.*, 1991b; Kreienkamp *et al.*, 1995).

Two models for the assembly of the muscle nAChR subunits have been proposed so far (for a review see Green, 1999). Both models agree that assembly involves the progressive formation of defined intermediates of the four subunits that then assemble

into the $\alpha_{(2)}\beta\gamma\delta$ pentamer. The two models are summarised in figures 1.3.8.a. and 1.3.8.b.

1.3.7.a. The 'hetero dimer' model

This was proposed on the basis of data obtained from the expression of single or paired subunits (Blount *et al.*, 1990; Gu *et al.*, 1991b; Saedi *et al.*, 1991; Kreienkamp *et al.*, 1995).

Here the majority of the subunit folding is thought to be required postranslationally before hetero-oligomerisation can proceed. During this slow folding, the cysteine loop between the cysteine residues 128 and 142 (*Torpedo* α1 numbering) forms in the α subunit and is required for α-Bgt binding (Blount *et al.*, 1990). The epitope recognised by the monoclonal antibody mAb35 also forms during this slow folding period, to form the 'mature' α subunit (note that mAb35 was raised against the native nAChR; Saedi *et al.*, 1990). The 'mature' α subunit then associates with free γ or δ subunits to assemble into αγ or αδ heterodimers, which provide different affinity binding sites for +-tubo (Blount & Merlie, 1989, see above). The two heterodimers are then thought to associate with the free β subunit to form the $\alpha_{(2)}\beta\gamma\delta$ pentamer.

1.3.7.b. The sequential model

In contrast to the 'heterodimer' model, data for the 'sequential' model has been acquired in the presence of all four subunits, using the pulse-chase method (Green & Claudio, 1993; Green & Wanamaker, 1997; Green & Wanamaker, 1998; Green, 1999). Here the assembly intermediates are identified by co-immunoprecipitation using subunit specific

antibodies, by immunoprecipitation with conformation-dependent antibodies or by precipitation with affinity resin (Green, 1999).

In this model the rapid assembly of α, β and γ subunits into αγβ *trimers* (majority of the trimers formed within 5 min) is required *before* the slow folding of the α subunit can proceed to form the cysteine loop between residues 128 and 142 (*Torpedo* α1 numbering), as identified by co-immunoprecipitation with mAb 35 (conformation dependent antibody specific for the α subunit) and precipitation by the α subunit cysteine loop specific mAb 259 (Green & Claudio, 1993; Green & Wanamaker, 1997). The formation of the trimers occurs too quickly for the experiments to be able to detect pairs of subunits. It is possible that all the possible heterodimers (αβ, αγ, βγ) are adequate precursors to trimer assembly (Green & Claudio, 1993). Because the formation of the trimers is so fast, Green & Claudio (1993) propose that it may occur co-translationally, while the ribosome is still producing the protein, in order to prevent misfolding of key functional domains.

The trimer continues to fold and shortly after the formation of the cysteine loop between residues 128 and 142 on the α subunit, the α subunit undergoes a conformational change, making the cysteine loop inaccessible to mAb 259 binding. Folding continues and the first α-Bgt binding site is formed (Green & Wanamaker, 1997; Green, 1999; Mitra *et al.*, 2001). Further conformational changes in the trimer occur over the next 2 hours, with the appearance of an epitope specifically recognised by mAb 14. This step is quickly followed by the addition of the δ subunit to the trimer and formation of the αβγδ tetramer (which also binds mAb 14).

Next, the disulphide bond forms between Cys 192 and Cys 193 in the α subunit, exposing an epitope for mAb383c. Shortly after the disulphide bond formation, the first

ACh binding site appears, between α and γ subunits (α_γ ACh binding site), indicated by the appearance of the mAb 247g epitope (Green & Wanamaker, 1998; Mitra *et al.*, 2001). In the next step, the cysteine loop between residues 128 and 142 on the β subunit undergoes a conformational change, which is required for the addition of the next subunit, i.e. the second α subunit (as demonstrated by deletion of cysteine 128; Green & Wanamaker, 1997). Shortly after the second α subunit associates with the tetramer, the second ACh and α-Bgt binding sites form between the second α and the δ subunit (α_δ ACh binding site), resulting in the final assembled $\alpha_{(2)}\beta\gamma\delta$ nAChR complex. The whole process takes more than 40 hours to complete for *Torpedo* nAChR subunits expressed in mouse fibroblasts and pulse chased at 20°C in order to reduce the rate of assembly and provide more accurate isolation of assembly intermediates (Green & Claudio, 1993; Green & Wanamaker, 1998; Mitra *et al.*, 2001). Green & Claudio (1993) verified the sequential model data (for mouse muscle nAChR) at 37°C, where assembly is much faster (within 2 hours).

Thus in the sequential model, subunit folding continues throughout assembly. Recent data from Green & Wanamaker (1998) suggests that 'late' folding events occur outside the endoplasmic reticulum, along the secretory pathway at a site close to where the receptor is targeted, and is required for correct channel function.

1.3.8. The heterodimer model vs. the sequential model

Most of the evidence for the heterodimer model comes from experiments in which only a limited number of subunits were expressed. Green & Claudio (1993) point out that the prediction of the sequential model only differ from those of the heterodimer model if the full complement of subunits is expressed. Green (1999) also suggests that differences in

the techniques used for isolating assembly intermediates may also be important. This is because data in support of the heterodimer model tend to come from experiments with relatively harsh solubilisation conditions, whereas data for the sequential model tend to use milder detergents, i.e. conditions that avoid the dissociation of assembled intermediates (Green & Claudio, 1993).

More recent data from chimeric subunits support the sequential model of assembly and indicate that the N-terminal domain is important for the rapid formation of assembly intermediates and that the C-terminal of the γ subunit is required in order to allow addition of the δ and second α subunit to the $\alpha\beta\gamma$ trimer (Eertmoed & Green, 1999).

Figure 1.3.8.a. **The heterodimer model of assembly**

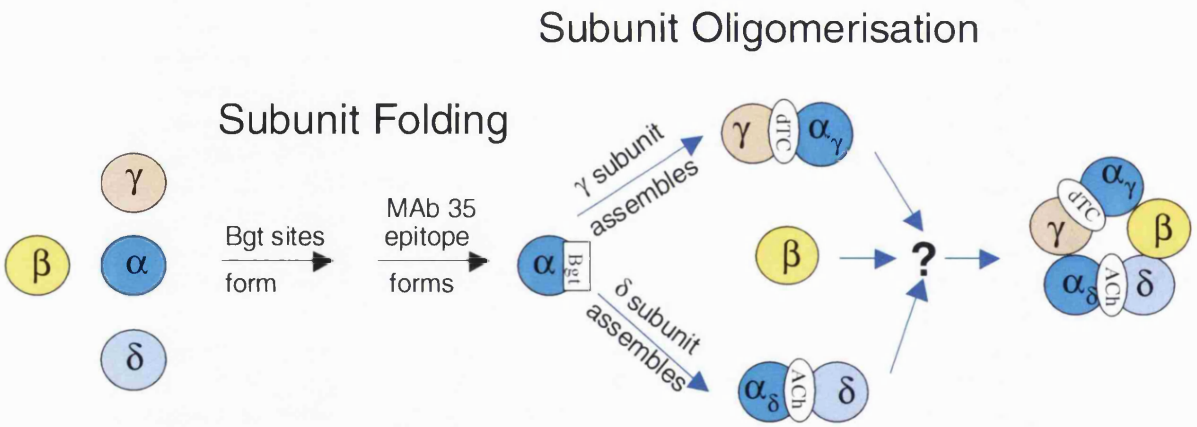

Figure 1.3.8.a. Show a schematic diagram of the heterodimer model of nAChR assembly. Subunit folding reactions are denoted by the black arrows and oligomerisation events by the blue arrows. Formation of the α-Bgt binding sites and the mAb 35 epitope precedes all subunit associations. The two different ACh binding sites, the high affinity +-Tubo site (dTC) and the low affinity +-Tubo site (ACh), appear on α_γ or α_δ heterodimers, respectively (adapted from Green, 1999).

Figure 1.3.8.b. **The sequential model of assembly**

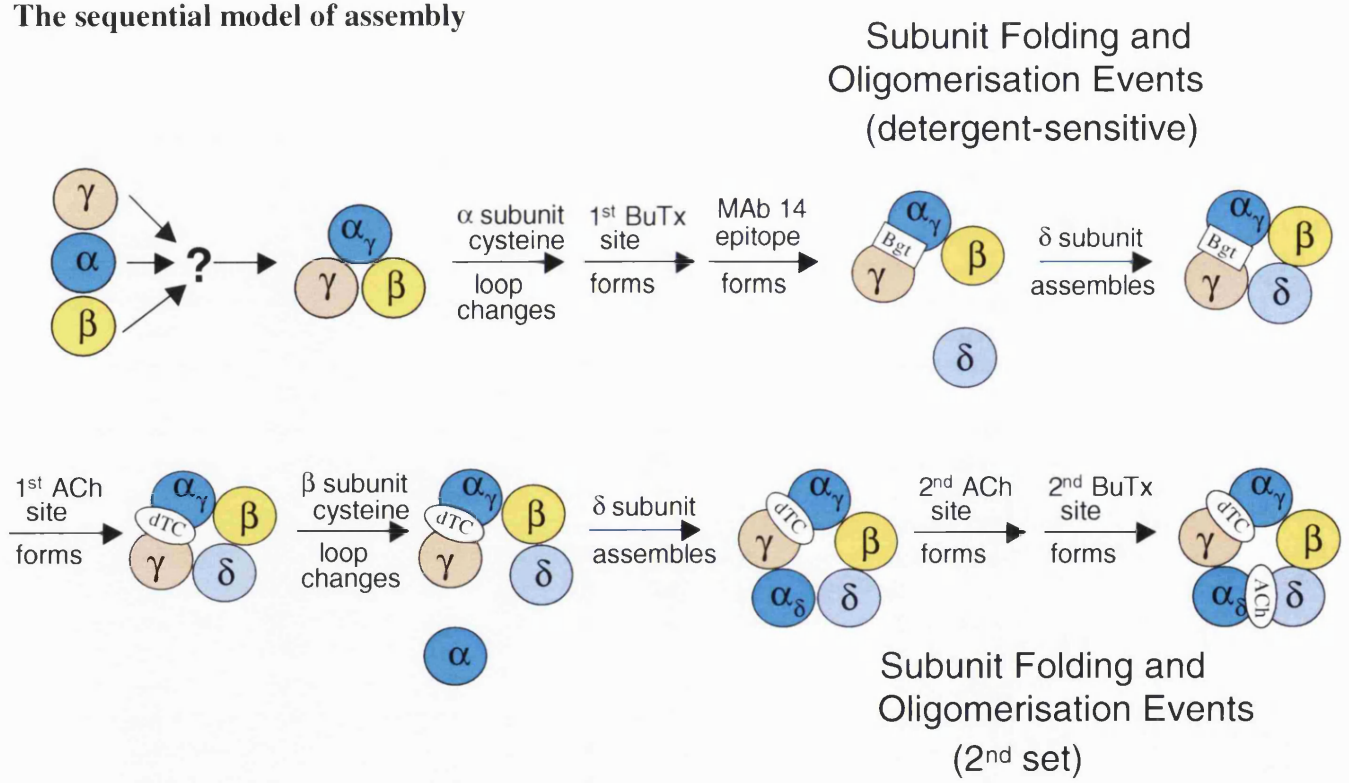

Figure 1.3.8.b. Show a schematic diagram of the sequential model of nAChR assembly. Subunit folding reactions are denoted by the black arrows and oligomerisation events by the blue arrows. The trimers rapidly form shortly after translation. Next the α subunit cysteine loop region undergoes a conformational change, followed by the formation of the first α-Bgt (Bgt) binding site and the appearance of the mAb 14 epitope on the αβγ trimers, shortly followed by the addition of the δ subunit, forming the αβγδ tetramer. Next the disulphide bond forms between cysteine 192 and 193 in the α subunit and the first ACh binding site is formed between α and γ subunits. Next the β subunit cysteine loop region undergoes a conformational change, followed the addition of the second α subunit. Finally the second α-Bgt and ACh binding sites appear on $\alpha_2\beta\gamma\delta$ pentamers between α and δ subunits (adapted from Green, 1999). Note the two different ACh binding sites, the high affinity +-Tubo site (dTC) and the low affinity +-Tubo site (ACh),

1.3.9. The channel gate

It is widely accepted that the gate of the channel is located within the pore-lining TM2 region. However, the identity and precise location of the gate still remains controversial.

One hypothesis is based on substituted-cysteine accessibility data (Akabas *et al.*, 1992; Akabas *et al.* 1994). In this technique, residues in the TM2 domain of the α1 subunit are mutated one at a time to cysteine. The activated muscle nAChR is permeable to methanethiosulfonate-ethylammonium (MTSEA), which reacts with the sulfhydryl (-SH) group on cysteine. When applied to the mutant receptor, MTSEA will react with any cysteine residue that it can reach, bind covalently and block the channel. Thus the residues mutated to cysteine provide binding sites for MTSEA within TM2. Upon removal of MTSEA, the extent of block it has produced can be assessed. If MTSEA is applied to the channel in the absence of agonist, then it will only reach as far down the channel as the gate.

Akabas *et al.* (1994) proposed that the gate is located at least as close to the intracellular end of the channel as the 3rd residue downstream from the NH_2-terminal end of TM2 (Leu 3').

In contrast to the location proposed by Akabas, a more extracellular position of the channel gate has been proposed on the basis of photoaffinity labelling data from open channel blocking non-competitive antagonists. Here radiolabelled photoreactive derivatives of compounds such as chlorpromazine - CPZ, triphenylmethyl-phosphonium - TPMP, meproadifen - Mep mustard or trifluoromethyliodophenyl-diazirine - TID are co-applied with agonist and subjected to an intense flash of U.V. light. Thus the

compounds block the open channel and covalently bind to neighbouring amino acid side chains upon U.V. activation, labelling pore-lining residues involved in the binding site of the compound used. All the compounds studied to date bind with highest affinity to sites within TM2 (Giraudat *et al.*, 1986; Hucho *et al.*, 1986; Pedersen & Cohen, 1990; White & Cohen, 1992; for a review see Karlin & Akabas, 1995). Interestingly, CPZ labels 3 rings of 5 residues, contributed by all subunit, near the middle of the pore (Giraudat *et al.*, 1987; for a review see Karlin & Akabas, 1995). These rings are: the highly conserved ring of Leu, located 9 residues downstream from the NH_2-terminal end of TM2 (Leu 9' in the numbering of Miller, 1989); the ring of threonines, located 6 residues downstream from the NH_2-terminal end of TM2 (Thr 6'); the ring of serines, located 2 residues downstream from the NH_2-terminal end of TM2 (Ser 2'; see figure 1.3.10.e.).

Further evidence in support of a more extracellular position of the gate comes from experiments using the permanently charged quaternary ammonium compound QX222, which only blocks the nicotinic channel in the open state when applied extracellularly (Leonard *et al.* 1988; Charnet *et al.*, 1990; reviewed in Ionic channels of excitable membranes, Hille, 2nd edition, p 430). The equilibrium binding affinity and the dwell time of QX222 in the open channel of both wild-type and TM2 mutant receptors is compared in two papers from Lester's group (Leonard *et al.* 1988; Charnet *et al.* 1990). Here the TM2 mutations were: polar Ser or Thr in 2', 6' or 10' to non-polar alanine (Ala) and *vice versa*. The mutants were progressively introduced into the subunits of the receptor complex, with a maximum copy number of 5. Affinity and dwell time of QX222 in the open channel decrease by approximately 35 % for each Ala residue introduced in 6', whereas an approximate 29 % increase in affinity and dwell time was

observed for each Ala residue introduced in the more extracellular 10' (Leonard *et al.* 1988; Charnet *et al.*, 1990).

Charnet *et al.*, (1990) propose that the basis for this opposite effect in 6' and 10' is due to the charged amino moiety of QX222 binding to the polar residues in 6' and the nonpolar end binding to the polar residues in 10'. Thus decreasing the number of polar residues in 6' reduces the ability of the charged amino moiety to bind at 6', resulting in a reduction in binding affinity and dwell time, whereas decreasing the number of polar residues in 10' *increases* the ability of the non-polar end to bind at 10', increasing binding affinity and dwell time (Charnet *et al.*, 1990). Thus, the binding site for QX222 extends as intracellularly as 6' (Leonard *et al.* 1988; Charnet *et al.*, 1990). Because QX222 only blocks the open channel from the extracellular side, it would seem reasonable to assume that the QX222 binding site is beyond (towards the cytoplasmic side) the channel gate and therefore the channel gate would be more extracellular than 6'.

Indications of a more extracellular location of the gate than 6' are in agreement with Unwin's hypothesis that the gate is near the hydrophobic residue in 9'. This hypothesis is attractive because 9' is a hydrophobic amino acid in this superfamily of ligand gated ion channels. Indeed 9' is a Leu residue conserved not only throughout the nicotinic subunits (except $\alpha 5$ and $\beta 3$ which have valine in 9'), but also in $GABA_A$ & $5\text{-}HT_3$.

What is possibly the strongest evidence in favour of the role of 9'Leu as the channel gate comes from Unwin's electron microscope data of tubular crystals of *Torpedo* nAChRs at 9Å (Unwin, 1993). Unwin proposed that the inactive channel is held closed

by hydrophobic interaction between the side chains of the ring of 5 conserved 9'Leu residues.

Unwin later went on to describe the *Torpedo* nAChRs in the open state, after a brief spray of carbachol, before rapidly freezing the receptors in the open state (Unwin, 1998). This data further supports the role for 9' as the channel gate (Unwin, 1998). His analysis indicates that the TM2 domains that form the pore-lining region of the channel are bent α helices. The bend in the five α helices is located approximately at the midpoint of the pore and occludes the channel in the closed state, forming the channel gate. Unwin initially proposed that the channel gate is the highly conserved ring of 9' leucine residues, with each leucine projecting its hydrophobic side chain into the pore (Unwin, 1998). In the closed state, the leucine residues would form a narrow hydrophobic ring, impermeable to hydrated ions.

However, more recent data at 4.6 Å resolution from the same group, suggests that the leucine side chains are not close enough in the closed pore to form a simple hydrophobic ring (Unwin, 2000). This data describes the closed state as having a hole, with a radius of approximately 3.5 Å at the position of the gate. This radius is smaller than the radius of hydrated Na^+ (5.6 Å) or K^+ (3.8 Å) ions and therefore, in order to provide an efficient barrier to ion permeation, the gate must prevent surrounding polar groups in the 6' ring (Ser) and 2' ring (Ser/Thr) from removing part of the ion hydration shell (Unwin, 2000). Unwin proposes that ion permeation is prevented by a hydrophobic 'girdle', formed between the conserved 9'Leu ring and the conserved 13' valine ring, located one turn of the α helix above 9'Leu. Further, Unwin proposes that in the closed state the 9'Leu side chains weakly interact with neighbouring side chains on serine or alanine residues in 10', providing a limited stability to the 'girdle'. Upon ACh binding,

these weak side chain interaction would be readily disrupted by conformational changes in the receptor, destabilising the girdle and allowing ion permeation.

Additional, indirect evidence comes from site directed mutagenesis studies of the homomeric neuronal nACh α7 receptors, which demonstrate a role for 9' in the receptor sensitivity to ACh (Revah *et al.*, 1991). Revah *et al.* (1991) introduced hydrophobic valine (Val) or phenylalanine (Phe), or hydrophilic threonine (Thr) or serine (Ser) into the 9' position of α7. Because α7 is a homomeric receptor (see below), mutant receptors contained 5 copies of the mutation (one from each α subunit). Revah *et al.* (1991) report that these 9' mutations increase the sensitivity of the receptor to ACh. The ACh EC_{50} was decreased from its wild-type value of 115 μM to 30 μM and 6.2 μM for $\alpha7^{9'Phe}$ and $\alpha7^{9'Val}$ respectively. Hydrophilic mutations produced greater decreases in EC_{50}, to 0.8 μM and 0.7 μM for $\alpha7^{9'Ser}$ and $\alpha7^{9'Thr}$ respectively. Single channel data from wild-type and mutant receptors showed that the 9' mutations do not affect the main 46 pS conductance seen in the wild-type. However, 9' mutant channels display a second, higher conductance state of 80 pS. Revah *et al.* (1991) suggest that the 9' mutation makes the desensitised state conducting. This hypothesis is based on the observation that the mutant receptor is active at lower concentrations than the wild-type (desensitised states by definition have high affinity). Hence Revah *et al.* (1991) proposed that in the wild-type receptor the 9' residues swing into the channel in the desensitised state, blocking conductance.

However, in contrast to Revah *et al.* (1991), Filatov & White (1995) propose that 9'Leu does not swing into the channel to form a block in the desensitised state, because only one copy of the 9'Thr mutation is required to decrease the channel closing rate as determined from the open time distribution in the single channel records of wild-type

and mutant muscle nAChR (Filatov & White, 1995). Here $\alpha_{(2)}\beta\gamma^{9'Thr}\delta$ receptors have a mean open time of 174 ms vs. 2.4 ms (Filatov & White, 1995). Single channel data also revealed that wild-type and $\alpha_{(2)}\beta\gamma^{9'Thr}\delta$ receptors have the same single channel conductance (Filatov & White, 1995), with no additional conductance states.

Data from both Filatov & White (1995) and Labarca *et al.* (1995) provide further evidence for the role of 9' Leu in the gate of the channel. Both groups exploited the known stoichiometry of muscle nAChR (2:1:1:1 for α, β, γ and δ subunits) to investigate the effects of introducing increasing numbers of hydrophilic threonine (Filatov & White, 1995) or serine (Labarca *et al.*, 1995) residues into the 9' position. Whole cell data (looking at both binding and gating) demonstrated a subunit-independent, progressive decrease in ACh EC_{50} (approximately 10-fold for each copy of the mutation incorporated). Thus the channel became more sensitive to ACh as more copies of the mutation were introduced. These effects were interpreted in terms of changes in ACh efficacy.

The idea that 9' residues affect gating (and not binding) is supported by the observation that the *Kd* for +-tubo is unchanged for wild-type and mutated muscle nAChR (Filatov & White, 1995).

Data from Chang & Weiss, (1998) and Chang & Weiss (1999) also support the view that 9' mutations affect gating: mutating the 9'Leu to Ala, Gly, Ser, Thr, Val or Tyr in homomeric ρ1 $GABA_A$ receptors (containing 5 copies of the mutation Chang & Weiss, 1998) or to Ser in heteromeric $\alpha1\beta2\gamma2$ receptors (Chang & Weiss, 1999), produced spontaneous openings, indicated by an increase in holding current in the absence of agonists. The reversal potential of spontaneously active receptors was shifted to less

positive potentials upon reducing the external chloride concentration, indicating that this spontaneous current is a Cl^- conductance. Interestingly, the spontaneous activity of mutant ρ1 receptors was *reduced* by low GABA concentrations, resulting in a decrease in the holding current, suggesting that the agonist destabilises the spontaneously active state (R* + A) and the receptor proceeds to a bound, but inactive state (AR; $R^* \rightleftharpoons R + A \rightleftharpoons AR \rightleftharpoons A_2R \rightleftharpoons AR^*$).

Chang *et al.* (1996) also used 9'Leu to Ser mutations to examine the stoichiometry of rat α1β2γ2 $GABA_A$ receptors expressed in *Xenopus* oocytes. Receptors containing the 9'Ser mutation demonstrated increased sensitivity to GABA, indicated by a leftward shift in the GABA concentration response curve. However, in contrast to the findings of Filatov & White (1995) and Labarca *et al.* (1995) for the muscle nAChR, in α1β2γ2 $GABA_A$ receptors the magnitude of the shift was dependent on the subunit type which carried the mutation. The greatest decrease in EC_{50} was observed when the β2 subunit carried the mutation, producing a 1308-fold decrease in GABA EC_{50}, compared to a 153-fold and 46-fold decrease when γ2 or α1 carried the mutation (Chang *et al.*, 1996). Furthermore, in α1β2γ2 $GABA_A$ receptors, the magnitude of the decrease in GABA EC_{50} is only progressive up to a mutation copy number of two, whereupon additional copies of the mutation produce no further decrease in EC_{50} (Chang & Weiss, 1999). Because the effect of the mutation was dependent on the subunit type and only progressive up to a copy number of two, the stoichiometry of α1β2γ2 receptors could not be directly determined from changes in the EC_{50} as previously shown for the muscle nAChR Filatov & White (1995) and Labarca *et al.* (1995).

In order to tackle this problem, Chang *et al.* (1996) co-expressed mixtures of wild-type and mutant subunits, producing a heterogeneous population of wild-type and mutant

receptors. The principle being that if a subunit is present in two copies, then a mixed injection will produce a population of receptors which will include all wild-type, all mutant and hybrid receptors. Analysis of concentration response curve data from such mixed populations allowed the fitting of multiple components. When co-expressing mutant and wildtype α1 or mutant and wildtype β2 with wildtype and γ2, 3 components could be fitted (all wildtype, all mutant and hybrid), suggesting that these subunits are present in two copies. On the other hand, when co-expressing mutant or wildtype γ2 with wildtype α1 and β2, only 2 components could be fitted ($\alpha1\beta2\gamma2^{wt}$ and $\alpha1\beta2\gamma2^{9'Ser}$; Chang *et al.*, 1996). Chang *et al.* (1996) therefore proposed a stoichiometry of 2:2:1 for α1β2γ2 receptors. This stoichiometry is in good agreement with the findings of Farrar *et al.* (1999) using fluorescence energy transfer techniques.

Taking the data of Filatov & White (1995) and Labarca *et al.* (1995) together with those of Chang *et al.* (1996), we can conclude that mutating the 9'Leu ring can be a useful tool for analysing the stoichiometry of ligand gated ion channels, if we can verify that the mutation produces a subunit-independent and progressive reduction in the agonist EC_{50}.

1.3.10. The open pore

In the absence of ACh, the α_γ and α_δ subunits have different conformations around their ACh binding pockets. The binding of ACh is thought to cause rapid simultaneous twisting of the cavity lining rods of both α subunits, resulting in both subunits adopting a similar conformation (Unwin, 2000). Here the twisting of α_γ has the effect of pulling the β subunit away from α_δ, while α_δ twists into the space previously occupied by β. Thus ACh initiates localised disturbances in the α subunits, which are co-ordinated by the neighbouring δ and γ subunits (see figure 1.3.10.a.). The disturbances cause

further small rotations of the other subunits, causing the kinked TM2 α helices to twist to the side, disrupting the gate-forming residues (Unwin, 1998). In the open state, the twisting of the α helices not only transiently increases the pore diameter to allow ion permeation, but also exposes the small polar side chains of a line of serine or threonine residues at the narrowest portion of the pore (2'; Unwin, 1998). These residues are the most likely candidates for the channel selectivity filter, which is known to allow Na^+, K^+ and to some extent Ca^{2+} ions to permeate.

Figure 1.3.10.a. All subunits undergo a conformational change upon ACh binding

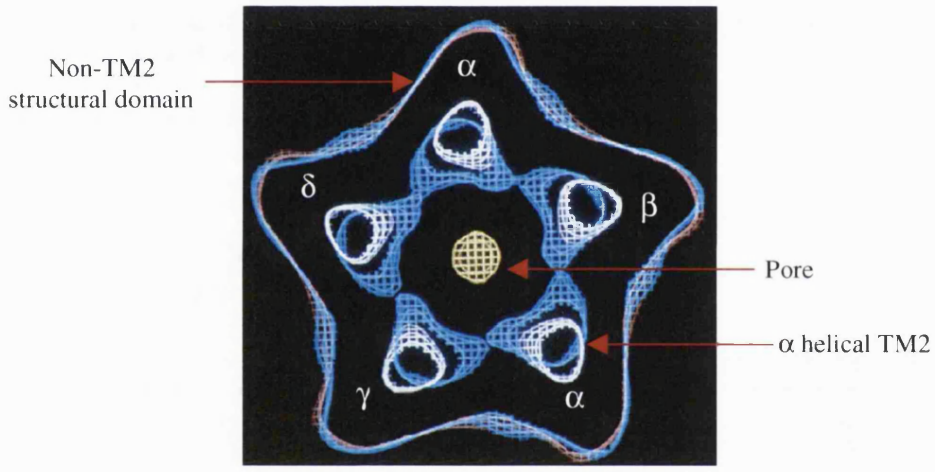

Figure. 1.3.10.a. Shown here is a computer generated model, based on electron microscope data, of the transition from the closed state (blue) to the open state (white) of tubular crystals of the nAChR of the *Torpedo* ray (adapted from Unwin, 1998). The α helical rods are represented in blue in the absence of ACh, with their final position in the presence of ACh traced in white. The structural, non-TM2 elements of the protein are represented by the star-shaped rim of electron density, blue in the absence of ACh and Red in the presence of ACh. Upon ACh binding, the α helical rods (from the TM2 domains of each subunit) simultaneously twist and move back towards the star shaped rim of electron density, transiently opening the channel.

Unwin's data are in good accord with the observations from site directed mutagenesis of the TM2 of *Torpedo* nAChRs (Imoto *et al.*, 1988; Imoto *et al.*, 1991). These studies indicated that four hydrophilic residues in and close to the TM2 domain of each subunit

face the pore and have a major effect on the single channel conductance of *Torpedo* nAChRs expressed in oocytes. These residues are; –4', -1', 2' and 20' (TM2; see figure 1.3.10.c.). Each subunit contributes these four residues to the formation of four 'rings' inside, and at the cytoplasmic face of the pore; -4' cytoplasmic ring; -1' intermediate ring; 2' central ring; 20' outer ring (Imoto *et al.*, 1988; Imoto *et al.*, 1991). The side chains of residues in the cytoplasmic, intermediate and outer rings all have an overall net negative charge. The residues of the central ring are hydrophilic and are uncharged (see figure 1.3.10.c.). The net charge and hydrophilic nature of these four rings is conserved throughout most of the nicotinic subunits (see figure 1.3.10.e.).

Cytoplasmic ring: In *Torpedo,* the –4' cytoplasmic ring has a net negative charge and is composed of aspartic acid (D) in α and β and glutamic acid (E) in δ, contributing negative charges. The remaining γ subunit has an uncharged glutamine (Q) residue in γ –4' (Imoto *et al.*, 1988). Thus the total charge of the cytoplasmic ring is –4 for *Torpedo* (this is the same for human adult muscle receptors; see figure 1.3.10.c. and 1.3.10.d).

Intermediate ring: The -1' intermediate ring also has a net negative charge and is composed of E in α, β and δ, contributing negative charges, with the remaining γ subunit contributing an uncharged Q. Thus in *Torpedo* and human adult muscle the total charge of the intermediate ring is also –4 (see figure 1.3.10.c. and 1.3.10.d).

Central ring: The 2' central ring is uncharged and it is composed of hydrophilic T in α and γ, and Serine (S) in β and δ. Thus in *Torpedo* and human adult muscle there is no charge on the central ring (see figure 1.3.10.c. and 1.3.10.d).

Outer ring: The 20' outer ring is composed of E in α and D in β, contributing negative charges, with uncharged Q in γ and δ. Thus in *Torpedo* the total charge of the cytoplasmic ring is –3. However, in human adult muscle the δ subunit contributes a positively charged K residue, with a total charge on the cytoplasmic ring of –2 (see figure 1.3.10.c. and 1.3.10.d).

Imoto *et al.* (1988) reports that reducing the net negative charge on the cytoplasmic, intermediate or outer 'ring' by inserting a positively charged Lysine (K) or neutral Q residue, decreases the single channel conductance of *Torpedo* nAChRs (summarised in table see figure 1.3.10.b.). The greatest decrease in conductance (measured as chord conductance) is observed when the –1' intermediate ring is mutated. Mutating the uncharged –1'Q to positively charged –1'K in the γ subunit reduces the net negative charge from –4 to –3 and the conductance from 85 to 18 pS (see table 1.3.10.b.). On the other hand, increasing the side chain length of uncharged residues in the 2' central ring reduces conductance, with the greatest reduction produced by hydrophobic side chains (Imoto *et al.*, 1991; Villarroel *et al.*, 1991). Note that the magnitude of this effect is dependant on the permeant ion i.e. little change for sodium, more for pure potassium and more still for rubidium, and also that β3 possess a serine residue in 2', whereas α3 and β4 contain threonine (see figure 1.3.10.e.). From the data of Imoto *et al.* (1991) it can be seen that a serine to threonine mutation, or *vice verse*, produces little change in conductance (10 pS at the most) in pure potassium and zero calcium. Thus the nature of the 2' is unlikely to effect sodium conductance.

Table 1.3.10.b. Summary of the effects on single channel conductance of mutations in the TM2 cytoplasmic, intermediate or outer rings of charges in *Torpedo* nicotinic receptors

-4' cytoplasmic ring mutants	Net charge	γ (pS)	-1' intermediate ring mutants	Net charge	γ (pS)	20' outer ring mutants	Net charge	γ (pS)
Wild-type	-4	85	Wild-type	-4	85	Wild-type	-3	85
α D-4'E	-4	80	α E-1'D	-4	80	γ Q20'K	-2	80
γ Q-4'K	-3	75	δ E-1'Q	-3	45	α E20'D	-3	78
δ E-4'K	-2	73	β E-1'Q	-3	40	δ Q20'K	-2	75
γ Q-4'K + δ E-4'K	-1	70	γ Q-1'K	-3	18	β D20'K	-1	72
α D-4'N	-2	65	α E-1'Q	-2	20	α E20'Q	-1	70
α D-4'K	-2	58				γ + δ Q20'K	-1	65
β D-4'K + γ Q-4'K	-1	55				β D20'K + γ Q20'K	0	60
β D-4'K + δ E-4'K	0	50				β D20'K + δ Q20'K	0	58
α D-4'K	0	45				α E20'K	+1	40
α D-4'R	0	42				β D20'K + γ Q20'K + δQ20'K	+1	38
β D-4'K + γ Q-4'K + δE-4'K	+1	40				α E20'R	+1	35
α D-4'K + γQ-4'K	+1	35				α E20'K + δ Q20'K	+2	25
α D-4'K + δ E-4'K	+2	30				α E20'K + β D20'K	+3	10
α D-4'K+ β D-4'K	+2	25						

Table 1.3.10.b: The mutations of the residues in the cytoplasmic (-4'), intermediate (-1'), central (2') and outer (20') rings (single letter amino acid code) and the resulting net charge are indicated. Positively charged residues are indicated in red, negatively charged residues in blue and uncharged residues in the black. γ is the resulting single channel conductance (pS). Table constructed from figures 2 and 3 from (Imoto *et al.*, 1988 and Imoto *et al.*, 1991).

Figure 1.3.10.c. The TM2 domains of *Torpedo* nicotinic receptors

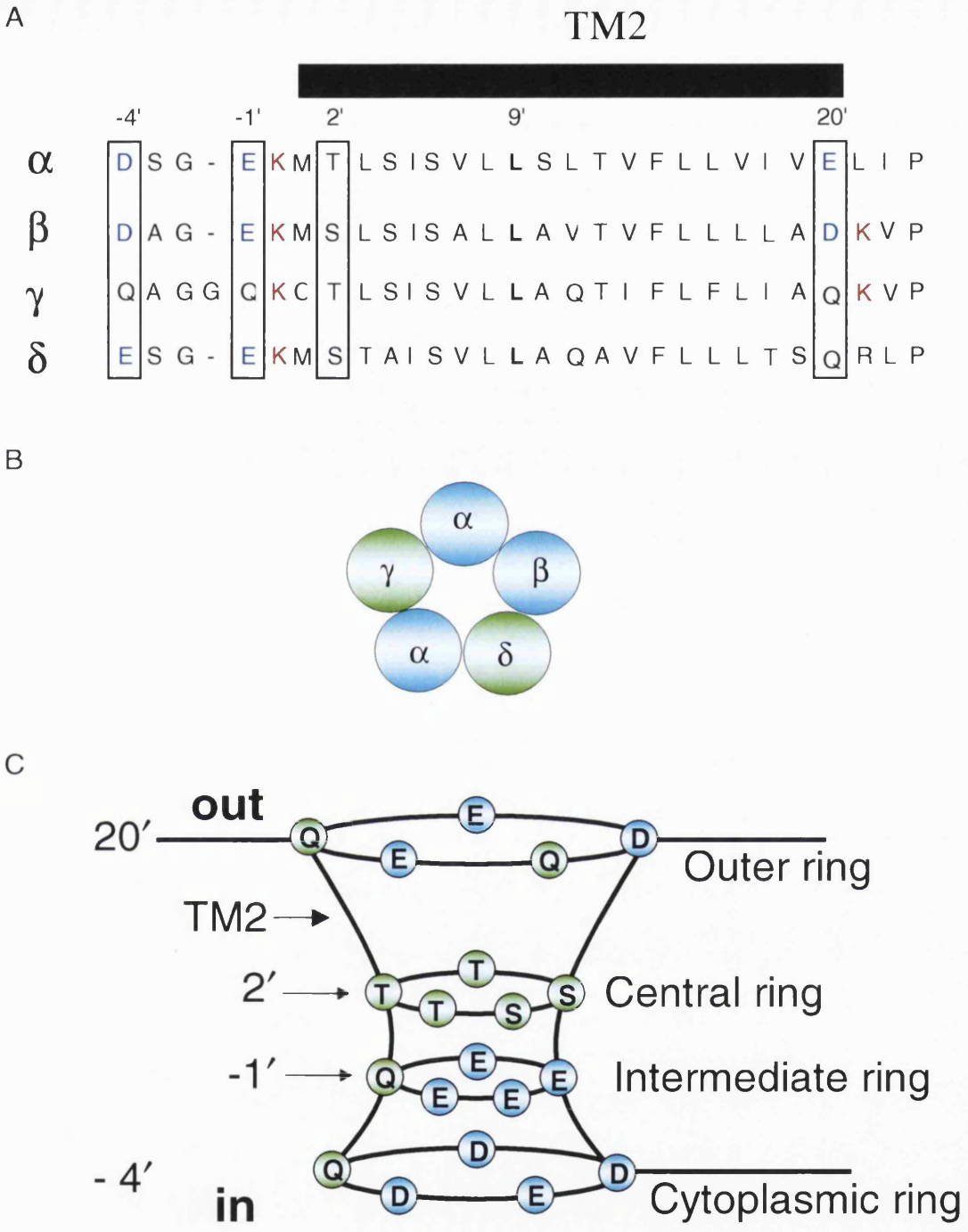

Figure 1.3.10.c. A shows the TM2 domain of α, β, γ and δ. Residues in A and C are labelled with the single letter amino acid code. The cytoplasmic (-4'), intermediate (-1'), central (2') and outer (20') rings are boxed and the 9' position of the reporter mutation is labelled for reference (bold). B shows a representation of what the *Torpedo* receptor may look like from the top. C shows a graphical representation of the pore of the channel, with the residues lining the pore forming the cytoplasmic (-4'), intermediate (-1'), central (2') and outer (20') rings. Note the constriction of the pore in-between the intermediate ring and the central ring. Positively charged residues are indicated in red, negatively charged residues in blue and neutral residues in green. The subunit arrangement shown is based on that described for the AChBP.

Figure 1.3.10.d. The TM2 domains of human adult muscle nicotinic receptors

A

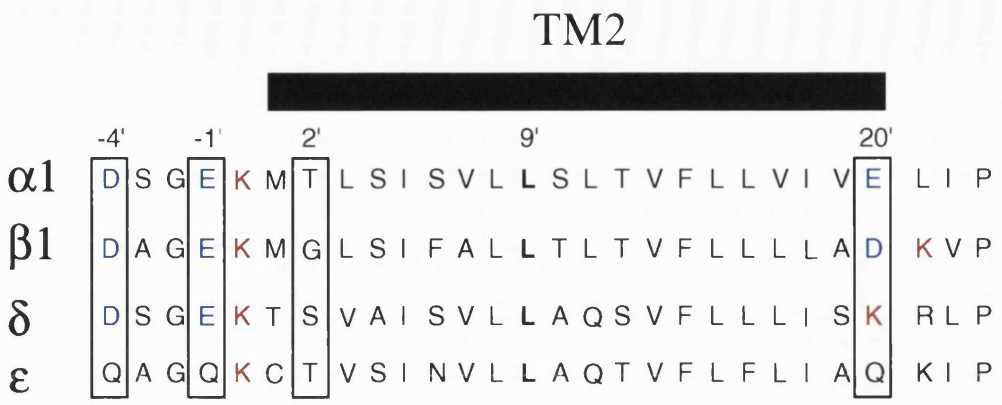

B

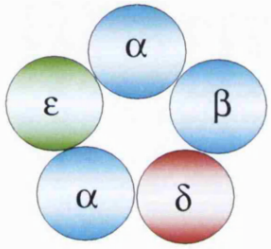

C

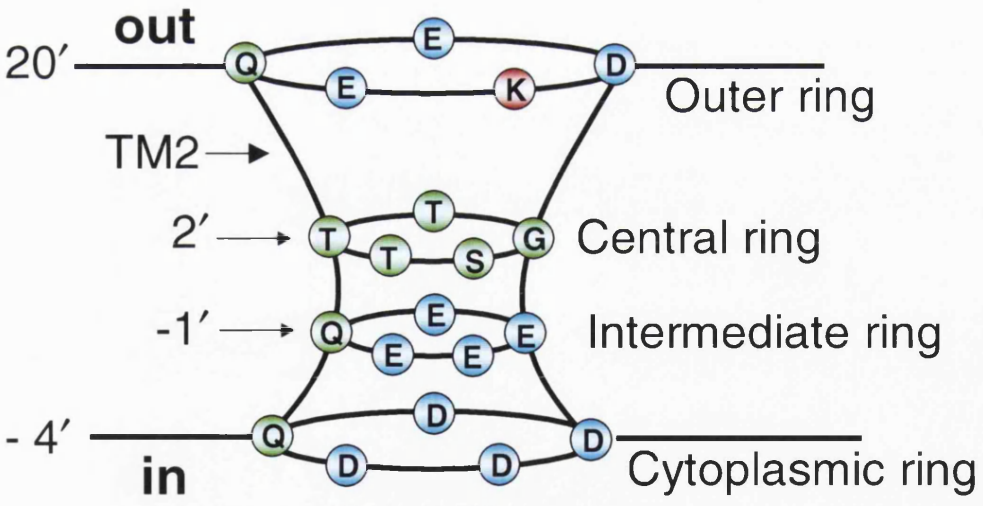

Figure 1.3.10.d. A shows the TM2 domain of α1, β1, δ and ε. See the legend to figure 1.3.10.c.

Figure 1.3.10.e. **Residues in the cytoplasmic, intermediate, central and outer rings of the human muscle and neuronal nicotinic acetylcholine receptor subunits**

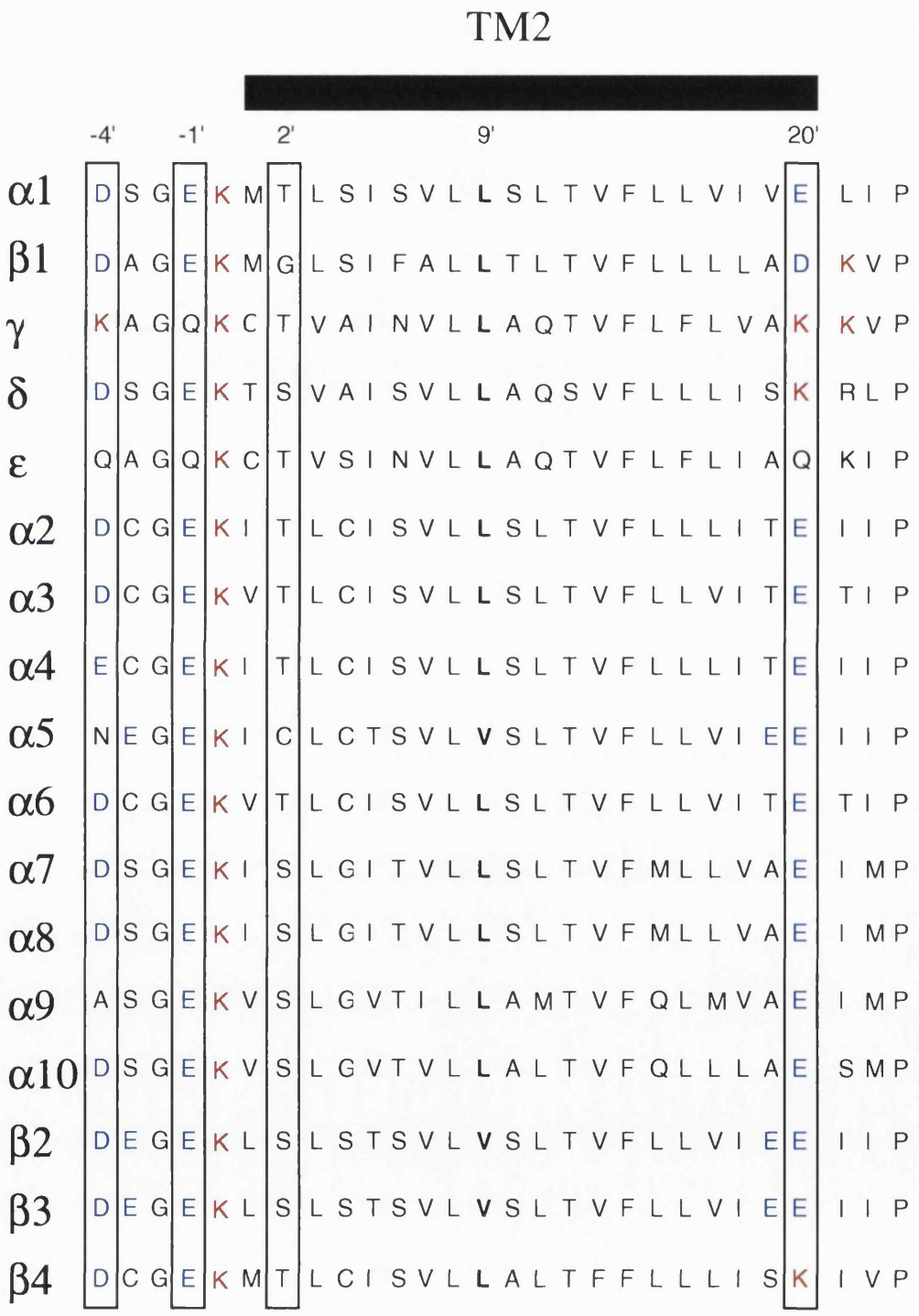

Figure 1.3.10.e. The residues of the cytoplasmic (-4'), intermediate (-1'), central (2') and outer (20') rings (rings indicated by boxed residues) for the human muscle and neuronal nicotinic acetylcholine receptor subunits are shown according to the single letter amino acid code. Note the α8 subunit is only found in chick and the sequence is only shown for comparison with the group. Positively charged residues are indicated in red and negatively charged residues in blue.

1.4. Function of the muscle nicotinic receptor at the neuromuscular junction

Fast synaptic transmission is well characterised at the synapses between the axons of spinal motor neurons and skeletal muscle fibres of vertebrates (NMJs). Here fast synaptic transmission is mediated by the neurotransmitter ACh acting on muscle nAChRs.

Activation of the motor neurone (presynaptic cell) results in action potentials that travel from the axon hillock, along the axon to the presynaptic terminal. Upon arrival at the presynaptic terminal, the action potential activates a number of voltage gated ion channels, including voltage gated Ca^{2+} channels in the presynaptic terminal membrane. The activation of the Ca^{2+} channels results in an influx of Ca^{2+} into the terminal, triggering the release of 'docked' ACh vesicles held close to the membrane by the cytoskeleton (exocytosis). Released vesicles fuse with the membrane and release ACh into the synaptic cleft. ACh then diffuses across the cleft, binding to, and transiently activating multiple muscle nAChRs located on the surface of junctional folds in the postsynaptic membrane of the skeletal muscle fibre. The resulting net influx of Na^{+} generates a rapid, transient depolarisation of the postsynaptic membrane, known as the endplate potential (EPP). The junctional folds in the postsynaptic membrane of the motor neurone are not electrically excitable, but the EPP spreads electrotonically to surrounding areas of the membrane that do contain voltage gated sodium channels. Here new action potentials are generated: these rapidly travel along the muscle fibre and cause the sarcoplasmic reticulum to release calcium, resulting in muscle contraction (Berne *et al* 1993; see figure 1.4.1.).

A large body of work has been produced on the study of the mechanism of activation of the muscle nAChR at the NMJ, including the factors that control the time course of the synaptic current (for review, see Edmonds *et al.*, 1995). The time course for the macroscopic synaptic current represents the sum of all the individual single-channel currents of the receptors on the postsynaptic membrane (Edmonds *et al.*, 1995). In principle, this time course should be determined by (a) the amount of transmitter released, (b) the time course of release, (c) the shape of the synaptic cleft and the location of the clustered postsynaptic receptors, (d) the rates at which diffusion, catabolic enzymes, and endocytosis mechanisms remove transmitter from the cleft, and (e) the rates of activation, deactivation, desensitisation, and block of the receptors by the transmitter (Edmonds *et al.*, 1995). In practice the main determinant is burst length and there is a good correlation between the time constant for the exponential decay of the synaptic current and the mean burst lifetime of the nAChR channel. This is because ACh in the synaptic cleft rapidly reaches millimolar concentrations, dropping sharply (within less than 1ms) as ACh both diffuses from the synaptic cleft into the extracellular space and becomes quickly hydrolysed by choline esterases associated with the postsynaptic membrane. Thus ACh that unbinds from the nAChR does not, on average, rebind. The high ACh concentration is sufficient to ensure a very fast on-rate, which drives binding of ACh to the subsynaptic nAChRs (reviewed in Edmonds *et al.*, 1995).

Figure 1.4.1. The muscle nicotinic receptor at the neuromuscular junction

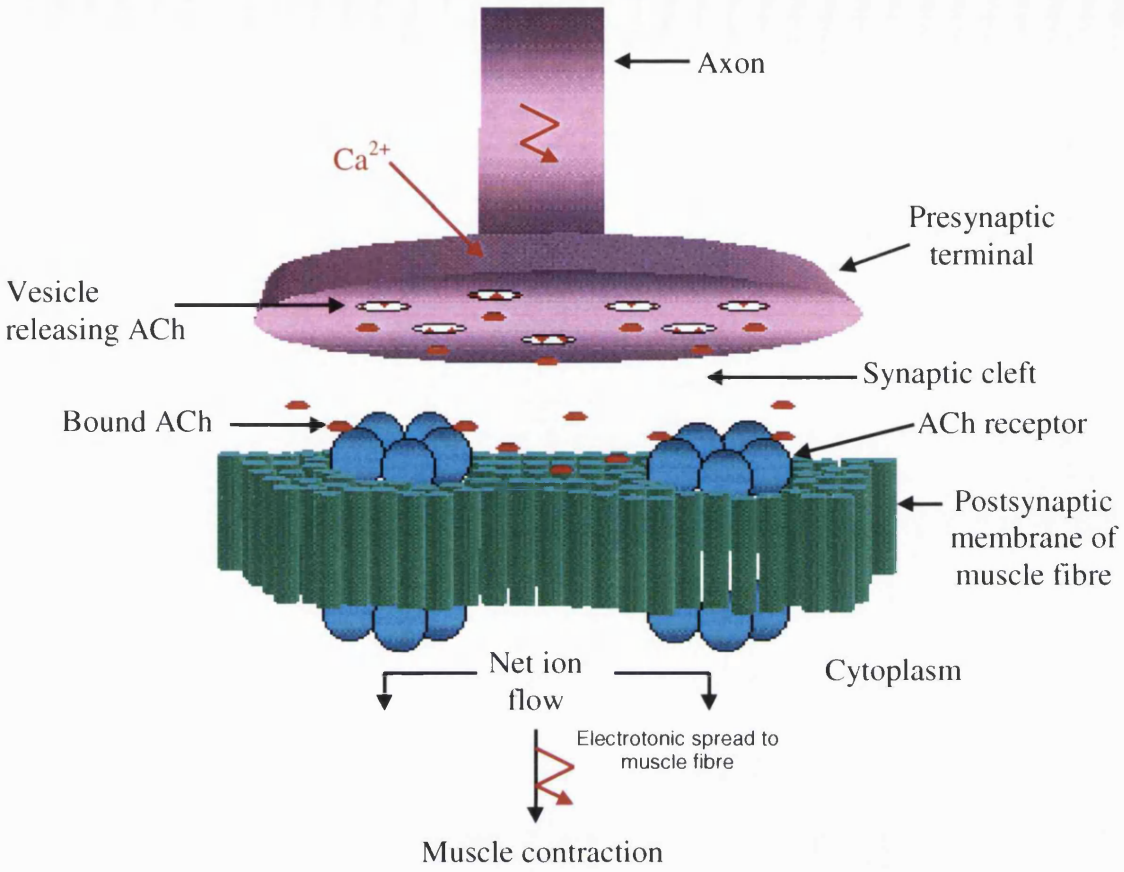

Figure 1.4.1. Shows a representation of fast synaptic transmission at the NMJ. The action potential (indicated by the red zigzag arrow) arrives at the presynaptic terminal, activating a Ca2+ influx through voltage gated Ca2+ channels. Ca2+ mediated phosphorylation events cause the release of docked ACh vesicles, which fuse with the membrane and release ACh (red dots) into the cleft. ACh then binds to the nAChR (indicated in blue) in the postsynaptic membrane of the muscle fibre and activates a net flow of Na+ into the muscle cell and K^+ out. The resulting depolarisation spreads in the muscle fibre, initiating an action potential and causing the muscle to contract.

1.5. Diversity of muscle nicotinic acetylcholine receptors

The earliest studies, by Katz and Miledi, on the structure and ion permeation of the nAChR channel had already demonstrated that there had to be more than one type of muscle nAChR. It was found that the receptor that is present in the non-junctional membrane of denervated muscle fibres differs from that found at the NMJ of normal adult endplates (Katz & Miledi, 1971). Later work showed that the receptors present in denervated rat muscle fibres are not the same as those in the non-junctional membrane of neonatal muscle endplates, and can be recognised because they have longer channel mean open times than receptors found in adult endplates (Sakmann & Brenner, 1978; Fischbach & Schuetze, 1980). On the basis of this data, Fischbach & Schuetze (1980) proposed that the neonatal type receptors are replaced by the adult type during postnatal development.

With the advent of molecular biology techniques, it became apparent that the difference between the two receptors resulted from replacement of the foetal γ subunit by the adult ε subunit, which is encoded by yet another gene. In terms of the TM2 domain, replacing γ with ε increases the net negative charge on both the cytoplasmic and extracellular rings of charges, which would predict an increase in single channel conductance for the adult receptor. Indeed, single channel data from adult and foetal bovine muscle nAChRs expressed in *Xenopus* oocytes demonstrate a single-channel conductance of 40 pS for $\alpha_{(2)}\beta\gamma\delta$ (foetal) vs. 60 pS for $\alpha_{(2)}\beta\varepsilon\delta$ (adult). The mean open lifetime of the channel also differed, 7.2 ms for $\alpha_{(2)}\beta\gamma\delta$ vs. 2.3 ms for $\alpha_{(2)}\beta\varepsilon\delta$. Thus, $\alpha_{(2)}\beta\gamma\delta$ (foetal) receptors have longer, smaller openings than the $\alpha_{(2)}\beta\varepsilon\delta$ (adult) receptors (Mishina *et al.*, 1986).

1.6. The neuronal nicotinic acetylcholine receptors

Even when briefly reviewed as in the previous section, the wealth of data on muscle nAChRs shows how well its structure, physiological function and kinetic behaviour are understood. The situation is much more complex for neuronal nAChR. On the one hand, in autonomic ganglia, neuronal nAChRs (mostly α3β4, see below) do mediate fast synaptic transmission (as at the NMJ; for a review see McGehee & Role, 1995). On the other hand, the role of neuronal nAChRs in the CNS is less clear. Irrespective of the physiological role of central nAChRs, the expression profile and composition of these nAChRs in the CNS was initially thought to be simple, given the high expression of α4 and β2 mRNA throughout the CNS. However, at least 9 subunits are expressed throughout the mammalian CNS (α2-α7, β2-β4) and more recent studies suggest that multiple subunits may be involved in the formation of functional receptors in the brain (discussed below). Consequently, the challenging questions to be answered are: What functional subunit combination exist in the CNS and what is the physiological significance of such diversity ? Before we can answer such questions, it is essential to establish which subunit combinations can be expressed in heterologous expression systems and ascertain their stoichiometry, pharmacological and biophysical properties in order to identify such receptors *in situ*. The following chapters will attempt to answer these questions for neuronal nAChRs containing the β3 subunit.

1.6.1. The cloning of the neuronal nicotinic subunits

The α3 subunit of the rat was the first neuronal nAChR subunit to be cloned by Boulter and colleagues in 1986 (Boulter *et al.*, 1986). Shortly afterwards the same group showed that α3, α4 and β2 could form functional α3β2 and α4β2 receptor when expressed in

Xenopus oocytes (Boulter *et al.*, 1987). Their work stimulated interest in the young field of neuronal nAChRs and a number of articles from various groups quickly followed, describing the newly cloned members of the growing neuronal nAChR family (see Sargent, 1993 for a review). The clones were classified as α subunits on the somewhat artificial criterion that their amino acid sequence should contain a pair of adjacent cysteines (Cys 192 and Cys 193; *Torpedo* α1 numbering) as 'markers' of the presumed ACh-binding site. Subunits lacking these two adjacent residues were labelled as non-α, later to be renamed β. It soon became apparent that the neuronal subunits, although related by a common ancestor to the muscle nAChR subunits, were far more diverse, having multiple α and β subunits. The human muscle α1 subunit has an amino acid sequence identity of 51 % with the neuronal α3 subunit, showing that divergence from a common evolutionary ancestor must have occurred a long time ago (Le Novère & Changeux, 1995). To date, 12 subunits have been identified as belonging to the neuronal nAChR family: α2-α10 (the muscle α subunit was renamed α1) and β2-4 (the muscle β subunit was renamed β1).

With 12 different subunits, a large number of combinations are theoretically possible (McGehee & Role, 1995). However, some simplifying assumptions can be made, as only some of the possible combinations can form functional channels when expressed in heterologous systems; for instance, in *Xenopus* oocytes some α subunits (α7 to α9) can form homomeric channels, sensitive to α-Bgt (see figure 1.6.1.a.). To date α10 has only been shown to form a functional channel when co-expressed with α9, the stoichiometry of which is currently unknown (Elgoyhen *et al.*, 2001; Sgard *et al.*, 2002). The majority of the other α subunits (namely α2-α4 and α6) can form functional channels only if co-expressed with a β subunit (either β2 or β4; see figure 1.6.1.a.). The latter type of receptor (which I shall refer to as a 'pair' receptor) is a pentamer with an α : β

stoichiometry of 2:3, as shown by radiolabelling and single channel studies on chick α4β2 receptors expressed in oocytes (Anand *et al.*, 1991; Cooper *et al.*, 1991).

Figure. 1.6.1.a. Examples of nAChR diversity from heterologous expression studies in *Xenopus* oocytes

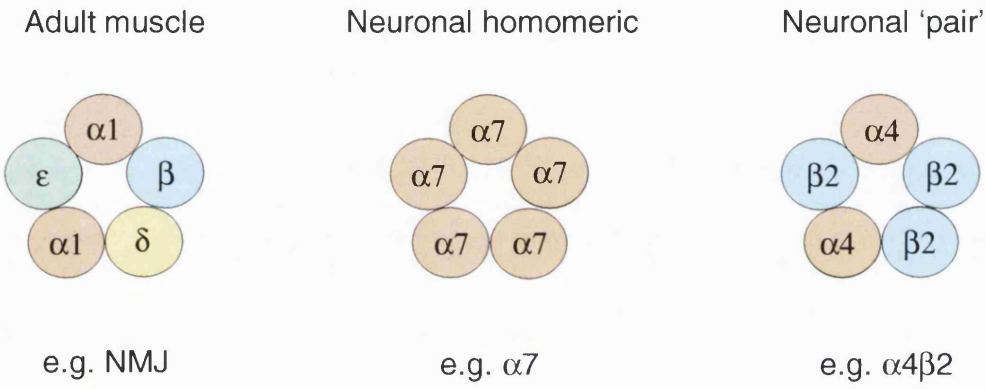

Figure 1.6.1.a. Shown is a graphical representation of each the three main nAChR types that have been expressed in *Xenopus* oocytes: $\alpha_{(2)}\beta\delta\varepsilon$ (adult muscle); α7 (neuronal homomeric) and α4β2 (neuronal pair). Note the subunit arrangement shown is based on that described for the AChBP.

1.6.2. Receptors with more than two types of subunit

The simple homomer or pair scheme does not account for subunits such as α5 and β3, which can only be assembled into functional receptors when co-expressed with another *two* different subunits, for instance as α4β2α5 or α3β4β3 receptors (which I shall refer to as 'triplet' receptors; see figure 1.6.2.a.).

Incorporation of α5 into functional receptors in *Xenopus* oocytes may manifest itself by changes in the properties of 'pair' nAChR: α4β2α5 receptors are 100-fold less sensitive to ACh than α4β2 (Ramirez-Latorre *et al.*, 1996). Single channel conductance increases (α4β2α5, Ramirez-Latorre *et al.*, 1996; Sivilotti *et al.*, 1997; Nelson & Lindstrom,

1999) and so do the rate and extent of desensitisation and calcium permeability (Gerzanich *et al.*, 1998).

Figure 1.6.2.a Triplet receptors expressed in *Xenopus* oocytes

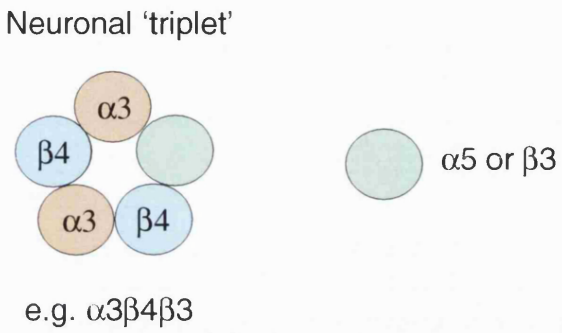

Figure 1.6.2.a. Shown is a graphical representation of triplet neuronal nAChRs expressed in *Xenopus* oocytes. Data in support of the stoichiometry shown are described in the results section. However, the arrangement of the subunits is unknown.

The β3 subunit was first cloned and identified as a neuronal nAChR subunit from rat brain (diencephalon) cDNA libraries by Deneris *et al.* (1989). They reported β3 as containing the same four transmembrane domain motif of the other neuronal nAChR subunits and lacking the adjacent cysteine residues 192 and 193, and therefore classed it as a β subunit.

Hernandez *et al.* (1995) analysed the amino acids sequence of chick β3 and found it to be most similar to the chick α5 subunit. If we include both identical amino acids and conservative substitutions for both α5 and β3, then the amino acid sequence similarity is 68.2 % for chick (Hernandez et al., 1995) and 80 % for human (Groot-Kormelink *et al.*, 1998). The α5 and β3 subunits have therefore been classified in a separate group within the nAChR phylogenetic tree (Tsunoyama & Gojobori, 1998).

Deneris *et al.* (1989) were unable to express functional β3 containing receptors with any of the known neuronal nAChR α subunits (α2 – α4 at the time) and β3 became labelled as an 'orphan' or pseudo gene, with no known function. However, in 1998 Groot-Kormelink *et al.* demonstrated the incorporation of β3 into an α3β4β3 triplet receptor when expressed with an α3β4 pair in oocytes, using a reporter mutation approach. More recently Palma *et al.* (1999) demonstrated the incorporation of β3 into a 'pair' α7β3 receptor.

The reporter mutation approach substituted the conserved hydrophobic 9' residue in TM2 of the β3 subunit (usually Leu, but Val in the case of β3 and α5) with a hydrophilic 9'Thr (see figure 1.6.2.b.). As previously discussed, mutating 9' to Thr or Ser increases the potency of agonists on α7 neuronal nAChRs (Revah *et al.*, 1991), muscle nAChRs (Filatov & White, 1995; Labarca *et al.*, 1995), ρ1 (Chang & Weiss, 1998) and α1β2γ2 $GABA_A$ receptors (Chang *et al.*, 1996).

Thus the incorporation of β3 into a α3β4β3 triplet receptor could be detected by an increase in the sensitivity of the receptor to ACh and a decrease in the wild type ACh EC_{50} from 180 μM to 42.6 μM for $\alpha3\beta4\beta3^{V9'T}$ (Groot-Kormelink *et al.*, 1998). However, the stoichiometry of such 'triplet' neuronal nAChR receptors and the effects of β3 incorporation on the pharmacological and biophysical properties of the 'pair' receptors are unknown. Chapters 3-6 aim to tackle these questions.

Figure 1.6.2.b. The reporter mutation

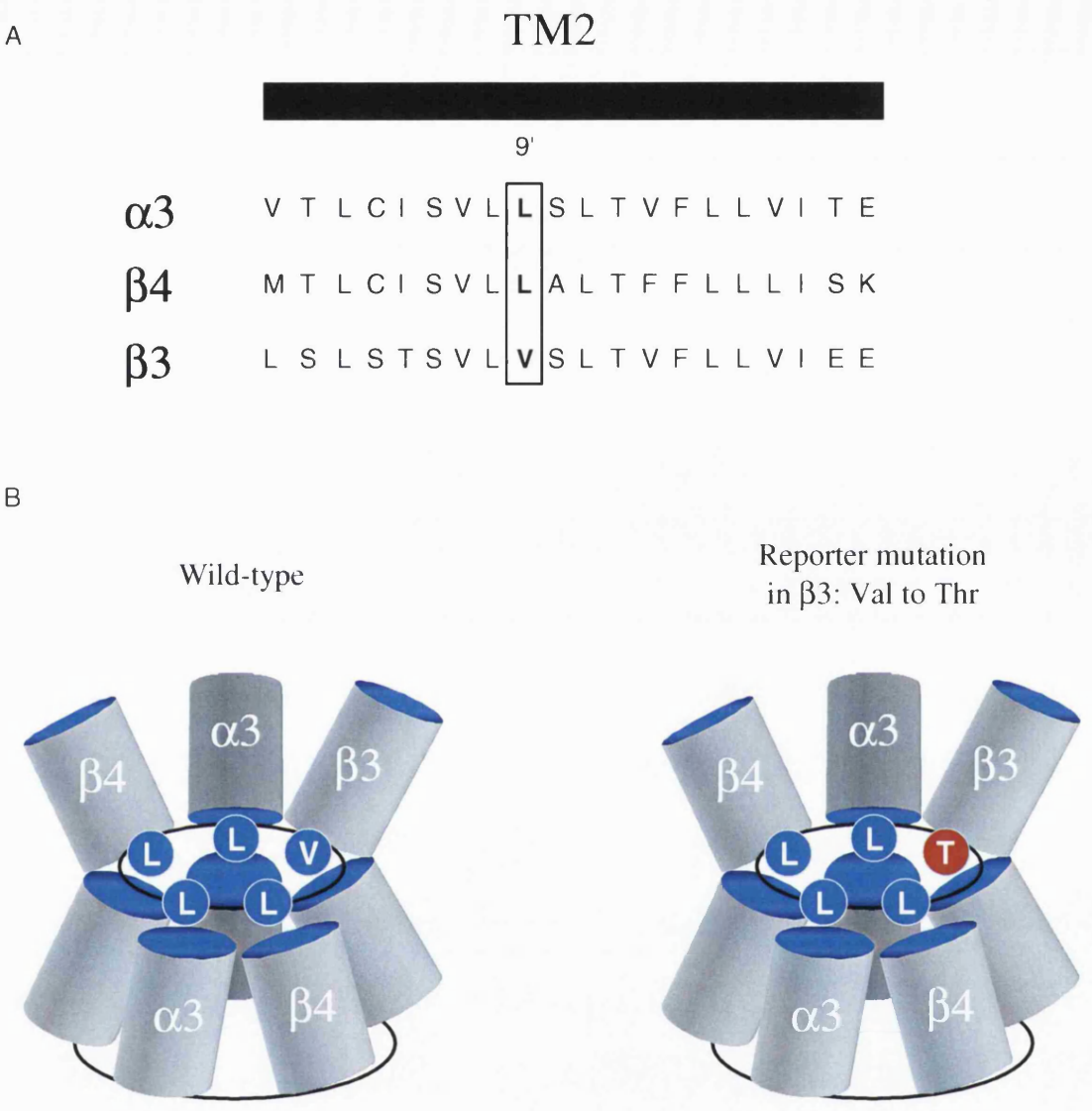

Figure 1.6.2.b. Diagrammatic representation of the arrangement of the TM2 domains in the closed state of a nAChR. The kinked TM2 domains are drawn according to Unwin (1998) and the 9' residues (which in this interpretation forms the channel gates) are highlighted with their one letter amino acid code. Note that the top half of the two TM2 domains at the front have been omitted for clarity, in order to emphasise the ring of hydrophobic residues at the channel gate.

1.6.3. Native receptors can contain more than two different subunits

There is increasing evidence to suggest that the 'either homomer or pair' rule is an oversimplification of the situation for native receptors. Just because one (or two) subunits are *sufficient* to produce a functional nAChR doesn't mean that native receptors are *necessarily* made in this minimally functional fashion, by just one or two types of subunit.

Subunit specific antibody data reports that in chick parasympathetic ciliary ganglia α5 co-immunoprecipitates with α3 and β4, and sometimes with β2 (Vernallis *et al.*, 1993; Conroy & Berg, 1995). On the basis of this data Conroy & Berg (1995) proposed that the main synaptic nAChR in chick parasympathetic ciliary ganglia is made up of three/four different subunits, α3, β4 and α5 (with or without β2).

Further evidence that receptors containing the α5 subunit occur in the autonomic nervous system comes from the work of Role and co-authors. Subunit specific deletion using antisense oligonucleotides targeted to the 5' region around the translation initiation site of the subunit in question reveals that chick sympathetic neurons express both α7 receptors and receptors containing α3 and/or α5 (Listerud *et al.*, 1991). The α5 containing receptors are insensitive to α-Bgt and have a single channel conductance of 35 pS (Yu & Role, 1998a). Furthermore, deletion of α5 or α3 results in an upregulation of α7 containing receptors, signified by an increase in α-Bgt sensitivity and the prevalence of an 18 pS conductance (Listerud *et al.*, 1991; Yu & Role, 1998a; Yu & Role, 1998b).

Conroy & Berg (1998) showed that a significant fraction of heteromeric receptors in embryonic chick brain contain not only α4 and β2, but also α5. This was confirmed by Balestra *et al.* (2000) who immunoprecipitated α2 containing receptors from chick optic lobe and α4 containing receptors from chick forebrain-cerebellum, and tested their high affinity epibatidine binding. These high affinity epibatidine binding sites could be precipitated by either β2 or α5 specific antibodies, indicating that α2 containing receptor from the optic lobe and α4 containing receptors from the forebrain-cerebellum also contain both β2 and α5.

Further, Balestra *et al.* (2000) report that the level of epibatidine binding increases during development, with significantly more binding in the optic lobe than in the forebrain at embryonic day 11 (47 to 225 vs. 47 to 77 fmol/mg of protein at postnatal day 1). The increase in binding coincides with an approximate 26-fold increase in α2 and α5 expression in the optic lobe and an approximate 6-fold increase in α4 and α5 expression in the forebrain (Balestra *et al.*, 2000). Balestra *et al.* (2000) propose that α5 forms developmentally regulated α2β2α5 and α4β2α5 receptors in the chick optic lobe and forebrain respectively.

An example of the complexity of neuronal nAChRs in the central nervous system involving β3 comes from the data of Forsayeth & Kobrin (1997). Using subunit specific antibodies, Forsayeth & Kobrin (1997) report that β3 and β4 co-immunoprecipitate with β2 in the cerebellum, indicating that all three β subunits are co-assembled. Furthermore, antibodies to α4, β2, β3 or β4 immunoprecipitated at least 75 % high affinity ACh binding sites (insensitive to κ-Bgt, 10 nM, in order to block ganglionic type receptors, and α-Bgt, 10 nM, in order to block α7 receptors; Forsayeth & Kobrin, 1997).

Forsayeth & Kobrin (1997) propose that α4 co-assembles with β2, β3 and β4 in the cerebellum, to form an α4β2β3β4 receptor. In support of this hypothesis, cotransfection of α4, β2, β3 and β4 in COS cells produced high affinity ACh binding sites and, in this heterologous system, the majority of the high affinity ACh binding sites were immunoprecipitated by antibodies specific for α4, β2, β3 or β4 as in the native receptors (Forsayeth & Kobrin, 1997).

More recent data show that the highest levels of β3 mRNA in the chick nervous system are found in the retina (Vailati *et al.*, 2000). In the retina, all high affinity radiolabelled epibatidine binding sites are precipitated by an α6 specific antibody and this precipitation reduces β3 specific antibody binding, suggesting that α6 and β3 co-assemble (Vailati *et al.*, 2000). The α6 precipitated receptors were then eluted from an α6 antibody immunoaffinity column and saturated with radiolabelled epibatidine before screening with antibodies specific for the other neuronal nAChR subunits. This showed that β4 immunoprecipitated all the α6 radiolabelled epibatidine binding sites. 50 % of these α6β4 receptors co-immunoprecipitated with β3 and 40 % with α3. Only 7.5 % were found to co-immunoprecipitate with β2 (Vailati *et al.*, 2000). When the screening was carried out on β3 containing receptors, the immunoaffinity column revealed that radiolabelled epibatidine binding sites were reduced by: 26 % for α2, 35 % for α3, 33 % for α4, 45 % for β2 and 42 % by β4 antibodies respectively. Finally, α-conotoxin MII (recently shown to be specific for α6 containing receptors Whiteaker *et al.*, 2002; Champtiaux *et al.*, 2002) inhibits radiolabelled epibatidine binding to receptors which co-immunoprecipitated with β3 and α6, but has no effect on receptors immunoprecipitated by β3 alone. On the basis of this data Vailati *et al.* (2000) propose that more than two populations of β3 containing receptor are present in the chick retina.

The first is α6β4β3, with the remaining populations consisting of β3 associated with any of the following subunits: α2, α3, α4, β2 and β4.

1.7. Evolution of nicotinic acetylcholine receptor subunits

The evolution of vertebrate nAChR subunits in both neuronal and muscle type receptors has been hotly debated in the literature (Le Novère & Changeux, 1995; Ortells & Lunt, 1995). It is generally accepted that two groups of nAChR subunits separated after the emergence of the subunits in insects and nematodes. However, the identity of the subunits constituting the two groups remains controversial, mainly because of differences in the methods used for constructing the evolutionary trees and in the definition of the data to be used (i.e. DNA vs. amino acid sequence).

On the basis of *DNA sequence* alignment, using only the first 2 codon positions from 270 shared codons from each subunit sequence (to avoid superimposed mutations which may affect the construction of the tree), Ortells & Lunt (1995) have constructed an evolutionary tree for the nAChR superfamily. In the construction of their tree, Ortells & Lunt (1995) have excluded "regions where there is no obvious sequence identity", which they define as:

"*the N-terminal domain; cytoplasmic loop between TM3 and TM4; and several other short sequences.*"

On the basis of these data, Ortells & Lunt propose that α7 and α8 neuronal nAChRs are the most primitive, splitting off from the early common ancestor before the other subunits (note that α9 was not included and α10 had not yet been cloned at the time).

Next, structural non-α subunits, lacking the adjacent cysteine residues (with the exception of β3) split off from the remaining α subunits, forming two main groups: one containing α1-α6 and β3 subunits and the other containing β1, β2, β4, γ, δ, and ε subunits. Subsequently the neuronal and the muscle type receptors split off into separate groups of α (including β3) and non-α subunits. Next the neuronal α subunits split off to form one group containing α2-α4 and α6 and the other group containing α5 and β3. The muscle non-α subunits also split off with γ, δ and ε in one group and β in the other.

In contrast to this, on the basis of *amino acid* sequence alignment (excluding signal peptide, non-conserved portion of N-terminal domain, cytoplasmic loop between TM3 and TM4 and C-terminus), Le Novère and Changeux (Le Novère & Changeux, 1995) propose that the muscle α1 subunit and all the neuronal subunits (α2-α6 and β2-β4) constitute one main group and all the muscle non-α subunits (*i.e.* β1, γ, δ, and ε) constitute the other main group.

More recently, Tsunomaya and Gojobori (Tsunoyama & Gojobori, 1998) constructed a phylogenetic tree on the basis of *amino acid* sequence alignment for all the nAChR subunits. Here they analysed the complete protein sequence (from start codon to stop codon) of 84 subunits divided over 18 different species, more nAChR subunits than the previous groups.

Here they also propose that initially the common ancestral subunit appeared in the nervous system and that homomeric receptor forming α7, α8 and α9 subunits are direct descendants of the common ancestor, with α9 diverging first (Tsunoyama & Gojobori, 1998). In agreement with the previous view of Ortells and Lunt (1995), this tree shows structural non-α subunits, lacking the adjacent cysteine residues (with the exception of

β3) split off from the α subunits, forming two main groups, the first eventually giving rise to α1-α6 and β3 subunits and the other to β1, β2, β4, γ, δ, and ε subunits (Tsunomaya & Gojobori, 1998). The same authors also distinguish five different subgroups within the neuronal subunits, distinguished on the basis of their sequence and functional analysis after over-expression in heterologous cells. The α7, α8, α9 subunits can all form homopentameric functional receptors and thus form the first group. In contrast, the α2/α4, α3/α6 and β2/β4 groups can form functional receptors as an "α/β" pair, but not the α5/β3 group. However, both α5 and β3 subunits are able to form functional receptors when co-expressed with an α/β pair, forming a 'triplet' receptor (as discussed above). The grouping of α5 and β3 into the same evolutionary group suggests that the β3 subunit may have a similar function to that of α5.

1.8. Distribution of the neuronal nicotinic acetylcholine receptor subunits

In situ hybridisation, immunohistochemistry, Northern blot analysis, and reverse transcriptase polymerase chain reaction (RT-PCR) analysis have established that of the 12 subunits cloned to date, 9 are expressed in the mammalian brain: α2, α3, α4, α5, α6 & α7 and β2, β3 & β4 (reviewed by Sargent, 1993; McGehee & Role, 1995). The main areas found to express nAChRs are: the periaqueductal grey matter, basal ganglia, thalamus, hippocampus, cerebellum and retina (for a review see Gotti *et al.*, 1997). The nAChR subunits are distributed throughout the mammalian cortex as follows: hippocampus contains α3, α4, α5, α7 and β2, β3 & β4; mesocorticolimbic system all 9 subunits listed above; the auditory cortex contains α7; retina contains all 9 subunits, whereas the chick optic lobe contains α2, α5, α7 and β2 (Clementi *et al.*, 2000). Steady state binding studies have shown that α4 and β2 represent the majority of high affinity

Nic binding sites and α7 represents the high affinity α-Bgt binding sites in the CNS (for a review see McGehee & Role, 1995).

Using subunit mRNA specific radiolabelled *in situ* hybridisation probes, Deneris *et al.* (1989) report that in the rat brain β3 mRNA is expressed along with α2, α3, α4 and β2 in the medial habenula (ventromedial part, see also Le Novère *et al.*, 1996), in rat substantia nigra *pars compacta* (SNc; also reported by Le Novère *et al.*, 1996; Han *et al.*, 2000), ventral tegmental area (VTA; also reported by Le Novère *et al.*, 1996; Han *et al.*, 2000) and the reticular nucleus of the thalamus. Le Novère *et al.* (1996) also report expression of β3 in the rat locus coeruleus. Thus β3 is particularly important in dopaminergic regions of basal ganglia. i.e. areas that are important in Parkinson's disease and nicotine addiction (see below).

More recent data using the same technique show that most dopaminergic neurons in SNc (~95 %) express α4, α5, α6, β2 and β3 mRNA. Other subunits are less common, with α3 and α7 being present in approximately 60 % of dopaminergic neurons and β4 only in less than 5 % of dopaminergic neurons (Azam *et al.*, 2002). Very similar results were obtained for dopaminergic neurons of the VTA . Some expression of α4, α7 and β2 mRNA was detected in GABA neurons within the SNc (Azam *et al.*, 2002).

Radiolabelled ligand binding data from Quik *et al.* (2000) demonstrate that the SNc contains both high affinity epibatidine and high affinity α-Bgt (selective for α7 receptors) binding sites, suggesting that heteromeric and α7 receptors are expressed in the SNc. Subunit specific *in situ* hybridisation data confirmed α4, α6, α7, β2, β3 and β4 mRNA expression in the SNc, with the greatest expression of α6 and β3 (Quik *et al.*, 2000).

The expression of β3 mRNA also seems to be affected by damage to the *substantia nigra* (SN). In order to produce Parkinson like damage to the dopaminergic neurons of the SN, Quik *et al.* (2000) studied the changes in the distribution of high affinity ligand binding sites and the expression of subunit mRNA produced by treatment of squirrel monkeys with the toxin 1-methyl-4-phenyl-1,2,3,6,tetrahydropyridine (MPTP). MPTP induced nigrostriatal damage was associated with a decrease in high affinity epibatidine binding sites, reduced β3 mRNA to 62 % and increased α6 mRNA to 143 % of control values (Quik *et al.*, 2000). These data suggest that β3 is incorporated into a receptor with high affinity for epibatidine within dopaminergic neurons of the SN. However, the functional implications of the reduction in β3 following nigrostriatal damage and the role of the α6 subunit relative to β3 are unclear.

A different technique for lesioning dopaminergic neurons, using the toxin 6-hydroxydopamine, abolishes mRNA signals for α3, α5, α6 and β4 subunits from the SN and α2, α3, α5, α6, α7 and β4 from the VTA of the rat. However, mRNA signals for α4, β2 and β3 were still present in the SN and VTA, suggesting that β3 is present in non-dopaminergic neurons of the SN and VTA (Charpantier *et al.*, 1998).

In contrast to the findings of Charpantier *et al.* (1998), Elliott *et al.* (1998) report that 6-hydroxydopamine lesions of the rat SN substantially reduce the mRNA signal for α5, α6 and, to a lesser extent, β3. This suggests that β3 is present in dopaminergic neurons in the SN.

Single cell RT-PCR data from Klink *et al.* (2001) showed that dopaminergic neurons in the SN and VTA express α3-α7 and β2-β4 mRNA, with the vast majority of neurons expressing α4, α5, α6, β3 and quite often α3. GABAergic projection neurons of the SN

also contained α5, α6 and β3, whereas α3, α4 and β2 were expressed in the VTA (Klink *et al.*, 2001). The same technique in isolated medial habenula neurons demonstrates that 95-100 % of neurons contain mRNA for α3-α5, β2 and β4, whereas only 40 % of cells were positive for α6, α7 and β3 and no cells contained α2 (Sheffield *et al.*, 2000).

Northern blot analysis of RNA isolated from various regions of the chick nervous system showed that β3 is expressed in retina, telencephalon, cerebellum and spinal cord (Hernandez *et al.* 1995).

As discussed above, immunoprecipitation studies by Forsayeth & Kobrin (1997) have shown that β3 is expressed together with α4, β2 and β4 in rat striatum, cerebellum and faintly in the hippocampus.

β3 has also been shown to be expressed in the peripheral nervous system. Polymerase chain reaction (PCR) analysis of the cochlea of the mouse has shown the co-expression of β3 with β2 and α2 – α6 (Drescher *et al.*, 1995) and rat cochlea (Anderson *et al.* 1997). Anderson *et al.* (1997) also report that β3 mRNA is co-expressed with in α2-α7, β2 and β4 in vestibular ganglia and with α3, α5 – α7, α9, β2 and β4 in vestibular end organs. The RT-PCR data of Morley *et al.* (1998) demonstrates the expression of β3 mRNA in the spiral ganglia of the rat cochlea.

Immunoprecipitation in chick retina demonstrates expression of α2-α4 and α6 and β2-β4, with at least two populations of β3 containing receptors are present: α6β4β3 and the second contains α2, α3, α4, β2, β3 and β4 without α6 (Vailati *et al.*, 2000).

In the chick periphery, β3 mRNA was found to be expressed in developing trigeminal and dorsal root ganglia, while low levels were detectable in superior cervical and sympathetic ganglia (Hernandez *et al.* 1995).

1.9. Function of neuronal nicotinic acetylcholine receptors in the CNS

In autonomic ganglia neuronal nAChRs are known to mediate the main excitatory synaptic events, i.e. fast synaptic transmission between preganglionic and postganglionic neurons, in both the sympathetic and parasympathetic system. Some presynaptic terminals may also have neuronal nAChRs (McGehee & Role, 1995; McGehee *et al.*, 1995; Coggan *et al.*, 1997).

In contrast to the situation in ganglia, in the CNS the role of neuronal nAChRs is unclear. In the CNS neuronal nAChRs are found in both the presynaptic and postsynaptic membranes (McGehee & Role, 1995; McGehee *et al.*, 1995; Coggan *et al.*, 1997).

1.9.1. Postsynaptic neuronal nicotinic acetylcholine receptors

Neuronal nAChRs mediate fast synaptic transmission in synapses between recurrent axons from spinal motoneurons and Renshaw cells (Eccles *et al.*, 1954). It took more than 40 years for the next report of nicotinic fast synaptic transmission in the nervous system to appear. This refers to the inner-plexiform layer of the developing retina, where cholinergic interneurons (termed starburst amacrine cells) mediate lateral interactions between bipolar cells and retinal ganglion cells, via activation of postsynaptic nAChRs (p349, Kandel and Schwartz, Principles of neural science, 2nd

edition; Feller *et al.*, 1996). Feller *et al.* (1996) propose that activation of postsynaptic nAChRs is important for propagating excitation in the developing retina. Roerig *et al.* (1997) describes spontaneous synaptic currents in the developing ferret visual cortex which are sensitive to dihydro-beta-erythroidine (DHβE; 100 μM) and insensitive to α-Bgt (100-200 nM), suggesting that heteromeric non-α7 receptors are involved in these spontaneous currents.

Growing evidence shows that nicotinic fast synaptic transmission takes place in the hippocampus. The hippocampus contains intrinsic cholinergic interneurons, GABAergic interneurons and excitatory glutamatergic neurons that receive cholinergic innervation from the septum. Thus cholinergic projections could excite GABAergic interneurons by releasing ACh onto nAChRs in their postsynaptic membranes. Indeed GABAergic neurons do have nicotinic receptors. The GABAergic interneurons can be separated into two groups on the basis of the type of agonist-evoked nicotinic currents they display. The first group has a fast decaying nicotinic inward current, reproduced by choline and sensitive to low concentrations of MLA and α-Bgt, thought to consist of α7 nAChRs (Jones & Yakel, 1997; Alkondon *et al.*, 1997; McQuiston & Madison, 1999; for a review see Jones *et al.*, 1999). This fast decaying current is abolished in α7 knockout mice (Orr-Urtreger *et al.*, 1997). The second group demonstrates two components: an initial fast decaying inward current, sensitive to choline, MLA and α-Bgt; and a slower decaying current sensitive to mecamylamine and DHβE. This second component is likely to be mediated by non-α7 receptors (Jones & Yakel, 1997; Alkondon *et al.* 1997; McQuiston & Madison, 1999; for a review see Jones *et al.*, 1999). Thus GABAergic interneurons can express more than one class of nAChR in their postsynaptic membrane.

Approximately 50 % of all hippocampal interneurons have the fast decaying α7 current (Jones & Yakel, 1997; McQuiston & Madison, 1999). Furthermore, α7 like currents have been described in cultured pyramidal cells (Albuquerque *et al.*, 2000) or mouse CA1 pyramidal neurons in acute slices (Ji *et al.*, 2001), suggesting that α7 may be important in interneurons that control input onto pyramidal cell dendrites.

The slower α-Bgt insensitive agonist induced currents are less common, present in approximately 10 % of hippocampal neurons in culture. This current is thought to be composed of mostly α4β2 and is highly sensitive to DHβE (10 nM), decreased by 100 nM MLA and blocked by 1 μM mecamylamine. Approximately 2 % of hippocampal neurons in culture display a second slow current, sensitive to 1 μM mecamylamine or 20 μM +-tubo and resistant to 100 nM MLA, thought to be composed of α3β4 (reviewed in Albuquerque et al., 2000).

Note that it is still controversial whether *pyramidal* cells do have nicotinic responses: there are reports of both fast α7-type responses (Albuquerque *et al.*, 2000; Ji *et al.*, 2001) and slow responses (Alkondon *et al.*, 1999).

The consensus for recent data is that α7 receptors are the main synaptic nicotinic receptor in the hippocampus. First of all, Fabian-Fine *et al.* (2001) report that α7 immunoreactivity is present at the *majority* of synapses in CA1 *stratum radiatum* (including GABAergic and glutamatergic ones). Alkondon *et al.* (1998) and Frazier *et al.* (1998) report α7-like receptors mediate fast synaptic transmission onto CA1 interneurons, on the basis of sensitivity of synaptic currents (both evoked and spontaneous) to desensitisation by choline, or block by MLA (50-150 nM) and α-Bgt

(100 nM). Such cholinergic currents were relatively rare and were found in only 17/125 of the interneurons. Nevertheless they contributed to approximately 10 % of the total evoked synaptic current. Hefft *et al.* (1999) has also reported α7-like synaptic currents in pyramidal cells from acute or organotypic slices, where the current is thought to contribute to less than 3 % of the total postsynaptic current.

1.9.2. Presynaptic neuronal nicotinic acetylcholine receptors

Neuronal nAChRs have also been shown to have a presynaptic and preterminal location at or near the nerve terminal, where they increase neurotransmitter release mainly via activation of voltage gated sodium and calcium channels (Wonnacott, 1997; MacDermott *et al.*, 1999; Wonnacott *et al.*, 2000). Both α7 and non-α7 receptors can play a presynaptic role. For example, α7 receptors enhance the release of glutamate in chick habenula/interpeduncular nucleus co-cultures (McGehee *et al.* 1995) and in mossy fiber terminals in rat hippocampus slices (Gray *et al.* 1996). However, the type of nAChR involved depends both on the brain region and on the nature of the terminal, i.e. on the transmitter released. Li *et al.* (1998) report that noradrenaline release in the dorsal raphe nucleus of the rat is sensitive to 100 nM methyllycaconitine (i.e. α7-like), whereas 5HT release is unaffected. In the hippocampus, both α7 and non-α7 receptors are thought to enhance GABA release (Alkondon *et al.*, 1999; Maggi *et al.*, 2001). Furthermore, dopaminergic and noradrenergic neurons express non-α7 nicotinic receptors, containing β2 or β4, which enhance the release of dopamine and noradrenaline respectively. However, modulation of neurotransmitter release may not be the only presynaptic role for nAChRs. It has been proposed that calcium entry through nAChRs, particularly through the highly calcium permeable α7 receptor ($P_{Ca}/P_{Na} > 10$; Seguela *et al.*, 1993), may depolarise the neuron and stimulate transmitter

release independently of voltage gated channels at resting and hyperpolarised membrane potentials (for a review see MacDermott *et al.*, 1999).

Given the well known addictive effects of Nic from tobacco smoke and the pharmaceutical interest in developing treatments for Nic abstinence, recent research has been concentrated on the role of neuronal nAChRs in areas of the brain implicated in reward and addiction. The VTA and the nucleus accumbens are both implicated in dopamine mediated reward. In particular, addictive drugs stimulate dopamine release in the VTA and nucleus accumbens.

The SNc is also of interest because a reduction in the number of dopaminergic neurons in the SNc causes Parkinson's disease and is accompanied with a reduction in radiolabelled Nic binding sites (Perry *et al.* 1995). Furthermore, nicotine from tobacco smoke is thought to protect against the development of Parkinson's disease (Janson *et al.*, 1988; for a review see Mihailescu & Drucker-Colin, 2000). In agreement with this, a protective effect of nicotine against nigrostriatal damage has been demonstrated in the rat (Jeyarasasingam *et al.*, 2002; Ryan *et al.*, 2001). This protective effect is sensitive to +-tubo, insensitive to α-Bgt and lost in α4 knockout mice (Jeyarasasingam *et al.*, 2002; Ryan *et al.*, 2001), suggesting that α4 containing nAChRs are important in this protective role, although it is unclear whether this protection is mediated by pre or postsynaptic receptors.

The VTA and SNc project dopaminergic terminals to the nucleus accumbens and the caudate putamen respectively. Systemic application of Nic in the VTA and SNc activates nAChRs both on postsynaptic neurons (Clarke & Pert, 1985; Picciotto *et al.*, 1998; Klink *et al.*, 2001; Jones *et al.*, 2001) and on presynaptic terminals (Rapier *et al.*,

1990; Grady *et al.*, 1992; el Bizri & Clarke, 1994; Soliakov & Wonnacott, 1996; Soliakov & Wonnacott, 2001; Jones *et al.*, 2001). Activation of postsynaptic nAChRs depolarises the dopaminergic neurons in the VTA and SNc, causing the release of dopamine in the nucleus accumbens and the caudate putmen (Imperato & Di Chiara, 1986; Mereu *et al.*, 1987; Benwell & Balfour, 1997; Pidoplichko *et al.*, 1997; Azam *et al.*, 2002).

The importance of neuronal nAChRs in the reward system is illustrated by the fact that β2 knockout mice do not self-administer Nic, unlike their wild type counterparts (Picciotto *et al.*, 1998). However, the subunit composition of the nAChR receptor subtypes involved in the reward system is unclear. This is because dopaminergic neurons in the VTA and SNc express mRNA for several neuronal nAChR subunits: α2, α3, α4, α5, α6, α7, β2, β3 and β4 subunits, with the largest expression of α3, α4, α5, α6, β2 and β3 (Elliott *et al.*, 1998; Charpantier *et al.*, 1998; Klink *et al.*, 2001; Azam *et al.*, 2002). Electrophysiological and pharmacological data from wild-type and gene knockout animal models suggests that at least 3 receptor subtypes are present in dopaminergic neurons. ACh evoked currents in these neurons have at least two components. The first component shows fast α7-like desensitisation, is activated by choline and blocked by α-Bgt and MLA (1 nM) and is abolished in α7 knockout mice (Klink *et al.*, 2001). The second component is a slower non-α7 desensitising current that is sensitive to block by mecamylamine (10 μM; Pidoplichko *et al.*, 1997; Fisher *et al.*, 1998; Klink *et al.*, 2001) and DHβE (2 μM; a concentration selective for β2 containing receptors; Klink *et al.*, 2001) and is abolished in β2 knockout mice (Klink *et al.*, 2001).

The second non-α7 component is likely to be mediated by two receptor subtypes. The first is insensitive to MLA and the second is sensitive to both -MLA (1 nM) and α–conotoxin MII (10 nM). The current amplitude of the second component is substantially reduced, but not abolished by α–conotoxin MII (10 nM) or MLA (1 nM; Klink *et al.*, 2001). Further, the degree of antagonism produced by α–conotoxin MII was unaffected by co-application of MLA (1 nM), suggesting that MLA and α–conotoxin MII affect the same receptor (Klink *et al.*, 2001).

Recent data from Champtiaux *et al.* (2002) demonstrates that α–conotoxin MII is selective for receptors containing the α6 subunit and suggests that the α–conotoxin MII and MLA sensitive receptor in the second component contains at least β2α6. Radio-labelled α–conotoxin MII binds with high affinity to areas in the brain including dopaminergic neurons in α3 knockout mice (Whiteaker *et al.*, 2002), but high affinity binding is abolished in α6 knockout mice along with high affinity epibatidine sites sensitive to α–conotoxin MII and resistant to the nAChR agonist cytisine (Cyt; Champtiaux *et al.*, 2002).

Furthermore, data from α4 knockout mice demonstrates that the MLA sensitive subtype consist of at least α4β2α6 and that the MLA insensitive subtype consist of β2α5 with at least another α subunit, probably α3. The second component of ACh evoked currents in α4 knockouts demonstrate a reduced amplitude and faster rate of decay, insensitive to MLA (1 nM; Klink *et al.*, 2001). Klink *et al.* (2001) propose that this speeding up of decay is due to a greater contribution of α5 containing receptors (probably in compensation for α4 being knocked out).

Through their effects on glutamate and GABA release, presynaptic nAChRs could modulate learning and memory formation. For example, activation of homomeric α7 receptors increases the release of glutamate from the presynaptic nerve terminal of mossy fibres onto hippocampal CA3 pyramidal cells, increasing the frequency of miniature glutamate mediated currents (Gray *et al.*, 1996; for a review see Wonnacott, 1997). Presynaptic α7 nAChRs have also been shown to selectively potentiate glutamate transmission mediated by NMDA receptors (implicated in synaptic plasticity and memory) in pyramidal cells of the rat prefrontal cortex and auditory cortex, between postnatal days 8 and 16 (Vidal & Changeux, 1993; Aramakis & Metherate, 1998; for a review see Jones *et al.*, 1999). Thus α7 nAChR may contribute to synaptic plasticity, mediated by NMDA receptors (Jones *et al.*, 1999).

In terms of effects on GABA release, presynaptic nAChRs (α7 and α/β heteromeric receptors) have been shown to increase GABA release from GABAergic interneurons in the hippocampus (Alkondon *et al.*, 1997; Alkondon *et al.*, 1999; Alkondon *et al.*, 2000; Zarei *et al.*, 1999).

In the developing rat hippocampus spontaneous network driven oscillatory events give rise to giant depolarising potentials (GDPs; Maggi *et al.*, 2001), which are thought to be important in promoting development of the hippocampus (Goodman & Shatz, 1993). GDPs are generated by a positive feedback system consisting of glutamate and GABA mediated excitation. Here glutamate released from pyramidal cells onto postsynaptic AMPA receptors on GABAergic interneurons depolarises the GABAergic interneurons and stimulates GABA release. GABA released from GABAergic interneurons is then thought to activate postsynaptic $GABA_A$ receptors on glutamatergic pyramidal cells, which in the developing hippocampus produce depolarising excitation (due the chloride

concentration gradient maintained by a developmentally expressed Cl importer, NKCC) and release further glutamate onto GABAergic interneurons (Rivera *et al.*, 1999; Maggi *et al.*, 2001). Glutamate is required for the generation of GDPs, as they are blocked by 20 μM DNQX (AMPA receptor antagonist; Maggi *et al.*, 2001). Maggi *et al.* (2001) reports that Nic produces a concentration dependent increase in GDP frequency, which is blocked by 50-100 μM DHβE and partially blocked by 50 nM MLA, suggesting that both α7 and α/β heteromeric receptors are involved. Maggi *et al.* (2001) propose that presynaptic nAChRs on GABAergic interneurons and glutamatergic pyramidal cells increase both GABA and glutamate release in the hippocampus, increasing the frequency of GDPs. Thus presynaptic nAChRs could be involved in promoting development within the hippocampus.

Neuronal nAChRs in the CNS have also been shown to be involved in cognition, since Nic enhances cognitive performance and loss of nAChRs is associated with ageing and Alzheimer's disease (AD). Patients with AD typically exhibit disruption of short-term memory and associative learning and are unable to recognise the names of familiar people or objects. It is thought that cholinergic pathways project from various basal ganglia to areas of the brain associated with learning and memory formation, namely the cerebral cortex, amygdala and the hippocampus. Post-mortem analysis of the brains of AD patients reveals substantial degeneration of these cholinergic pathways and a significant reduction in the levels of nAChRs throughout the brain, specifically in the hippocampus (for a review see Mihailescu & Drucker-Colin, 2000).

The data discussed above provides increasing evidence for the involvement of postsynaptic nAChRs in fast synaptic transmission in the CNS, although the subtypes and subunit composition of the receptors involved is complex. Given the widespread expression of mRNA for all the nAChR subunits it seems reasonable to assume that

neurons express multiple classes of nAChRs. Further, a proportion of these receptors has been shown to contain three or more different subunits, including β3. Thus it is important to characterise β3 containing receptors in expression systems in order to develop a pharmacological and biophysical 'finger print' for β3 if we are to determine its function in native receptors.

1.10. Aims of the research

The aim of this project is to investigate the molecular composition of neuronal nAChRs containing the related α5 or β3 subunits, with specific interest in the role of β3. A combination of electrophysiological and molecular biology techniques will be used. Knowing the subunit composition and stoichiometry of a receptor is important to our understanding of how the structure of the receptor determines its function and underlies the physiology of synaptic transmission for receptors that are synaptic. This information is also essential in order to express recombinant receptors that reproduce the properties of native receptors, a process of paramount importance in drug development.

What is the role of the β3 subunit in the assembly of neuronal nicotinic receptors ?

The first aim is to extend the reporter mutation approach to investigate the stoichiometry of the α3β4 pair and the α3β4β3 triplet:

Is the population of triplet receptors homogenous, or do the number of copies of β3 incorporated vary ?

If the stoichiometry of the triplet is constant, how many copies of β3 are present in the triplet ?

Does β3 replace an α or a β subunit ?

Does the related a5 subunit replace the same subunit type as β3 with the same copy number ?

If α5 replaces the same subunit type as β3 and the stoichiometry of the resulting triplet is unchanged, are a5 and β3 examples of a third class of subunits ?

The second aim is to investigate how the incorporation of β3 affects the properties of the α3β4 pair receptors:

Does β3 contribute to the formation of the agonist binding site ?

Does the presence of β3 change the receptor sensitivity to agonist and antagonists and/or the biophysical properties of the nAChR ?

If β3 incorporation does significantly affect the properties of the receptor, then we can move on to further investigation to discriminate β3 containing receptors from non-β3 containing receptors *in vivo*:

Do β3-containing receptors exist in native tissue ?

Do their properties resemble those of β3-containing recombinant receptors ?

Chapter 2: Materials and methods

2.1. Preparation of cRNA for oocyte expression

All cRNAs (wild-type and mutant) coding for the neuronal nAChR subunits used in this study were prepared, synthesised and sequenced by Dr. Paul Groot-Kormelink.

2.1.1. Plasmid cDNAs of the human neuronal nAChR α3, α5, β3, and β4 subunits

The human neuronal nAChR α3, α4, α5, β3, and β4 subunit cDNAs were a generous gift from the Janssen Research Foundation in Beerse, Belgium. All subunits had been isolated from the human neuroblastoma cell lines SH-SY5Y and/or IMR-32 by Dr. Paul Groot-Kormelink, using a 'nested PCR' approach (Groot-Kormelink & Luyten, 1997). The 'nested PCR' approach permits the selection of optimal primers for the first rounds of PCR to amplify a specific subunit from a cDNA pool. After amplification and purification of the desired fragment, the latter can then be used as a single template in the second round of PCR using less optimal 'nested' primers. These nested primers were designed in such a way that they would amplify the coding region only (from start to stop codon), resulting in cDNAs without any 5' or 3' untranslated regions (UTRs). Kakinuma *et al.* (1996) report that removing both 5' and 3' UTRs from thyroid stimulating hormone receptor (TSH) cDNA increases the cell surface expression of heterologously expressed TSH receptors by approximately 10 fold. Therefore, these regions were removed from the nAChR subunits in order to maximise receptor expression and to ensure that the subunits are transcribed with equal efficiency when co-expressed.

The protein translation was further increased by the addition of a general Kozak consensus sequence (GCCACC), introduced in the PCR primers, immediately upstream

of the start codon (Kozak, 1991). The Kozak consensus sequence is the consensus recognition site for the start of the translation of the protein by the ribosome complex. The GenBank accession numbers for the cDNA sequences used in this study are; α3, Y08418; α4, Y08421; α5, Y08419; β3, Y08417 and β4, Y08416 (Swiss-Prot accession numbers for the protein sequences are; α3, P32297; α4, P43681; α5, P30532; β3, Q05901 and β4, P30926). All cDNAs were provided in the pSP64T.GL vector, which contains 5' and 3' UTRs of the *Xenopus* β-globin gene (Akopian et al., 1996, see also figure 2.1.5.). *Xenopus* β-globin is a 'house keeping' gene, which is readily recognised by the ribosome and rapidly translated. Inserting the subunit coding sequence in-between these β-globin UTRs increases mRNA stability and improves translation, resulting in more than 1000 fold enhanced protein expression levels in *Xenopus* oocytes (personal communication, Dr. Paul Groot-Kormelink).

2.1.2. Creating the 9' mutants

Mutations were created using the QuickChange method (QuickChangeTM Site-Directed Mutagenesis Kit, Stratagene), courtesy of Dr. Paul Groot-Kormelink. Briefly, pairs of oligonucleotides (primers) complementary to the opposite strands of the subunit cDNA and bearing the desired mutation were designed. Primers were between 25 and 45 bases in length with a melting temperature (T_m) of approximately 78 °C.

The T_m values were calculated using the following equation:

$T_m = 81.5 + 0.41$ (% GC) - 675/N - % mismatch,

Where N is the primer length in base pairs, % GC is the % of sequence containing nucleotides G and C, % mismatch is the number of inserted nucleotides (mutation) divided by the length of the primer. i.e. Introducing two new nucleotides as the mutation and the primer length is 37 nucleotides. % mismatch is 2/37 x 100 % = 5.4 % (equation from QuickChangeTM Site-Directed Mutagenesis Kit, p4).

Primers were used in a PCR reaction directed to the pSP64T.GL vector containing the inserted subunit sequence of interest. The PCR reaction used *Pfu* DNA polymerase to extend the primers, producing nicked replicates of both strands of the parental plasmid bearing the desired mutation. Following PCR, the reaction mixture was treated with the restriction endonuclease *Dpn*I, which only digests methylated or hemi-methylated DNA. The parental plasmids (which were isolated from a methylating strain of E. coli) were susceptible to *Dpn*I digestion, whereas the PCR products were unmethylated and therefore unaffected by the endonuclease. Digestion thus eliminated the parental DNA and the remaining nicked vector DNA containing the desired mutation was subsequently transformed into E. coli and mutants were selected by sequencing over the mutation.

The cDNA sequence of the selected mutants were then fully verified on both strands to check for PCR artefacts. The following TM2 mutants (in the appropriate pSP64T.GL plasmid constructs) were used in this study; $\alpha3^{L279T}$, $\alpha5^{V290T}$, $\alpha5^{V290L}$, $\beta3^{V273T}$, $\beta3^{V273L}$, and $\beta4^{L272T}$ (for wild type sequences and corresponding position, see figure 2.1.4.). These mutants shall be referred to hereafter as $\alpha3^{L9'T}$, $\alpha5^{V9'T}$, $\alpha5^{V9'L}$, $\beta3^{V9'L}$, $\beta3^{V9'T}$, and $\beta4^{L9'T}$.

2.1.3. *In vitro* synthesis of subunit mRNA from cloned cDNA

All cDNA-containing pSP64T.GL plasmids were linearised by restriction enzyme digestion immediately downstream of the 3' untranslated β-globin sequence (in the available polylinker, see figure 2.1.5.), and subsequently the cRNA of mRNA polarity was transcribed with the SP6 mMESSAGE mMACHINE kit (Ambion). The mMESSAGE mMACHINE kit utilises the SP6 RNA polymerase (which specifically recognises the plasmid promoter sequence) to synthesise mRNA with a 7-methylguanosine cap at the 5' end. The 5' cap is required for the ribosome complex of the oocyte to bind to the mRNA and start translation.

The quality of the *in vitro* synthesised cRNA was checked by gel electrophoresis. The cRNA was considered to be of good quality if it produced a single band on the gel. The concentration of the *in vitro* synthesised cRNA was estimated by gel electrophoresis after staining with ethidium bromide (in order to visualise the cRNA under U.V. illumination) and comparison with RNA standards of comparable length and known concentration. Aliquots of different concentrations (10 ng, 40 ng, 100 ng, and 1 μg) for each cRNA were prepared in RNAse free water and stored at –80 °C. Before injecting the cRNA into oocytes, the cRNA aliquots were defrosted on ice and the desired subunit mixes were prepared and kept on ice until injection. Aliquots were used only once, never refrozen.

Figure 2.1.4. The 9' mutations

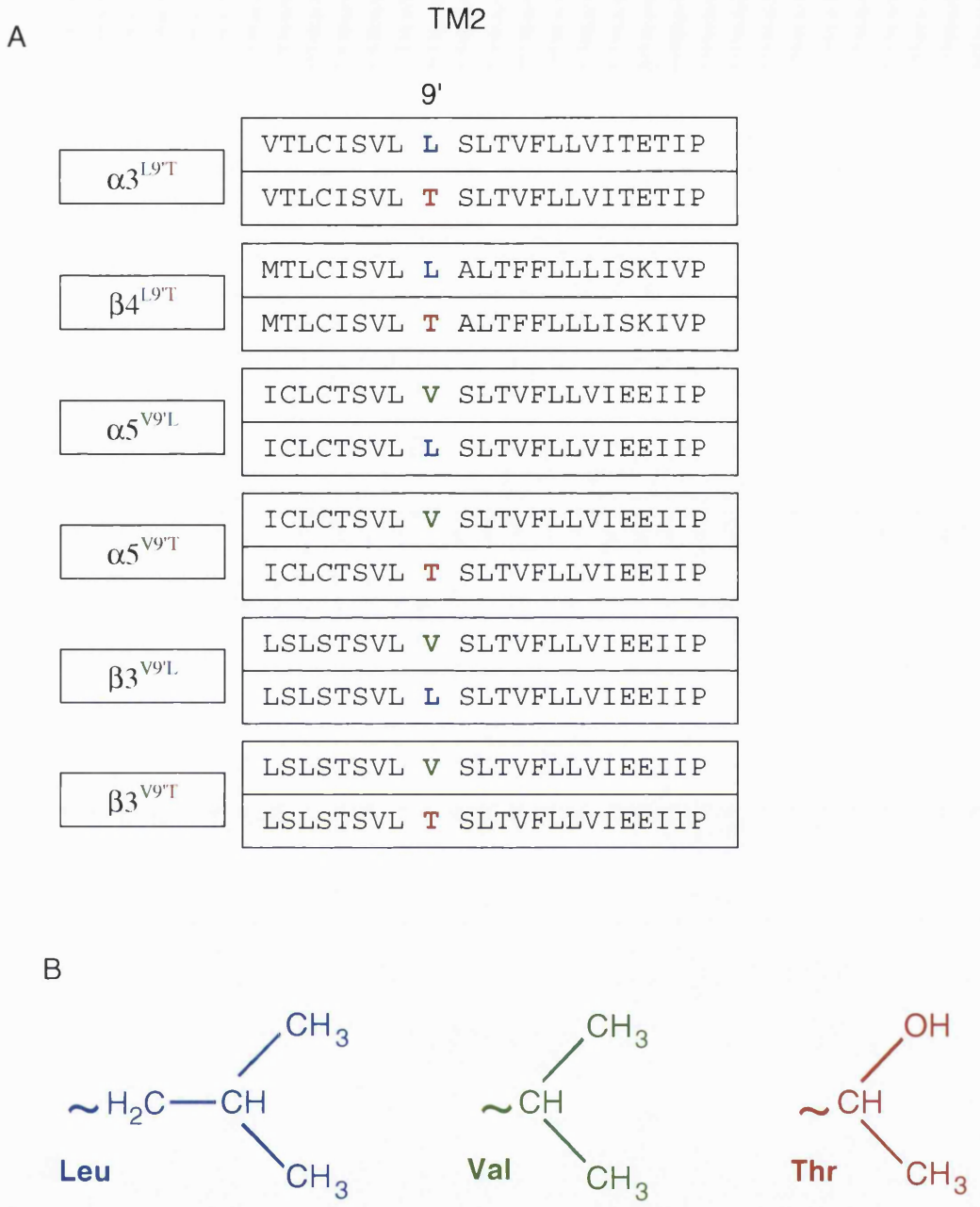

Figure 2.1.4. A, amino acid sequences of the second transmembrane domains (TM2) of the α3, α5, β3 and β4 subunits are shown. The wild type 9' residues are shown on the top row and the inserted 9' mutations on the bottom of each block. The 9' residues are labelled; V (valine); L (leucine) and T (threonine). B, amino acid side chains for the hydrophilic residues leucine (Leu) and valine (Val) and the hydrophobic residue threonine (Thr).

Figure 2.1.5. *In vitro* synthesis of subunit mRNA from cloned cDNA

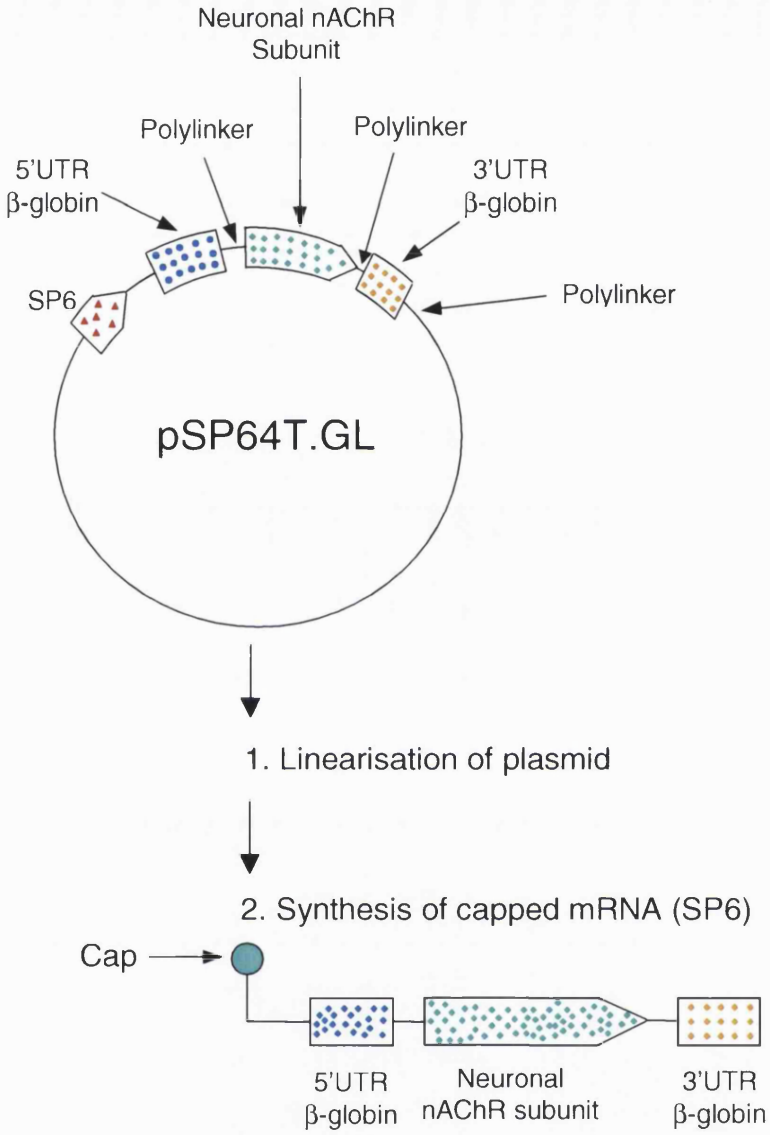

Figure 1.2.5. Shows a schematic diagram of the In *vitro* synthesis of subunit mRNA from cloned cDNA. The pSP64T.GL plasmid is indicated, with the SP6 promoter sequence (red dots) and the 5' (blues dots) and 3' UTRs (orange dots) of the *Xenopus* β-globin gene flanking the nAChR subunit insert (green dots). Step 1: the plasmid is linearised by restriction enzyme digestion in the polylinker immediately downstream of the 3' UTRs β-globin sequence. Step 2: the mRNA is synthesised using the SP6-mMESSAGE mMACHINE kit, resulting in capped mRNA, with the 5' and 3' β-globin UTRs flanking the neuronal nAChR subunit of interest.

2.2. The *Xenopus* oocyte expression system

Gurdon and co-workers first introduced the *Xenopus laevis* oocyte as a viable expression system for messenger RNA (mRNA) injected into the oocyte cytoplasm in 1971. When *Xenopus laevis* oocytes were injected with 9S mRNA coding for heterologous haemoglobin and incubated at 19°C, they rapidly and efficiently synthesised the haemoglobin protein (as revealed by radiolabelling with ^{3}H-histidine; see Gurdon *et al.*, 1971).

However, it was Sumikawa *et al* (1981) who first showed that *Xenopus laevis* oocytes could correctly assemble and express heterologous ion channels: using cat skeletal muscle mRNA, they obtained muscle nAChR. Boulter *et al.* (1987) were the first group to express a neuronal nAChR in the oocyte by injecting cRNA (rat $\alpha 3\beta 2$). Since these early experiments, the oocyte has become an established expression system used by many electrophysiologists to study various ion channels (Sigel, 1990). The *Xenopus* oocyte expression system was chosen for the present study because oocytes assemble nAChR efficiently and it is easy to control the proportion of subunits transfected for complex subunit combinations (for a review see Sivilotti *et al.*, 2000).

The *Xenopus laevis* oocyte is the precursor of the egg cell, which leaves the oviduct to become fertilised. Oocytes are stored in the ovaries in the abdominal cavity of the female *Xenopus*, from where they can be surgically removed for use in electrophysiological experiments (for a review see Smart and Krishek 1995). Oocytes are ideally suited for use in electrophysiological experiments due to their large size and ability to efficiently assemble and express exogenous proteins on their cell surface.

Because of its size, the oocyte is relatively resistant to damage by electrodes and can be injected individually with the genetic material coding for the receptor of choice.

2.2.1. *Xenopus* oocyte preparation

Female *Xenopus laevis* frogs (Blades, UK) were anaesthetised by immersion in neutralised ethyl m-aminobenzoate solution (tricaine, methanesulphonate salt; 0.2 % solution weight/volume; Sigma Chemical Co.), and killed by decapitation, followed by destruction of the brain and spinal cord (in accordance with Home Office guidelines) before removal of ovarian lobes. Clumps of approximately 300 cells freshly removed from the ovarian lobes were dissected in pre-incubation Barth's solution into groups of approximately 70 cells, discarding small immature cells that lacked well defined poles and uniform pigmentation. The dissected oocytes were gently shaken (Mini Orbital SO5, Stuart Scientific) in collagenase solution (245 collagen digestion units ml^{-1} in pre-incubation Barth's solution, 10-12 oocytes per ml; collagenase type IA, Sigma Chemical Co) for 65 minutes at 18 ±1° C ; repeatedly rinsed with fresh, syringe filtered Barth's solution (0.22 μm Millex GP; Millipore, Bedford, USA) and stored at 4° C overnight in sterile tissue culture dishes (Falcon, Becton Dickinson). Collagenase treated oocytes were then manually defolliculated in order to allow cRNA injection (watchmaker forceps, Precista No. 5; Excelta Corporation, Buellton, USA) and the largest cells with well defined poles and uniform pigmentation were chosen for cRNA injection.

2.2.2. nAChR injection and expression

The oocytes chosen for injection were placed on a nylon mesh (24 mm X 15 mm, with a 11 X 19 grid and each square of the grid measuring 1 mm X 1 mm, glued to a small Petri dish 37 mm in diameter) for support and immersed in pre-injection Barth's solution (see figure 2.2.2.a). Injection pipettes were pulled (Drummond glass # 3-000-203-G/X, pulled on List Medical L/M-3-PA) and broken to form a staggered tip of 12 – 16 μm (Narishige MF-830 micro forge). The staggered tip was then fire polished (Narishige MF-830 micro forge) and forged into the shape of a hypodermic needle, in order to minimise damage to the oocyte membrane. In order to reduce cRNA degradation by RNAses, cRNA for loading the injection pipettes was stored in ethanol washed and fire polished borosilicate glass (GC150-7.5; Clark Medical). Injection pipettes were backfilled with mineral oil (M-5904) and loaded from the tip with the appropriate cRNA, freshly defrosted from -80°C and centrifuged (to accumulate the solution at the bottom of the vial).

cRNA was then injected into the cytoplasm of the oocyte with a Drummond Nanoject (Drummond Instruments; see figure 2.2.2.a) and confirmed by a visible real time increase in the diameter of the oocyte ("plumping up"). Upon completion of the injection, the oocytes were rapidly transferred with a fire polished Pasteur pipette to individual wells in a multiwell plate (24 Multiwell, Falcon, Becton Dickinson), filled with syringe filtered post-injection Barth's solution (0.22 μm Millex GP; Millipore, Bedford, USA).

The ratio of α to β was 1:1 for α3β4. When expressing α3β4β3 or α3β4α5 receptors, a 1:1:20 ratio (α3:β4:β3/α5) was chosen to ensure that most of the current was carried by

triplet receptors (rather than by pair α3β4, Groot-Kormelink *et al.*, 1998). The amount of cRNA to be injected (in 46 nl of RNAse-free water) for each combination was determined empirically, with the aim of achieving a maximum ACh-evoked current of 1.5-2 μA. The maximum amount of cRNA injected for each combination is described in table 2.4.2.a.

The oocytes were then incubated for approximately 60 hours at 18° C (BDH cooled incubator; BDH). After incubation, oocytes were stored at 4° C until needed for recording. Experiments were carried out at a room temperature of 18-20° C between 2.5 and 14 days from injection.

Figure 2.2.2.a. The oocyte cRNA injection setup

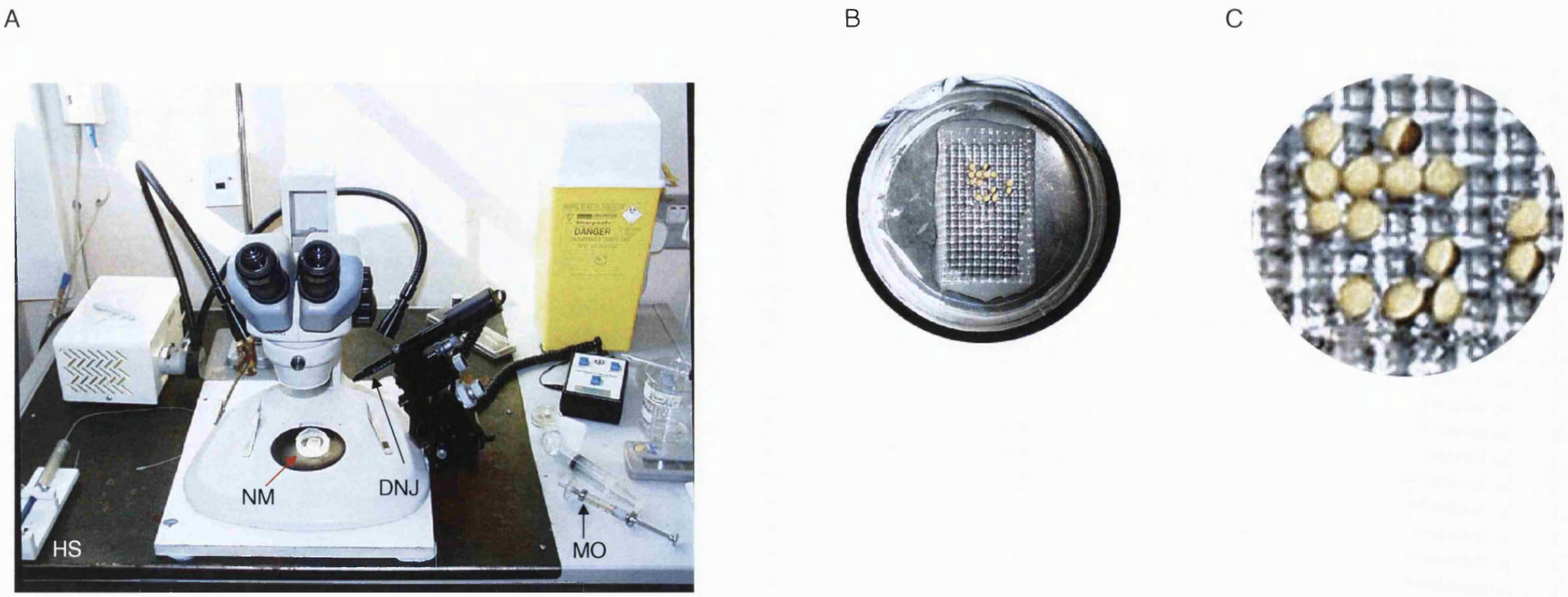

Figure 2.2.2.a. A shows the general set up for the cRNA injection of oocytes. HS = Hamilton syringe used for dispensing cRNA, DNJ = Drummond Nanoject, MO = syringe filled with mineral oil for backfilling injection pipettes, NM = nylon mesh for supporting oocytes. B shows the nylon mesh providing support for oocytes immersed in pre-injection Barth's solution, awaiting injection. C shows a magnified image of B.

2.3. Electrophysiological recording

Oocytes were firmly held in place by a square shaped 'cage' formed by 4 metal pins (approximately 0.5 mm in diameter and 6 mm in length) stuck in a layer of Sylgard® at the bottom of the chamber. The caged oocyte was protected from the outflow of the bath by a thin nylon mesh, forming a second compartment in the bath where both the bath ground Ag/AgCl pellet and the outflow suction were located (see figure 2.3.1). The bath had a volume of 0.2 ml (the full dimensions of the bath are shown in figure 2.3.1.) and oocytes were continuously superfused with the appropriate Ringer solution at 4.5 ml/min by a gravity fed system (see figure 2.3.2.). The bath level was kept constant by suction (Dymax 30 pump, Charles Austen Pumps, Surrey, UK). Cannulae with a 0.46 mm internal diameter were used for both application and removal of the superfusate (see figure 2.3.1). The end of the suction cannula was cut at an angle and positioned away from the bath walls in order to reduce excessive fluctuations in the bath volume during perfusion. Dedicated valves were used to switch the superfusion from the different Ringer solutions (T1) to various agonist/antagonist concentrations (T2; see figure 2.3.2.). The oocytes were voltage clamped at the chosen potential, using the two-electrode clamp mode of an Axoclamp-2B amplifier (Axon Instruments) and a gain of at least 10,000 V/V and a phase lag of 0.15 ms or better. Electrodes were pulled from Clark borosilicate glass GC150TF (Warner Instrument Corporation) and filled with 3 M KCl. The electrode resistances were 0.5 - 1 MΩ for ME_i and 1 – 3 MΩ for ME_v. Experiments were terminated if the total holding current exceeded 2 μA, in order to minimise series resistance errors (see clamp errors section).

Figure 2.3.1. The oocyte bath

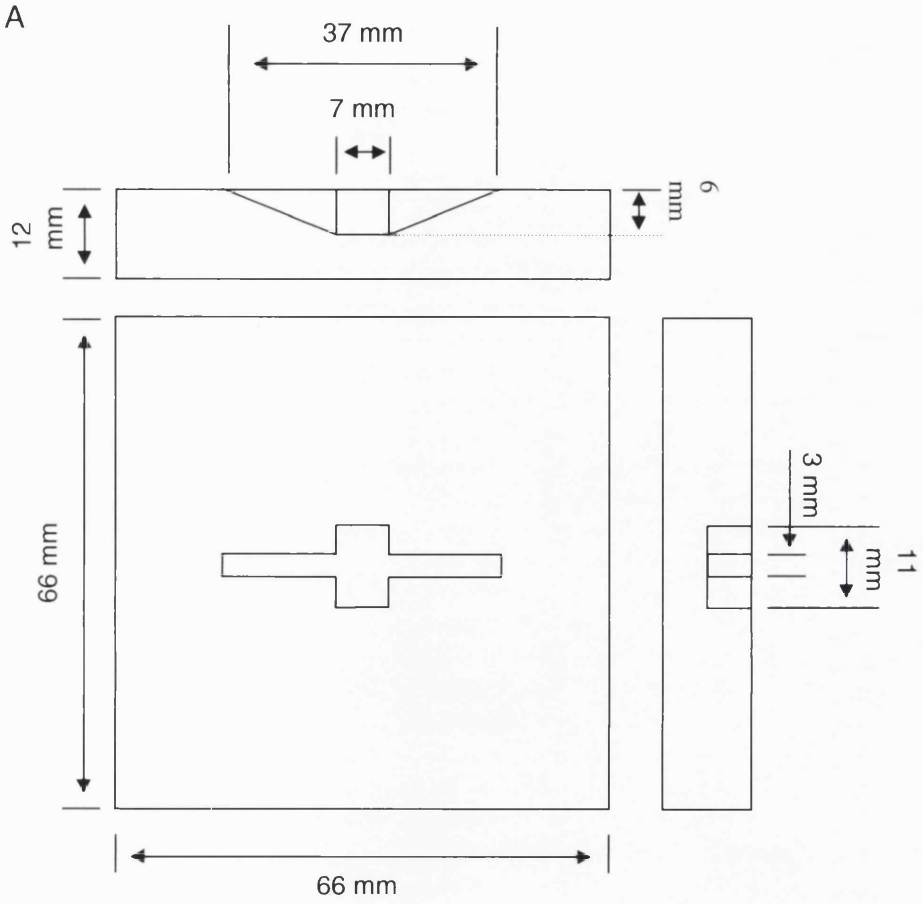

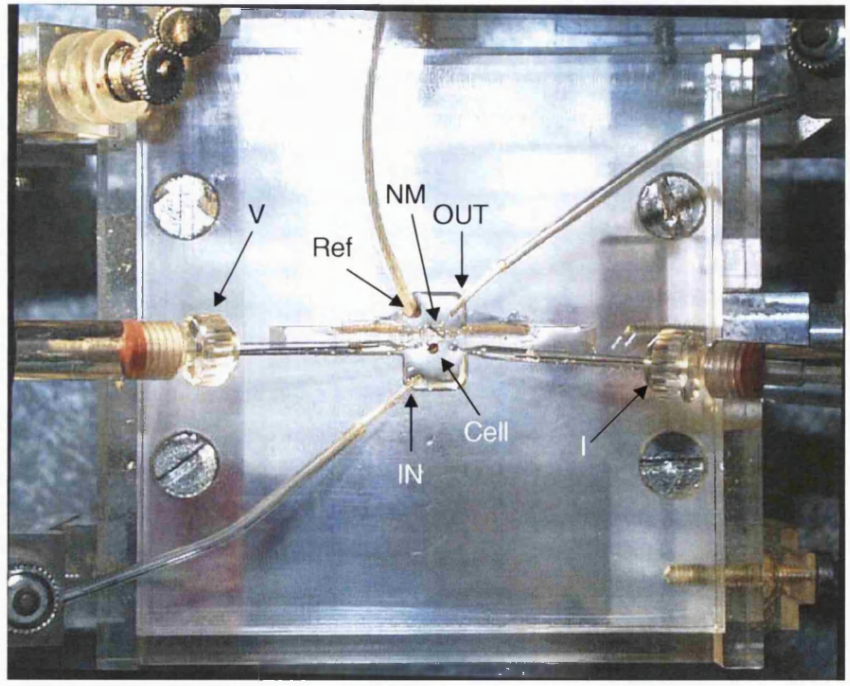

Figure 2.3.1. Shown are a schematic diagram of the oocyte bath used, with dimensions in mm (A) and a photo of the bath during recording (B). V = recording microelectrode, I = current injecting electrode, IN = the inflow for Ringer and agonist application, OUT = outflow of waste, Ref = the bath ground electrode, NM = thin nylon mesh, Cell = the oocyte.

Figure 2.3.2. The two electrode voltage clamp setup

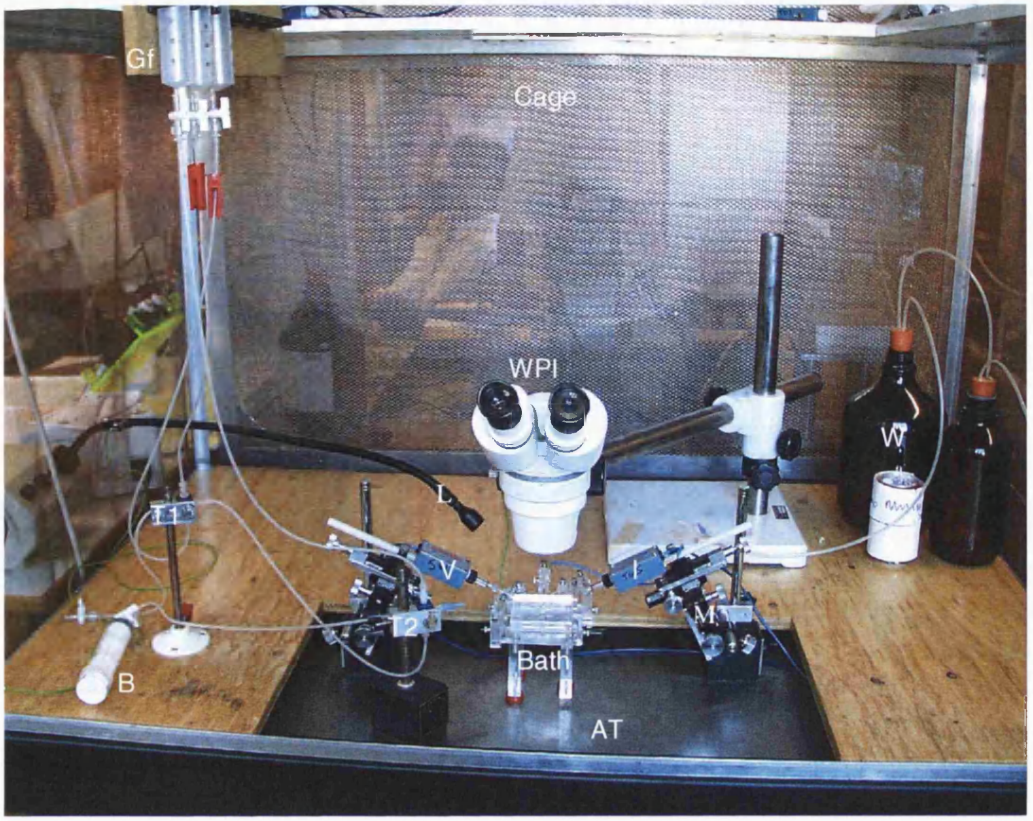

Figure 2.3.2. The bath is shown mounted on a Perspex base and attached to the vibration isolation table (AT) by magnets. The voltage recording (V) and current injecting (I) headstages are shown attached to the Narishige manipulators (M). Valve T1 was used for switching Ringer solutions and valve T2 for switching between Ringer and agonist / antagonist. The WPI dissection microscope is labelled and illuminated by the fibreoptic light (L), both were kept off the air table to reduce vibrations. B, is the bleed syringe for removing air bubbles from the gravity fed perfusion system (Gf), with the waste stored in W.

The agonist solutions (ACh chloride; carbamycholine chloride - CCh; cytisine - Cyt; 1-1-dimethyl-4-phenyl-piperazinium iodide - DMPP; +-epibatidine; +-lobeline hydrochloride; nicotine hydrogen tartate - Nic; Sigma Chemical Co.) were freshly prepared from aliquots of frozen stock solutions and applied via the bath perfusion. Application was continued for a period sufficient to obtain a stable plateau response (at low concentrations) or the beginning of a sag after a peak (at the higher concentrations); the resulting inward current was recorded on a flat bed chart recorder (Kipp & Zonen) for later analysis.

2.4. The voltage clamp

The voltage clamp technique relies on Ohm's law to measure the flow of ionic currents across the cell membrane.

Ohm's law: $V = IR$

Where V = potential difference or voltage, I = current and R = resistance

In a voltage clamp experiment the membrane potential (V_m) is kept constant (clamped) and set to a desired membrane potential (V_{cmd}) by the experimenter. The voltage clamp amplifier uses a negative feedback circuit to instantaneously inject current (I) into the cell, through a microelectrode of resistance R, and hold the membrane at the set potential (V_H).

2.4.1. Two electrode voltage clamp

The two-electrode voltage clamp (TEVC) technique is used to record large currents produced by multiple ion channels in whole cell recording, most commonly in the *Xenopus* oocyte expression system (see figure 2.4.1.a.).

Figure 2.4.1.a. The voltage clamp circuit

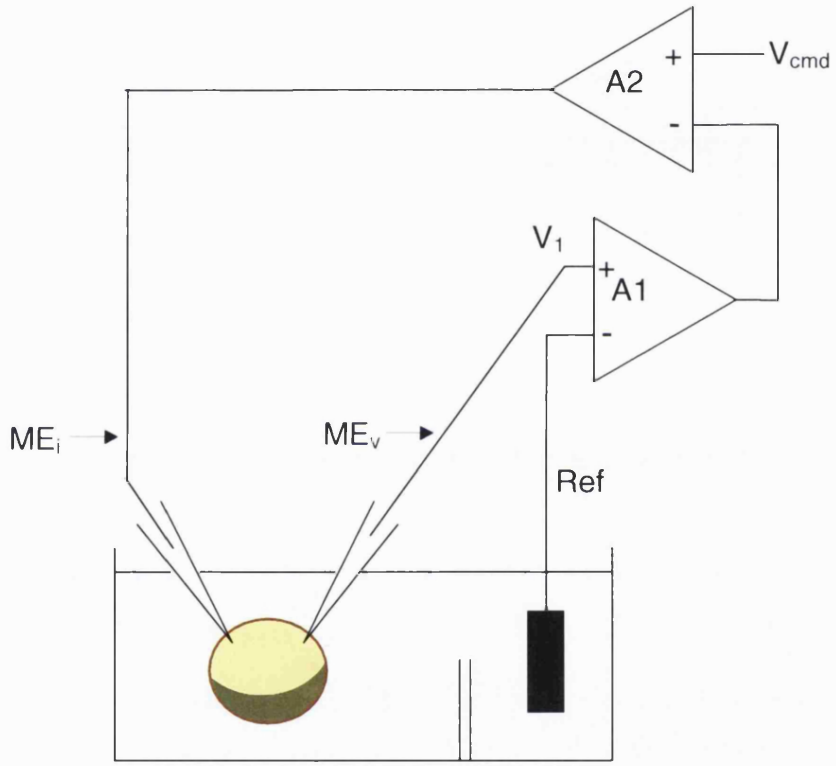

Figure 2.4.1.a. A graphical representation of the TEVC circuit. Where A1 represents the high impedance unity-gain preamplifier and A2, the high gain current injecting amplifier of the Axon voltage clamp amplifier; ME_v, recording electrode; ME_i current injecting electrode; ref, bath ground Ag/AgCl pellet; V_1, potential measured by ME_v; V_{cmd}, clamp command potential.

TEVC uses a fast, high gain current injecting amplifier (A2) to provide a negative feedback system to 'clamp' the cell membrane. The membrane potential (V_m) is measured by the recording electrode inserted in the membrane (ME_V of resistance R_V) and connected to the high impedance unity-gain preamplifier (A1) with respect to

ground (Ref). The high impedance of A1 ensures that the amplifier draws negligible current from the oocyte and that the potential reaching the input of A1 (V_1) is as close to V_m as possible. A1 then passes on this signal to A2 for comparison with the set holding potential (V_{cmd}). Any change in V_m, caused by the net flow of ions across the membrane through activated ion channels, triggers A2 to instantaneously inject current (I) into the cell through the current injecting electrode (ME_i of resistance R_i) inserted in another part of the membrane and clamp the membrane at V_{cmd}.

The efficiency of the clamp and the accuracy with which the amplifier reaches $V_m = V_{cmd}$ for a given ionic current (current flow through activated ion channels) depends on the gain on the amplifier and the access resistance (current injection electrode resistance + cytoplasmic resistance).

For a given ionic current:

$$V_m = V_{cmd}\frac{A}{1+A} - \frac{RaI}{I+A}$$

Where V_m is the membrane potential (mV), V_{cmd} is the clamp command potential set on the amplifier, A is the gain of the amplifier, R_a is the access resistance and *I* is the ionic current (equation from The Plymouth Workshop Handbook: Microelectrode Techniques. p19).

In order to increase the accuracy of the clamp we can increase the gain (A) of the amplifier; pull electrodes of lower resistance to reduce the access resistance (R_a) and reduce the expression of the ion channel to reduce the ionic current (*I*). However, the access resistance is not eliminated and there will still be an error (see clamp errors section).

The speed at which $V_m = V_{cmd}$ is reached will be affected by the membrane capacitance (C_m). When injecting current into the cell, the amplifier must first charge the membrane capacitance before $V_m = V_{cmd}$ with time constant τ (see equation 2.3.4.b.).

Equation 2.4.1.b. Time taken to charge the membrane capacitance

$$\tau = \frac{R_i C_m}{A}$$

Where τ = time constant, R_i = current injection electrode resistance, C_m = membrane capacitance and A is the amplifier gain (Axon guide p93).

Hence, charging time increases with membrane capacitance and electrode resistance and decreases with amplifier gain. Large cells like the *Xenopus* oocyte have large surface area and thus large membrane capacitance. This is important when trying to clamp fast voltage gated currents (which last for less than 10 ms), but in the case of ligand gated currents the exchange time (Ringer to agonist, greater than 500 ms) of the solution in the oocyte bath and at the receptors will exceed the charging time of the oocyte membrane and thus the value of τ becomes less significant.

For all experiments the clamp was tuned to allow a gain of at least 10,000 V/V, with a phase lag of 0.15 ms or better in order to avoid oscillation. Electrode resistances were recorded before each oocyte impalement and were typically 0.5 - 1 MΩ for the current injecting electrode and 0.5 – 2 MΩ for the voltage-recording electrode.

2.5. Clamp errors

The potential that we measure in practice is measured with a series resistance error. This is because current flows in a complete circuit, thus the reference electrode is used both for the measurement of V_m and for the return of the holding current (I_H) to the amplifier. Current that is being injected must return to the amplifier through everything that is in-between the oocyte and reference electrode input of the amplifier, passing through a series resistance (R_s see figure 2.5.2.). This R_s is the sum of the resistance of the bath (R_{bath}), the resistance of the reference electrode (R_{ref}) and the resistance of any agar bridge present (R_{agar} ; see equation 2.5.1.).

Equation 2.5.1. Series resistance

$$R_s = R_{bath} + R_{ref} + R_{agar}$$

R_s = the series resistance, R_{bath} = resistance of the bath, R_{ref} = resistance of the Ag/AgCl ground electrode, R_{agar} = resistance of the agar bridge.

As R_s is small, but finite, the current return will produce a potential across R_s, termed V_s. V_s contributes to the measured potential ε (see figure 2.5.2.), but is not present across the membrane of the oocyte, hence it is a source of error in the value of ε. Indeed ε is the sum of the 'true' V_m plus V_s, resulting in the oocyte being clamped at a potential that is different to the set V_{cmd} (see equation 2.5.3.). Furthermore, due to Ohm's law, the size of this error will increase as more current is passed (see equation 2.5.3.).

Figure 2.5.2. Series resistance in two-electrode voltage clamp

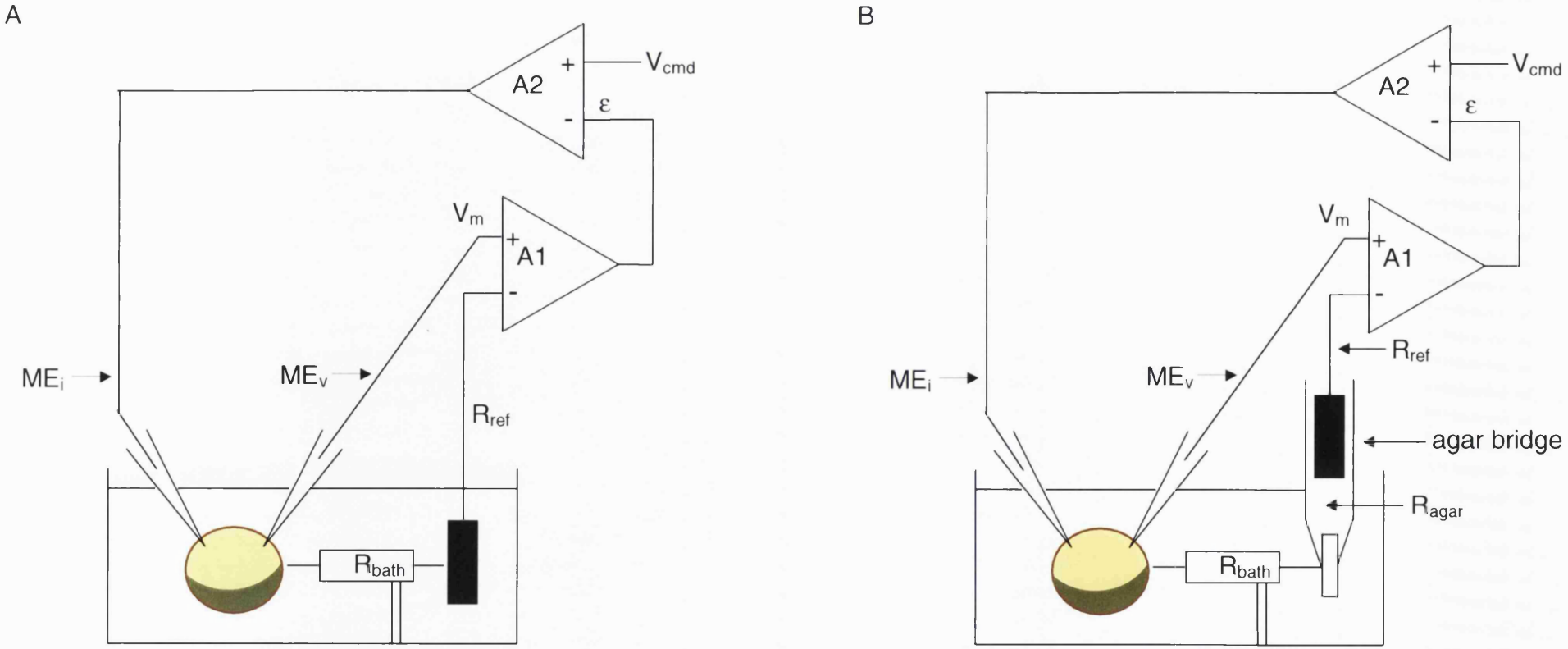

Figure 2.5.2. Shown are graphical representations of series resistance in a two-electrode voltage clamp circuit with (B) or without an agar bridge (A). A1 = the high impedance unity-gain preamplifier and A2, the high gain current injecting amplifier of the Axon voltage clamp amplifier; ME_v, recording electrode; ME_i current injecting electrode; ref, bath ground Ag/AgCl pellet; V_m, membrane potential; ε, measured membrane potential; V_{cmd}, clamp command potential.

Equation 2.5.3. The series resistance error

$$\varepsilon = V_m + V_s$$

and

$$V_s = IR_s$$

Where ε = the membrane potential reaching amplifier V2, V_m = the 'true' membrane potential and V_s = the potential of the series resistance, R_s = the series resistance and I = the current injected in order to maintain the clamp.

A typical value for R_{bath} for an oocyte in Ringer is 150-200 Ω (Axon guide p 39) and typical values for the resistance of the 1 mm diameter Ag/AgCl pellet (R_{ref}) are 300-600 Ω, with lower values of R_{ref} achieved when the whole of the pellet is submerged in the recording solution (Axon Guide, p39). Therefore, the value of R_s for our experiments without the agar bridge was at best 450 Ω and at worst 800 Ω.

In the current study, in all experiments without the agar bridge we aimed to keep total holding current below 2 μA. In practice, the maximum total current (response + holding current) recorded was 2.63 μA ($\alpha 3\beta 4^{L9'T}\alpha 5^{wt}$ see table 2.6.3.). The largest total currents were recorded in concentration-response curve experiments and they are reported in table 2.6.3.

Given the largest total current measured, we can calculate the degree of series resistance error produced by V_s in a worst case scenario (Rs = 1 $K\Omega$):

$$V_s = IR_s$$

$$V_s = 2.63 \times 1$$

$$= 2.63 \text{ mV}$$

Therefore, in a worse case scenario, the holding potential would be wrong by 2.63 mV. Assuming a reversal potential of 0 mV, this corresponds to 2.63/70 = 3.8 % error in the driving force, which is likely to be within the experimental variability for the data in the current study.

2.6. Estimating V_s in our experimental conditions

While the figure for V_s presented above is an estimate based on typical values of bath resistance, we obtained direct evidence that this estimate is reasonable and that we operated within the limits in which current was correctly measured in a series of preliminary experiments using the α4β4 combination (the first clones available to us at the time). In order to do this, steady state responses to a single concentration of ACh were obtained at different holding potentials for two different receptor expression levels, in order to construct two current/voltage (I/V) curves with different maximum currents (see figure 2.6.2.). If our R_s is large, then we would expect to see a distortion in the I/V curve with the greatest maximum current.

Oocytes expressing α4β4 receptors (0.5, or 0.05 ng/46nl cRNA) were initially held at -70 mV and 5 μM ACh was applied at an interval of 5 minutes between applications, as

this was found to be sufficient to ensure reproducible steady state responses. Each application was obtained at a different holding potential, between –70 and –20 mV. In order to check and compensate for possible decreases in agonist sensitivity throughout the experiment (using the same method described in section 2.9.1.), a standard steady state response was recorded at –70 mV every second response. The experiment was started only after checking that this standard gave reproducible responses at –70 mV.

Because the I/V curves were obtained from separate oocytes expressing different levels of the receptor, the effect of response rundown on the recorded responses will differ between the experiments. For this reason I have chosen to use the compensated ACh response data for the I/V curves, in order to remove any distorting affect of the response rundown. Thus any distortion in the scaling of the two I/V curves would be caused by V_s.

Comparing the I/V curve for α4β4 0.05ng/46nl with α4β4 0.5ng/46nl revealed that the shape of the I/V curve was unchanged (see table 2.6.1. and figure 2.6.2.).

Table 2.6.1. Summary I/V data for low and high α4β4 receptor expression

	Low expression 0.05 ng		High expression 0.5 ng	
	-50 mV	-70 mV	-50 mV	-70 mV
ACh Response (nA)	192	490	480	1175
Holding current (nA)	131	130	70	85
Total current (nA)	**323**	**620**	**550**	**1260**
Compensated ACh response (nA)	203	490	481	1175

Table 2.6.1. ACh response = the response (nA) elicited by bath application of ACh. Holding current = holding current before ACh application. Total current = the sum of the holding current and the ACh response. The compensated ACh response = the calculated ACh response after compensation for rundown.

Figure 2.6.2. Measuring the series resistance error

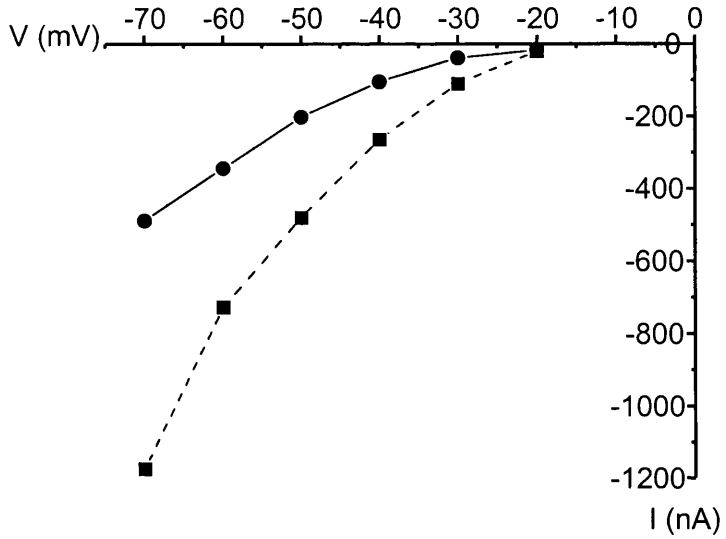

Figure 2.6.2. Shown are the I/V plots for α4β4 0.05 ng/46 nl (●) and α4β4 0.5 ng/46 nl (■). Note the lack of distortion in the scaling of the I/V curves at –70 mV.

Because we are only changing the expression level of the receptor (and thus the total current), if we had no significant error produced by our value of V_s, then we should be able to directly scale the two I/V curves.

We can now calculate the scaling factor between α4β4 0.5ng/46nl and α4β4 0.05 ng/46nl at –50 mV from the compensated ACh response:

$$\text{Scale factor} = \frac{481}{203}$$

$$= 2.37$$

Thus at –70 mV α4β4 0.5 ng/46 nl should produce a maximum current of:

$$490 \times 2.37 = 1161 \text{ nA}$$

Compared to the actual value of 1175 nA. If we assume that all of the very small discrepancy was caused by Vs, then the amount of error produced would be:

$$\left(\frac{1175-1161.3}{1161.3}\right)\times 100$$

= 1.18 % error at a maximum total current of 1.26 μA.

This corresponds to 70*0.0118 = 0.83 mV error in the driving force.

Given Ohm's law, we can now calculate our value of R_s :

$$R_s = \frac{V_{error}}{I_{total}}$$

$$R_s = \frac{0.83}{1.26}$$

$$R_s = 0.66\ \text{K}\Omega$$

Where I_{total} = The agonist induced current + the holding current

Which shows that we are well within the R_s estimate of 1 KΩ.

Table 2.6.3. Summary of maximum current passed for all concentration response curves

	Max total current (nA)	*Max error due to V_s (%)*	*Mean total current (nA)*	I_H (nA)	*No. of batches*	*n*	*cRNA injected* (ng)
$\alpha3\beta4$	2095	2.0 %	1014 ± 173	184 ± 57	2	7	0.5 - 1
$\alpha3^{L9'T}\beta4$	945	0.9 %	802 ± 44	85 ± 29	2	6	0.5
$\alpha3\beta4^{L9'T}$	1890	1.8 %	813 ± 386	200 ± 83	2	4	0.25 – 0.5
$\alpha3\beta4\beta3^{wt}$	930	0.9 %	755 ± 115	300 ± 83	2	6	0.1 - 10
$\alpha3\beta4\beta3^{V9'L}$	508	0.5 %	411 ± 64	230 ± 63	2	4	1 - 5
$\alpha3\beta4\beta3^{V9'T}$	1200	1.1 %	695 ± 87	175 ± 24	4	10	0.1 - 5
$\alpha3^{L9'T}\beta4\beta3^{V9'L}$	1650	1.6 %	1144 ± 182	148 ± 56	3	4	1
$\alpha3\beta4^{L9'T}\beta3^{V9'L}$	1340	1.3 %	1084 ± 162	90 ± 16	3	4	1 - 5
$\alpha3^{L9'T}\beta4\beta3^{V9'T}$	1815	1.7 %	1674 ± 78	80 ± 20	2	4	5
$\alpha3\beta4^{L9'T}\beta3^{V9'T}$	1425	1.3 %	1016 ± 145	83 ± 23	2	4	10
$\alpha3\beta4\alpha5^{wt}$	840	0.8 %	631 ± 91	126 ± 33	2	5	5 - 10
$\alpha3\beta4\alpha5^{V9'L}$	1720	1.6 %	901 ± 217	96 ± 31	3	5	5 – 10
$\alpha3\beta4\alpha5^{V9'T}$	865	0.8 %	647 ± 40	74 ± 19	4	7	1 - 5
$\alpha3^{L9'T}\beta4\alpha5^{wt}$	1095	1.0 %	968 ± 88	68 ± 17	2	4	1
$\alpha3^{L9'T}\beta4\alpha5^{V9'L}$	713	0.7 %	661 ± 32	185 ± 75	3	4	1
$\alpha3\beta4^{L9'T}\alpha5^{wt}$	2628	2.5 %	1761 ± 328	68 ± 39	3	6	0.5
$\alpha3\beta4^{L9'T}\alpha5^{V9'L}$	1060	1.0 %	686 ± 105	76 ± 23	4	5	0.5

Table 2.6.1. Maximum total current = the sum of the holding current and the maximum response. Max error due to V_s = the % of error in the driving force produced by V_s when the maximum total current was passed at –70 mV, where R_s = 0.66 KΩ. Mean total current = mean (± S.D of the mean) of the total current. IH = the mean (± SD of the mean) initial holding current at the start of the experiment.

2.7. The problem of Vs with an agar bridge

For all calcium permeability data (discussed below) an agar bridge was used to connect the bath ground to the amplifier. A typical value for R_{agar} for an agar bridge 1 mm in diameter and 10 mm in length, filled with 3 M KCl, is 510 Ω (Axon guide p 39) and 130 Ω for an agar bridge 2 mm in diameter and 10 mm in length. Our agar bridge consisted of two parts (see below). First the capillary tube, 1.17 mm in diameter and approximately 75 mm in length. Second, part of the syringe filled with agar, 5 mm in diameter and 18 mm in length.

Thus in a worse case scenario, the value of R_{agar} for our agar bridge was:

$R_{agar} = 510 \times 7.5 + 130 \text{ x } 1.8$

$= 4059\ \Omega$

$= 4\text{K}\ \Omega$

If we add this to our measured value of R_{bath}:

$R_{bath'} = 0.66 + 4$

$= <5\text{K}\ \Omega$

For all calcium permeability data, the maximum total current recorded was 522 nA at a holding potential of –40 mV (see chapter 6). Thus in the worst case scenario the series resistance errors produced by V_s when the agar bridge was used, were:

$V_s = 0.52 \times 5$

$= 2.6$ mV

Therefore, in a worse case scenario, the holding potential would be wrong by 2.6 mV. However, for the I/V curve experiments we were only interested in the value of the reversal potential, where current injection is zero. Hence our data would not be affected by the large value of R_s.

2.8. Experimental design

2.8.1 Solutions

2.8.1.a. Oocyte Ringer

All oocyte Ringer was prepared in water stored only in glass containers (as opposed to plastic containers) in order to avoid contamination from plasticisers, which have been shown to inhibit nAChRs (Papke *et al.*, 1994). Atropine (0.5 μM) was added to all oocyte Ringer in order to block mAChRs endogenous to the oocyte and prevent their contribution to the recording (for an example, see Davidson *et al.*, 1991).

Data for full and partial concentration-response curves and negative controls were obtained using nominally calcium-free Ringer solution, chosen in order to minimise the contribution of Ca^{2+}-gated chloride conductance. This conductance is endogenous to the *Xenopus* oocyte and may be activated by Ca^{2+} entry through neuronal nAChRs (see for an example Sands *et al.*, 1993). The calcium-free Ringer had the following composition (mM): NaCl 150, KCl 2.8, HEPES 10, $MgCl_2$ 2, 0.5 μM atropine sulphate; pH 7.2 adjusted with 5 M NaOH.

Data for all antagonist experiments were obtained in Ringer containing calcium (1 mM), as the presence of calcium was found empirically to reduce the holding current of the

oocyte and improve the rate of success of the experiments. As the Schild method is a null method, any distorting affect on the recorded response caused by the endogenous Ca^{2+}-gated chloride conductance would be negligible because the responses were matched. The calcium Ringer had the following composition (mM): NaCl 150, KCl 2.8, HEPES 10, $MgCl_2$ 2, $CaCl_2$ 1, 0.5 μM atropine sulphate; pH 7.2 adjusted with 5 M NaOH.

Data for calcium permeability experiments were obtained in chloride free, 1.8 and 18 mM calcium Ringer solutions, with osmolarity adjusted by using sucrose (based on solutions used by Gerzanich *et al.*, 1998), after oocytes had been depleted of chloride by incubation in chloride free solution (see below). Chloride free Ringer and low chloride electrode solutions were used in order to reduce the contribution of the calcium activated chloride current endogenous to the oocyte (activated by calcium entry through the nAChR) and improve the sensitivity of our method. All chloride free recordings were made using an agar bridge for the ground electrode (see below).

1.8 mM calcium Ringer, composition (mM): $Ca(OH)_2$ 1.8, NaOH 115, K-gluconate 2.5, HEPES 10, sucrose 35, 0.5 μM atropine bromide (osmolarity 263); pH 7.2 adjusted with methanesulphonic acid.

18 mM calcium Ringer, composition (mM): $Ca(OH)_2$ 18, NaOH 115, K-gluconate 2.5, HEPES 10, 0.5 μM atropine bromide (osmolarity 261); pH 7.2 adjusted with methanesulphonic acid.

Low chloride electrode solution, composition: K-acetate 2.5 M, KCl 10 mM (for the Ag/AgCl electrode).

2.8.1.b. Agonist and Antagonist solutions

All agonist and antagonist stock solutions were prepared in calcium-free Ringer, aliquoted out and frozen for future use (except Trimetaphan camsylate, kept at 4°C). For recording, agonist and antagonist solutions were freshly prepared from frozen stock aliquots in the appropriate recording solution and the thawed aliquot discarded at the end of the day.

2.8.1.c. Oocytes culture solution – Barth's

The Barth's solution had the following composition: NaCl 88; KCl 1; $MgCl_2$ 0.82; $CaCl_2$ 0.77; $NaHCO_3$ 2.4; Tris-HCl 15; with 50 U ml^{-1} penicillin and 50 mg ml^{-1} streptomycin; pH 7.4 adjusted with NaOH.

The Barth's solution was sterile filtered (0.2 μm Cyclopore, Whatman, UK) once before storage (4°C) and a second time before applying to the oocytes. The solution was discarded after 7 days and a fresh stock made for each oocyte batch. Initially all oocytes were cultured in Barth's solution until selected for recording.

A constant concern is the health of the cultured oocytes, as this affects the experimental yield. We found that the addition of 5 % horse serum to the Barth's solution after cRNA injection consistently decreased the initial holding current (I_H) when recording from treated oocytes (for data see table 2.8.1.c.i.). This decrease in holding current was seen to indicate an improvement in the health of the oocyte and increased the yield of data from treated cells in agreement with the findings of Quick *et al.* (1992).

During the course of three years of experiments that form the basis of this thesis it was found that the health of the *Xenopus* toads held at UCL had deteriorated. It was suggested that a concentration of zinc toxic to the *Xenopus* may be present in the water. Because very low concentrations of contaminants could be potentially detrimental to oocyte health, as an extra precaution I switched to using HPLC water (rather than using distilled water) for preparing the Barth's solution.

Table 2.8.1.c.i. Incubating in 5 % horse serum decreases the initial holding current of oocytes expressing neuronal nicotinic receptors

	Mean I_H (nA)	*n*	*n batches*	*p*
Barth's	-364.38 ± 81.32	16	2	
Barth's + 5 % Horse serum	-161.76 ± 31.89	17	2	0.03

Table 2.4.1.c.i. Where Mean IH = mean (± S.D. of mean) of the initial holding current at the start of each experiment recorded at –70 mV. *p* = result from a 2 tail *t*-test assuming unequal variance. Note the significant improvement in I_H for oocytes stored in Barth's + 5 % horse serum.

Pre-injection Barth's solution for oocyte collagenase treatment and peeling, had a composition of (mM): NaCl 88; KCl 1; $MgCl_2$ 0.82; $CaCl_2$ 0.77; $NaHCO_3$ 2.4; Tris-HCl 15; with 50 U ml^{-1} penicillin and 50 mg ml^{-1} streptomycin; pH 7.4 adjusted with NaOH.

Post-injection Barth's solution for oocyte incubation, had a composition of (in mM): NaCl 88; KCl 1; $MgCl_2$ 0.82; $CaCl_2$ 0.77; $NaHCO_3$ 2.4; Tris-HCl 15; with 50 U ml^{-1} penicillin and 50 mg ml^{-1} streptomycin, 5 % heat inactivated horse serum; pH 7.4 adjusted with NaOH.

For all recording conditions, oocytes were held in a 0.2 ml bath and continuously superfused with the appropriate Ringer solution at a rate of 4.5 ml min^{-1} using the apparatus described above. Agonist or agonist + antagonist solutions were applied via the bath perfusion for a period sufficient to obtain a stable plateau response (at low concentrations) or the beginning of a sag after a peak (at higher concentrations). The resulting peak inward current from each response was recorded on a flat bed chart recorder (Kipp & Zonen) for later analysis.

2.8.2. Concentration-response curves

The range of ACh concentrations to be applied in order to obtain a full concentration-response curve was determined empirically for each combination tested. Responses to agonist applications were plotted (after compensation for rundown) as the experiment progressed, in order to make sure that the maximum of the concentration-response curve was reached.

Oocytes were held at –70 mV and ACh was applied at 5 minute intervals, as this was found to be sufficient to ensure reproducible responses (except for $\alpha3\beta4\alpha5^{V9'L}$, for which a 10-minute interval had to be chosen to allow recovery from desensitisation). In order to check and compensate for possible decreases in agonist sensitivity throughout the experiment, a standard concentration of ACh (approximately EC_{20} for the particular combination used) was applied every third response. The experiment was started only after checking that this standard concentration gave reproducible responses.

2.8.3. Agonist potency ratios

Recombinant α3β4 and α3β4β3 receptors were characterised by testing their sensitivity to a range of agonists. This method was chosen to assess relative potency ratios for the agonists concerned and assess any differences between the 'pair' and 'triplet'.

Oocytes were held at –60 mV, in order to minimise agonist self block of the channel, and parallel partial concentration-response curves for each receptor combination (α3β4 and $\alpha3\beta4\beta3^{wt}$) were obtained for all agonists at low agonist concentrations (less than EC_{20}), in order to avoid agonist self block and minimise the contribution of the desensitised state. The range of agonist concentrations to be applied in order to obtain a partial concentration-response curve, parallel to a reference partial concentration-response curve of ACh, was determined empirically. Responses to agonist applications were plotted on a log/log scale (after compensation for rundown) as the experiment progressed, in order to make sure that the partial concentration-response curves were indeed parallel with the ACh curve and within the same range of response magnitude. As previously done for concentration response curves, a standard concentration of ACh (approximately EC_{20} for the particular combination used) was applied every third response, in order to check and compensate for possible decreases in agonist sensitivity throughout the experiment. The experiment was started only after checking that this standard concentration gave reproducible responses. An interval of 5 minutes was allowed between agonist applications, as this was found to be sufficient to ensure reproducible responses.

2.8.4. Schild experiments

Recombinant α3β4 and α3β4β3 receptors were further characterised by testing their sensitivity to a range of antagonists. This method was chosen in order to establish whether the antagonist tested acted competitively and to measure the equilibrium dissociation constant for comparing antagonists.

The experimental design is similar to that for agonist potency ratio measurements. For each receptor combination (α3β4 and $\alpha3\beta4\beta3^{wt}$) oocytes were held at –70 mV and reference parallel partial concentration-response curves were obtained for ACh at low concentrations (less than EC_{20}), to minimise the contribution of desensitisation and open channel block. The experiment was only started once this reference curve was found to be reproducible. Ringer containing the appropriate antagonist was then applied to the oocyte for a period determined empirically, in order to achieve equilibrium with the receptors (assessed by reaching a stable reduction in the ACh response). The range of agonist and antagonist concentrations to be co-applied in order to obtain a partial concentration-response curve, parallel to the reference ACh partial concentration-response curve, was determined empirically. Responses were plotted as the experiment progressed, in order to make sure that the partial concentration-response curves were parallel with the ACh curve and within the same range of response magnitude. Note that only one concentration of antagonist was tested in each oocyte in order to minimise any effects of rundown.

2.8.5. Calcium permeability experiments

As part of the characterisation of recombinant α3β4 and α3β4β3 receptors I carried out measurements of calcium permeability, by the reversal potential method in chloride depleted oocytes.

For all I/V ramps, due to the use of chloride free solutions, the bath ground AgCl pellet was connected to the bath via an agar bridge. The agar bridge consisted of a 1 ml syringe glued to a capillary tube (7.5 mm in length, 1.17 mm internal diameter, see figure 2.8.5.a). The tube and syringe were filled with approximately 300 µl (5 mm in diameter and 18 mm in length) of 5 % agar dissolved in 3 M KCl, interfacing with approximately 300 µl of 3 M KCl solution. The AgCl pellet was submerged in the 3 M KCl solution and connected to the bath ground input on ME_i. At the start of each recording day a fresh piece of agar, approximately 2 mm in length, was expelled from the syringe in order to allow the agar to make sufficient contact with the Ringer solution in the bath. The tip of the agar bridge was then immersed in 1 mM calcium Ringer (chloride free, see solutions) for approximately 30 mins, in order to produce a stable recording of the electrode tip potential. At the end of each day of recording, the agar bridge was removed and stored in 3 M KCl solution.

All oocytes were transferred from the Barth's solution to 1.8 mM calcium Ringer (chloride free, see solutions) for 24-30 hours prior to recording, in order to minimise free chloride inside the cell and minimise the calcium activated chloride current (activated by calcium entry through activated nAChRs) endogenous to the oocyte.

Oocytes were held at –40 mV and the holding potential was ramped from –40 to 40 mV (Axon Digidata 1320 interface and pClamp 8.1.) over a period of 2 seconds, recording the change in holding current in response to the voltage ramp. An initial delay of 50 ms before the start of each ramp allowed the holding current in the absence of the ramp to be recorded, marking the start of the experiment. A group of 4 ramps, with each ramp separated by 10 seconds, were used for each response. Leak currents were measured by applying control ramps before agonist application. ACh responses were obtained in 1.8 and 18 mM calcium Ringer (see solutions) and ramps were only initiated once the agonist response had reached a steady state plateu, in order to measure the effect of the ramp at a constant P_{open}. An interval of 10 minutes was allowed between ACh applications, as this was found to be sufficient to allow the desensitised receptor to recover and allow reproducible responses to be obtained. Responses were sampled at 2 KHz (Axon Digidata 1320), filtered at 500 Hz (CJC 8-pole Bessel filter) and stored on disk for later analysis.

Figure 2.8.5.a. The agar bridge

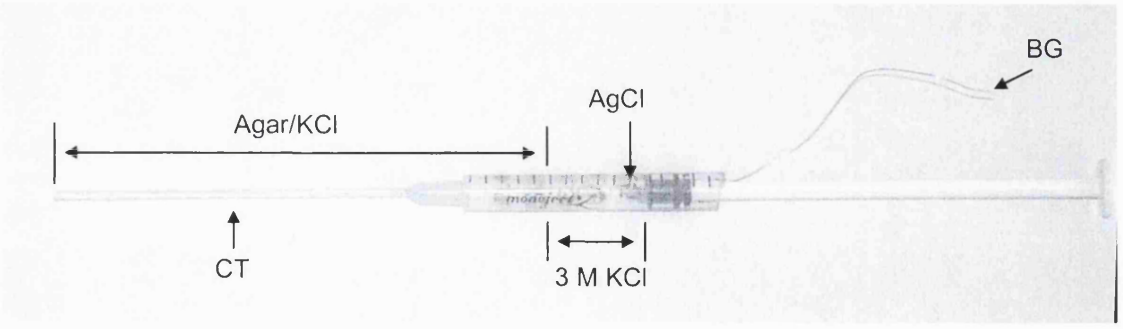

Figure 2.8.5.a. Shown above is the agar bridge constructed from a 1ml syringe, containing 5 % agar + 3 M KCl (Agar/KCl). The interface of the agar with the 3 M KCl containing the AgCl pellet (AgCl) is indicated. CT = The capillary tube filled with 5 % agar and BG = the bath ground connection (note this was later soldered and insulated before connecting to the ground input of the current injecting headstage via a 2 mm gold pin).

2.9. Data analysis

2.9.1. Full concentration-response curves

As described above, a standard concentration of ACh was applied at the start of the experiment and then re-applied every third response (1^{st}, 4^{th}, 7^{th}, 10^{th} application etc.), bracketing two ACh concentration-response curve data points. Because all the data points were bracketed by a known standard, the degree of rundown was assumed to be linear for the short period between standard applications and could thus be calculated and corrected for each data point.

First, the response of each application of the standard was recorded and the degree of reduction (if any) in response was calculated and expressed as a percentage of the initial standard in the form of a normalisation factor (see equation 2.5.1.a).

Equation 2.9.1.a. Response rundown calculation

3^{rd} standard normalisation factor $= 3^{rd}$ standard / 1^{st} standard

$= 90 / 100$

$= 90\ \%$

Next, the resulting normalisation factor for each standard was used to interpolate and correct for any response rundown in the ACh concentration-response curve data points bracketed by the standard (see equation 2.9.1.b.).

Equation 2.9.1.b. Rundown compensation and correction

$$X_{1'} = \frac{X_1}{S_1 - \left(\frac{S_1 - S_2}{3}\right)} \times 100$$

and

$$X_{2'} = \frac{X_2}{S_1 - 2\left(\frac{S_1 - S_2}{3}\right)} \times 100$$

Where $X_{1'}$ = Corrected ACh data point 1, X_1 = ACh data point 1, $X_{2'}$ = Corrected ACh data point 2, X_2 = ACh data point 2, S_1 = initial standard and S_2 = standard at the end of the bracket.

The resulting corrected ACh concentration-response curves data points were then fitted with the Hill equation.

$$I = I_{\max} \frac{[\mathrm{A}]^{n_H}}{[\mathrm{A}]^{n_H} + EC50^{n_H}},$$

Where I is the response, measured at its peak, [A] is the agonist concentration, I_{max} is the maximum response, EC_{50} is the agonist concentration for 50 % maximum response and n_H is the Hill coefficient. The Hill equation is an empirical description of the concentration-response curve.

Fitting was done in stages, as follows. Each concentration-response curve was fitted separately, individual responses being equally weighted, in order to obtain estimates for I_{max}, EC_{50} and n_H. These separate estimates were used to calculate the means and standard deviation of the means (see the results section).

Each response in a particular oocyte was then normalised to the fitted I_{max} for that experiment; all the normalised responses for a given combination were then pooled.

The pooled normalised data points were then fitted again with the Hill equation (with weight given by the reciprocal of their variance), in order to obtain the curves displayed in chapters 3, 4 and 5. These pooled fits were done for display purposes and to obtain fits under the constraint of parallelism when we needed to estimate the horizontal distance between the concentration response curves. In any case estimates of EC_{50} and slope from the pooled and separate fits agreed well. For instance, the constrained fits to the normalised pooled experiments were used to estimate the horizontal distance between the concentration-response curves (*i.e.* the potency ratio) obtained from receptors carrying different 9' mutations (see chapter 3 and 4). Potency ratios were expressed relative to either triplet or pair receptors which had only Leu in 9' (which therefore had potency ratios of 1). These constrained fits allowed the estimate of 2.01-unit likelihood intervals for the potency ratios (or the EC_{50} for the two reference combinations, $\alpha3\beta4$ and $\alpha3\beta4\beta3^{V9'L}$): these correspond to 95 % confidence limits (± 2 standard deviations) for a normally-distributed variable (Colquhoun & Sigworth 1995), but have the advantage of being robust to distribution assumptions.

Least squares fitting was used for both partial and full concentration-response curves by the program CVFIT, courtesy of D. Colquhoun and I. Vais, available from http://www.ucl.ac.uk/Pharmacology/dc.html.

2.9.2. Potency ratios for agonists and Schild experiments with antagonists

All parallel partial concentration-response curves for the various agonist were compensated for rundown as described above for full concentration-response curves. The data were then plotted on a log/log scale (in order to produce linear plots) and fitted

with a power function. This derives from the Hill equation (see below) if we assume that the agonist concentration is far smaller than the EC_{50}.

The power function corresponds to a straight line in log-log co-ordinates and has the general form:

$$\log_{10}(I) = K + n_H \log_{10}[A]$$

Where I is the response, measured at its peak, [A] is the agonist concentration, K is a constant and n_H is the Hill coefficient. The two free parameters are n_H and K.

Partial concentration-response curves for the range of agonists (or for agonist in the presence of antagonist), used in each oocyte were fitted simultaneously with equal weighting and the constraint of equal Hill slopes in order to obtain estimates of the horizontal distance between the partial concentration-response curves (*i.e.* the potency ratios for agonists or dose ratio for antagonists).

Potency ratios for all agonists were expressed as fractions of ACh potency (relative potencies), assigning to ACh the standard potency of 1. In this notation, a potency ratio of less than 1 means the agonist is more potent than ACh.

In the case of antagonists, the fitted dose ratios obtained for all antagonist concentrations were then re-fitted to the Schild equation and the antagonist equilibrium constant (K_B) derived from the x axis intercept.

The Schild equation:

$$r - 1 = \frac{x_B}{K_B}$$

where r is the dose ratio, x_B is the antagonist concentration, and K_B is the equilibrium constant for antagonist binding (it is the only free parameter in this case, because the slope is unity in the Schild equation. i.e. it assumes that the antagonist is competitive).

The fitted relative potencies for each agonist, or the fitted K_B for each antagonist, were then compared between α3β4 and α3β4β3 receptors in a two-tailed *t*-test assuming unequal variance. The *t*-test assessed the significance of any difference between α3β4 and α3β4β3 receptors for a given agonist or antagonist, expressed as a p value. Here p values of 0.05 or less were taken to indicate a significant difference.

2.9.3. Permeability data

The sampled data for each group of 4 ramps was averaged using pClamp 8.1 in order to reduce the noise on the sampled recording. The noise is reduced by the square root of the number of records, thus the greater the number of records, the less significant the noise.

Averaged leak currents were then subtracted from ramps obtained during nAChR activation, allowing the measurement of agonist dependent currents. The resulting leak subtracted ramps were then imported into Origin 6 and used to construct current/voltage curves (I/V curves). The plotted I/V curves were then smoothed using a rolling average of 100 data points in order to aid the measurement of the reversal potential of each oocyte for later analysis.

The reversal potential for both 1.8 and 18 mM calcium conditions was measured as the holding potential at which the recorded current was equal to zero. The shift in reversal potential from 1.8 to 18 mM calcium was then measured and compared between $\alpha3\beta4$ and $\alpha3\beta4\beta3$ receptors in a two-tailed *t*-test assuming unequal variance. The *t*-test assessed the significance of any difference between $\alpha3\beta4$ and $\alpha3\beta4\beta3$ receptors in the change in reversal potential caused by the increase in external calcium, expressed as a *p* value. Here *p* values of 0.05 or less indicate a significant difference and values greater than 0.05 indicate no significant difference between the two receptors.

2.10. Computer software used

All text and figures have been produced using Adobe Photoshop 6, Microsoft Office 97 suite and Microcal Origin 6. All traces were scanned into Adobe Photoshop 6 using a Hewlett Packard 4200C USB scanner (set to 300 DPI and 1:1 scale), processed and stored in the JPEG format. All I/V ramps were generated and analysed in Pclamp 8.1 (Axon instruments).

Table 2.11. Table of materials

	Supplier
Acetylcholine chloride (ACh) Atropine methyl bromide & atropine sulphate Calcium hydroxide Carbamylcholine chloride (carbachol) Collagenase (Type IA), (-)-cytisine hydrochloride (Cys) Dihydro-beta erythroidine hydrobromide (DHβE) 1-1-dimethy-4-phenyl-piperazinium iodide (DMPP) (+)-Epibatidine hydrochloride (Epi) Ethyl m-aminobenzoate methanesulphonate salt (Tricaine) (-)-Lobeline hydrochloride (Lob) Mecamylamine hydrochloride Methansulphonic acid Mineral oil (M-5904) (-)-nicotine hydrogen tartrate (Nic) Potassium acetate and potassium gluconate (+)-tubocurarine chloride Trizma hydrochloride (Tris; SigmaUltra)	Sigma, UK.
Trimethaphan camsylate	Cambridge Laboratories Ltd, Wallsend, Tyne and Wear, UK
Calcium chloride HiPerSolv (HPLC water), Magnesium chloride N-2-hydroxyethylpiperazine-N-2-ethansulphonic acid (HEPES) Potassium chloride Sodium chloride, Sodium hydrogen carbonate and Sodium hydroxide Sucrose	BDH Laboratory Supplies, Poole, UK (analytical grade)
Heat inactivated horse serum Penicillin/Streptomycin (Pen/Strep)	Life Technologies Ltd, Paisley, UK
0.22 μm pore syringe filters (Millex GP)	Millipore, Bedford, USA.
Falcon sterile multiwells and dishes	Beckton Dickinson, NJ, USA
Clark borosilicate glass (GC150TF) for pulling electrodes Electrode holders (QSW-T15N) silver electrode wire and silver chloride bath ground pellets	Warner Instrument Corporation, Hamden, CT, USA

Table 2.12. Table of equipment

Axoclamp 2B HS–2A headstage (gain x 10 - current passing) and HS–2A headstage (gain x 1, recording)	Axon Instruments, Foster City, CA, USA
Hamilton 0.025 ml syringe used to displace RNA and the Hamilton 4-way (4-4) opposing valve, for switching the perfusion	Hamilton, Nevada, USA
50 ml monoject syringes, used in the perfusion	Tyco Healthcare, Gosport, UK
Capillary glass for pulling injection needles Drummond Nanoject system	Laser Lab Systems Ltd, UK
Single channel flat bed chart recorder	Kipp & Zonen, Lincoln, UK
List Medical L/M-3P-A electrode puller (used for pulling injection needles),	Darmstadt, Germany
Narishige MF- 830 microforge (used for polishing injection needles) Narishige MM-3 micromanipulators (use for recording) Narishige PC-10 Patch electrode puller (used for pulling recording electrodes	Narishige, Tokyo, Japan
Nikon SMZ645 Microscope for oocyte dissection and injection	Nikon, Tokyo, Japan
Tektronix TDS 210 oscilloscope,	Tektronix, OR, USA
Neurolog system	Digitimer, Hertfordshire, UK
Preamp 1 and 8 pole bessel filter	CJC electronics, London, UK
Dymax 30 pump,	Charles Austen Pumps, Surrey, UK
Gilson P20, P200 and P1000 micro pipettes	Gilson, Wisconsin, USA

Chapter 3: Stoichiometry of 'pair' α3β4 neuronai nicotinic acetylcholine receptors

As discussed in chapter 1, the stoichiometry of 'pair' neuronal nAChR is known to be 2 α : 3 β subunits (see for chick α4β2 receptors Anand *et al.*, 1991; Cooper *et al.*, 1991). The first aim of the project was to test if the reporter mutation approach (see chapter 1) could be used to study stoichiometry in neuronal nAChR. If the reporter mutation approach is to be an effective tool to analyse the stoichiometry of neuronal nAChR, the increase in receptor sensitivity to ACh must be independent of which subunit type carries it. Additionally, the effect of the 9' Thr mutations on agonist EC_{50} should be progressive, increasing with the mutation copy number in the assembled receptor complex. While data on muscle nAChRs make these assumptions broadly reasonable (Labarca et al., 1995; Filatov & White, 1995), they do not hold for $GABA_A$ receptors (Chang *et al.*, 1996; using serine mutations; see chapter 1). Because of this, I checked the validity of these experiments in a nAChR whose stoichiometry is known, before applying the method to the new 'triplet' nAChR. Thus the reporter mutation 9' Thr was introduced in either subunit of 'pair' α3β4 receptors.

The magnitude of the shift in the dose response curve produced by a hydrophilic 9' mutation depends on the nature of the mutation, being greater for a Leu to Ser than for a Leu to Thr mutation (Revah *et al.*, 1991; Chang & Weiss, 1998; Chang & Weiss, 1999). The Leu to Thr mutation was chosen as it has been previously shown by Groot-Kormelink *et al.* (1998) to produce a shift in the dose-response curve sufficient to demonstrate incorporation of β3.

3.1. Mutating either subunit of the α3β4 'pair' increases the receptor sensitivity to ACh

Full concentration response curves were obtained by bath-application of ACh to oocytes expressing 'pair' α3β4 wild type or mutant ($\alpha3^{L9'T}\beta4$ or $\alpha3\beta4^{L9'T}$) receptors, using the protocol described in chapter 2. The data were then fitted as described in chapter 2 to obtain the mean and standard error of the mean values for all the fitted parameters (EC_{50}, I_{max} and Hill slope), shown in panel D of figures 3.1.1-3.2.1.

$\alpha3\beta4^{wt}$ pair receptors had a mean EC_{50} of 180 ± 17 μM ACh and a mean n_H of 1.81 ± 0.09 (n = 7), broadly in agreement with that reported in the literature for human α3β4 receptors expressed in *Xenopus* oocytes (in the range of 160 to 203 μM ACh; see Gerzanich *et al.*, 1995; Wang *et al.*, 1996; Chavez-Noriega *et al.*, 1997 and Groot-Kormelink *et al.*, 1998). $\alpha3^{L9'T}\beta4$ and $\alpha3\beta4^{L9'T}$ receptors had much lower mean EC_{50} values of 5.8 ± 1 and 0.75 ± 0.05 respectively. There was also a decrease in n_H (1.15 ± 0.08 and 0.92 ± 0.08 respectively; see table 3.2.4.). Note that in order to estimate the size of the shift in the EC_{50}, the data for the wildtype and mutant receptors were refitted with the constraint of a common Hill slope. The constrained fit allowed the estimate of the horizontal distance between concentration response curves, expressed as dose ratios (termed *r*) in relation to the wildtype (where wild type $r = 1$; see table 3.2.4.). For mutations that increase the receptor sensitivity to ACh, *r* is greater than 1, a decrease in sensitivity is indicated by *r* smaller than 1 (see figure 3.2.2. for a graphical description of how *r* is measured). The figures show the pooled fits, both with and without the constraint of parallelism. It can be seen that the distortion introduced by this constraint is not serious.

Figure 3.1.1. Reference α3β4 'pair' receptor concentration response curves

A

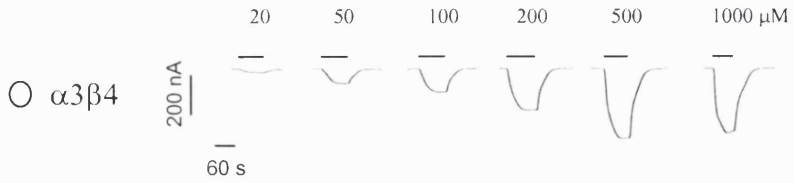

B

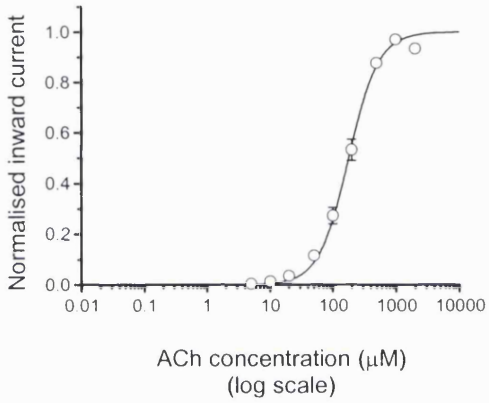

C

EC_{50} (μM)	I_{max} (nA)	n_H	I_H (nA)	*Rundown (%)*	*No. of batches*	*n*	*cRNA injected* (ng)
180 ± 17.0	1430 ± 425	1.81 ± 0.09	184 ± 57.2	25.4 ± 4.2	2	7	0.5 - 1

Figure 3.1.1. A shows examples of inward currents elicited by bath-applied ACh in oocytes expressing α3β4. B shows the ACh concentration-response curves pooled from experiments such as the ones shown in A: Pooled normalised results were fitted with the Hill equation as a free fit (O). C shows a summary of the fitted parameters: EC_{50}, I_{max} and n_H are the mean (± S.D. of mean) of parameter estimates obtained by fitting separately each concentration-response curve with a Hill equation. I_H is the mean (± S.D. of mean) holding current recorded at the start of the experiment. Rundown is the % (± S.D. of mean) of the response of the initial standard observed when the standard was applied at the end of the experiment. No. of batches are the number oocyte batches used. cRNA injected is the range of cRNA injected in order to produce acceptable expression levels for the experiments in A.

Figure 3.1.2. Mutating the α3 subunit of the α3β4 'pair' increases the receptor's sensitivity to ACh

A

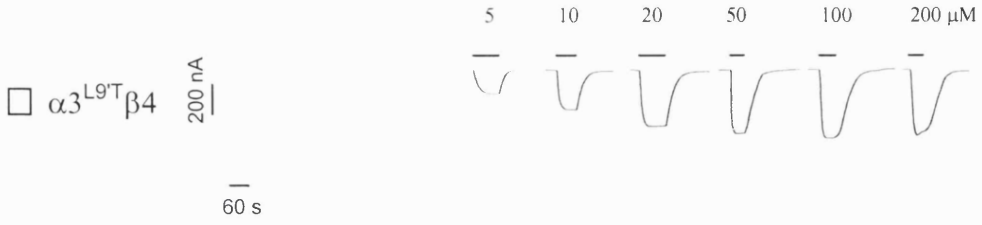

B

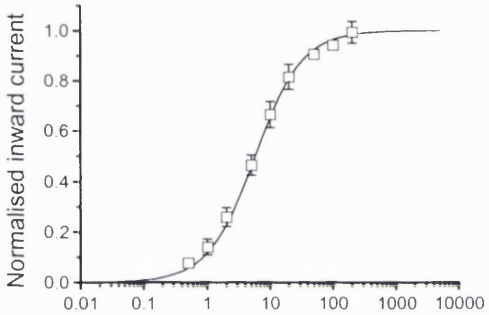

C

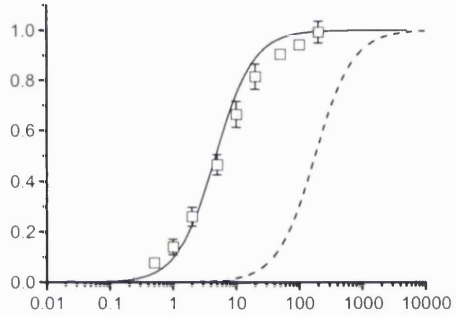

D

EC_{50} (μM)	I_{max} (nA)	n_H	I_H (nA)	*Rundown (%)*	*No. of batches*	*n*	*cRNA injected* (ng)
$\alpha3^{L9'T}\beta4$							
5.8 ± 1.0	1043 ± 411	1.15 ± 0.08	85 ± 28.7	54.7 ± 8.6	2	6	0.5

Figure 3.1.2. A shows examples of inward currents elicited by bath-applied ACh in oocytes expressing $\alpha3^{L9'T}\beta4$. B and C show ACh concentration-response curves pooled from experiments such as the ones shown in A. Pooled normalised results were fitted with the Hill equation either as free fit (panel B) or under the constraint of equal slopes (panel C), in order to estimate the horizontal distance between the curves as a dose-ratio. The concentration-response curves refer to oocytes injected with $\alpha3^{L9'T}\beta4$ (□). Panel C also shows for reference (dashed curve with no symbols) the concentration-response curve for $\alpha3\beta4^{wt}$. D shows a summary of the fitted parameters: EC_{50}, I_{max} and n_H are the mean (± S.D. of mean) of parameter estimates obtained by fitting separately each concentration-response curve with a Hill equation. I_H is the mean (± S.D. of mean) holding current recorded at the start of the experiment. Rundown is the % (± S.D. of mean) of the response of the initial standard observed when the standard was applied at the end of the experiment. No. of batches are the number of oocyte batches used. cRNA injected is the range of cRNA injected in order to produce acceptable expression levels for the experiments in A.

3.2. Mutating the β4 subunit is not equivalent to mutating the α3 subunit in α3β4 'pair' nAChRs

Inserting the 9'T mutation into the β4 subunit produced a greater increase in α3β4 'pair' receptor sensitivity to ACh than when the mutation was in the α3 subunit, shifting the EC_{50} to 0.75 ± 0.05 μM ACh (see table 3.2.4.). A summary of the responses, separate and constrained fits for wild type and mutant receptors are shown in figure 3.2.2.

Therefore, $\alpha3\beta4^{L9'T}$ receptors were approximately six-fold more sensitive to ACh than $\alpha3^{L9'T}\beta4$ receptors (r = 292, 95 % confidence intervals [267-318]; see table 3.2.4.), which in turn were 37-fold more sensitive than α3β4 receptors (r = 37.2 [31.2-44.6]; see table 3.2.4.). This is consistent with the receptor containing more copies of β4 than α3. It is attractive to hypothesise that there are three copies of β4 to two copies of α3 in the pentameric α3β4 receptor. These data also confirm the hypothesis that in neuronal nAChR the effect of the reporter mutation on the agonist EC_{50} is roughly independent of the subunit type and progressive, increasing with the mutation copy number, as Labarca *et al* (1995) showed for the muscle nAChR (see discussion).

If the effect of each hydrophobic to hydrophilic substitution in 9' is independent of position and multiplicative on the ACh EC_{50} (i.e. additive in terms of free energy), then plotting the logarithm of the ACh EC_{50} against the presumed number of mutations in each pentamer channel should yield a linear plot. Figure 3.2.5. shows that this is indeed the case for the α3β4 pair, which shows an approximately linear relation between log EC_{50} and the putative number of mutations in the receptor for up to 3 copies of the mutation. Note, there is a reduction in the Hill slope as we proceed from the α3β4 wild-type to $\alpha3^{L9'T}\beta4$ and to $\alpha3\beta4^{L9'T}$ (see figure 3.2.2).

Figure 3.2.1. Mutating the β4 subunit is not equivalent to mutating the α3 subunit in α3β4 'pair' nAChRs

A

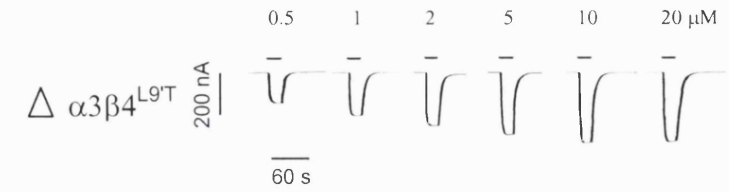

B

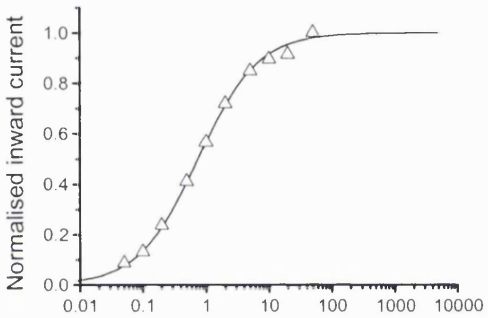

C

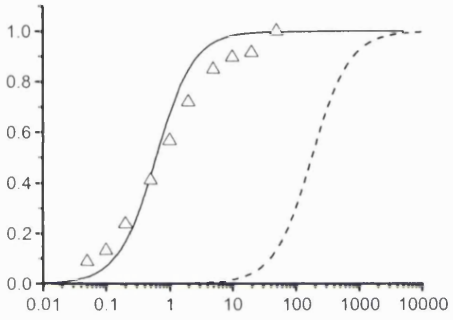

D

EC_{50} (μM)	I_{max} (nA)	n_H	I_H (nA)	*Rundown (%)*	*No. of batches*	*n*	*cRNA injected* (ng)
0.75 ± 0.05	562 ± 264	0.92 ± 0.08	200 ± 83	77.4 ± 9.5	2	4	0.25 – 0.5

Figure 3.2.1 A shows examples of inward currents elicited by bath-applied ACh in oocytes expressing $\alpha3\beta4^{L9'T}$. B and C show ACh concentration-response curves pooled from experiments such as the ones shown in A. Pooled normalised results were fitted with the Hill equation either as free fit (panel B) or under the constraint of equal slopes (panel C), in order to estimate the horizontal distance between the curves as a dose-ratio. The concentration-response curves refer to oocytes injected with $\alpha3\beta4^{L9'T}$ (Δ). Panel C also shows for reference (dashed curve with no symbols) the concentration-response curve for $\alpha3\beta4^{wt}$. D shows a summary of the fitted parameters: EC_{50}, I_{max} and n_H are the mean (± S.D. of mean) of parameter estimates obtained by fitting separately each concentration-response curve with a Hill equation. I_H is the mean (± S.D. of mean) holding current recorded at the start of the experiment. Rundown is the % (± S.D. of mean) of the response of the initial standard observed when the standard was applied at the end of the experiment. No. of batches are the number of oocyte batches used. cRNA injected is the range of cRNA injected in order to produce acceptable expression levels for the experiments in A.

Figure 3.2.2. Summary of the effect of the separate mutations in α or β in α3β4 receptors

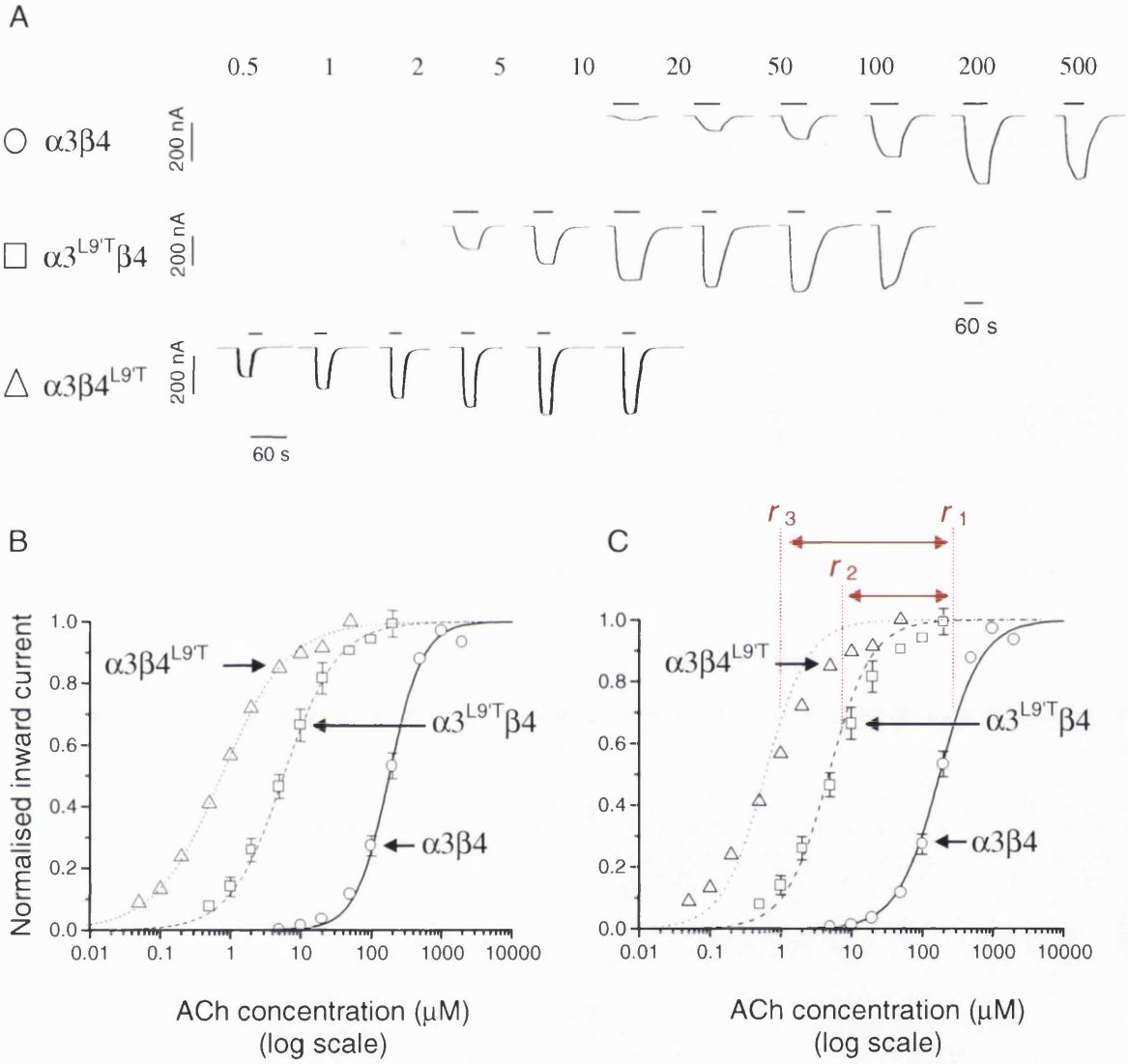

Figure 3.2.2. A, examples of inward currents elicited by bath-applied ACh in oocytes expressing α3β4, $\alpha3^{L9'T}\beta4$ or $\alpha3\beta4^{L9'T}$. B and C show ACh concentration-response curves pooled from experiments such as the ones shown in A (*n* = 4 - 7 oocytes). Pooled normalised results were fitted with the Hill equation either as free fit (panel B) or under the constraint of equal slopes (panel C) in order to estimate the horizontal distance between the curves as a dose-ratio, indicated by the red dotted lines; *r* 1 (dose ratio for α3β4); *r* 2 ($\alpha3^{L9'T}\beta4$); *r* 3 ($\alpha3\beta4^{L9'T}$); values of *r* are shown in table 3.2.4.). The concentration-response curves refer to oocytes injected with α3β4 (○), $\alpha3^{L9'T}\beta4$ (□) or $\alpha3\beta4^{L9'T}$ (△). Note that the greater increase in ACh sensitivity produced by mutating β4.

Table 3.2.3. Comparison of EC_{50} and Hill slope values from separate fits and pooled fits

	EC_{50} (μM)		n_H	
	Separate fit	Pooled fit	Separate fit	Pooled fit
$\alpha3\beta4^{wt}$	180 ± 17.0	172.4 ± 9.66	1.81 ± 0.09	1.62 ± 0.11
$\alpha3^{L9'T}\beta4$	5.8 ± 1.0 (p	5.36 ± 0.6 (p	1.15 ± 0.08 (p	1.08 ± 0.11 (p
$\alpha3\beta4^{L9'T}$	0.75 ± 0.05 (p	0.72 ± 0.05 (p	0.92 ± 0.08 (p	0.91 ± 0.05 (p

Table 3.2.3. A summary of the fitted data. For the separate fits: EC_{50} and n_H are the mean (± S.D. of mean) of parameter estimates obtained by fitting separately each concentration-response curve with a Hill equation. For the pooled fits: EC_{50} and n_H (± S.D. of mean) are parameter estimates obtained by fitting averaged normalised data points with the Hill equation with no constraints.

Table 3.2.4. Summary table for α3β4 wild type and mutant receptors

	EC_{50} (μM)	I_{max} (nA)	n_H	*dose ratios*	*square root of dose ratios*	*cube root of dose ratios*	*n*
$\alpha3\beta4^{wt}$	180 ± 17.0 [163.6-193.9]	1430 ± 425	1.81 ± 0.09	1			7
$\alpha3^{L9'T}\beta4$	5.8 ± 1.0	1043 ± 411	1.15 ± 0.08	37.3 [31.2-44.6]	6.11 [5.58-6.68]		6
$\alpha3\beta4^{L9'T}$	0.75 ± 0.05	562 ± 264	0.92 ± 0.08	292 [267-318]		6.63 [6.44-6.83]	4

Table 3.2.4. A summary of the fitted data: EC_{50}, I_{max} and n_H are the mean (± S.D. of mean) of parameter estimates obtained by fitting separately each concentration-response curve with a Hill equation. I_H is the mean (± S.D. of mean) holding current recorded at the start of the experiment. Dose ratios were estimated from fits in which curves were constrained to have the same slope (summarised in panel C of figure 3.2.2) for comparison with wild type α3β4 curves, in order to estimate the horizontal distance between the curves as a dose-ratio, where α3β4 = 1. The same parallel fits allowed estimation of 2.01-unit likelihood intervals (in square brackets under the means of the parameters they refer to; see Methods section): these are equivalent to 95 % confidence intervals.

Figure 3.2.5. Relation between ACh EC_{50} and putative number of Thr mutations

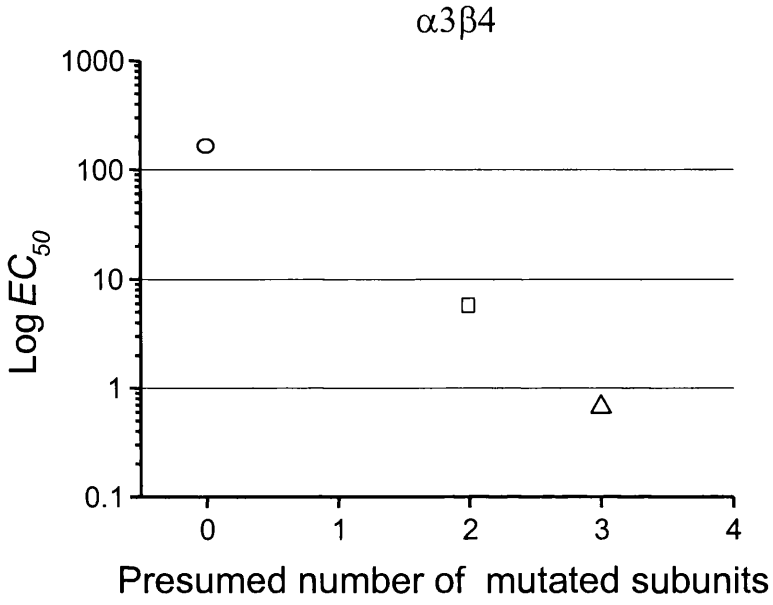

Figure 3.2.5. EC_{50} values for the various α3β4 Thr mutants are plotted on a log scale against the presumed number of mutated subunits in receptor complex. This number was calculated on the basis of a stoichiometry of 2:3 for α3β4. The symbols refer to α3β4 (○), $\alpha3^{L9'T}\beta4$ (□) and $\alpha3\beta4^{L9'T}$ (△). Note the approximate linearity of the decline in EC_{50} as the presumed mutation copy number increases.

3.3. Expression of single subunits

While it has been reported in the literature that injection of wildtype α3 or β4 alone does not form a functional nAChR, there is no evidence about $\alpha3^{L9'T}$ or $\beta4^{L9'T}$ mutants. Hence, I carried out a series of control experiments to show that injection of one subunit alone (wild-type or mutant, namely α3, $\alpha3^{L9'T}$, β4, $\beta4^{L9'T}$) did not result in the expression of functional nAChRs (*i.e.* current responses to 1 mM ACh were less than 1 nA; n = 5-7 subunit tested; total cRNA injected 10 ng). In non-injected oocytes responses to 1 mM ACh were also negligible (less than 1 nA, n = 5). These results are summarised in table 3.3.1.

Comparing the initial holding currents for wildtype and mutant single subunits in a two-tailed *t*-test assuming unequal variance, revealed a significant increase for mutated subunits. The mean initial holding current for α3 increased from 29 ± 5.4 nA to 208 ± 28.2 nA for $\alpha3^{L9'T}$ (*p* 0.003) and from 47 ± 6.8 nA for β4 to 187 ± 43.2 nA for $\beta4^{L9'T}$ (*p* 0.03; see table 3.3.1.).

Table 3.3.1. Single subunits do not produce functional nAChRs

	Mean I_H	Mean Response to 1 mM ACh (nA)	batches	N
α3	29 ± 5.4	<1	2	5
$\alpha3^{L9'T}$	208 ± 28.2 **(*p* 0.003)**	<1	3	5
β4	47 ± 6.8	<1	3	7
$\beta4^{L9'T}$	187 ± 43.2 **(*p* 0.03)**	<1	4	5

Table 3.3.1. Mean I_H = Mean initial holding current (± S.D. of the mean) at the start of the experiment. Where *p* is the result of a 2 tailed *t*-test assuming unequal variance, comparing the change in holding current produced by the 9' mutation. Here *p* values of 0.05 or less were taken to indicate a significant difference. Note that the holding current in both mutant subunits is significantly different from the respective wild type subunits.

3.4. Discussion

3.4.1. Assumptions of the reporter mutation approach

The data described above show that the main effect of introducing the 9'T mutation in α3 or β4 in α3β4 pair receptors is a shift towards higher agonist potency. This shift appears to be almost parallel. When α3 is mutated the EC_{50} is shifted by approximately 37-fold compared to 292-fold when β4 is mutated. These results are what would be

predicted by a stoichiometry of 2 α : 3 β and confirm that the reporter mutation method can be used in neuronal nAChRs.

From the data presented above, we propose that the shift in the ACh dose response curve produced by introducing the L9'T mutation in either the α3 or the β4 subunit in 'pair' α3β4 receptors, are in agreement with a stoichiometry of 2 α : 3 β. This stoichiometry has been thought to hold for 'pair' nAChRs since the work of Anand *et al.* (1991) and Cooper *et al.* (1991) in chick α4β2 'pair' receptors.

Anand *et al.* (1991) determined a 2 α : 3 β stoichiometry for chick α4β2 receptors on the basis of the ratio of the radioactivity produced by each subunit in ^{35}S-methionine-labelled receptors. Briefly, oocytes injected with chick α4β2 RNA were incubated in ^{35}S-methionine rich media and the resulting assembled receptors were solubilised and affinity purified on a bromoacetylcholine column. The bound assembled receptors were then eluted and sedimented on a 5-20 % sucrose gradient and fractionated on the basis of radioactivity by liquid scintillation counting. The resulting two peak fractions of assembled receptors were then further affinity purified, fractionated by SDS-gel electrophoresis into α4 and β2 bands and assayed for radioactivity by liquid scintillation counting. The results of the assay revealed a β/α ratio of 1.46, in good agreement with a stoichiometry of 2 α : 3 β.

Cooper *et al.* (1991) assessed the stoichiometry of chick α4β2 receptors expressed in *Xenopus* oocytes on the basis of the single channel conductance of wild type and TM2 20' mutant receptors. As discussed in chapter 1, increasing the net negative charge of the extracellular 20' ring increases single channel conductance, whereas decreasing the net negative charge decreases it. Cooper *et al.* (1991) mutated the negatively charged α4

20' glutamate (E) residue to a positively charged lysine (K, $\alpha4^{20'K}$) and the positively charged β2 20'K to a negatively charged E ($\beta2^{20'E}$). Thus receptors that incorporate $\alpha4^{20'K}$ will demonstrate a reduced single channel conductance compared to the wild type, whereas receptors that incorporate $\beta2^{20'E}$ will demonstrate an increased single channel conductance compared to the wild type.

Co-expressing $\alpha4^{wt}$ and $\alpha4^{20'K}$ with $\beta2^{20'E}$ produced 3 receptor populations with different single channel conductances: $\alpha4^{wt}{}_{(2)}\beta2^{20'E}{}_{(3)}$, $\alpha4^{20'K}\alpha4^{wt}\beta2^{20'E}{}_{(3)}$ and $\alpha4^{20'K}\beta2^{20'E}{}_{(3)}$. On the other hand, co-expressing $\alpha4^{wt}$ with $\beta2^{wt}$ and $\beta2^{20'E}$ produced 4 receptor populations with different single channel conductances: $\alpha4^{wt}{}_{(2)}\beta2^{20'E}{}_{(3)}$, $\alpha4^{wt}{}_{(2)}\beta2^{wt}{}_{(1)}\beta2^{20'E}{}_{(2)}$, $\alpha4^{wt}{}_{(2)}\beta2^{wt}{}_{(2)}\beta2^{20'E}{}_{(1)}$ and $\alpha4^{wt}{}_{(2)}\beta2^{wt}{}_{(3)}$. Thus Cooper *et al.* (1991) propose a 2 α : 3 β stoichiometry for α4β2 nAChRs.

In contrast to these data, variable stoichiometries have been proposed for neuronal nAChRs on the basis of the results of expressing 1:1, 1:9 and 9:1 α to β ratios in *Xenopus* oocytes (α2β2, Papke et al. 1989 and α4β2 Zwart & Vijverberg, 1998). Papke et al. (1989) reported two independently occurring single channel conductances of 34 pS and 16 pS in oocytes expressing α2β2 in a 1:1 ratio. Further, when expressing α2β2 in a 1:9 ratio, only a single 12.3 pS conductance was observed. On the basis of these data Papke et al. (1989) propose that oocytes expressing 1:1 α2β2 assemble two receptor populations with differing β subunit stoichiometries, whereas increasing the ratio of β subunits to 1:9 results in the formation of a single population of receptors with the greatest number of β subunits.

However, neuronal nAChRs commonly display multiple conductance levels (Papke, 1993). Thus an alternative explanation of this data is that the different conductance levels observed are produced by different states of the same molecular complex, as proposed for rat SCG neurons by Sivilotti et al. (1997).

Zwart & Vijverberg (1998) report that expressing α4β2 in a 1:9 α:β ratio produces a marked increase in receptor sensitivity to ACh. Here the wild-type (1:1 α:β) ACh concentration response curve is shifted to the left by approximately 30-fold and a reduction in the Hill slope is observed. Zwart & Vijverberg (1998) report that the ACh concentration response curve and +-tubo concentration responses curve for 1:9 α4β2 injected oocytes are best fitted with two components. On the basis of this data Zwart & Vijverberg (1998) propose that the 1:9 α4β2 injected oocytes expresses α4β2 receptors with differing stoichiometries.

3.4.2. The independent and progressive effect of the 9'Thr mutation

There is little in the literature to tell us whether the effects of 9' hydrophilic mutations on neuronal nAChR are predictable like those described for muscle nAChR or resemble those described for $GABA_A$ receptors. 9' hydrophilic TM2 mutations in a neuronal nAChR have been extensively investigated (see Revah *et al.*, 1991) and found to enhance the potency of ACh on α7 receptors. As recombinant α7 receptors are homomeric, 5 copies of the mutation are incorporated, thus these findings cannot address the relation between the magnitude of the shift and the number of mutated subunits. We have therefore ourselves obtained corroborating evidence that in neuronal nAChR the effect of each copy of the 9' mutation can be approximated as being independent and equivalent.

The central type α4β2 'pair' neuronal nAChR has been shown in the chick to contain α and β subunits in a 2:3 ratio (Anand *et al.*, 1991; Cooper *et al.*, 1991). It would seem reasonable to assume that 'pair' combinations of related subunits have the same stoichiometry, irrespective of the species they were cloned from. We found that in α3β4 receptors, the increase in ACh potency produced by mutating α (which we term $r_{\alpha 3}$) is 37.3-fold (see dose ratio values in table 2.3.4.), whereas the increase in ACh potency produced by mutating β ($r_{\beta 4}$) is 292-fold (see table 2.3.4.). Assuming a 2:3 ratio for αβ subunits, it can be seen that $\sqrt[2]{r_{\alpha 3}} \cong \sqrt[3]{r_{\beta 4}}$

The actual values observed were $^2\sqrt{37.3} = 6.11$ and $^3\sqrt{292} = 6.63$, respectively, in good agreement with the 2:3 α/β ratio prediction. This is what we expect if the effect of each copy of the reporter mutation is equivalent, irrespective of whether it is carried by the α or the β subunits. However, in order to validate our interpretation of the data, a few assumptions about the reporter mutation approach must be made.

The first condition is that the reporter mutation should not affect the correct assembly and therefore the subunit stoichiometry of the neuronal nAChR. The reporter mutation chosen is in TM2, *i.e.* in the pore-lining region: mutations in this area are not expected to influence assembly directly, since the sequence determinants for subunit assembly are not in the pore-lining region, but in the NH_2-terminal domain preceding the first transmembrane domain (Gu *et al.*, 1991a; Kreienkamp *et al.*, 1995). An indirect, long-range effect of a channel mutation on assembly cannot in principle be excluded, but would appear to be unlikely, as no such effect was reported by the numerous studies which have mutated TM2 residues in order to establish which amino acids are accessible from the open or closed pore and how these residues influence nAChR channel conductance and ionic permeability. For instance, if muscle nAChR carrying 9'

mutations had a stoichiometry different from the normal (2:1:1:1 for α:β:γ:δ, respectively), detectable changes in single-channel conductance would be expected, because of the differences in the TM2 domains of the α, β, γ, δ subunits (see Imoto *et al.,* 1988): these are not seen when 9' is mutated to Ser, Thr or isomers of Leu (Labarca *et al.*, 1995; Filatov & White, 1995; Kearney *et al.,* 1996). Evidence that the 9' Thr mutation does not significantly affect the ligand-binding site is provided by the observation that the *Kd* for the competitive antagonist +-tubo on recombinant muscle nAChRs is not affected by introducing the 9' Thr mutation in the γ subunit (Filatov & White, 1995; see chapter 1).

In order to be able to interpret our results reliably, in terms of subunit stoichiometry, other conditions must also be verified. In particular, the overall effect of the reporter mutation must depend only on the number of mutations incorporated in the channel, not on the type of subunit that carries the mutation. Secondly, the relation between number of mutants and magnitude of the observed change in ACh potency must be a simple one, the ideal case being that the effect of each additional mutation is independent of the number of mutations already in the channel. Thirdly, the receptors considered must have a uniform stoichiometry.

These criteria have been shown to hold true for the muscle nAChR: in this receptor (which has a stoichiometry of 2:1:1:1 for α:β:γ:δ, respectively) the introduction of a progressively greater number of 9' Ser or 9' Thr mutations has a consistent effect on ACh EC_{50}, an effect which is independent and similar for each additional mutation. Each Ser in 9' produced roughly a 10-fold shift in EC_{50}: there was no overlap between the range of EC_{50} observed for combinations with the different mutation copy numbers (Labarca *et al.*, 1995). In a further analysis of muscle nAChR, Kearney *et al.* (1996)

have investigated the lack of full subunit equivalence (probably due to asymmetry in the pore and interactions between adjacent subunits) by introducing in 9' a wide range of unnatural amino acid residues with progressive increments in side-chain length or branching.

However, the situation appears quite different for the $GABA_A$ receptor. Introduction of 9' Leu to Ser mutations in $\alpha1\beta2\gamma2$ $GABA_A$ recombinant receptors is very effective in increasing the receptor sensitivity to GABA, but the effectiveness of each mutation depends on which subunit type carries it. Consequently, stoichiometry could not be deduced from the EC_{50} shifts directly, but had to be confirmed by ascertaining how many dose-response components result from injecting mixtures of cRNA for the wild-type and mutant subunits (Chang *et al.*, 1996). In $GABA_A$ receptors, a further complication is that the shift in EC_{50} saturates when more than two subunits carry the mutation (Chang & Weiss, 1999).

There is another confounding factor, which in principle may impinge differently on different receptors (and perhaps explain some of the discrepancies observed). The linearity and multiplicativity of the effect of each mutated subunit that we observed would be expected if the mutation produces linearly additive changes in the free energy of one or more steps of channel activation. That is because free energy values are related to the logarithm of rate (and equilibrium) constants. However, 9' hydrophilic mutations are also known to affect desensitisation: changes in desensitisation should also alter the observed agonist EC_{50} to an extent which may depend on the impact of desensitisation on the wild-type dose-response curve. An increase in desensitisation would reduce the observed maximum response and thus shift the EC_{50} to the left, whereas a decrease in desensitisation would produce an apparent increase in EC_{50},

shifting the curve to the right. Since the extent to which desensitisation affects an agonist dose-response curve is difficult to determine macroscopically, this additional action of the mutation could make the final effect of the mutation unpredictable and estimates of stoichiometry unreliable.

3.4.3. The Hill slope of mutant receptors

The most likely explanation for the observation that the Hill slope decreases in receptors containing the 9' mutation, is that the contribution of monoliganded openings increases as the proportion of mutant subunits in the receptor rises. Monoliganded openings are known to occur in muscle nAChRs (although they are relatively rare at all but the lowest concentrations, Colquhoun & Sakmann, 1985); their contribution to the total current can be expected to increase with mutation number, if the reporter mutation does indeed destabilise the closed state. A receptor which needs the binding of only a single agonist molecule to open can be expected to give rise to an equilibrium dose-response curve with a slope of one. Hence, a greater contribution of monoliganded openings can be expected to make the curve shallower. Similar effects were observed by Chang & Weiss (1998) in $GABA_A$ receptors.

3.4.4. The holding current of oocytes expressing single mutant subunits

A possible explanation for the observed increase in initial holding current in oocytes injected with mutant α3 or β4 or β3 subunits, is the formation of spontaneously active homomeric receptors. For example, the expression of wildtype α3 alone may result in the formation of homomeric receptors, which however would be non-functional as they lack the complementary residues contributed by the β subunit and required for the

formation of the ACh binding site (see chapter 1). Such a receptor may still possess a gating mechanism, yet lack the ability for ligands to activate it. It can be seen that introducing 5 copies (assuming a pentamer is formed) of the 9' mutation into a homomeric channel lacking an ACh binding site, may produce spontaneous openings in the absence of agonists as previously observed in homomeric ρ1 $GABA_A$ receptors (Chang & Weiss, 1998) and in heteromeric α1β2γ2 receptors (Chang & Weiss, 1999), indicated by an increase in holding current.

A more attractive hypothesis is that the injection of 10 ng of RNA, 10 times the concentration of RNA used for the expression of the α3β4 'control', is detrimental to the health of injected oocytes. Such an affect on oocyte health would be reflected as an increase in the initial holding current. It is likely that if the sample size for the *t*-test was larger, then the differences observed in initial holding current would no longer be significant. This hypothesis is re-enforced by the data for the injection of wildtype or mutant β3 alone or with either α3 or β4, where the injection of $\alpha3^{L9'T}\beta3^{V9'T}$ results in an initial holding current not significantly different than that of α3β3 (102 ± 20 vs. 94 ± 25, p 0.92; see table 4.8.1.).

Chapter 4: Stoichiometry of 'triplet' α3β4β3 neuronal nicotinic acetylcholine receptors

Groot-Kormelink *et al.* (1998) have previously shown that β3 is incorporated into a functional α3β4β3 'triplet' receptor, but the position and copy number of β3 is unknown. α5, like β3, can only form functional receptors when expressed together with an α/β 'pair', forming an αβα5 'triplet' receptor (Ramirez-Latorre *et al.*, 1996; Wang *et al.*, 1996). As discussed previously in Chapter 1, in terms of amino acid sequence α5 and β3 are very similar, but distant from the rest of the group of neuronal nAChR subunits and have been classified together in tribe III-3 of the evolutionary nAChR tree (Corringer *et al.*, 2000). Thus the labels α5 and β3 may be somewhat misleading. These 'triplet' forming subunits may play more of a structural role in the formation of 'triplet' receptors, analogous to the β subunit in the muscle nAChR.

The next aim of the project was to apply the reporter mutation method (validated by our own α3β4 'pair' receptor data) to the problem of the stoichiometry of 'triplet' receptors containing the β3 subunit.

4.1. The α3β4β3 nAChR, comparing the mutant $\beta3^{V9'L}$ with the $\beta3^{wt}$ subunit

4.1.1. $\beta3^{wt}$ vs. $\beta3^{V9'L}$

In all subunits belonging to the nAChR superfamily, the midpoint (9') residue in the second transmembrane domain is highly conserved, being occupied by a hydrophobic amino acid. This is a Leu in all vertebrate nAChR subunits (see chapter 1), except for β3 and α5, which have a Val in 9' (position 273 for β3; see figure 4.1.1.a.).

Figure 4.1.1.a. The β3 subunit has a valine residue in the 9' position

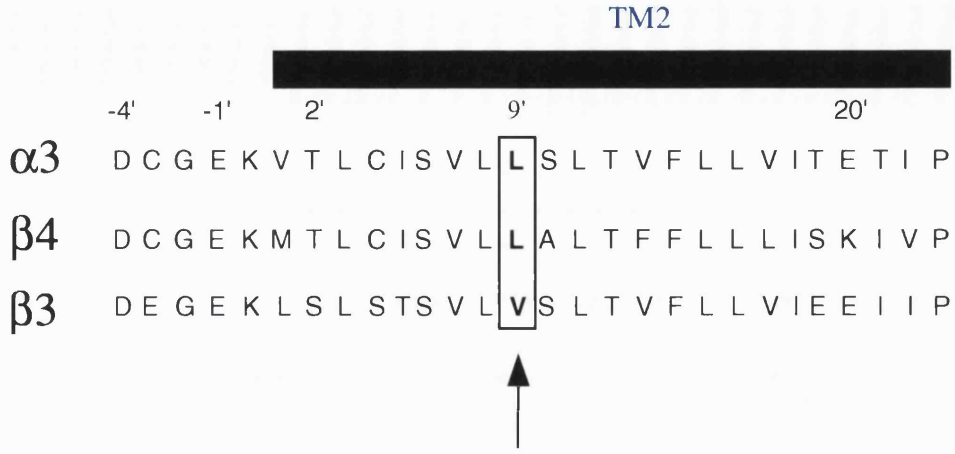

Figure 4.1.1.a. In this alignment of the TM2 region the conserved hydrophobic residue in 9' (Leu or Val) is boxed and marked by an arrow. The numbering of the TM2 domain follows Miller (1989). The 9' residues refer to $\alpha3^{L279}$, $\beta4^{L272}$ and $\beta3^{V273}$. Note the Val residue in 9' of the β3 subunit.

In homomeric receptors formed by subunits which have Leu in 9', introducing a Val in this position increases agonist sensitivity, slows desensitisation (see for homomeric α7 nAChR, Revah *et al.*, 1991 and for muscle nAChR Kearney *et al.*, 1996) and increases spontaneous openings (for $GABA_C$ ρ1 receptors, see Chang & Weiss, 1998). Such effects of a Leu to Val mutation in 9' are smaller, but similar to those of the Leu to Thr mutation we planned to use in our investigation. Additionally, the crucial assumption for the interpretation of our experiments in terms of stoichiometry is that the main determinant for the effect of the 9' Thr mutations on agonist EC_{50} should be their copy number in the assembled receptor complex. This assumption was validated by data from the 'pair' α3β4 receptor, which has only Leu residues in 9' (see Chapter 3). It was therefore considered possible that the presence of one or more non-Leu residues in the position (which would be contributed by wild-type β3 subunits to the assembled triplet receptor) might confound the effect of progressively introducing Thr in the different subunits. This would reduce the sensitivity of our experimental design. In order to

avoid this potential problem, we introduced a Val9'Leu (i.e. V9'L) mutation in β3, and used $\beta3^{V9'L}$ rather than $\beta3^{wt}$ in all the experiments (unless otherwise specified).

4.1.2. Insertion of a Leu residue in the β3 subunit of 'triplet' α3β4β3 receptors increases sensitivity to ACh

Full concentration response curves were obtained by bath-application of ACh to oocytes expressing 'triplet' α3β4β3 wild type or mutant receptors using the protocol described in chapter 2. Example responses from one oocyte expressing 'triplet' α3β4β3 wild type or mutant receptors are shown in panel A of figures 4.1.2.a. - 4.4.2 and 4.5.1- 4.7.1.

The resulting concentration response curves were then fitted as previously discussed in chapter 3 to determine the EC_{50}, I_{max} and Hill slope values for each experiment. The mean and standard error of the mean values for all fitted parameters (EC_{50}, I_{max} and Hill slope) are shown in panel C of figure 4.1.2.a. and panel D of figure 4.1.2.b. - 4.4.2. and 4.5.1 – 4.6.1. Averages of responses normalised to the fitted maximum are shown as the data points in panels B and C of figures 4.1.2.a. – 4.6.1., with the resulting fitted curve shown in panel B.

The ACh sensitivity of $\alpha3\beta4\beta3^{wt}$ receptors (see figure 4.1.2.a.) was compared with that of $\alpha3\beta4\beta3^{V9'L}$ receptors (see figure 4.1.2.b.) and, contrary to expectations, found to be consistently increased in $\alpha3\beta4\beta3^{V9'L}$ receptors (summarised in figure 4.1.2.b.). Although the decrease in the EC_{50} of ACh was relatively small (from 242.7 ± 44.1 μM to 163.1 ± 13.4 μM, see table 4.4.3.), it was still thought preferable to use $\beta3^{V9'L}$ rather than $\beta3^{wt}$ in the stoichiometry experiments, in order to introduce subunits carrying the 9' Thr mutation into receptors which only had Leu in the 9' position. Note that $\alpha3\beta4\beta3^{V9'L}$

receptors show a slight increase in the speed of desensitisation when compared to $\alpha3\beta4\beta3^{wt}$ (see panel A of figure 4.1.b.). This is more pronounced when comparing $\alpha3\beta4\beta3^{V9'L}$ receptors with $\alpha3\beta4\beta3^{V9'T}$ (see panel A of figure 4.4.2.).

Averaged normalised responses recorded from $\alpha3\beta4\beta3^{V9'L}$ and from 'triplet' receptors bearing the 9' mutation in different subunits were then re-fitted with the curves constrained to be parallel (i.e. with equal Hill slopes) in order to estimate the horizontal distance between concentration response curves, expressed as dose ratios (termed *r*) taking $\alpha3\beta4\beta3^{V9'L}$ as a reference (where $\alpha3\beta4\beta3^{V9'L}$ $r = 1$; see table 4.7.2). All constrained fits are shown in panel C of figures 4.2.1. - 4.4.2. and 4.5.1. – 4.7.1. The free and constrained fit curves were similar, differing only when the presumed mutation copy number was high (see panels B and C of figure 4.5.1. and 4.6.1.).

Figure 4.1.2.a. 'Triplet' $\alpha3\beta4\beta3^{wt}$ concentration response curves

A

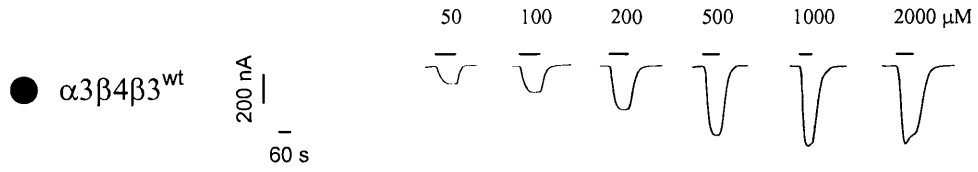

B

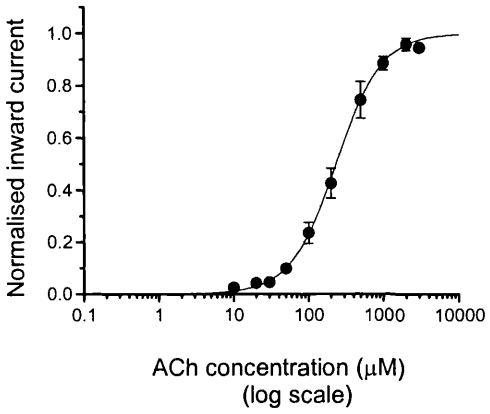

C

EC_{50} (µM)	I_{max} (nA)	n_H	I_H (nA)	*Rundown (%)*	*No. of batches*	*n*	*cRNA injected* (ng)
242.7 ± 44.1	1333 ± 373	1.42 ± 0.1	300 ± 83.4	43.34 ± 8.92	2	6	0.1 - 10

Figure 4.1.2.a. A shows examples of inward currents elicited by bath-applied ACh in oocytes expressing $\alpha3\beta4\beta3$. B shows ACh concentration-response curves pooled from experiments such as the ones shown in A: Pooled normalised results were fitted with the Hill equation as a free fit (panel B; see chapter 3). The concentration-response curves refer to oocytes injected with $\alpha3\beta4\beta3^{wt}$ (●). C shows a summary of the fitted parameters: EC_{50}, I_{max} and n_H are the mean (± S.D. of mean) of parameter estimates obtained by fitting separately each concentration-response curve with a Hill equation. I_H is the mean (± S.D. of mean) holding current recorded at the start of the experiment. Rundown is the % (± S.D. of mean) of the response of the initial standard observed when the standard was applied at the end of the experiment. No. of batches are the number of oocyte batches used. cRNA injected is the range of cRNA injected in order to produce acceptable expression levels for the experiments in A.

Figure 4.1.2.b. Reference 'triplet' $\alpha3\beta4\beta3^{V9'L}$ concentration response curves

A

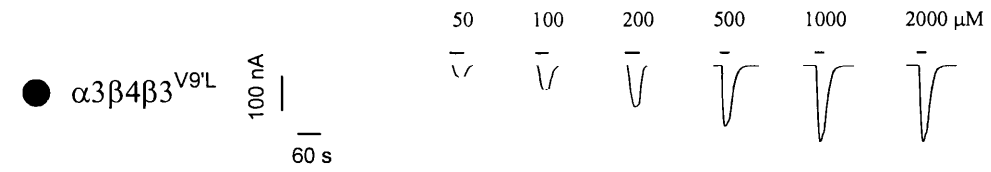

B

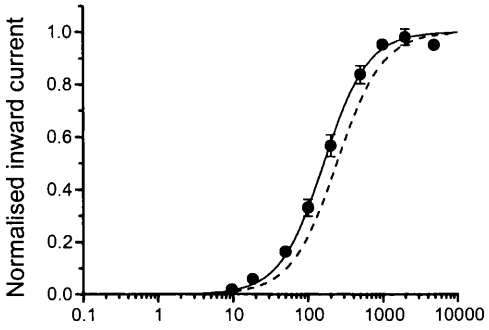

C

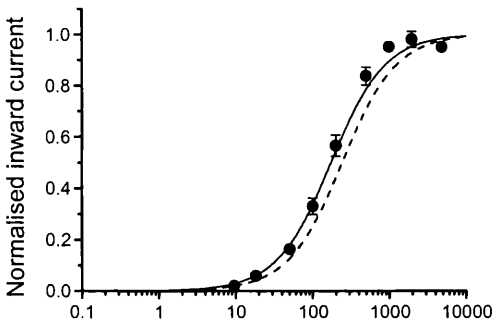

D

EC_{50} (μM)	I_{max} (nA)	n_H	I_H (nA)	*Rundown (%)*	*No. of batches*	*n*	*cRNA injected* (ng)
163.1 ± 13.4	305.7 ± 69.3	1.47 ± 0.08	230 ± 63.1	82.2 ± 7.2	2	4	1 - 5

Figure 4.1.2.b. A shows examples of inward currents elicited by bath-applied ACh in oocytes expressing $\alpha3\beta4\beta3^{V9'L}$. B and C show ACh concentration-response curves pooled from experiments such as the ones shown in A: Pooled normalised results were fitted with the Hill equation either as free fit (panel B) or under the constraint of equal slopes (panel C) for comparison with other mutant curves, in order to estimate the horizontal distance between the curves as a dose-ratio, where $\alpha3\beta4\beta3^{V9'L}$ = 1. The concentration-response curves refer to oocytes injected with $\alpha3\beta4\beta3^{V9'L}$ (●). Panels B and C also show for reference (dashed curve with no symbols) the concentration-response curve for $\alpha3\beta4\beta3^{wt}$. D shows a summary of the fitted parameters: EC_{50}, I_{max} and n_H are the mean (± S.D. of mean) of parameter estimates obtained by fitting separately each concentration-response curve with a Hill equation. I_H is the mean (± S.D. of mean) holding current recorded at the start of the experiment. Rundown is the % (± S.D. of mean) of the response of the initial standard observed when the standard was applied at the end of the experiment. No. of batches are the number of oocyte batches used. cRNA injected is the range of cRNA injected in order to produce acceptable expression levels for the experiments in A.

4.2. Inserting a 9' Thr mutation in the β3 subunit of 'triplet' α3β4β3 receptors increases sensitivity to ACh

The insertion of the 9' Thr mutation in the β3 subunit increased the α3β4β3 'triplet' receptor sensitivity to ACh, in agreement with the findings of Groot-Kormelink *et al.* (1998). The mean EC_{50} was significantly reduced approximately 4-fold, from 163.1 ± 13.4 μM for $\alpha3\beta4\beta3^{V9'L}$ (see panel D, figure 4.1.5 and table 4.7.2.) to 43.4 ± 2.2 μM (p 0.003; see table 4.7.2) for the $\alpha3\beta4\beta3^{V9'T}$ mutant (dose ratio of $r = 4.12$ [3.77-4.52]; see panel D of figure 4.2.1 and table 4.7.2.). Comparing the initial holding currents and Hill slope of $\alpha3\beta4\beta3^{V9'L}$ with $\alpha3\beta4\beta3^{V9'T}$ in a two-tailed t-test assuming unequal variance, revealed no significant difference. Oocytes expressing $\alpha3\beta4\beta3^{V9'L}$ had a mean initial holding current of 230 ± 63.1 nA and a mean Hill slope of 1.47 ± 0.08 compared to 175 ± 23.5 nA (p 0.46) and 1.28 ± 0.04 (p 0.10) for $\alpha3\beta4\beta3^{V9'T}$ (see table 4.7.2.).

Figure 4.2.1. Inserting a 9' Thr mutation in the β3 subunit of 'triplet' α3β4β3 receptors increases sensitivity to ACh

A

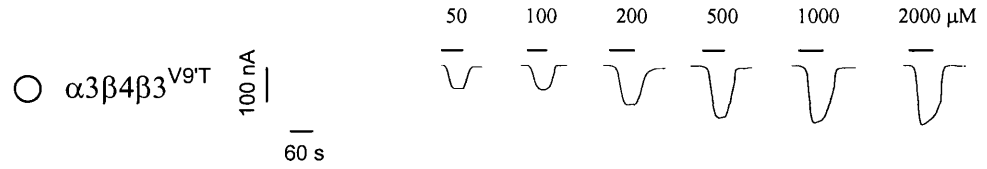

B

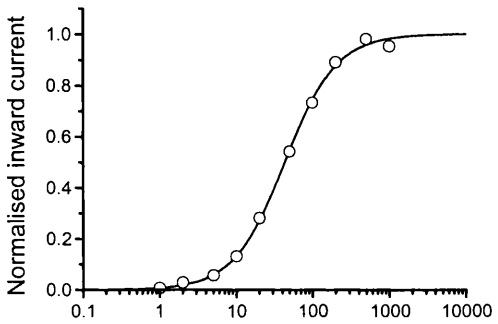

C

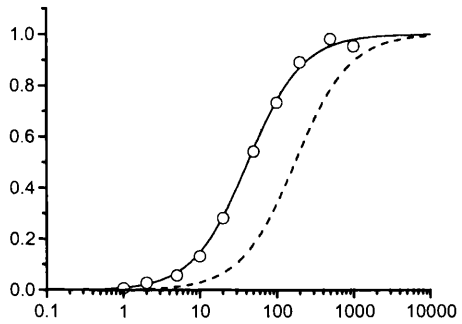

D

EC_{50} (μM)	I_{max} (nA)	n_H	I_H (nA)	*Rundown (%)*	*No. of batches*	*n*	*cRNA injected* (ng)
43.4 ± 2.2	240.9 ± 41.3	1.28 ± 0.04	175 ± 23.5	67.8 ± 7.31	4	10	0.1 - 5

Figure 4.2.1 A shows examples of inward currents elicited by bath-applied ACh in oocytes expressing $\alpha3\beta4\beta3^{V9'T}$. B and C show ACh concentration-response curves pooled from experiments such as the ones shown in A: Pooled normalised results were fitted with the Hill equation either as free fit (panel B) or under the constraint of equal slopes (panel C) for comparison with other mutant curves, in order to estimate the horizontal distance between the curves as a dose-ratio, where $\alpha3\beta4\beta3^{V9'L}$ = 1. The concentration-response curves refer to oocytes injected with $\alpha3\beta4\beta3^{V9'T}$ (○). Panel C also shows for reference (dashed curve with no symbols) the concentration-response curve for $\alpha3\beta4\beta3^{V9'L}$. D shows a summary of the fitted parameters: EC_{50}, I_{max} and n_H are the mean (± S.D. of mean) of parameter estimates obtained by fitting separately each concentration-response curve with a Hill equation. I_H is the mean (± S.D. of mean) holding current recorded at the start of the experiment. Rundown is the % (± S.D. of mean) of the response of the initial standard observed when the standard was applied at the end of the experiment. No. of batches are the number of oocyte batches used. cRNA injected is the range of cRNA injected in order to produce acceptable expression levels for the experiments in A.

4.3. Inserting a 9' Thr mutation in the α3 subunit of 'triplet' α3β4β3$^{V9'L}$ receptors produces a greater effect than mutating the β3 subunit

Inserting the 9' Thr mutation in α3 produced a greater increase in α3β4β3$^{V9'L}$ 'triplet' receptor sensitivity to ACh than when the mutation was in the β3 subunit. The mean EC_{50} was reduced sixteen-fold, to 10.5 ± 1.4 μM ACh (dose ratio of r = 17.1 [14.9-19.7]; see panel D of figure 4.3.1. and table 4.7.2.) compared to the EC_{50} of 163.1 ± 13.4 μM for α3β4β3$^{V9'L}$ receptors (see table 4.7.2.). Comparing the initial holding currents and Hill slope of α3β4β3$^{V9'L}$ with α3$^{L9'T}$β4β3$^{V9'L}$ in a two-tailed t-test assuming unequal variance, revealed a significant reduction in Hill slope for α3$^{L9'T}$β4β3$^{V9'L}$. Oocytes expressing α3β4β3$^{V9'L}$ had a mean initial holding current of 230 ± 63.1 nA and a mean Hill slope of 1.47 ± 0.08 compared to 148 ± 56.3 nA (p 0.37) and 1.14 ± 0.06 (p 0.02) for α3$^{L9'T}$β4β3$^{V9'L}$ (see table 4.7.2.). Thus, mutating the α3 subunit produces approximately a four times greater shift than mutating the β3 subunit and significantly reduces the Hill slope compared to the 'control' α3β4β3$^{V9'L}$.

Figure 4.3.1. Inserting a 9' Thr mutation in the α3 subunit of 'triplet' $\alpha3\beta4\beta3^{V9'L}$ receptors produces a greater effect than mutating the β3 subunit

A

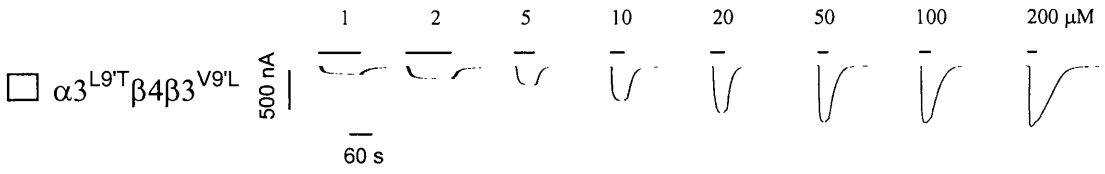

B

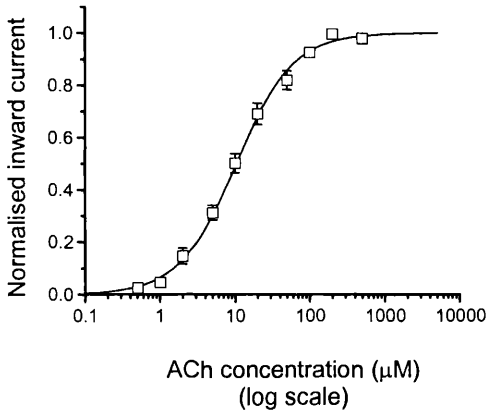

C

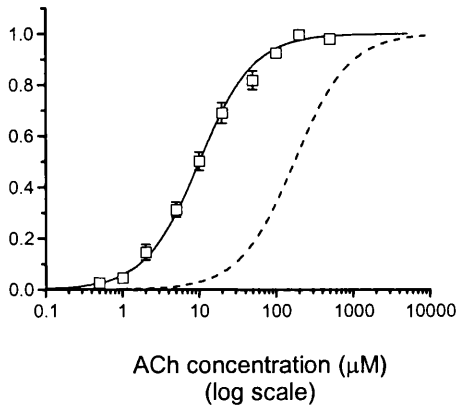

D

EC_{50} (μM)	I_{max} (nA)	n_H	I_H (nA)	*Rundown (%)*	*No. of batches*	*n*	*cRNA injected (ng)*
10.5 ± 1.4	993 ± 157	1.14 ± 0.06	148 ± 56.3	92.2 ± 19.6	3	4	1

Figure 4.3.1 A shows examples of inward currents elicited by bath-applied ACh in oocytes expressing $\alpha3^{L9'T}\beta4\beta3^{V9'L}$. B and C show ACh concentration-response curves pooled from experiments such as the ones shown in A: Pooled normalised results were fitted with the Hill equation either as free fit (panel B) or under the constraint of equal slopes (panel C) for comparison with other mutant curves, in order to estimate the horizontal distance between the curves as a dose-ratio, where $\alpha3\beta4\beta3^{V9'L}$ = 1. The concentration-response curves refer to oocytes injected with $\alpha3^{L9'T}\beta4\beta3^{V9'L}$ (□). Panel C also shows for reference (dashed curve with no symbols) the concentration-response curve for $\alpha3\beta4\beta3^{V9'L}$. D shows a summary of the fitted parameters: EC_{50}, I_{max} and n_H are the mean (± S.D. of mean) of parameter estimates obtained by fitting separately each concentration-response curve with a Hill equation. I_H is the mean (± S.D. of mean) holding current recorded at the start of the experiment. Rundown is the % (± S.D. of mean) of the response of the initial standard observed when the standard was applied at the end of the experiment. No. of batches are the number of oocyte batches used. cRNA injected is the range of cRNA injected in order to produce acceptable expression levels for the experiments in A.

4.4. Inserting 9' Thr mutations in both α3 and β3 subunits of 'triplet' $\alpha3\beta4\beta3^{V9'L}$ receptors produces a greater effect than mutating α3 or β3 alone

Inserting the 9' Thr mutation in *both* α3 and β3 produced a greater increase in $\alpha3\beta4\beta3^{V9'L}$ 'triplet' receptor sensitivity to ACh than when the mutation was in α3 or β3 alone. The mean EC_{50} was reduced by approximately forty two-fold, to 4.49 ± 0.37 μM ACh (dose ratio of $r = 41.6$ [37.6-46.0]; see panel D of figure 4.4.1. and table 4.7.2.) compared to the 'control' $\alpha3\beta4\beta3^{V9'L}$ (see table 4.7.2.). Note the progressive increase in the potency of ACh as the 9' Thr mutation was introduced in β3 (four times), α3 alone (seventeen times) or α3 and β3 (forty two times; summarised in figure 4.4.2).

Comparing the initial holding currents and Hill slope of $\alpha3\beta4\beta3^{V9'L}$ with $\alpha3^{L9'T}\beta4\beta3^{V9'T}$ in a two-tailed *t*-test assuming unequal variance, revealed a significant reduction in Hill slope for $\alpha3^{L9'T}\beta4\beta3^{V9'T}$. Oocytes expressing $\alpha3\beta4\beta3^{V9'L}$ had a mean initial holding current of 230 ± 63.1 nA and a mean Hill slope of 1.47 ± 0.08 compared to 80 ± 20.4 nA (p 0.09) and 1.13 ± 0.04 (p 0.02) for $\alpha3^{L9'T}\beta4\beta3^{V9'T}$ (see table 4.7.2.). Note the progressive, but slight reduction in Hill slope in this series of mutants.

Figure 4.4.1. Inserting 9' Thr mutations in both α3 and β3 subunits of 'triplet' $\alpha3\beta4\beta3^{V9'L}$ receptors produces a greater effect than mutating α3 or β3 alone

A

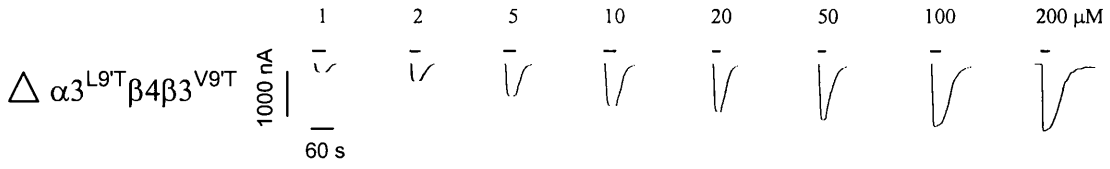

B

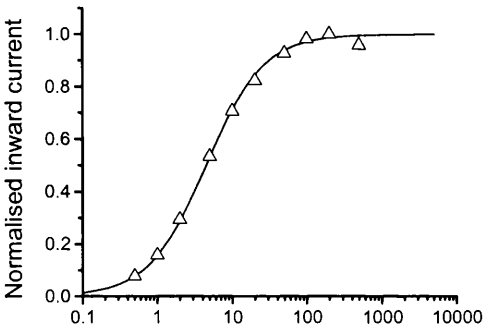

C

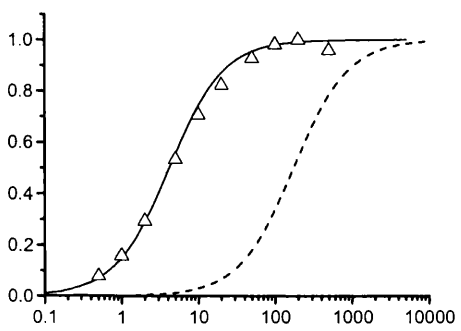

D

EC_{50} (μM)	I_{max} (nA)	n_H	I_H (nA)	*Rundown (%)*	*No. of batches*	*n*	*cRNA injected* (ng)
4.49 ± 0.37	1866 ± 276	1.13 ± 0.04	80 ± 20.4	88.6 ± 17.1	2	4	5

Figure 4.4.1. A shows examples of inward currents elicited by bath-applied ACh in oocytes expressing $\alpha3^{L9'T}\beta4\beta3^{V9'T}$. B and C show ACh concentration-response curves pooled from experiments such as the ones shown in A: Pooled normalised results were fitted with the Hill equation either as free fit (panel B) or under the constraint of equal slopes (panel C) for comparison with other mutant curves, in order to estimate the horizontal distance between the curves as a dose-ratio, where $\alpha3\beta4\beta3^{V9'L}$ = 1. The concentration-response curves refer to oocytes injected with $\alpha3^{L9'T}\beta4\beta3^{V9'T}$ (Δ). Panel C also shows for reference (dashed curve with no symbols) the concentration-response curve for $\alpha3\beta4\beta3^{V9'L}$. D shows a summary of the fitted parameters: EC_{50}, I_{max} and n_H are the mean (± S.D. of mean) of parameter estimates obtained by fitting separately each concentration-response curve with a Hill equation. I_H is the mean (± S.D. of mean) holding current recorded at the start of the experiment. Rundown is the % (± S.D. of mean) of the response of the initial standard observed when the standard was applied at the end of the experiment. No. of batches are the number of oocyte batches used. cRNA injected is the range of cRNA injected in order to produce acceptable expression levels for the experiments in A.

Figure 4.4.2. Summary of the effects of 9' Thr mutations in α3 and β3 subunits

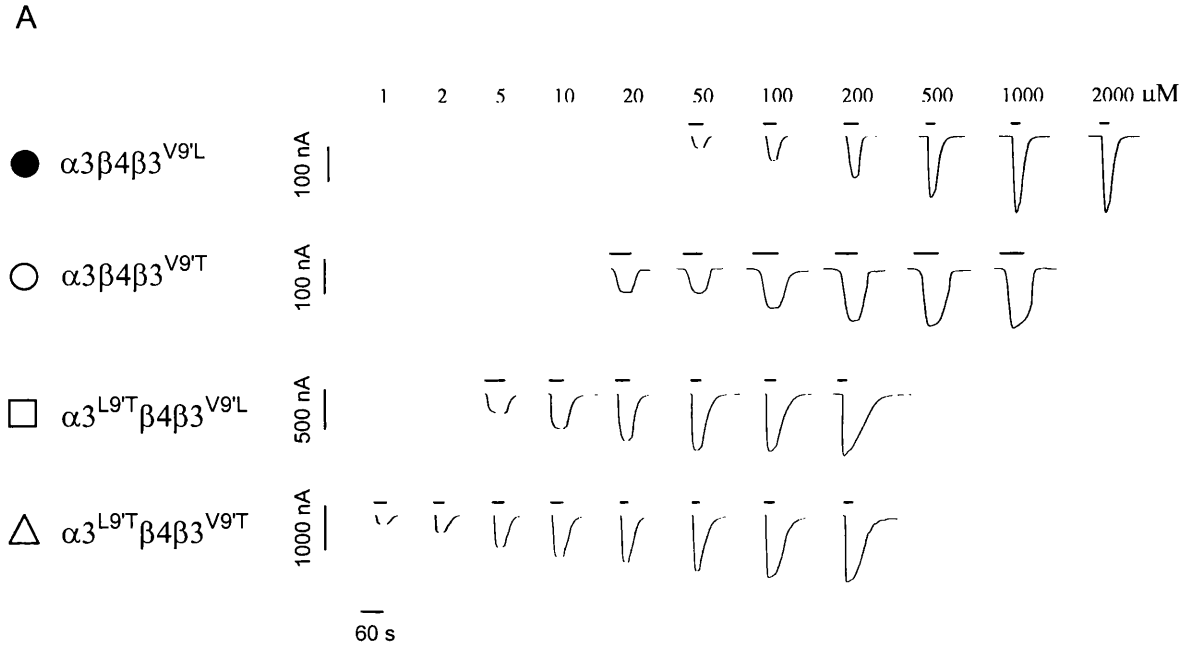

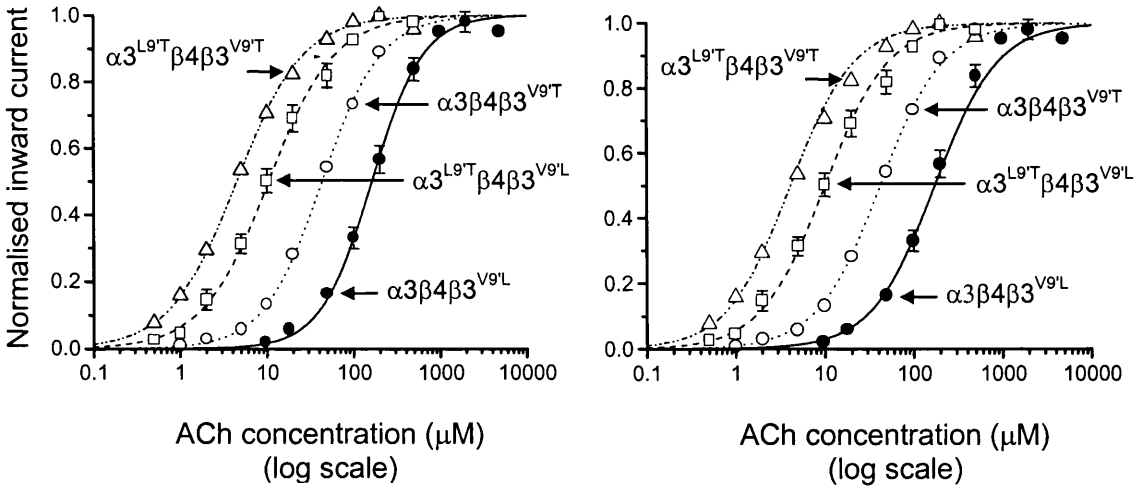

Figure 4.4.2. A, examples of inward currents elicited by a representative range of ACh concentrations (see values above the application bars) in oocytes expressing $\alpha3\beta4\beta3^{V9'L}$, $\alpha3\beta4\beta3^{V9'T}$, $\alpha3^{L9'T}\beta4\beta3^{V9'L}$ or $\alpha3^{L9'T}\beta4\beta3^{V9'T}$. B,C show ACh concentration-response curves pooled from experiments such as the ones shown in A (*n* = 4-10 oocytes). Pooled normalised results were fitted with the Hill equation either as free fit (panel B) or under the constraint of equal slopes (panel C) in order to estimate the horizontal distance between the curves as a dose-ratio (see Table 4.4.3). The concentration-response curves shown refer to oocytes injected with $\alpha3\beta4\beta3^{V9'L}$ (●), $\alpha3\beta4\beta3^{V9'T}$ (○), $\alpha3^{L9'T}\beta4\beta3^{V9'L}$ (□) and $\alpha3^{L9'T}\beta4\beta3^{V9'T}$ (△); bars show standard deviation of the mean (when larger than the symbol). Note the progressive increase in the potency of ACh as the 9' Thr mutation was introduced in β3, α3 alone or α3 and β3.

Table 4.4.3. Summary table of 9' Thr mutations in α3 and β3 subunits

	EC_{50} (μM)	I_{max} (nA)	n_H	*Dose ratios*	*Square root of dose ratios*	*cube root of dose ratios*	*n*
$\alpha3\beta4\beta3^{wt}$	242.7 ± 44.1	1333 ± 373	1.42 ± 0.1				6
$\alpha3\beta4\beta3^{V9'L}$	163.1 ± 13.4 [159.5-189.8]	305.7 ± 69.3	1.47 ± 0.08	1			4
$\alpha3\beta4\beta3^{V9'T}$	43.4 ± 2.2	240.9 ± 41.3	1.28 ± 0.04	4.12 [3.77-4.52]			10
$\alpha3^{L9'T}\beta4\beta3^{V9'L}$	10.5 ± 1.4	993 ± 157	1.14 ± 0.06	17.1 [14.9-19.7]	4.14 [3.86-4.44]		4
$\alpha3^{L9'T}\beta4\beta3^{V9'T}$	4.49 ± 0.37	1866 ± 276	1.13 ± 0.04	41.6 [37.6-46.0]		3.46 [3.35-3.58]	4

Table 4.4.3. A summary of the fitted data: EC_{50}, I_{max} and n_H are the mean (± S.D. of mean) of parameter estimates obtained by fitting separately each concentration-response curve with a Hill equation. Dose ratios were estimated from fits in which curves were constrained to have the same slope (summarised in panel C of figure 4.4.2) for comparison with other mutant curves, in order to estimate the horizontal distance between the curves as a dose-ratio, where $\alpha3\beta4\beta3^{V9'L}$ = 1. The same parallel fits allowed estimation of 2.01-unit likelihood intervals (in square brackets under the means of the parameters they refer to; see Methods section): these are equivalent to 95 % confidence intervals.

4.5. Inserting a 9' Thr mutation in the β4 subunit of 'triplet' α3β4β3$^{V9'L}$ receptors is equivalent to mutating α3 alone

If the α3β4β3 receptor contains two copies of α3 and one of β3, it follows that the receptor should also contain two copies of β4, in order to make up the total subunit number of five. This would predict that mutating β4 should have the same effect as mutating α3. This question was addressed by the next set of experiments.

Inserting the 9' Thr mutation in the β4 subunit produced an increase in α3β4β3$^{V9'L}$ 'triplet' receptor sensitivity to ACh, equivalent to mutating the α3 subunit alone. The mean EC_{50} was reduced to 9.54 ± 2.1 μM ACh (dose ratio of r = 21.9 [18.6-25.6]; see panel D of figure 4.6 and table 4.7.2.) compared to 10.5 ± 1.4 μM (*p 0.71*) and a dose ratio of r = 17.1 [14.9-19.7] for α3$^{L9'T}$β4β3$^{V9'L}$ (see table 4.7.2.).

Comparing the initial holding current and Hill slope of α3β4β3$^{V9'L}$ with α3β4$^{L9'T}$β3$^{V9'L}$ in a two-tailed *t*-test assuming unequal variance, revealed a significant reduction in Hill slope for α3β4$^{L9'T}$β3$^{V9'L}$. Oocytes expressing α3β4β3$^{V9'L}$ had a mean initial holding current of 230 ± 63.1 nA and a mean Hill slope of 1.47 ± 0.08 compared to 90 ± 15.8 nA (*p* 0.11) and 1.12 ± 0.06 (*p* 0.02) for α3β4$^{L9'T}$β3$^{V9'L}$ (see table 4.7.2.). Thus, mutating the β4 subunit significantly reduces the Hill slope compared to the 'control' α3β4β3$^{V9'L}$.

Figure 4.5.1. Inserting a 9' Thr mutation in the β4 subunit of 'triplet' $\alpha3\beta4\beta3^{V9'L}$ receptors is equivalent to mutating α3 alone

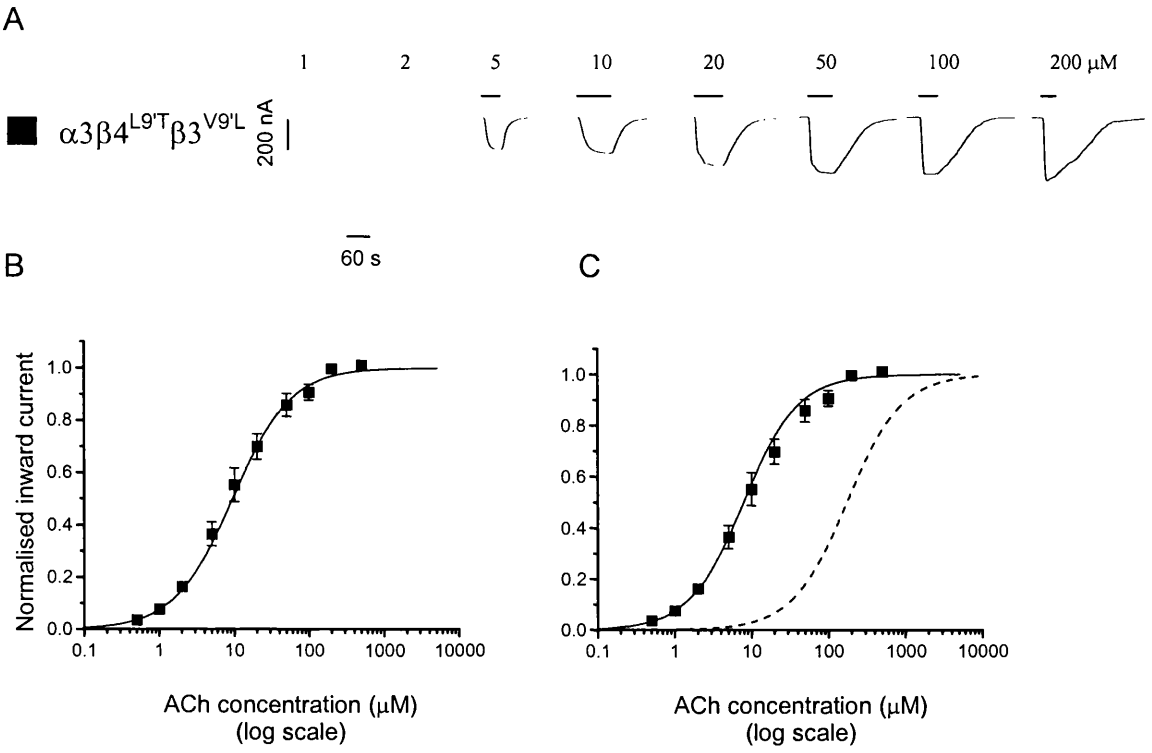

D

EC_{50} (μM)	I_{max} (nA)	n_H	I_H (nA)	*Rundown (%)*	*No. of batches*	*n*	*cRNA injected* (ng)
9.54 ± 2.1	963.6 ± 107.1	1.12 ± 0.06	90 ± 15.8	77.6 ± 21.8	3	4	1 - 5

Figure 4.5.1. A shows examples of inward currents elicited by bath-applied ACh in oocytes expressing $\alpha3\beta4^{L9'T}\beta3^{V9'L}$. B and C show ACh concentration-response curves pooled from experiments such as the ones shown in A: Pooled normalised results were fitted with the Hill equation either as free fit (panel B) or under the constraint of equal slopes (panel C) for comparison with other mutant curves, in order to estimate the horizontal distance between the curves as a dose-ratio, where $\alpha3\beta4\beta3^{V9'L}$ = 1. The concentration-response curves refer to oocytes injected with $\alpha3\beta4^{L9'T}\beta3^{V9'L}$ (■). Panel C also shows for reference (dashed curve with no symbols) the concentration-response curve for $\alpha3\beta4\beta3^{V9'L}$. D shows a summary of the fitted parameters: EC_{50}, I_{max} and n_H are the mean (± S.D. of mean) of parameter estimates obtained by fitting separately each concentration-response curve with a Hill equation. I_H is the mean (± S.D. of mean) holding current recorded at the start of the experiment. Rundown is the % (± S.D. of mean) of the response of the initial standard observed when the standard was applied at the end of the experiment. No. of batches are the number of oocyte batches used. cRNA injected is the range of cRNA injected in order to produce acceptable expression levels for the experiments in A.

4.6. Inserting a 9' Thr mutation in both β4 and β3 subunits of 'triplet' $\alpha3\beta4\beta3^{V9'L}$ receptors produces a greater effect than mutating β4 or β3 alone

Inserting the 9' Thr mutation in both β4 and β3 produced a greater increase in $\alpha3\beta4\beta3^{V9'L}$ 'triplet' receptor sensitivity to ACh than when the mutation was in β4 or β3 alone. The mean EC_{50} was reduced by approximately fifty-fold, to 3.22 ± 0.53 μM ACh (dose ratio of r = 50.3 [43.7-58.0]; see panel D of figure 4.6.1.and table 4.7.2.) compared to $\alpha3\beta4^{L9'T}\beta3^{V9'L}$ and $\alpha3\beta4\beta3^{V9'T}$ (see table 4.7.2). Note the progressive increase in the potency of ACh as the 9' Thr mutation was introduced in β3 (four times), β4 alone (twenty two times) or β4 and β3 (fifty times; summarised in figure 4.6.1.).

Comparing the initial holding current and Hill slope of $\alpha3\beta4\beta3^{V9'L}$ with $\alpha3\beta4^{L9'T}\beta3^{V9'T}$ in a two-tailed *t*-test assuming unequal variance, revealed a significant reduction in Hill slope for $\alpha3\beta4^{L9'T}\beta3^{V9'T}$. Oocytes expressing $\alpha3\beta4\beta3^{V9'L}$ had a mean initial holding current of 230 ± 63.1 nA and a mean Hill slope of 1.47 ± 0.08 compared to 83 ± 23.0 nA (p 0.10) and 0.94 ± 0.04 (p 0.004) for $\alpha3\beta4^{L9'T}\beta3^{V9'T}$ (see table 4.7.2.).

Figure 4.6.1. Inserting a 9' Thr mutation in both β4 and β3 subunits of 'triplet' $\alpha3\beta4\beta3^{V9'L}$ receptors produces a greater effect than mutating β4 or β3 alone

A

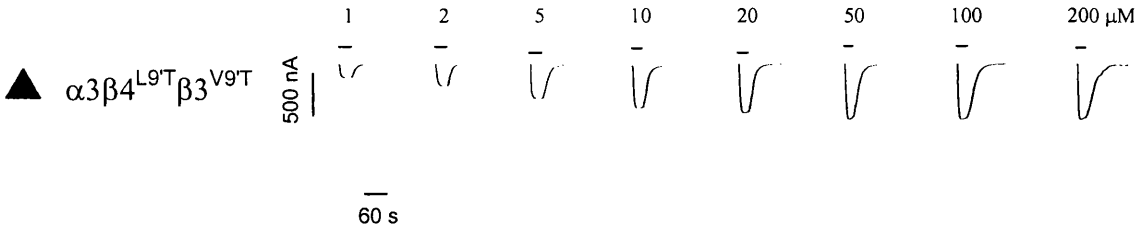

B

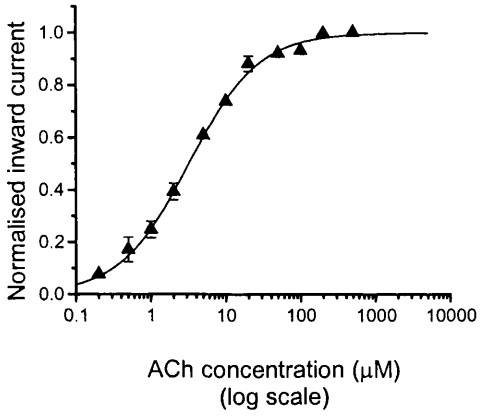

C

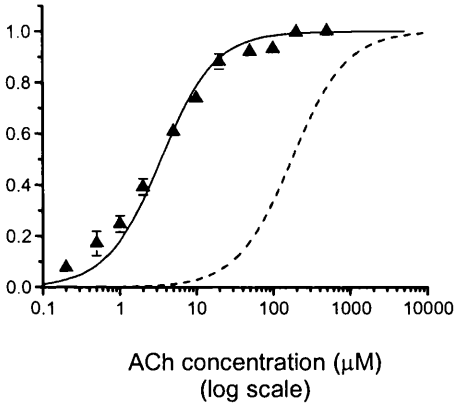

D

EC_{50} (μM)	I_{max} (nA)	n_H	I_H (nA)	*Rundown (%)*	*No. of batches*	*n*	*cRNA injected* (ng)
3.22 ± 0.53	592 ± 177	0.94 ± 0.04	83 ± 23	119.0 ± 11.0	2	4	10

Figure 4.6.1. A shows examples of inward currents elicited by bath-applied ACh in oocytes expressing $\alpha3\beta4^{L9'T}\beta3^{V9'T}$. B and C show ACh concentration-response curves pooled from experiments such as the ones shown in A: Pooled normalised results were fitted with the Hill equation either as free fit (panel B) or under the constraint of equal slopes (panel C) for comparison with other mutant curves, in order to estimate the horizontal distance between the curves as a dose-ratio, where $\alpha3\beta4\beta3^{V9'L}$ = 1. The concentration-response curves refer to oocytes injected with $\alpha3\beta4^{L9'T}\beta3^{V9'T}$ (▲). Panel C also shows for reference (dashed curve with no symbols) the concentration-response curve for $\alpha3\beta4\beta3^{V9'L}$. D shows a summary of the fitted parameters: EC_{50}, I_{max} and n_H are the mean (± S.D. of mean) of parameter estimates obtained by fitting separately each concentration-response curve with a Hill equation. I_H is the mean (± S.D. of mean) holding current recorded at the start of the experiment. Rundown is the % (± S.D. of mean) of the response of the initial standard observed when the standard was applied at the end of the experiment. No. of batches are the number oocyte batches used. cRNA injected is the range of cRNA injected in order to produce acceptable expression levels for the experiments in A.

4.7. Inserting a 9' Thr mutation in both β4 and β3 subunits of 'triplet' $\alpha3\beta4\beta3^{VL}$ receptors is equivalent to mutating both α3 and β3

Inserting the 9' Thr mutation in the β4 and β3 subunits produced an increase in $\alpha3\beta4\beta3^{V9'L}$ 'triplet' receptor sensitivity to ACh, equivalent to that seen after mutating the α3 and β3 subunits. The mean ACh EC_{50} was 3.22 ± 0.53 μM for $\alpha3\beta4^{L9'T}\beta3^{V9'T}$ vs. 4.49 ± 0.37 μM for $\alpha3^{L9'T}\beta4\beta3^{V9'T}$ (p 0.10; see table 4.7.2).

The concentration-response curves for the $\alpha3\beta4^{L9'T}\beta3^{V9'L}$ mutant were very close to those for the $\alpha3^{L9'T}\beta4\beta3^{V9'L}$ mutant (shown for reference as dashed curves in figure 4.7.1, panels B and C); indeed the 2-unit likelihood intervals for the dose ratios (see table 4.7.2) overlap both for $\alpha3^{L9'T}\beta4\beta3^{V9'L}$ (r = 17.1 [14.9-19.7]) and $\alpha3\beta4^{L9'T}\beta3^{V9'L}$ (r = 21.9 [18.6-25.6]) and for $\alpha3^{L9'T}\beta4\beta3^{V9'T}$ (r = 41.6 [37.6-46.0]) and $\alpha3\beta4^{L9'T}\beta3^{V9'T}$ (r = 50.3 [43.7-58.0]). Again the simplest explanation for these results is that α3β4β3 receptors contain two copies of α3 and β4, but only one copy of the β3 subunit. Figure 4.7.3. shows clearly that the effect of the mutation did not saturate up to a presumed mutation copy number of three, producing a progressive leftward shift in the ACh concentration response curve. There was also a reduction in the Hill slope in $\alpha3\beta4^{L9'T}\beta3^{V9'T}$, from 1.12 ± 0.06 for the $\alpha3\beta4^{L9'T}\beta3^{V9'L}$ mutant to 0.94 ± 0.04 (see figure 4.7.3).

As previously discussed for the α3β4 receptor (see Chapter 3), if the effect of each hydrophobic to hydrophilic substitution in 9' is independent of position and multiplicative on the ACh EC_{50} (i.e. additive in terms of free energy), then plotting the logarithm of the ACh EC_{50} against the presumed number of mutations in each pentamer

channel should yield a linear plot. Figure 4.7.3. shows that this is indeed the case also for the α3β4β3 'triplet', which shows an approximately linear relation between log EC_{50} and the putative number of mutations in the receptor. However, there is an apparent reduction in the Hill slope from 2 to 3 copies of the mutation for $\alpha3^{L9'T}\beta4\beta3^{V9'T}$ and $\alpha3\beta4^{L9'T}\beta3^{V9'T}$ compared to $\alpha3\beta4\beta3^{wt}$ and $\alpha3\beta4\beta3^{V9'T}$ (see figure 4.7.1. and table 4.7.2.). In terms of the dose ratios for $\alpha3^{L9'T}\beta4\beta3^{V9'L}$ vs. $\alpha3^{L9'T}\beta4\beta3^{V9'T}$ (41.6 / 17.1) and $\alpha3\beta4^{L9'T}\beta3^{V9'L}$ vs. $\alpha3\beta4^{L9'T}\beta3^{V9'T}$ (50.3 / 21.9), the apparent shift in the receptor sensitivity to ACh is increased further for both $\alpha3^{L9'T}\beta4\beta3^{V9'T}$ and $\alpha3\beta4^{L9'T}\beta3^{V9'T}$, suggesting that the effect of the mutation is still progressive, although nearing saturation. i.e. 41.6 / 17.1 and 50.3 / 21.9 are both smaller than 4.14 and 4.68 (the square roots of the dose ratios for $\alpha3^{L9'T}\beta4\beta3^{V9'L}$ and $\alpha3\beta4^{L9'T}\beta3^{V9'L}$).

Figure 4.7.1. Inserting a 9' Thr mutation in both β4 and β3 subunits of 'triplet' $\alpha3\beta4\beta3^{V9'L}$ receptors is equivalent to mutating both α3 and β3

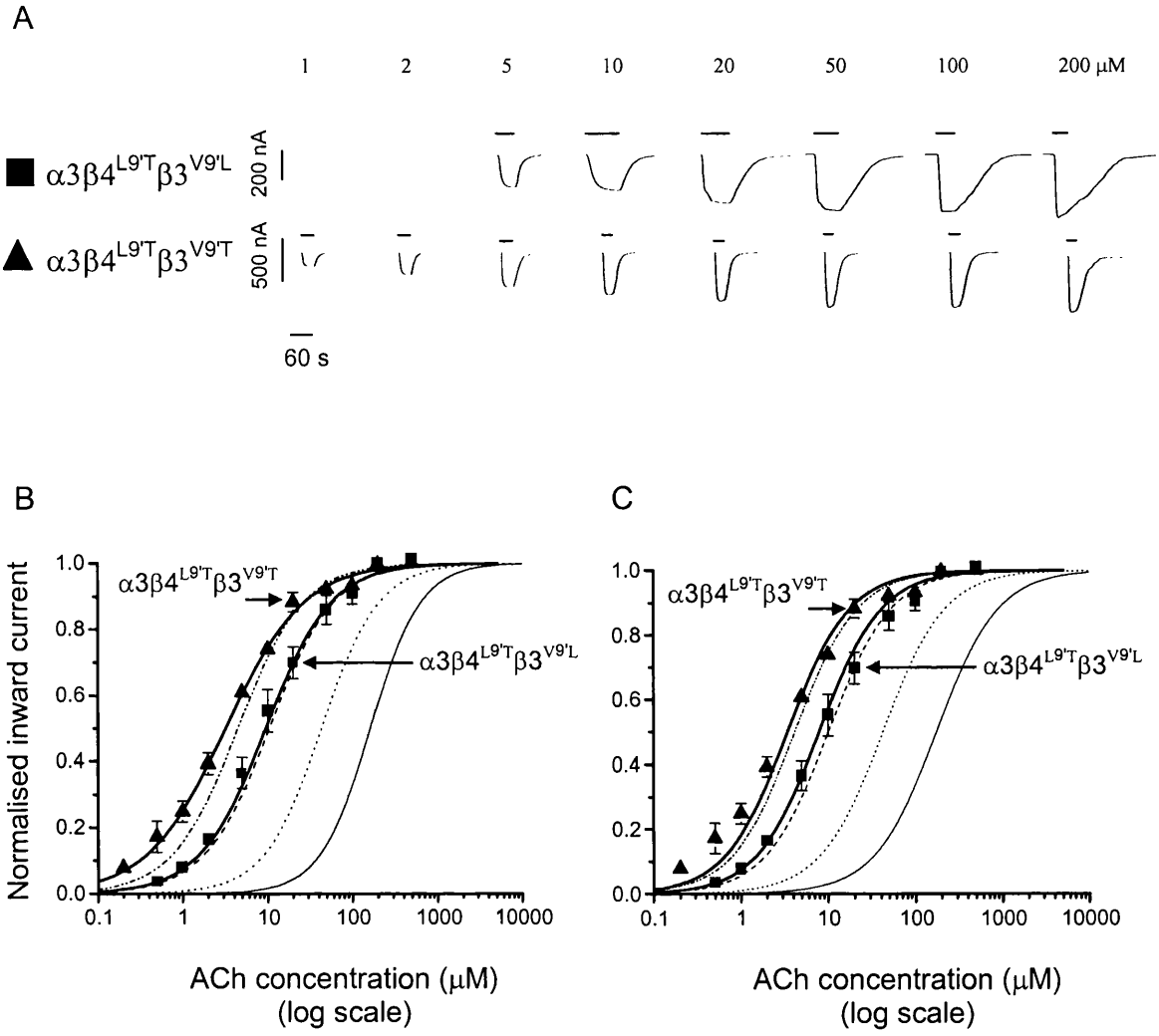

Figure 4.7.1. A, examples of inward currents elicited by a representative range of ACh concentrations (see values above the application bars) in oocytes expressing $\alpha3\beta4^{L9'T}\beta3^{V9'L}$ or $\alpha3\beta4^{L9'T}\beta3^{V9'T}$. B and C show ACh concentration-response curves pooled from experiments such as the ones shown in A (*n* = 4 oocytes). Pooled normalised results were fitted with the Hill equation either as free fit (panel B) or under the constraint of equal slopes (panel C) in order to estimate the horizontal distance between the curves as a dose-ratio (see Table 4.7.2). The concentration-response curves shown refer to oocytes injected with $\alpha3\beta4^{L9'T}\beta3^{V9'L}$ (■) and $\alpha3\beta4^{L9'T}\beta3^{V9'T}$ (▲); bars show standard deviation of the mean (when larger than the symbol). Panels B and C also show for reference (curves with no symbols, reproduced from Figure.2) the concentration-response curves relating to 9' Thr mutations in α3 and/or β3. Note that the effect of mutating β4 is similar to that of mutating α3.

Table 4.7.2. Summary table of 9' Thr mutations in α3, β4 and β3 subunits

	EC_{50} (μM)	n_H	I_H (nA)	*Rundown (%)*	*Dose ratios*	*Square root of dose ratios*	*cube root of dose ratios*	*n*
$\alpha3\beta4\beta3^{V9'L}$	163.1 ± 13.4 [159.5-189.8]	1.47 ± 0.08	230 ± 63.1	82.2 ± 7.2	1			4
$\alpha3\beta4\beta3^{V9'T}$	43.4 ± 2.2 **(*p* 0.003)**	1.28 ± 0.04 (*p* 0.10)	175 ± 23.5 (*p* 0.46)	67.8 ± 7.3 (*p* 0.19)	4.12 [3.77-4.52]			10
$\alpha3^{L9'T}\beta4\beta3^{V9'L}$	10.5 ± 1.4	1.14 ± 0.06 **(*p* 0.02)**	148 ± 56.3 (*p* 0.37)	92.2 ± 19.6 (*p* 0.66)	17.1 [14.9-19.7]	4.14 [3.86-4.44]		4
$\alpha3\beta4^{L9'T}\beta3^{V9'L}$	9.54 ± 2.1 (*p* 0.71)	1.12 ± 0.06 **(*p* 0.02)**	90 ± 15.8 (*p* 0.11)	77.7 ± 21.8 (*p* 0.86)	21.9 [18.6-25.6]	4.68 [4.31-5.06]		4
$\alpha3^{L9'T}\beta4\beta3^{V9'T}$	4.49 ± 0.37	1.13 ± 0.04 **(*p* 0.02)**	80 ± 20.4 (*p* 0.09)	88.6 ± 17.1 (*p* 0.75)	41.6 [37.6-46.0]		3.46 [3.35-3.58]	4
$\alpha3\beta4^{L9'T}\beta3^{V9'T}$	3.22 ± 0.53 (*p* 0.10)	0.94 ± 0.04 **(*p* 0.004)**	83 ± 23 (*p* 0.10)	119.0 ± 11.0 (*p* **0.05**)	50.3 [43.7-58.0]		3.69 [3.52-3.87]	4

Table 4.7.2. A summary of the fitted data: EC_{50}, I_{max} and n_H are the mean (± S.D. of mean) of parameter estimates obtained by fitting separately each concentration-response curve with a Hill equation. I_H is the mean (± S.D. of mean) holding current recorded at the start of the experiment. Rundown is the % (± S.D. of mean) of the response of the initial standard observed when the standard was applied at the end of the experiment. Dose ratios were estimated from fits in which curves were constrained to have the same slope (summarised in see panel C of figure 4.7.1) for comparison with other mutant curves, in order to estimate the horizontal distance between the curves as a dose-ratio, where $\alpha3\beta4\beta3^{V9'L}$ = 1. The same parallel fits allowed estimation of 2.01-unit likelihood intervals (in square brackets under the means of the parameters they refer to; see Methods section): these are equivalent to 95 % confidence intervals. *p* values are the result of a two-tailed *t*-test assuming unequal variance, comparing the Hill slope, initial holding current and extent of rundown of all mutant combinations and the EC_{50} of $\alpha3\beta4\beta3^{V9'T}$, with the $\alpha3\beta4\beta3^{V9'L}$ 'control'. The EC_{50} values of double and triple mutants are compared as indicated, in order to test equivalence of the mutation copy number. Here *p* values of 0.05 or less were taken to indicate a significant difference.

Figure 4.7.3. Relation between ACh EC_{50} and putative number of 9' Thr mutations

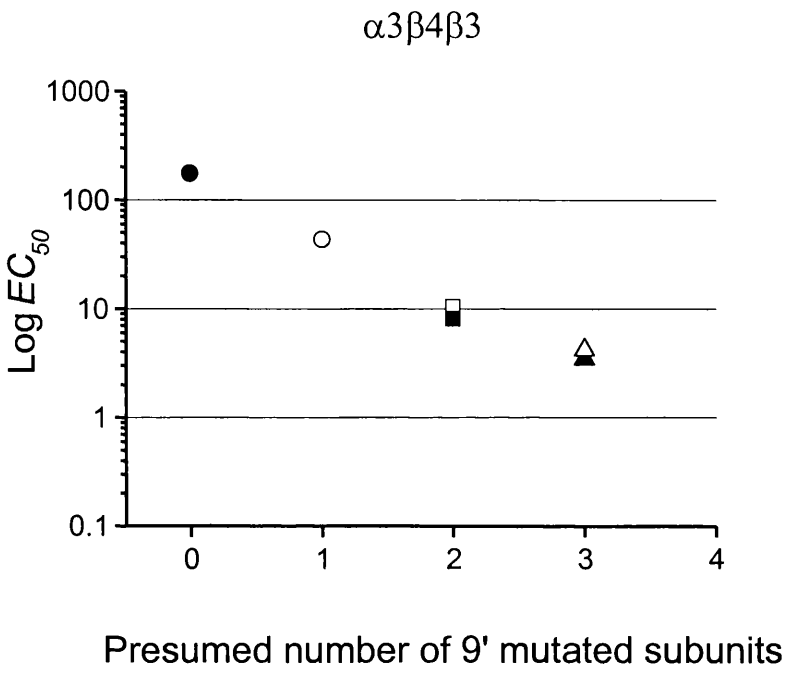

Figure 4.7.3. EC_{50} values for the various α3β4β3 9' Thr mutants are plotted on a log scale against the presumed number of mutated subunits in receptor complex. This number was calculated on the basis of a stoichiometry of 2:2:1 for α3β4β3. The symbols refer to $\alpha3\beta4\beta3^{V9'L}$ (●), $\alpha3\beta4\beta3^{V9'T}$ (○), $\alpha3^{L9'T}\beta4\beta3^{V9'L}$ (□), $\alpha3\beta4^{L9'T}\beta3^{V9'L}$ (■), $\alpha3^{L9'T}\beta4\beta3^{V9'T}$ (Δ) and $\alpha3\beta4^{L9'T}\beta3^{V9'T}$ (▲). Note the approximate linearity of the decline in EC_{50} as the presumed mutation copy number increases.

4.8. Expression of β3 alone or with either α3 or β4

As discussed previously, little is known about the expression of mutant subunits alone. Furthermore, wildtype combinations of α or β subunits co-expressed with wildtype β3 as α/β3 or β/β3 do not form functional receptors. However, there is no data on α/β3 or β/β3 mutants. Hence, I carried out a series of control experiments, injecting β3 alone (wild-type or mutant, namely β3, $\beta3^{V9'L}$, $\beta3^{V9'T}$) or in 'pair' combinations with either α3 (α3β3, $\alpha3\beta3^{V9'L}$, $\alpha3\beta3^{V9'T}$, $\alpha3^{L9'T}\beta3$, $\alpha3^{L9'T}\beta3^{V9'L}$, $\alpha3^{L9'T}\beta3^{V9'T}$,) or β4 (β4β3, $\beta4\beta3^{V9'L}$, $\beta4\beta3^{V9'T}$, $\beta4^{L9'T}\beta3$, $\beta4^{L9'T}\beta3^{V9'L}$, $\beta4^{L9'T}\beta3^{V9'T}$, 10 ng total). These experiments did not result in the expression of functional nAChRs (i.e. current responses to 1 mM ACh were less than 1 nA; n = 5-6 for each combination tested; total cRNA injected 10 ng; 1:1 ratio for the pairwise combinations). In non-injected oocytes responses to 1 mM ACh were also negligible (less than 1 nA, n = 5). These results are summarised in table 4.8.1.

Comparing the initial holding currents for wildtype and mutant single subunits and non-functional pairs in a two-tailed *t*-test assuming unequal variance, revealed no significant change in holding current. For example, oocytes injected with α3β3 had a mean initial holding current of 94 ± 25 nA vs. 102 ± 20 nA for oocytes injected with $\alpha3^{L9'T}\beta3^{V9'T}$ (*p* 0.92; see table 4.8.1.).

Table 4.8.1. Expression of β3 alone or with either α3 or β4

	Mean *IH*	Mean Response to 1 mM ACh (nA)	*n*	batches
β3	52 ± 20	<1	5	5
$\beta3^{V9'L}$ (*p* 0.88)	56 ± 13	<1	5	2
$\beta3^{V9'T}$ (*p* 0.89)	56 ± 14	<1	5	2
α3β3	94 ± 25	<1	5	1
$\alpha3\beta3^{V9'L}$ (*p* 0.64)	44 ± 5	<1	5	1
$\alpha3\beta3^{V9'T}$ (*p* 0.12)	108 ± 12	<1	5	1
$\alpha3^{L9'T}\beta3$ (*p* 0.60)	58 ± 16	<1	5	1
$\alpha3^{L9'T}\beta3^{V9'L}$ (*p* 0.95)	96 ± 25	<1	5	1
$\alpha3^{L9'T}\beta3^{V9'T}$ (*p* 0.92)	102 ± 20	<1	6	2
β4β3	96 ± 21	<1	5	1
$\beta4\beta3^{V9'L}$ (*p* 0.13)	132 ± 49	<1	5	2
$\beta4\beta3^{V9'T}$ (*p* 0.25)	70 ± 36	<1	5	1
$\beta4^{L9'T}\beta3^{wt}$ (*p* 0.74)	48 ± 24	<1	5	1
$\beta4^{L9'T}\beta3^{V9'L}$ (*p* 0.22)	90 ± 29	<1	5	1
$\beta4^{L9'T}\beta3^{V9'T}$ (*p* 0.28)	100 ± 32	<1	5	2

Table 4.8.1. Mean *IH* = Mean initial holding current (± S.D. of the mean) at the start of the experiment. *p* is the result of a 2 tail *t*-test assuming unequal variance, comparing wild-type values to the indicated mutant subunit combination. Here *p* values of 0.05 or less were taken to indicate a significant difference.

4.9. Discussion

The α3β4 data showed that the assumptions of the reporter mutation approach to stoichiometry are satisfied in this type of 'pair' neuronal nAChR. The data on α3β4β3 'triplet' receptors show that mutations in α3 or β4 are equivalent in effect, and that they shift the ACh dose-response curve to the left by an amount log(*r*) (where *r* is the dose ratio of Table 4.4.3.) that is approximately twice the shift observed if β3 is mutated. If

the mutation is inserted in *both* the β3 *and* the α3 (or β4) subunits, the magnitude of the resulting log (*r*) shift is approximately the sum of the shifts caused by each mutation separately, although some reduction in the magnitude of the shift is observed. A possible explanation for this is the reduced contribution of the desensitised state in receptors with high copy numbers of the 9' mutation. A decrease in the extent of desensitisation would be expected to increase the observed agonist EC_{50} (shifting the concentration response curve to the right), counteracting the effect of the mutation on agonist efficacy (see chapter 5).

Thus each additional mutation has a similar effect in neuronal nAChR, irrespective of the number of mutations already incorporated in the pore as seen for the α3β4 'pair' (again see the linearity of plot in Figure 4.7.3.). Given this independent and progressive effect of the 9' mutation, the equal shifts in the ACh EC_{50} produced by mutating either α3 or β4, indicates that α3 and β4 must be present in the same copy number. Because the nAChR is a pentamer, α3, β4 and β3 subunits can only be present in a 2:2:1 ratio.

4.9.1. The slope of the ACh concentration-response curves in mutant receptors

The greatest shifts in agonist sensitivity (*i.e.* those observed in $\alpha3^{L9'T}\beta4\beta3^{V9'T}$, $\alpha3\beta4^{L9'T}\beta3^{V9'T}$) were associated with a significant decrease in the slope of the concentration-response curves (see table 4.7.2.). Such changes often result from receptor heterogeneity (the EC_{50}s for two receptor types have to differ by something approaching 100-fold before the presence of two components becomes detectable in dose-response curves, if the Hill coefficient values are similar to those observed for this type of receptors). While this explanation cannot be discounted in principle for our data, it is difficult to see why receptor heterogeneity should increase with the increase in

the number of mutant subunits in the receptor, particularly since the decrease in slope is not limited to the 'triplet' receptors, but can be observed for the α3β4 'pair' receptors (see the $\alpha3\beta4^{L9'T}$ curve, chapter 3, figure 3.2.2.). Another more likely explanation is that the slope decreases because monoliganded openings contribute more current as the proportion of mutant subunits in the receptor rises. Monoliganded openings are known to occur in muscle nAChRs (although they are relatively rare at all but the lowest concentrations, Colquhoun & Sakmann, 1985); their contribution to the total current can be expected to increase with mutation number, if the reporter mutation does indeed destabilise the closed state. A receptor which needs the binding of only a single agonist molecule to open can be expected to give rise to an equilibrium dose-response curve with a slope of one. Hence, a greater contribution of monoliganded openings can be expected to make the curve shallower. Similar effects were observed by Chang & Weiss (1998) in $GABA_A$ receptors.

These observations substantiate our conclusions that the subunit stoichiometry in the α3β4β3 triplet is indeed 2:2:1. This stoichiometry fits in well with what is known of non-homomeric neuronal nAChR, namely that their pentameric structure contains at least two agonist binding sites, each requiring the presence of an α subunit; as in the muscle nAChR (Colquhoun & Sakmann, 1985), it is likely that both binding sites must be occupied for channel opening to occur effectively. The presence of at least two binding sites (which on average must be occupied for the channel to open) is in good accord with the observation of a Hill slope greater than 1 (1.42 for the wild-type triplet). It is unlikely that β3 can play the role of an α subunit with respect to agonist binding, given that the sequence of the β3 presumed binding domains is very similar to that of the other β subunits.

4.9.2. The rundown of mutant receptors

Comparing the extent of rundown in mutant receptors with $\alpha3\beta4\beta3^{V9'L}$ in a two-tailed *t*-test assuming unequal variance, revealed a significant reduction in the extent of rundown for $\alpha3\beta4^{L9'T}\beta3^{V9'T}$. Here the mean extent of rundown in $\alpha3\beta4\beta3^{V9'L}$ was 82.2 ± 7.2 % vs. 119.0 ± 11.0 % for oocytes expressing $\alpha3\beta4^{L9'T}\beta3^{V9'T}$ (p 0.05; see table 4.7.2.), indicating a significant potentiation compared to the $\alpha3\beta4\beta3^{V9'L}$ 'control'. Kuryatov *et al.* (1997) and Figl *et al.* (1998) report a similar use dependant potentiating effect for 6' serine to phenylalanine mutations inserted in rat α4 when co-expressed with wildtype β2 in oocytes. Figl *et al.* (1998) propose that this potentiation is the result of use dependant unblocking of mutant receptors. Thus inserting the 9' mutation in β3 in combination with β4 may create a novel binding site for a molecule to block the channel in the closed state. Such a blocker would be expected to have high affinity for the closed state and hence repeated activation of mutant receptors would release the block, producing a progressive potentiation as the block is removed and more channels become active. Further, such a potentiation would be more pronounced at the low agonist concentrations used for the control response, where P_{open} is small.

Chapter 5: Stoichiometry of 'triplet' α3β4α5 neuronal nicotinic acetylcholine receptors

The next aim of the project was to see if the 2:2:1 stoichiometry of 'triplet' receptors containing the β3 subunit applies to 'triplet' receptors containing the α5 subunit.

As discussed in chapter 1, α5 and β3 are very similar in amino acid sequence and are classed together in tribe III-3 of the evolutionary 'nAChR tree' (Corringer *et al.*, 2000). A further similarity with β3 is the fact that α5 can only form functional receptors when expressed together with an α/β 'pair', forming an αβα5 'triplet' receptor (Ramirez-Latorre *et al.*, 1996; Wang *et al.*, 1996). In this chapter we extend the reporter mutation strategy used for β3 to nAChRs containing α5.

5.1. Co-expression of wild-type α5 does not affect the ACh sensitivity of α3β4 'pair' nAChRs

Full concentration response curves were obtained by bath-application of ACh to oocytes expressing 'triplet' α3β4α5 wild type (figure 5.1.1.) or mutant receptors (figs 5.2.1 – 5.7.3) using the protocol described in chapter 2. Example responses from one oocyte expressing 'triplet' α3β4α5 wild type or mutant receptors are shown in panel A of figure 5.2.1.

The resulting concentration response curves were then fitted as previously discussed in chapter 3 to determine the EC_{50}, I_{max} and Hill slope values for each experiment. The mean and standard error of the mean values for all fitted parameters (EC_{50}, I_{max} and Hill slope) are shown in panel C of figs 5.2.1 - 5.7.3. Average responses normalised to the maximum for each oocyte are shown as the data points and the resulting fitted curve in panel B of figs 5.2.1 - 5.7.3.

As previously reported by Wang and co-authors (1996), expressing the α5 subunit together with α3 and β4 had no apparent effect on the α3β4 'pair' ACh concentration-response curve, making it difficult to be sure of incorporation of α5 (see figure 5.1.1.). Mean EC_{50} values were similar, 180 ± 17.0 μM ACh for the α3β4 'pair' and 207 ± 25.6 μM ACh (p 0.40, see table 5.7.4.) for the α3β4α5^{wt} 'triplet' (see panel C of figure 5.1.1.). Thus, the incorporation of α5 is not obvious from a first glance at the dose-response relationship.

The ACh concentration-response curve of oocytes expressing α3β4 + α5 has a significantly shallower mean Hill slope than the α3β4 'pair' (1.39 ± 0.08 vs. 1.81 ± 0.09 respectively, p 0.01; see panel C of figure 5.1.1. and table 5.3.3.). Furthermore, the time course of ACh responses recorded from oocytes expressing all three subunits was clearly different from that of α3β4 'pair' receptors. Such 'triplet' responses (shown in panel A of figure 5.1.2.) had a much faster 'sag' to the sustained application of high ACh concentrations (indicating faster desensitisation, as noted by Wang *et al.* 1996 and Gerzanich *et al.* 1998).

Comparing the holding curret, I_{max} and extent of rundown in oocytes expressing α3β4α5^{wt} with α3β4 in a two-tailed t-test assuming unequal variance, revealed a significant reduction in the extent of rundown when co-expressing α5 wildtype. The mean extent of rundown in α3β4 was 25.4 ± 4.2 % vs. 74.3 ± 15.3 % for oocytes expressing α3β4α5^{wt} (p 0.004; see table 5.7.4.).

Figure 5.1.1. Co-expression of wild-type α5 does not affect the ACh sensitivity of α3β4 'pair' nAChRs

A

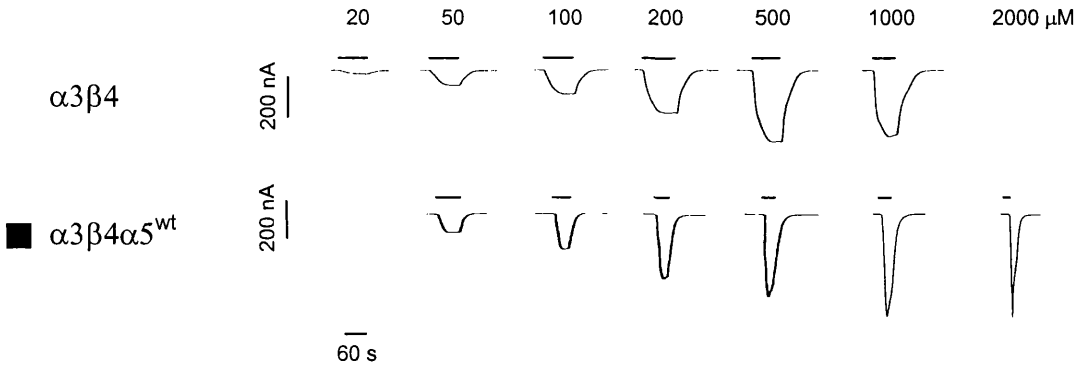

B

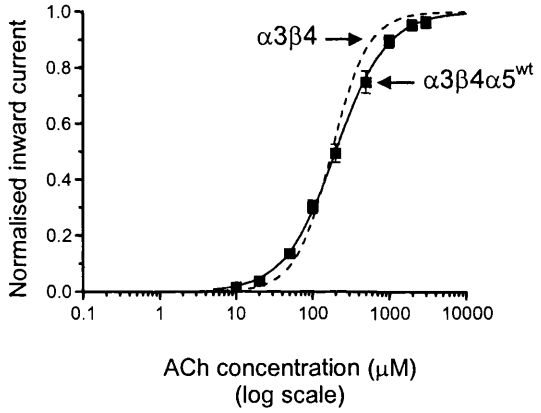

C

	EC_{50} (μM)	I_{max} (nA)	n_H	I_H (nA)	*Rundown (%)*	*No. of batches*	*n*
α3β4	180 ± 17.0	1430 ± 425	1.81 ± 0.09	184 ± 57.2	25.4 ± 4.2	2	7
α3β4α5^{wt}	207 ± 25.6	1098 ± 245	1.39 ± 0.08	126.0 ± 33.1	74.3 ± 15.3	2	5

Figure 5.1.1. A shows examples of inward currents elicited by bath-applied ACh in oocytes expressing α3β4 or α3β4α5^{wt}. B shows ACh concentration-response curves pooled from experiments such as the ones shown in A: Pooled normalised results were fitted with the Hill equation as a free fit (panel B; see chapter 3). The concentration-response curves refer to oocytes injected with α3β4α5^{wt} (■). B also shows for reference (dashed curve with no symbols, reproduced from figure 3.1.1) the concentration response curve relating to α3β4. C shows a summary of the fitted parameters: EC_{50}, I_{max} and n_H are the mean (± S.D. of mean) of parameter estimates obtained by fitting separately each concentration-response curve with a Hill equation. I_H is the mean (± S.D. of mean) holding current recorded at the start of the experiment. Rundown is the % (± S.D. of mean) of the response of the initial standard observed when the standard was applied at the end of the experiment. No. of batches are the number of oocyte batches used.

5.2. Inserting a 9' Leu in α5 does not affect the ACh sensitivity of α3β4 'pair' nAChRs

As previously discussed for 'triplet' receptors containing the β3 subunit (see Chapter 4), we mutated the 9' Val residue of α5 to Leu in order to start off with a receptor containing only Leu residues in 9'.

The insertion of the 9' Leu mutation in the α5 subunit of α3β4α5 'triplet' receptors did not change the ACh EC_{50} of the 'triplet', which remained indistinguishable from the α3β4 'pair'. Mean ACh EC_{50} values were 206 ± 15.5 μM (see figure 5.3.1) compared to 180 ± 17.0 μM for the α3β4 'pair' (p 0.28, see table 5.7.4.) and 207 ± 25.6 μM for the $\alpha3\beta4\alpha5^{wt}$ 'triplet' (figure 5.3.2., table 5.3.3).

Once again the time course of the responses showed a fast sag at the higher concentrations of ACh, in all likelihood indicating an increase in the rate of desensitisation, compared to both the α3β4 'pair' and the α3β4α5 wild type 'triplet' (see panel A figure 5.3.2). Thus the only noticeable effect of the presence of the α5 subunit in α3β4α5 receptors was a change in the shape of the response to high agonist concentrations, irrespective of the nature of the hydrophobic residue in the 9' position of α5.

Comparing the Hill slope, holding curret, I_{max} and extent of rundown in oocytes expressing $\alpha3\beta4\alpha5^{V9'L}$ with α3β4 in a two-tailed t-test assuming unequal variance, revealed a significant reduction in *both* the Hill slope and the extent of rundown when co-expressing $\alpha5^{V9'L}$. The mean Hill slope for α3β4 was 1.81 ± 0.09 vs. 1.47 ± 0.05 for oocytes expressing $\alpha3\beta4\alpha5^{V9'L}$ (p 0.01; see table 5.7.4.). The mean extent of rundown in α3β4 was 25.4 ± 4.2 % vs. 95.5 ± 17.0 % for oocytes expressing $\alpha3\beta4\alpha5^{V9'L}$ (p 0.013; see table 5.7.4.).

Figure 5.2.1. Inserting a 9' Leu in α5 does not affect the ACh sensitivity of α3β4 'pair' nAChRs

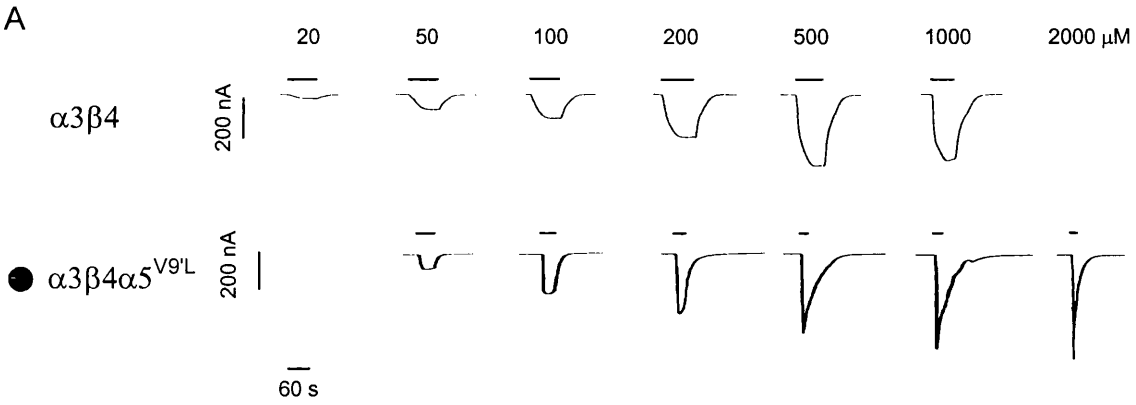

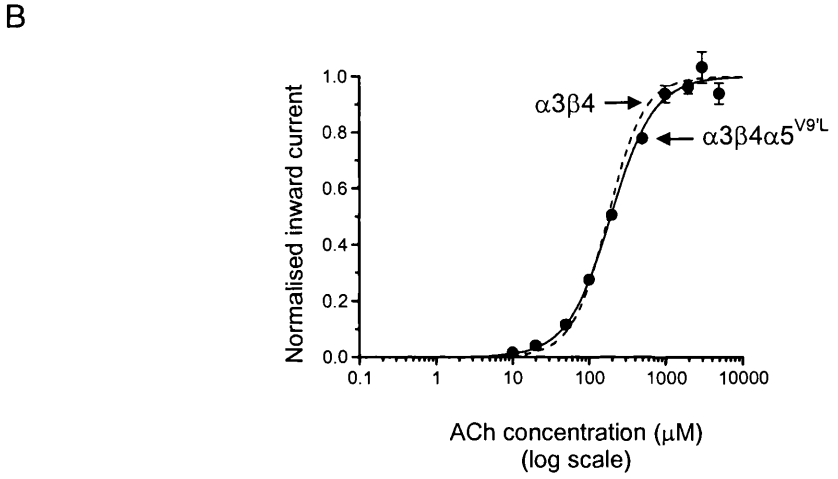

C

	EC_{50} (μM)	I_{max} (nA)	n_H	I_H (nA)	*Rundown (%)*	*No. of batches*	*n*
α3β4	180 ± 17.0	1430 ± 425	1.81 ± 0.09	184 ± 57.2	25.4 ± 4.2	2	7
$\alpha3\beta4\alpha5^{V9'L}$	206 ± 15.5	966 ± 367	1.47 ± 0.05	96.0 ± 31.1	95.5 ± 17.0	3	5

Figure 5.2.1. A shows examples of inward currents elicited by bath-applied ACh in oocytes expressing α3β4 or $\alpha3\beta4\alpha5^{V9'L}$. Note the change in time course of the responses to high concentrations (500 – 2000 μM) of ACh in oocytes expressing $\alpha3\beta4\alpha5^{V9'L}$ compared to α3β4. B shows ACh concentration-response curves pooled from experiments such as the ones shown in A: Pooled normalised results were fitted with the Hill equation as a free fit (panel B; see chapter 3). The concentration-response curves refer to oocytes injected with $\alpha3\beta4\alpha5^{V9'L}$ (●). B also shows for reference (dashed curve with no symbols, reproduced from figure 3.1.1) the concentration response curve relating to α3β4. Note the close similarity between the curves.

Figure 5.2.2. Comparing the effect of $\alpha5^{wt}$ and $\alpha5^{V9'L}$ on the ACh sensitivity of $\alpha3\beta4$ nAChRs

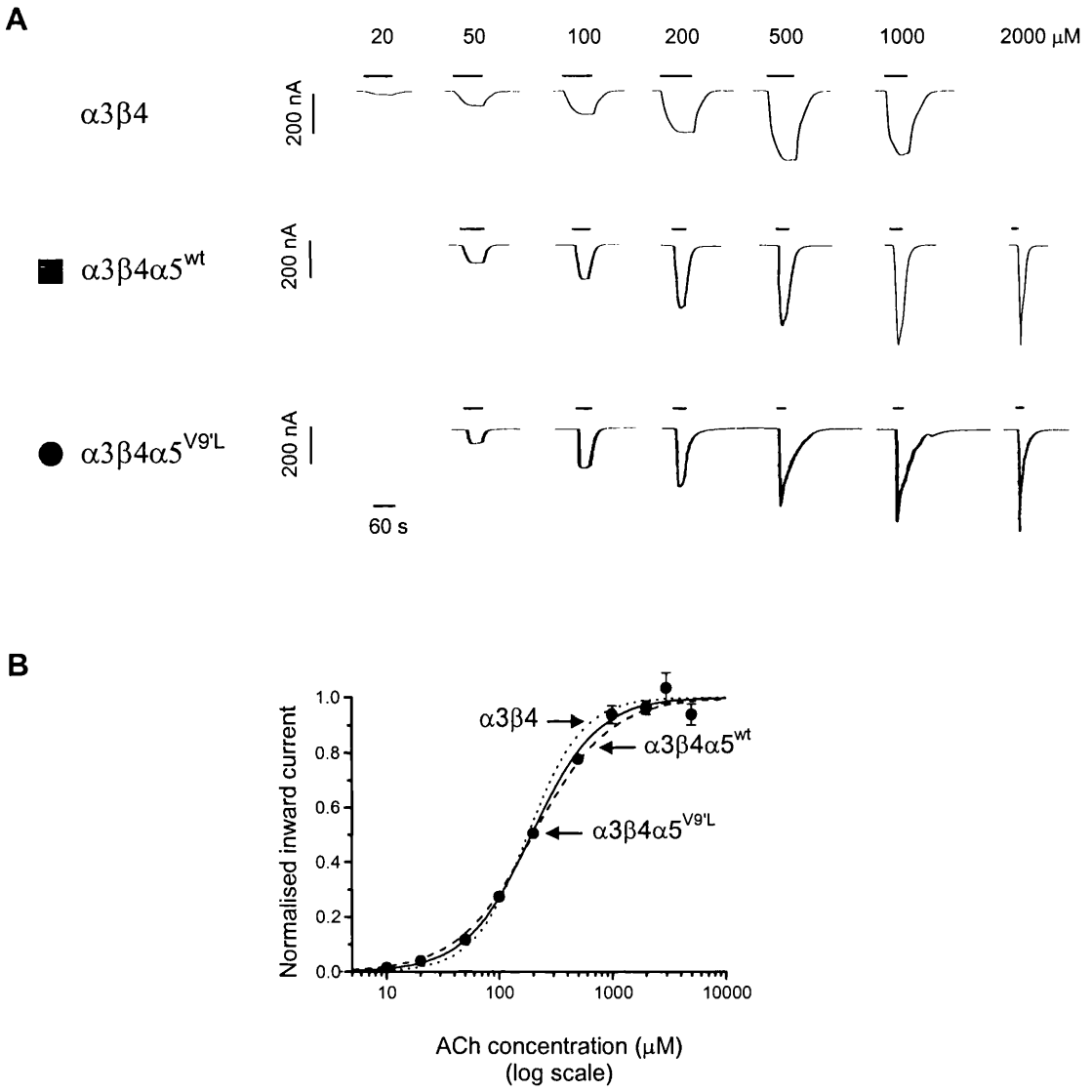

Figure 5.2.2. A shows examples of inward currents elicited by bath-applied ACh in oocytes expressing $\alpha3\beta4$, $\alpha3\beta4\alpha5^{wt}$ or $\alpha3\beta4\alpha5^{V9'L}$. Note the change in time course of the responses to high concentrations (500 – 2000 μM) of ACh in oocytes expressing $\alpha3\beta4\alpha5^{V9'L}$ compared to $\alpha3\beta4\alpha5^{wt}$. B shows ACh concentration-response curves pooled from experiments such as the ones shown in A: Pooled normalised results were fitted with the Hill equation as a free fit (panel B; see chapter 3). The concentration-response curves refer to oocytes injected with $\alpha3\beta4\alpha5^{wt}$ (dashed curve with no symbols) and $\alpha3\beta4\alpha5^{V9'L}$ (●). B also shows for reference (dotted curve with no symbols, reproduced from figure 3.1.1) the concentration response curve relating to $\alpha3\beta4$. Note the close similarity between the curves.

5.3. Inserting a 9' Thr in α5 does not affect the ACh sensitivity of nAChRs resulting from expression of $\alpha3\beta4\alpha5^{V9'L}$

In order to confirm the incorporation of α5 into an α3β4α5 'triplet' and to establish what proportion of current –if any- is due to the α3β4 'pair', we inserted a 9' Thr reporter mutation in α5 (as we did for the β3 subunit, see chapter 4). As discussed in chapter 4, all subunits belonging to the nAChR superfamily bear a hydrophobic amino acid in this position (termed 9'), namely a leucine or (in the case of α5 and β3) a valine. Mutation of this 9' residue to a hydrophilic amino acid, such as threonine or serine, is known to increase the agonist sensitivity (Revah *et al.*, 1991). The magnitude of this increase is proportional to the number of copies of the mutation incorporated into the receptor for muscle nAChRs (Labarca *et al.*, 1995). The data presented in chapters 3 and 4 indicate that this approximately holds, up to a mutation copy number of three, in α3β4 'pair' and α3β4β3 'triplet' neuronal nAChRs.

Surprisingly, we found that inserting a 9' Thr mutation in α5 had little effect on the properties of nAChRs produced by oocytes injected with α3, β4 and $\alpha5^{V9'T}$. Such receptors were indistinguishable from either wild-type 'triplet' receptors or from 'pair' α3β4 receptors in their sensitivity to ACh. Mean ACh EC_{50} values were 183 ± 11.0 μM (see figure 5.2.1) compared to 180 ± 17.0 μM for the α3β4 'pair' (p 0.89, see table 5.7.4.) and 207 ± 25.6 μM ACh for the $\alpha3\beta4\alpha5^{wt}$ 'triplet' (figure 5.2.2, Table 5.2.3). The only noticeable difference was in the time course of the responses to high ACh concentrations, which, in the $\alpha5^{V9'T}$ mutant, lost the fast desensitisation which is seen in receptors containing $\alpha5^{wt}$ or $\alpha5^{V9'L}$ (see panel A, figure 5.2.2).

Comparing the Hill slope, holding current, I_{max} and extent of rundown in oocytes expressing $\alpha3\beta4\alpha5^{V9'T}$ with $\alpha3\beta4$ in a two-tailed *t*-test assuming unequal variance, revealed a significant reduction in *both* the Hill slope and the extent of rundown when co-expressing $\alpha5^{V9'T}$. The mean Hill slope for $\alpha3\beta4$ was 1.81 ± 0.09 vs. 1.19 ± 0.08 for oocytes expressing $\alpha3\beta4\alpha5^{V9'T}$ (*p* 0.002; see table 5.7.4.). The mean extent of rundown in $\alpha3\beta4$ was 25.4 ± 4.2 % vs. 74.5 ± 12.3 % for oocytes expressing $\alpha3\beta4\alpha5^{V9'T}$ (*p* 0.005; see table 5.7.4.).

Figure 5.3.1. Inserting a 9' Thr in α5 does not affect the ACh sensitivity of α3β4 'pair' nAChRs

A

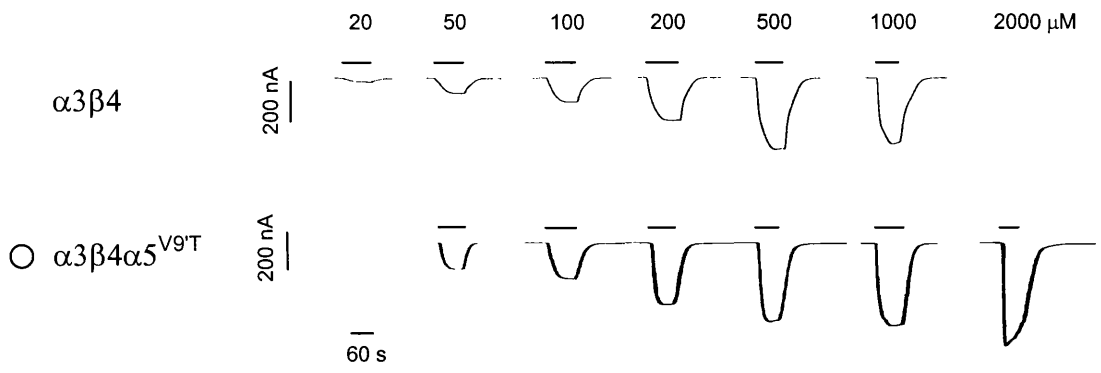

B

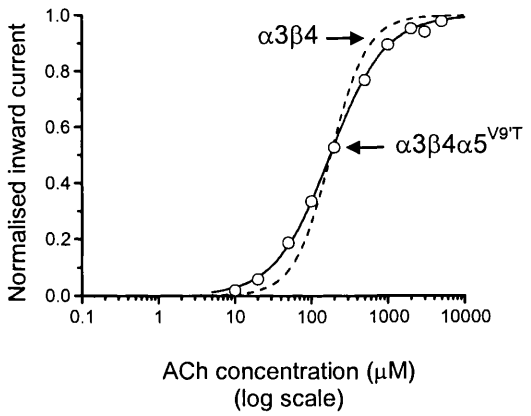

C

	EC_{50} (μM)	I_{max} (nA)	n_H	I_H (nA)	*Rundown (%)*	*No. of batches*	*n*
α3β4	180 ± 17.0	1430 ± 425	1.81 ± 0.09	184 ± 57.2	25.4 ± 4.2	2	7
$\alpha3\beta4\alpha5^{V9'T}$	183 ± 11.0	646 ± 97.8	1.19 ± 0.08	73.8 ± 19.2	74.5 ± 12.3	4	7

Figure 5.3.1. A shows examples of inward currents elicited by bath-applied ACh in oocytes expressing α3β4 or $\alpha3\beta4\alpha5^{V9'T}$. B shows ACh concentration-response curves pooled from experiments such as the ones shown in A: Pooled normalised results were fitted with the Hill equation as a free fit (panel B; see chapter 3). The concentration-response curves refer to oocytes injected with $\alpha3\beta4\alpha5^{V9'T}$ (○). B also shows for reference (dashed curve with no symbols, reproduced from figure 3.1.1) the concentration response curve relating to α3β4. Note the close similarity between the curves.

Figure 5.3.2. Mutations in the 9' position of α5 do not change the ACh sensitivity of α3β4 'pair' receptors

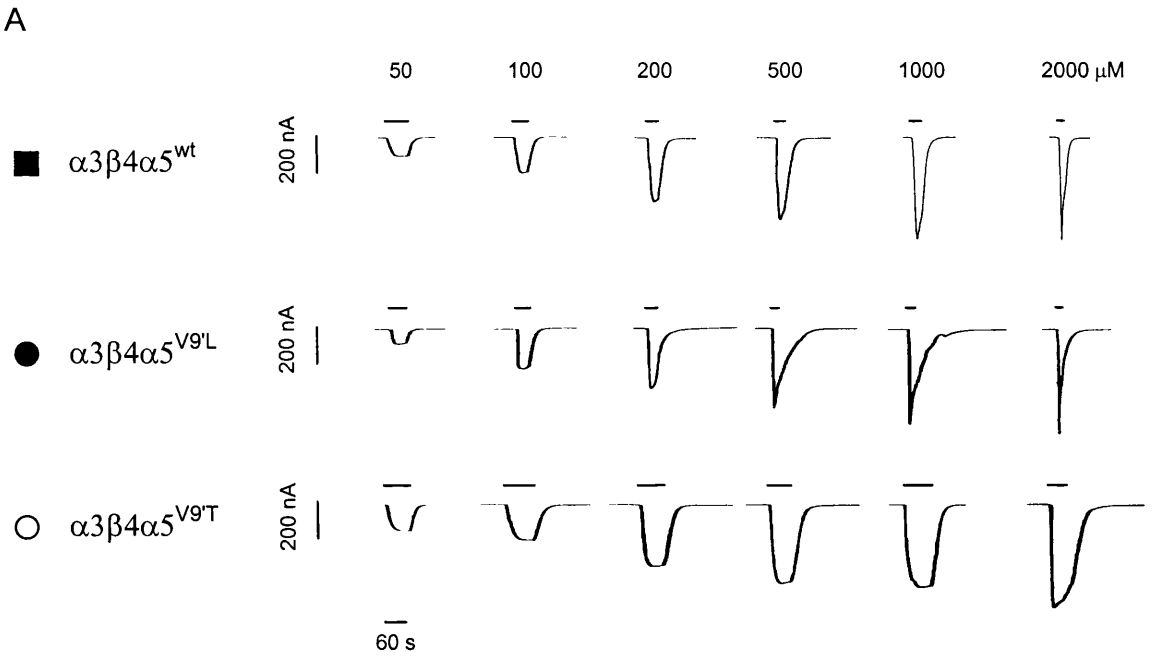

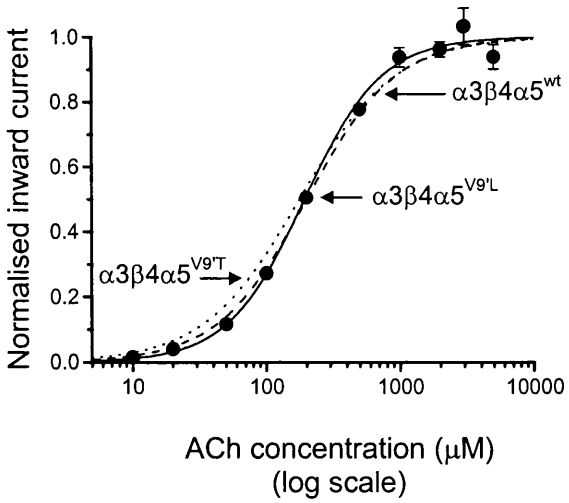

Figure 5.3.2 A shows examples of inward currents elicited by bath-applied ACh in oocytes expressing $\alpha3\beta4\alpha5^{wt}$, $\alpha3\beta4\alpha5^{V9'L}$ or $\alpha3\beta4\alpha5^{V9'T}$. Note the difference in time course of the responses to high concentrations (500 – 2000 μM) of ACh in oocytes expressing $\alpha3\beta4\alpha5^{wt}$, $\alpha3\beta4\alpha5^{V9'L}$ or $\alpha3\beta4\alpha5^{V9'T}$. B shows ACh concentration-response curves pooled from experiments such as the ones shown in A: Pooled normalised results were fitted with the Hill equation as a free fit (panel B; see chapter 3). The concentration-response curves refer to oocytes injected with $\alpha3\beta4\alpha5^{wt}$ (■), $\alpha3\beta4\alpha5^{V9'L}$ (●) and $\alpha3\beta4\alpha5^{V9'T}$ (○). B also shows for reference (dashed curve with no symbols, reproduced from figure 3.1.1) the concentration response curve relating to α3β4. Note the close similarity between the curves.

Table 5.3.3. Summary of α3β4α5 'triplet' receptors

	EC_{50} (μM)	I_{max} (nA)	n_H	n
α3β4	180 ± 17.0	1430 ± 425	1.81 ± 0.09	7
$\alpha3\beta4\alpha5^{wt}$	207 ± 25.6 (*p* 0.40)	1098 ± 245	1.39 ± 0.08 (***p* 0.01**)	5
$\alpha3\beta4\alpha5^{V9'L}$	206 ± 15.5 (*p* 0.28)	966 ± 367	1.47 ± 0.05 (***p* 0.01**)	5
$\alpha3\beta4\alpha5^{V9'T}$	183 ± 11.0 (*p* 0.89)	646 ± 97.8	1.19 ± 0.08 (***p* 0.002**)	7

Table 5.3.3. A summary of the fitted data for the concentration response curves from oocytes expressing α3β4, $\alpha3\beta4\alpha5^{wt}$, $\alpha3\beta4\alpha5^{V9'L}$ or $\alpha3\beta4\alpha5^{V9'T}$: EC_{50}, I_{max} and n_H are the mean (± S.D. of mean) of parameter estimates obtained by fitting separately each concentration-response curve with a Hill equation. Note the similar EC_{50} and Hill slope values for all three combinations. No. of batches are the number of oocyte batches used. Where *p* is the result of a 2 tail *t*-test assuming unequal variance, comparing α3β4 values to the indicated subunit combination. Here *p* values of 0.05 or less were taken to indicate a significant difference. Note the significant difference in the Hill slope produced by the co-expression of α5.

5.4. Co-expression of $\alpha5^{wt}$ decreases the ACh sensitivity of $\alpha3\beta4^{L9'T}$ receptors

Co-expressing $\alpha5^{wt}$ or α5 mutants with the α3β4 'pair' did not affect the ACh concentration response curve of α3β4, one possible explanation is that α5 does not form functional α3β4α5 'triplet' receptors in oocytes, as argued by Fucile *et al.* (1997). However, the difference in the time course of the responses between oocytes expressing α3β4 and α3β4 + α5 wild-type, or mutant, would suggest incorporation of α5 into an α3β4α5 'triplet'.

Following on from the stoichiometry experiments with β3, the next set of experiments incorporated 9' Thr mutations into the α3 and β4 subunits of 'triplet' α3β4α5 receptors.

Full ACh concentration response curves were obtained from oocytes expressing $\alpha3\beta4^{L9'T} + \alpha5^{wt}$ (see figure 5.4.1). Comparing $\alpha3\beta4^{L9'T} + \alpha5^{wt}$ ACh concentration response curves with those previously obtained for the $\alpha3\beta4^{L9'T}$ mutant (see Chapter 3) revealed a dramatic 30 fold rightward shift in the ACh concentration response curve for $\alpha3\beta4^{L9'T} + \alpha5^{wt}$, demonstrating the incorporation of α5 into an α3β4α5 'triplet' (see panel B, figure 5.4.1.). Oocytes expressing $\alpha3\beta4^{L9'T} + \alpha5^{wt}$ had mean EC_{50} values of 30.7 ± 1.63 μM ACh compared to 0.75 ± 0.05 μM ACh for $\alpha3\beta4^{L9'T}$ receptors (see panel C, figure 5.4.1). The time course of the responses show a fast sag in their response to the higher concentrations of ACh when compared to $\alpha3\beta4^{L9'T}$ (see panel A, figure 5.4.1).

The aim of the next set of experiments was to determine if this dramatic effect of α5 on the $\alpha3\beta4^{L9'T}$ concentration-response curve was dependent on the nature of the residue in the 9' position of α5.

5.5. The decrease in ACh sensitivity produced by α5 incorporation into $\alpha3\beta4^{L9'T}$ is similar for $\alpha5^{wt}$, $\alpha5^{V9'L}$ & $\alpha5^{V9'T}$

Inserting a 9'Leu in the α5 subunit and co-expressing $\alpha5^{V9'L}$ with $\alpha3\beta4^{L9'T}$, produced a decrease in the ACh sensitivity of $\alpha3\beta4^{L9'T}$ receptors. Oocytes expressing $\alpha3\beta4^{L9'T} + \alpha5^{V9'L}$ had mean EC_{50} values of 29.2 ± 1.57 μM ACh (see figure 5.5.1) compared to 0.75 ± 0.05 μM ACh for $\alpha3\beta4^{L9'T}$ receptors (see figure 5.5.2). Comparison with oocytes expressing $\alpha3\beta4^{L9'T} + \alpha5^{wt}$ indicated that the observed decrease in ACh sensitivity was independent of the residue in the 9' position, with mean ACh EC_{50} values of 30.7 ± 1.63 μM (see figure 5.5.3). The time course of the responses for $\alpha3\beta4^{L9'T}\alpha5^{V9'L}$ show a fast

sag in their response to the higher concentrations of ACh when compared to $\alpha3\beta4^{L9'T}$ (see panel A, figure 5.5.2). Comparing responses from $\alpha3\beta4^{L9'T}\alpha5^{wt}$ with $\alpha3\beta4^{L9'T}\alpha5^{V9'L}$ shows a faster sag in response to the higher concentrations of ACh for $\alpha3\beta4^{L9'T}\alpha5^{wt}$ (see panel A, figure 5.5.3). Thus co-expression of α5 with $\alpha3\beta4^{L9'T}$ causes an approximate 40-fold change in ACh sensitivity, increasing the ACh EC_{50} from approximately 0.75 μM to approximately 30 μM, irrespective of whether α5 carried a V, an L or a T residue in 9'.

5.6. Co-expression of $\alpha5^{wt}$ decreases the ACh sensitivity of $\alpha3^{L9'T}\beta4$ receptors

Co-expressing $\alpha5^{wt}$ with $\alpha3^{L9'T}\beta4$ produced a decrease in the ACh sensitivity of $\alpha3^{L9'T}\beta4$ receptors, producing a rightward shift in the ACh concentration response curve (figure 5.6.2). Oocytes expressing $\alpha3^{L9'T}\beta4 + \alpha5^{wt}$ had mean EC_{50} values of 22.7 ± 2.02 μM ACh (figure 5.6.1) compared to 5.8 ± 1.0 μM ACh for $\alpha3^{L9'T}\beta4$ (p 0.001, see table 5.7.4. and figure 5.6.2). Comparison with oocytes expressing $\alpha3\beta4^{L9'T} + \alpha5^{wt}$ indicated that the observed decrease in ACh sensitivity for $\alpha3^{L9'T}\beta4\alpha5$ was much smaller, i.e. approximately 4 fold (compared to 39 fold for $\alpha3\beta4^{L9'T}\alpha5$; see table 5.7.4.). The time course of the responses for $\alpha3^{L9'T}\beta4\alpha5^{wt}$ show a faster sag in their response to the higher concentrations of ACh when compared to $\alpha3^{L9'T}\beta4$ (see panel A, figure 5.6.2).

Figure 5.4.1. Co-expressing $\alpha5^{wt}$ decreases the ACh sensitivity of $\alpha3\beta4^{L9'T}$

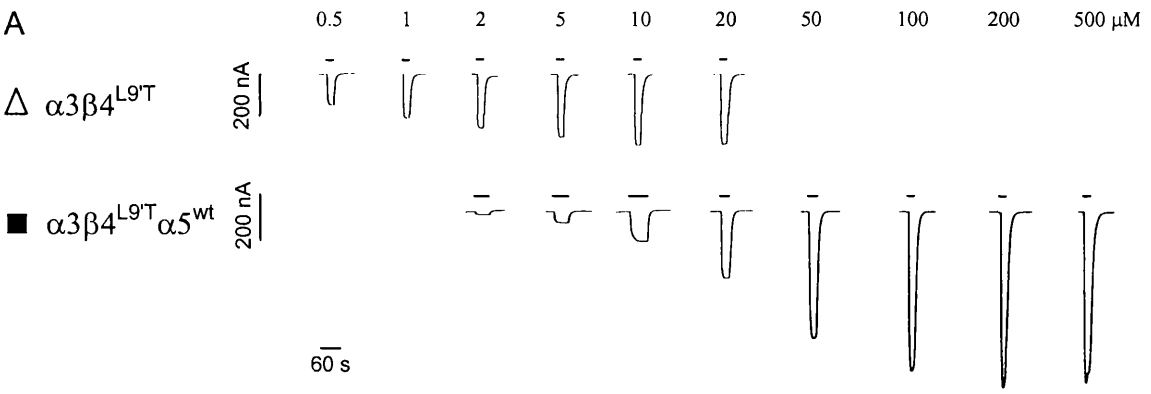

B

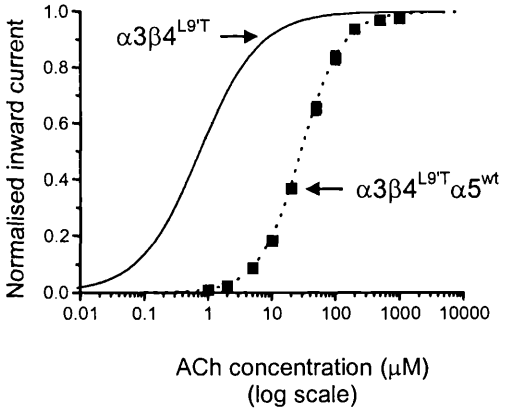

C

	EC_{50} (μM)	I_{max} (nA)	n_H	I_H (nA)	*Rundown (%)*	*No. of batches*	*n*
$\alpha3\beta4^{L9'T}$	0.75 ± 0.05	562 ± 264	0.92 ± 0.08	200 ± 83	77.4 ± 9.5	2	4
$\alpha3\beta4^{L9'T}\alpha5^{wt}$	30.7 ± 1.6	2546 ± 518	1.36 ± 0.10	68.3 ± 39.4	68 ± 8.2	3	6

Figure 5.4.1. A shows examples of inward currents elicited by bath-applied ACh in oocytes expressing $\alpha3\beta4^{L9'T}$ or $\alpha3\beta4^{L9'T}\alpha5^{wt}$. B shows ACh concentration-response curves pooled from experiments such as the ones shown in A: Pooled normalised results were fitted with the Hill equation as a free fit (panel B; see chapter 3). The concentration-response curves refer to oocytes injected with $\alpha3\beta4^{L9'T}\alpha5^{wt}$ (■). B also shows for reference (solid curve with no symbols, reproduced from figure 3.) the concentration response curve relating to $\alpha3\beta4^{L9'T}$. C shows a summary of the fitted parameters: EC_{50}, I_{max} and n_H are the mean (± S.D. of mean) of parameter estimates obtained by fitting separately each concentration-response curve with a Hill equation. I_H is the mean (± S.D. of mean) holding current recorded at the start of the experiment. Rundown is the % (± S.D. of mean) of the response of the initial standard observed when the standard was applied at the end of the experiment. No. of batches are the number of oocyte batches used.

Figure 5.5.1. Co-expressing $\alpha5^{V9'L}$ decreases the ACh sensitivity of $\alpha3\beta4^{L9'T}$

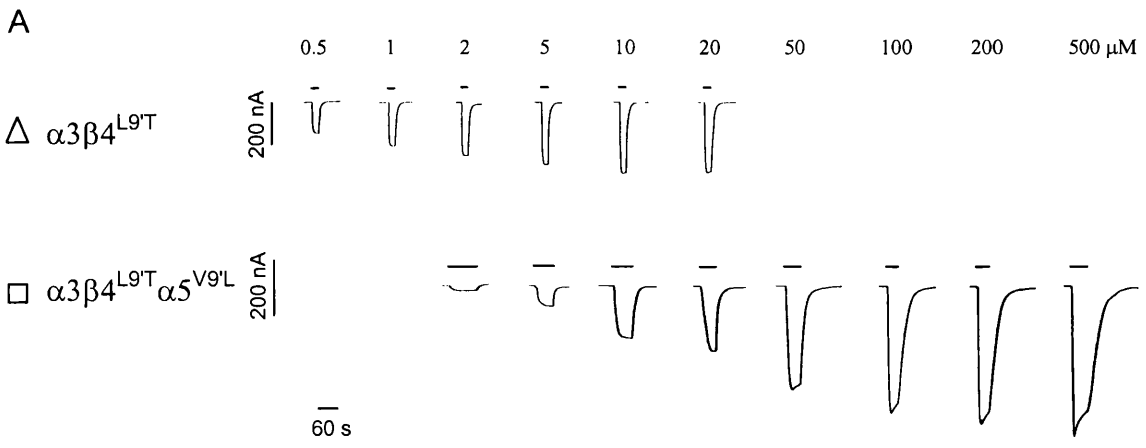

B

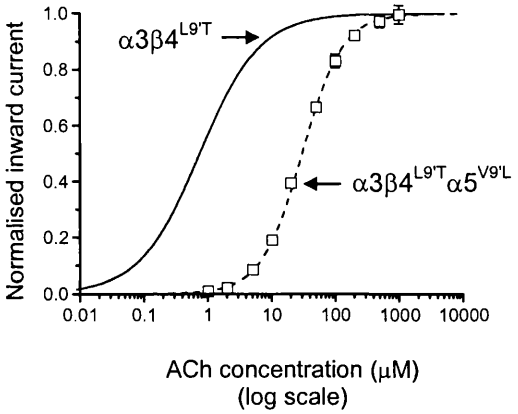

C

	EC_{50} (μM)	I_{max} (nA)	n_H	I_H (nA)	*Rundown (%)*	*No. of batches*	*n*
$\alpha3\beta4^{L9'T}$	0.75 ± 0.05	562 ± 264	0.92 ± 0.08	200 ± 83	77.4 ± 9.5	2	4
$\alpha3\beta4^{L9'T}\alpha5^{V9'L}$	29.2 ± 1.57	792 ± 209	1.31 ± 0.03	76.0 ± 22.9	81.2 ± 8.4	4	5

Figure 5.5.1. A shows examples of inward currents elicited by bath-applied ACh in oocytes expressing $\alpha3\beta4^{L9'T}$ or $\alpha3\beta4^{L9'T}\alpha5^{V9'L}$. B shows ACh concentration-response curves pooled from experiments such as the ones shown in A: Pooled normalised results were fitted with the Hill equation as a free fit (panel B; see chapter 3). The concentration-response curves refer to oocytes injected with $\alpha3\beta4^{L9'T}\alpha5^{V9'L}$ (□). B also shows for reference (solid curve with no symbols, reproduced from figure 3.) the concentration response curve relating to $\alpha3\beta4^{L9'T}$. C shows a summary of the fitted parameters: EC_{50}, I_{max} and n_H are the mean (± S.D. of mean) of parameter estimates obtained by fitting separately each concentration-response curve with a Hill equation. I_H is the mean (± S.D. of mean) holding current recorded at the start of the experiment. Rundown is the % (± S.D. of mean) of the response of the initial standard observed when the standard was applied at the end of the experiment. No. of batches are the number of oocyte batches used.

Figure 5.5.2. Co-expressing $\alpha5^{V9'T}$ decreases the ACh sensitivity of $\alpha3\beta4^{L9'T}$

A

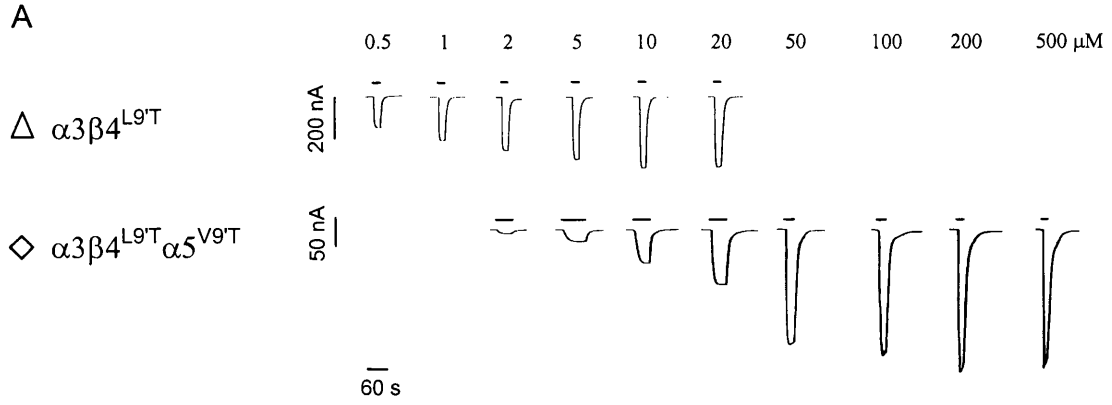

B

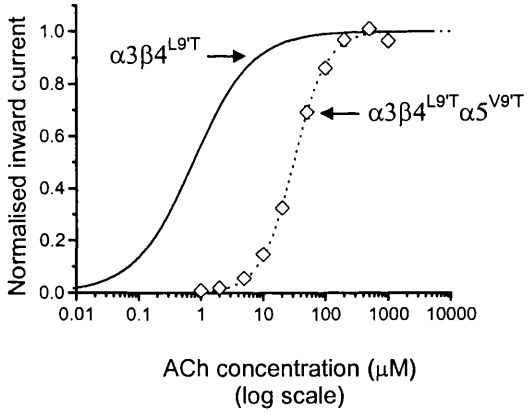

C

	EC_{50} (μM)	I_{max} (nA)	n_H	I_H (nA)	*Rundown (%)*	*No. of batches*	*n*
$\alpha3\beta4^{L9'T}$	0.75 ± 0.05	562 ± 264	0.92 ± 0.08	200 ± 83	77.4 ± 9.5	2	4
$\alpha3\beta4^{L9'T}\alpha5^{V9'T}$	31.1 ± 1.40	1476 ± 450	1.63 ± 0.12	62.5 ± 14.9	64.9 ± 10.4	3	4

Figure 5.5.2. A shows examples of inward currents elicited by bath-applied ACh in oocytes expressing $\alpha3\beta4^{L9'T}$ or $\alpha3\beta4^{L9'T}\alpha5^{V9'T}$. B shows ACh concentration-response curves pooled from experiments such as the ones shown in A: Pooled normalised results were fitted with the Hill equation as a free fit (panel B; see chapter 3). The concentration-response curves refer to oocytes injected with $\alpha3\beta4^{L9'T}\alpha5^{V9'T}$ (◇). B also shows for reference (solid curve with no symbols, reproduced from figure 3.) the concentration response curve relating to $\alpha3\beta4^{L9'T}$. C shows a summary of the fitted parameters: EC_{50}, I_{max} and n_H are the mean (± S.D. of mean) of parameter estimates obtained by fitting separately each concentration-response curve with a Hill equation. I_H is the mean (± S.D. of mean) holding current recorded at the start of the experiment. Rundown is the % (± S.D. of mean) of the response of the initial standard observed when the standard was applied at the end of the experiment. No. of batches are the number of oocyte batches used.

Figure 5.5.3. The effect of α5 co-expression on the ACh sensitivity of $\alpha3\beta4^{L9'T}$ 'pair' receptors is independent of the residue in position 9' of α5

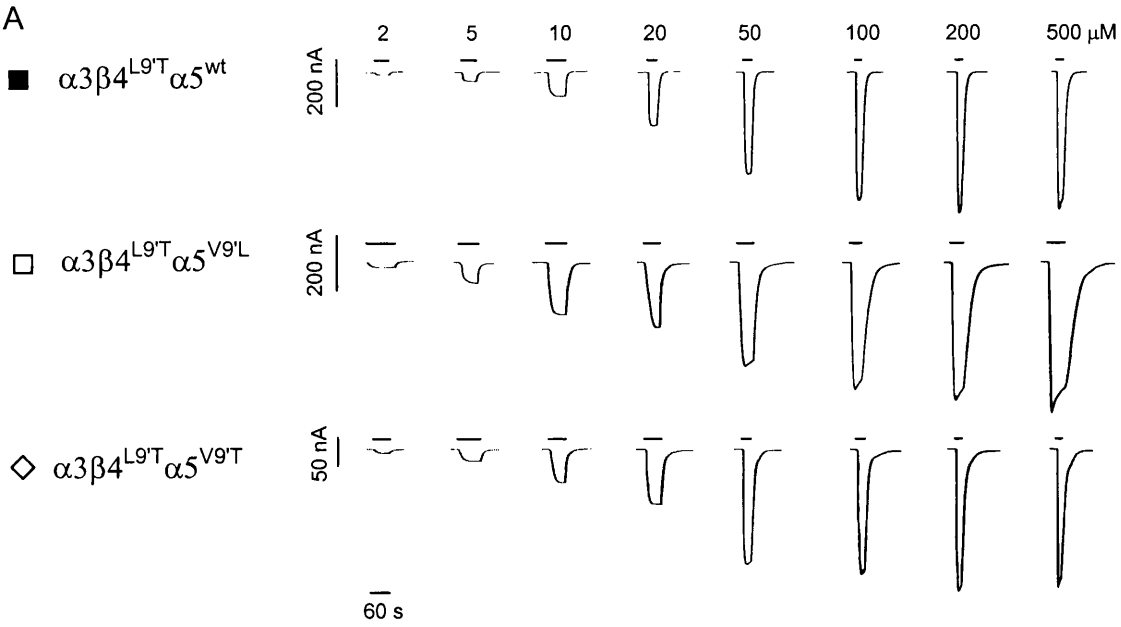

B

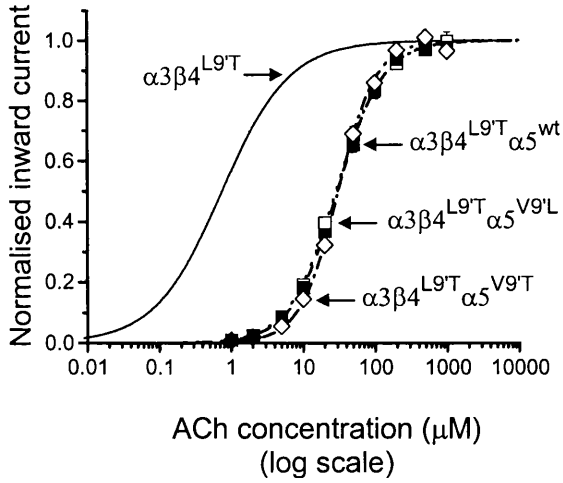

Figure 5.5.3. A shows examples of inward currents elicited by bath-applied ACh in oocytes expressing $\alpha3\beta4^{L9'T}\alpha5^{wt}$, $\alpha3\beta4^{L9'T}\alpha5^{V9'L}$ or $\alpha3\beta4^{L9'T}\alpha5^{V9'T}$. B shows ACh concentration-response curves pooled from experiments such as the ones shown in A: Pooled normalised results were fitted with the Hill equation as a free fit (panel B; see chapter 3). The concentration-response curves refer to oocytes injected with $\alpha3\beta4^{L9'T}\alpha5^{wt}$ (■), $\alpha3\beta4^{L9'T}\alpha5^{V9'L}$ (□) or $\alpha3\beta4^{L9'T}\alpha5^{V9'T}$ (◇). B also shows for reference (solid curve with no symbols, reproduced from figure 3.) the concentration response curve relating to $\alpha3\beta4^{L9'T}$.

Figure 5.6.2. Co-expressing $\alpha5^{wt}$ decreases the ACh sensitivity of $\alpha3^{L9'T}\beta4$

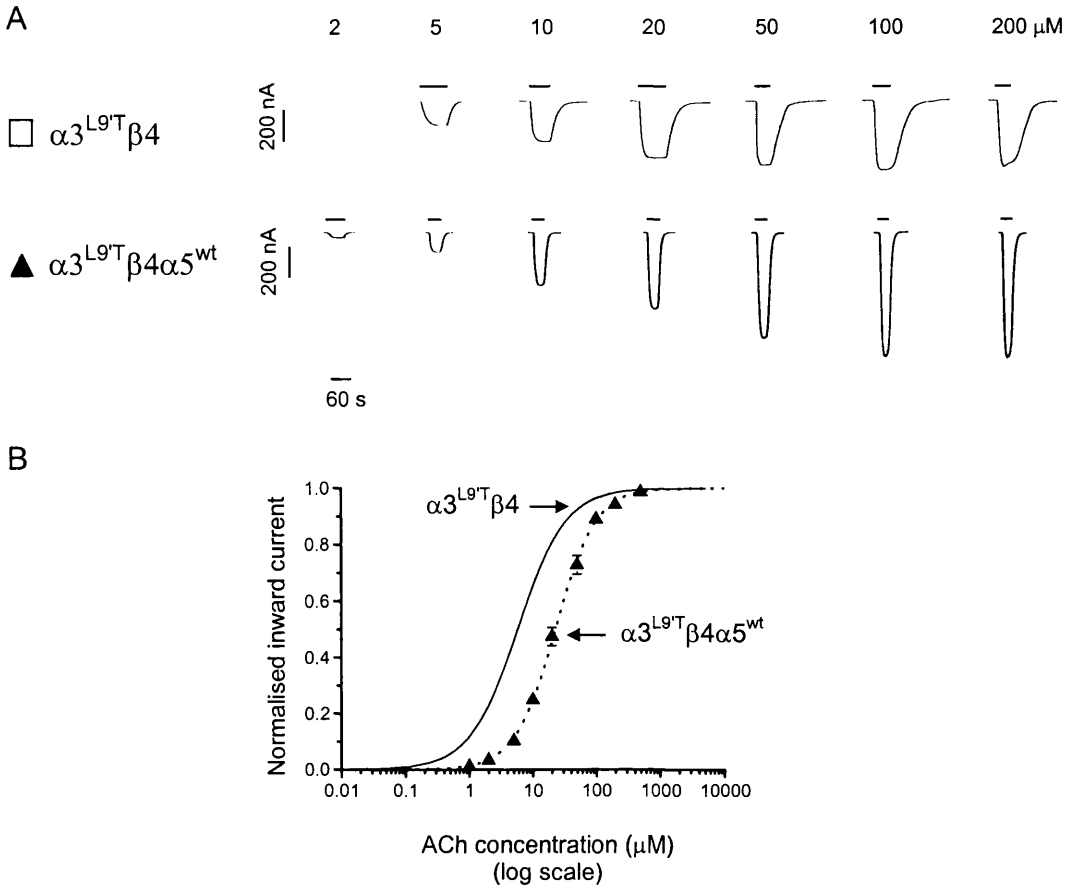

C

	EC_{50} (μM)	I_{max} (nA)	n_H	I_H (nA)	*Rundown (%)*	*No. of batches*	*n*
$\alpha3^{L9'T}\beta4$	5.8 ± 1.0	1043 ± 411	1.15 ± 0.08	85 ± 28.7	54.7 ± 8.6	2	6
$\alpha3^{L9'T}\beta4\alpha5^{wt}$	22.7 ± 2.02	1122 ± 197	1.40 ± 0.07	67.5 ± 16.52	67 ± 8.56	2	4

Figure 5.6.2 A shows examples of inward currents elicited by bath-applied ACh in oocytes expressing $\alpha3^{L9'T}\beta4$ or $\alpha3^{L9'T}\beta4\alpha5^{wt}$. B shows ACh concentration-response curves pooled from experiments such as the ones shown in A: Pooled normalised results were fitted with the Hill equation as a free fit (panel B; see chapter 3). The concentration-response curves refer to oocytes injected with $\alpha3^{L9'T}\beta4\alpha5^{wt}$ (▲). B also shows for reference (solid curve with no symbols, reproduced from figure 3.) the concentration response curve relating to $\alpha3^{L9'T}\beta4$. C shows a summary of the fitted parameters: EC_{50}, I_{max} and n_H are the mean (± S.D. of mean) of parameter estimates obtained by fitting separately each concentration-response curve with a Hill equation. I_H is the mean (± S.D. of mean) holding current recorded at the start of the experiment. Rundown is the % (± S.D. of mean) of the response of the initial standard observed when the standard was applied at the end of the experiment. No. of batches are the number of oocyte batches used.

5.7. The decrease in ACh sensitivity produced by α5 incorporation into $\alpha3^{L9'T}\beta4$ is similar for $\alpha5^{wt}$, $\alpha5^{V9'L}$ or $\alpha5^{V9'T}$

Co-expressing $\alpha5^{V9'L}$ with $\alpha3^{L9'T}\beta4$ produced a decrease in the ACh sensitivity of $\alpha3^{L9'T}\beta4$ receptors, producing a rightward shift in the ACh concentration response curve to a mean ACh EC_{50} of 17.6 ± 1.90 μM (figure 5.7.1.). Co-expressing $\alpha5^{V9'T}$ with $\alpha3^{L9'T}\beta4$ produced a decrease in the ACh sensitivity of $\alpha3^{L9'T}\beta4$ receptors, producing a rightward shift in the ACh concentration response curve to a mean ACh EC_{50} of 18.2 ± 1 μM (figure 5.7.2.).

Thus co-expression of α5 with $\alpha3^{L9'T}\beta4$ causes a 3 to 4 fold decrease in ACh sensitivity, with an EC_{50} change from approximately 6 μM to approximately 20 μM irrespective of whether α5 carried a V, a L or a T residue in 9' (see figure 5.7.3. and table 5.7.4.). Note that this shift is considerably smaller than that observed when α5 mutant or wt subunits are introduced into the $\alpha3\beta4^{L9'T}$ receptor. This suggests that α5 replaces a β4 subunit in the formation of the α3β4α5 receptor (see discussion).

Comparing I_{max} and the extent of rundown in mutant receptors with α3β4 and $\alpha3^{L9'T}\beta4$ in a two-tailed *t*-test assuming unequal variance, revealed a significant reduction in the extent of rundown when co-expressing $\alpha5^{V9'L}$ or $\alpha5^{V9'T}$ and a significant reduction in I_{max} for $\alpha3^{L9'T}\beta4\alpha5^{V9'L}$. The mean extent of rundown in $\alpha3^{L9'T}\beta4$ was 54.7 ± 8.6 % vs. 86.5 ± 7.5 % for oocytes expressing $\alpha3^{L9'T}\beta4\alpha5^{V9'L}$ (p 0.02; see table 5.7.4.) and 124.9 ± 8.5 % for oocytes expressing $\alpha3^{L9'T}\beta4\alpha5^{V9'T}$ (p 0.001; see table 5.7.4.). The mean I_{max} for α3β4 was 1430 ± 425 nA vs. 491 ± 104 nA for oocytes expressing $\alpha3^{L9'T}\beta4\alpha5^{V9'L}$ (p 0.02; see table 5.7.4.).

Figure 5.7.1. Co-expressing $\alpha5^{V9'L}$ decreases the ACh sensitivity of $\alpha3^{L9'T}\beta4$

A

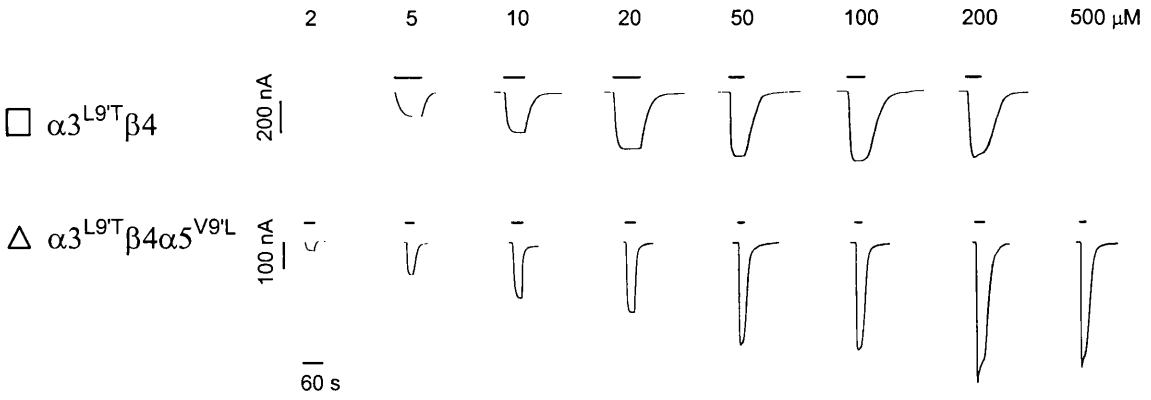

B

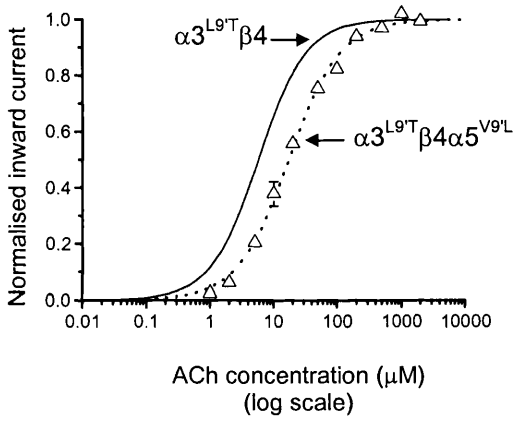

C

	EC_{50} (μM)	I_{max} (nA)	n_H	I_H (nA)	*Rundown (%)*	*No. of batches*	*n*
$\alpha3^{L9'T}\beta4$	5.8 ± 1.0	1043 ± 411	1.15 ± 0.08	85 ± 28.7	54.7 ± 8.6	2	6
$\alpha3^{L9'T}\beta4\alpha5^{V9'L}$	17.6 ± 1.90	491 ± 104	1.08 ± 0.04	185.0 ± 75.3	86.5 ± 7.5	3	4

Figure 5.7.1. A shows examples of inward currents elicited by bath-applied ACh in oocytes expressing $\alpha3^{L9'T}\beta4$ or $\alpha3^{L9'T}\beta4\alpha5^{V9'L}$. B shows ACh concentration-response curves pooled from experiments such as the ones shown in A: Pooled normalised results were fitted with the Hill equation as a free fit (panel B; see chapter 3). The concentration-response curves refer to oocytes injected with $\alpha3^{L9'T}\beta4\alpha5^{V9'L}$ (Δ). B also shows for reference (solid curve with no symbols, reproduced from figure 3.) the concentration response curve relating to $\alpha3^{L9'T}\beta4$. C shows a summary of the fitted parameters: EC_{50}, I_{max} and n_H are the mean (± S.D. of mean) of parameter estimates obtained by fitting separately each concentration-response curve with a Hill equation. I_H is the mean (± S.D. of mean) holding current recorded at the start of the experiment. Rundown is the % (± S.D. of mean) of the response of the initial standard reproduced by the standard at the end of the experiment. No. of batches are the number of oocyte batches used.

Figure 5.7.2. Co-expressing $\alpha5^{V9'T}$ decreases the ACh sensitivity of $\alpha3^{L9'T}\beta4$

A

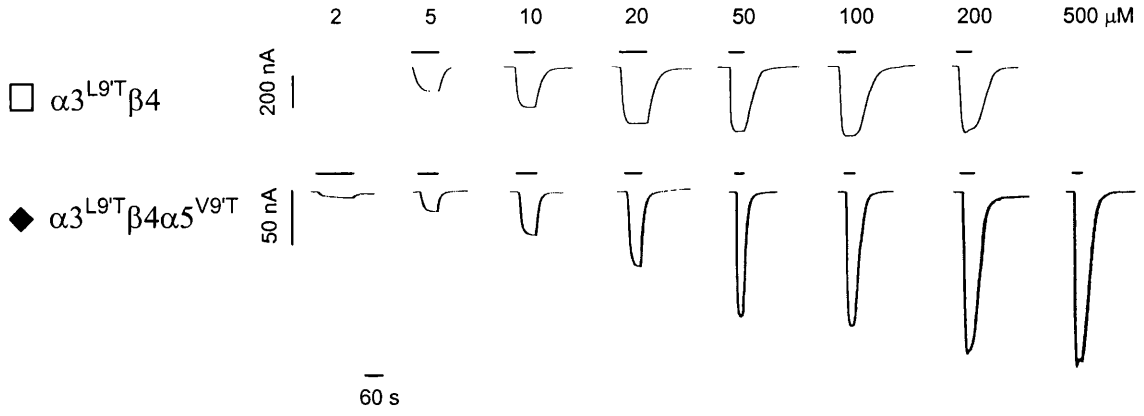

B

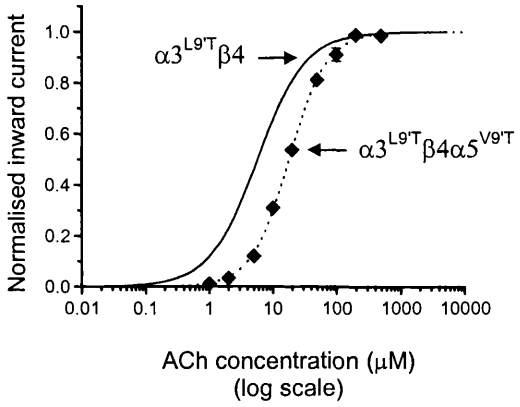

C

	EC_{50} (μM)	I_{max} (nA)	n_H	I_H (nA)	*Rundown (%)*	*No. of batches*	*n*
$\alpha3^{L9'T}\beta4$	5.8 ± 1.0	1043 ± 411	1.15 ± 0.08	85 ± 28.7	54.7 ± 8.6	2	6
$\alpha3^{L9'T}\beta4\alpha5^{V9'T}$	18.2 ± 1.00	1215 ± 280	1.45 ± 005	77.5 ± 30.4	124.90 ± 8.53	1	4

Figure 5.7.2. A shows examples of inward currents elicited by bath-applied ACh in oocytes expressing $\alpha3^{L9'T}\beta4$ or $\alpha3^{L9'T}\beta4\alpha5^{V9'T}$. B shows ACh concentration-response curves pooled from experiments such as the ones shown in A: Pooled normalised results were fitted with the Hill equation as a free fit (panel B; see chapter 3). The concentration-response curves refer to oocytes injected with $\alpha3^{L9'T}\beta4\alpha5^{V9'T}$ (◆). B also shows for reference (solid curve with no symbols, reproduced from figure 3.) the concentration response curve relating to $\alpha3^{L9'T}\beta4$. C shows a summary of the fitted parameters: EC_{50}, I_{max} and n_H are the mean (± S.D. of mean) of parameter estimates obtained by fitting separately each concentration-response curve with a Hill equation. I_H is the mean (± S.D. of mean) holding current recorded at the start of the experiment. Rundown is the % (± S.D. of mean) of the response of the initial standard reproduced by the standard at the end of the experiment. No. of batches are the number of oocyte batches used.

Figure 5.7.3. The effect of α5 co-expression on the ACh sensitivity of $\alpha3^{L9'T}\beta4$ 'pair' receptors is independent of the residue in position 9' of α5

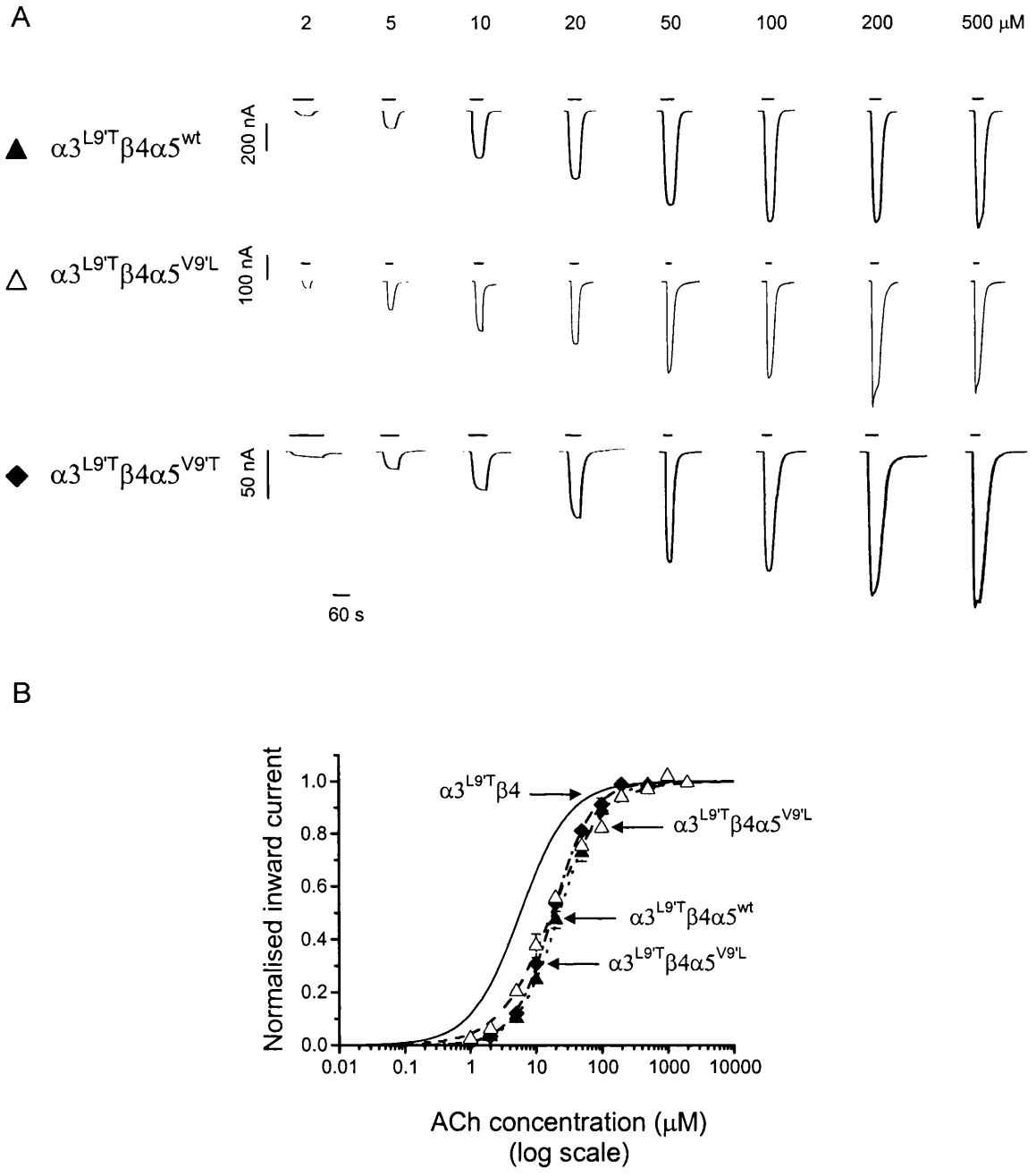

Figure 5.7.3. A shows examples of inward currents elicited by bath-applied ACh in oocytes expressing $\alpha3^{L9'T}\beta4\alpha5^{wt}$, $\alpha3^{L9'T}\beta4\alpha5^{V9'L}$ or $\alpha3^{L9'T}\beta4\alpha5^{V9'T}$. B shows ACh concentration-response curves pooled from experiments such as the ones shown in A: Pooled normalised results were fitted with the Hill equation as a free fit (panel B; see chapter 3). The concentration-response curves refer to oocytes injected with $\alpha3^{L9'T}\beta4\alpha5^{wt}$ (▲), $\alpha3^{L9'T}\beta4\alpha5^{V9'L}$ (△) or $\alpha3^{L9'T}\beta4\alpha5^{V9'T}$ (◆). B also shows for reference (solid curve with no symbols, reproduced from figure 3.) the concentration response curve relating to $\alpha3^{L9'T}\beta4$.

Table 5.7.4. A summary of the affect of α5 on wild type and mutant α3β4 'pair' receptors

	EC_{50} (μM)	I_{max} (nA)	n_H	I_H (nA)	Rundown (%)	No. of batches	n	cRNA injected (ng)
α3β4	180 ± 17.0	1430 ± 425	1.81 ± 0.09	184.0 ± 57.2	25.4 ± 4.2	2	7	0.5 - 1
$\alpha3\beta4\alpha5^{wt}$	207 ± 25.6 (*p* 0.40)	1098 ± 245 (*p* 0.51)	1.39 ± 0.08 **(*p* 0.01)**	126.0 ± 33.1 (*p* 0.40)	74.3 ± 15.3 **(*p* 0.004)**	2	5	5 - 10
$\alpha3\beta4\alpha5^{V9'L}$	206 ± 15.4 (*p* 0.28)	966 ± 367 (*p* 0.43)	1.47 ± 0.05 **(*p* 0.01)**	96.0 ± 31.1 (*p* 0.21)	95.5 ± 17.0 **(*p* 0.013)**	3	5	5 – 10
$\alpha3\beta4\alpha5^{V9'T}$	182 ± 27.1 (*p* 0.89)	709 ± 106 (*p* 0.14)	1.27 ± 0.11 **(*p* 0.002)**	73.8 ± 19.2 (*p* 0.11)	74.5 ± 12.3 **(*p* 0.005)**	4	8	1 - 5
$\alpha3^{L9'T}\beta4$	5.8 ± 1.0	1043 ± 411	1.15 ± 0.08	85.0 ± 28.7	54.7 ± 8.6	2	6	0.5
$\alpha3^{L9'T}\beta4\alpha5^{wt}$	22.7 ± 2.0 **(*p* 0.001)**	1122 ± 197 (*p* 0.77)	1.40 ± 0.07 **(*p* 0.05)**	67.5 ± 16.5 (*p* 0.45)	67 ± 8.6 (*p* 0.34)	2	4	1
$\alpha3^{L9'T}\beta4\alpha5^{V9'L}$	17.6 ± 1.9 (*p* 0.12)	491 ± 104 **(*p* 0.02)**	1.08 ± 0.04 (*p* 0.47)	185.0 ± 75.3 (*p* 0.29)	86.5 ± 7.5 **(*p* 0.02)**	3	4	1
$\alpha3^{L9'T}\beta4\alpha5^{V9'T}$	18.2 ± 1.0 (*p* 0.11)	1215 ± 280 (*p* 0.62)	1.45 ± 0.05 **(*p* 0.02)**	77.5 ± 30.4 (*p* 0.78)	124.9 ± 8.5 **(*p* 0.001)**	1	4	0.5
$\alpha3\beta4^{L9'T}$	0.75 ± 0.1	562 ± 264	0.92 ± 0.08	200.0 ± 83	89.0 ± 9.0	2	4	0.25 – 0.5
$\alpha3\beta4^{L9'T}\alpha5^{wt}$	30.7 ± 1.6 **(*p* 8.62 X 10^{-6})**	2546 ± 518 **(*p* 0.01)**	1.36 ± 0.10 **(*p* 0.01)**	68.3 ± 39.4 (*p* 0.22)	68.0 ± 8.2 (*p* 0.12)	3	6	0.5
$\alpha3\beta4^{L9'T}\alpha5^{V9'L}$	29.2 ± 1.6 (*p* 0.50)	792 ± 209 (*p* 0.52)	1.31 ± 0.03 **(*p* 0.01)**	76.0 ± 22.9 (*p* 0.24)	81.2 ± 8.4 (*p* 0.53)	4	5	0.5
$\alpha3\beta4^{L9'T}\alpha5^{V9'T}$	31.1 ± 1.4 (*p* 0.88)	1476 ± 450 (*p* 0.14)	1.63 ± 0.12 **(*p* 0.004)**	62.5 ± 14.9 (*p* 0.20)	64.9 ± 10.4 (*p* 0.13)	3	4	0.25

Table 5.7.4. A summary of the fitted data: EC_{50}, I_{max} and n_H are the mean (± S.D. of mean) of parameter estimates obtained by fitting separately each concentration-response curve with a Hill equation. I_H is the mean (± S.D. of mean) holding current recorded at the start of the experiment. Rundown is the % (± S.D. of mean) of the response of the initial standard reproduced by the standard at the end of the experiment. No. of batches are the number oocyte batches used. cRNA injected is the range of cRNA injected in order to produce acceptable expression levels for the experiments. Where *p* is the result of a 2 tail *t*-test assuming unequal variance, assessing the effect of wild-type or mutant α5 co-expressing on the values measured for the subunit combination indicated. Here *p* values of 0.05 or less were taken to indicate a significant difference.

5.8. Pair combinations containing $\alpha3^{L9'T}$ and α5 respond to ACh

A series of control experiments showed that injection of one subunit alone (wild-type or mutant), namely α5, $\alpha5^{V9'L}$, $\alpha5^{V9'T}$ or of 'pair' combinations of α5 with either α3 (α3α5, $\alpha3\alpha5^{V9'L}$, $\alpha3\alpha5^{V9'T}$) or β4 (β4α5, $\beta4\alpha5^{V9'L}$, $\beta4\alpha5^{V9'T}$, 10 ng total) did not result in the expression of functional nAChRs (*i.e.* current responses to 1 mM ACh were less than 1 nA; n = 5 for each combination tested; total cRNA injected 10 ng; 1:1 ratio for the pairwise combinations). In non-injected oocytes responses to 1 mM ACh were also negligible (less than 1nA, n = 5).

'Pair' combinations containing the $\alpha3^{L9'T}$ subunit together with α5 did produce detectable ACh responses. Nevertheless such inward currents in response to 1 mM ACh were small (maximum responses were 149 ± 47 and 142 ± 50 nA, n= 5 for $\alpha3^{L9'T}\alpha5$ and $\alpha3^{L9'T}\alpha5^{V9'L}$, respectively). Only the $\alpha3^{L9'T}\alpha5^{V9'T}$ combination produced a larger inward current (362 ± 145 nA, n = 5; summarised in table 5.8.2., see and figure 5.8.3. for a concentration response curve). Note however that the EC_{50} for these responses is very high, 746.8 μM, n=1. The corresponding triplet combination, $\alpha3^{L9'T}\beta4\alpha5^{V9'T}$ produced a much larger average maximum current (1215 ± 280 nA; see table 5.8.2.) in response to a considerably lower ACh concentration (200 μM, EC_{50} 18.2 μM, see table 5.7.4.). The maximum ACh concentration used for the corresponding 'triplet' concentration response curves was 500 μM for $\alpha3^{L9'T}\beta4\alpha5^{wt}$ and $\alpha3^{L9'T}\beta4\alpha5^{V9'T}$ and 2 mM for $\alpha3^{L9'T}\beta4\alpha5^{V9'L}$. Further, ACh responses for the 'pair' $\alpha3^{L9'T}\alpha5$ combinations were obtained after injecting 10 ng of cRNA, compared to 0.5 – 1 ng for the corresponding 'triplets' (see table 5.7.4.). Thus the formation of $\alpha3^{L9'T}\alpha5$ 'pair' combinations would have a negligible effect on our data.

$\beta4^{L9'T}$ combinations with $\alpha5$, $\alpha5^{V9'L}$ or $\alpha5^{V9'T}$ responded to 1 mM ACh with small *outward* currents (less than or equal to 55 nA, n = 5; total cRNA injection 10 ng; 1:1 ratio for all pair wise combinations). These results are summarised in table 5.8.1.

Comparing the initial holding currents for wildtype and mutant single subunits and non-functional pairs in a two-tailed *t*-test assuming unequal variance, revealed no significant change in holding current. For example, oocytes injected with $\alpha3\alpha5$ had a mean initial holding current of 36 ± 9.3 nA vs. 174 ± 66.8 nA for oocytes injected with $\alpha3^{L9'T}\alpha5^{V9'T}$ (*p* 0.11; see table 4.8.1.).

Table 5.8.1. The experimental controls

	Mean *IH*	Mean Response to 1 mM ACh (nA)	*n*	batches
α5	52 ± 13.2	0	5	2
$\alpha5^{V9'L}$	36 ± 9.8 (*p* 0.36)	0	5	1
$\alpha5^{V9'T}$	24 ± 2.4 (*p* 0.10)	0	5	2
α3α5	36 ± 9.3	0	5	1
$\alpha3\alpha5^{V9'L}$	95 ± 21.8 (*p* 0.07)	0	5	3
$\alpha3\alpha5^{V9'T}$	34 ± 4.0 (*p* 0.88)	0	5	2
$\alpha3^{L9'T}\alpha5^{wt}$	120 ± 60.7 (*p* 0.24)	115 ± 52.3	5	2
$\alpha3^{L9'T}\alpha5^{V9'L}$	126 ± 78.7 (*p* 0.32)	Outward 24 ± 7.7	5	2
$\alpha3^{L9'T}\alpha5^{V9'T}$	174 ± 66.8 (*p* 0.11)	140.6 ± 49.8	5	2
β4α5	90 ± 21.2	0	5	2
$\beta4\alpha5^{V9'L}$	114 ± 35.4 (*p* 0.58)	0	5	2
$\beta4\alpha5^{V9'T}$	60 ± 9.5 (*p* 0.25)	0	5	2
$\beta4^{L9'T}\alpha5^{wt}$	134 ± 26.9 (*p* 0.24)	Outward 16 ± 4	5	2
$\beta4^{L9'T}\alpha5^{V9'L}$	144 ± 38.5 (*p* 0.26)	283 ± 106.4	5	3
$\beta4^{L9'T}\alpha5^{V9'T}$	124 ± 20.4 (*p* 0.28)	Outward 19 ± 4.3	5	2

Table 5.8.1. Mean *IH* = Mean initial holding current (± S.D. of the mean) at the start of the experiment. Where *p* is the result of a 2 tailed *t*-test assuming unequal variance, comparing the change in holding current produced by introducing increasing copies of the 9' mutation into the subunit combinations indicated. Here *p* values of 0.05 or less were taken to indicate a significant difference. Note that the 9' mutation does not significantly affect the holding current of any of the combinations.

Table 5.8.2. $\alpha3^{L9'T}\alpha5^{V9'T}$ vs. $\alpha3^{L9'T}\beta4\alpha5^{V9'T}$

	EC_{50} (μM)	I_{max} (nA)	n_H	I_H (nA)	*No. of batches*	*n*
$\alpha3^{L9'T}\alpha5^{V9'T}$	746.8	908	3.95	340	1	1
$\alpha3^{L9'T}\beta4\alpha5^{V9'T}$	18.2 ± 1.00	1215 ± 280	1.45 ± 0.05	77.5 ± 30.4	1	4

Table 5.8.2. Summary of the fitted data: EC_{50}, I_{max} and n_H are the mean (± S.D. of mean) of parameter estimates obtained by fitting separately each concentration-response curve with a Hill equation. I_H is the mean (± S.D. of mean) holding current recorded at the start of the experiment. No. of batches are the number of oocyte batches used.

Figure 5.8.3. $\alpha3^{L9'T}\alpha5^{V9'T}$ produces a functional receptor that does not resemble $\alpha3^{L9'T}\beta4\alpha5^{V9'T}$ receptors

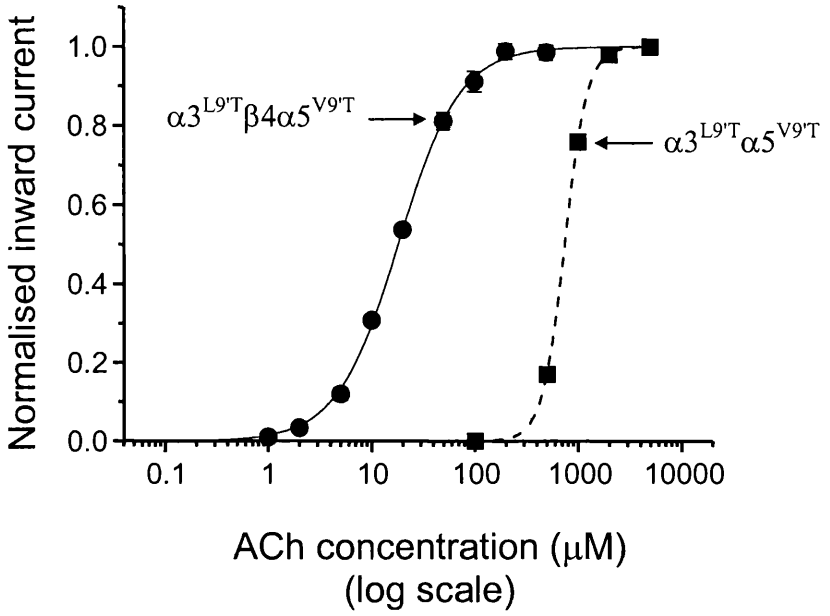

Figure 5.8.3. Shows ACh concentration-response curves pooled from experiments such as the ones shown in 5.7.3.: Pooled normalised results were fitted with the Hill equation as a free fit (see chapter 3). The concentration-response curves refer to oocytes injected with $\alpha3^{L9'T}\beta4\alpha5^{V9'T}$ (●) and $\alpha3^{L9'T}\alpha5^{V9'T}$ (■).

5.9. Discussion

The experiments presented above were performed as a continuation of the work on the stoichiometry of the α3β4β3 'triplet' receptor. It seemed plausible that the same approach would allow us to establish whether 'triplet' receptors containing α5 have the same 2:2:1 stoichiometry.

It has been shown previously that in α4β2α5 'triplet' receptors, the incorporation of α5 is detected by the appearance of a new receptor population, considerably less sensitive

to the agonist action of ACh. Lindstrom and co-workers however report that the effect of the presence of α5 depends on the nature of the 'parent' pair of subunits with which α5 is co-expressed. For instance, in oocytes α5 markedly *increased* the ACh sensitivity of human α3β2α5 receptors, but left unchanged that of α3β4α5 nAChRs (Wang *et al.*, 1996; Gerzanich *et al.*, 1998). The same authors report that in α3β4α5 nAChRs, α5 incorporation is manifest because of changes in the desensitisation and calcium permeability of the receptor. On the other hand, if *chick* subunits are expressed, α5 *decreases* α3β4 agonist sensitivity in mammalian cells, but has no effect if these subunits are expressed in oocytes (Fucile *et al.*, 1997). Indeed, these data have been taken to indicate lack of co-assembly of this particular 'triplet' receptor in oocytes.

Nevertheless more evidence for α5 incorporation is provided by single channel experiments. α5-containing nAChRs also have a higher single channel conductance than the 'parent' pair receptors both for an α4β2 background (Ramirez-Latorre *et al.*, 1996) and for an α3β4 background (Sivilotti *et al.*, 1997; Nelson & Lindstrom, 1999). These data not only confirm incorporation, but suggest that α5 replaces a β subunit in the formation of the 'triplet' (see below).

5.9.1. The incorporation of α5 into functional α3β4α5 triplet receptors

Recombinant nAChRs containing α3 and α5 were previously characterised by Lindstrom and co-workers (Gerzanich *et al.*, 1998; Wang *et al.*, 1996; Wang *et al.*, 1998; Nelson & Lindstrom, 1999). Our data agree with their observation that α5 does not affect the EC_{50} of the wildtype α3β4 concentration-response curve to ACh (see table 5.7.4.). However, α5 does increase apparent desensitisation to high ACh concentrations

and decreases the Hill slope (see table 5.7.4.), most notably in $\alpha3\beta4\alpha5^{V9'L}$ receptors (see figure 5.2.2.). Interestingly, neither of these effects are shared by β3 (see α3β4β3 data in chapter 4).

Additionally, our data suggest efficient assembly of α3β4α5 receptors in oocytes in agreement with the findings of Wang *et al.* (1996). This is demonstrated by the consistent reduction in ACh sensitivity observed when α5 was expressed with $\alpha3^{L9'T}\beta4$ or $\alpha3\beta4^{L9'T}$. In these mutant nAChRs, addition of α5 increased the ACh EC_{50} by four-fold ($\alpha3^{L9'T}\beta4$) or forty-fold ($\alpha3\beta4^{L9'T}$; see figures 5.5.3 & 5.7.3.). Our interpretation assumes that 9' mutations do not affect subunit assembly in nAChRs: indeed such an effect of 9' mutations has never been reported and is not observed for mutant α3β4 or α3β4β3 receptors (see chapters 3 & 4).

Furthermore, α5 incorporation in receptors mutated in α3 or β4 was clear regardless of whether α5 itself was expressed as $\alpha5^{wt}$, $\alpha5^{V9'L}$ or $\alpha5^{V9'T}$. The magnitude of the EC_{50} shift was much larger if the 9'T mutation was in β4 (40-fold *vs.* approximately four-fold for $\alpha3^{L9'T}$ nAChRs). A plausible explanation for this disparity is that α5 (like β3) replaces a β4 subunit in the receptor. If that is the case and if the mutation is carried by β4, α5 would affect ACh EC_{50} not just because of its incorporation, but also because it decreases the number of copies of the mutation. Wang *et al.* (1996) first suggested that α5 replaces a β subunit. This is reasonable, because α5 differs from a typical α in the putative agonist binding domain sequences, containing a negatively charged aspartate residue in position 190 of loop C (in common with β3; *Torpedo* α1 numbering) compared to neutral tyrosine found in all other α subunits. Thus α5 may not be able to play the role of an α subunit. This would also be in agreement with the consistent

increase in single-channel conductance produced by α5 incorporation (Ramirez-Latorre *et al.*, 1996). As discussed in chapter 1, Imoto *et al.* (1988) describe 3 rings of charges in the TM2 domain, whose net charge affects single channel conductance of nAChRs. If α5 replaces a β subunit, it would increase the net negative charge of the extracellular ring of charges in position 20' of TM2, by replacing the positively charged lysine residue contributed by β4 with a negatively charged glutamate residue (see figure 5.8.1.a). This would be expected to increase the single-channel conductance of the resulting α3β4α5 triplet (Imoto *et al.*, 1988). However, the net charge in the extracellular ring would not change if α5 replaced an α subunit (see figure 5.8.1.b).

Table 5.9.1.a. α5 replacing β4 in the α3β4α5 triplet receptor

Receptor	Subunit	Copy number	Cytoplasmic ring	Intermediate ring	Outer ring
			-4'	-1'	20'
α3β4	α3	2	D (-)	E (-)	E (-)
	β4	3	D (-)	E (-)	K (+)
Net charge			- 5	- 5	+ 1
α3β4α5	α3	2	D (-)	E (-)	E (-)
	β4	2	D (-)	E (-)	K (+)
	α5	1	N (0)	E (-)	E (-)
Net charge			- 4	- 5	- 1

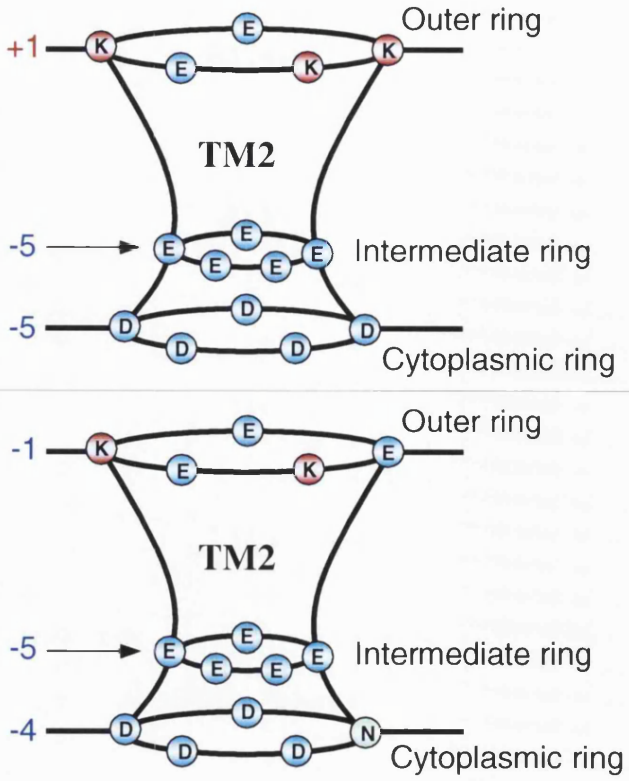

Table 5.9.1.a. Shown are the residues in the TM2 cytoplasmic (-4'), intermediate (-1') and outer (20') rings of charges for the α3, β4 and α5 subunits. The residues are indicated using the single letter amino acid code. The presumed stoichiometry for both α3β4 and α3β4α5 receptors is indicated by the subunit copy number. The net charge for each ring of charges is calculated on the basis of the subunit copy number. A graphical representation of the pore of the channel, with the residues lining the pore forming the cytoplasmic (-4'), intermediate (-1'). Note that the subunit arrangement shown is based on that of the ACh binding protein.

Table 5.9.1.b. α5 replacing α3 in the α3β4α5 triplet receptor

Receptor	Subunit	Copy number	Cytoplasmic ring	Intermediate ring	Outer ring
			-4'	-1'	20'
α3β4	α3	2	D (-)	E (-)	E (-)
	β4	3	D (-)	E (-)	K (+)
Net charge			- 5	- 5	+ 1
α3β4α5	α3	1	D (-)	E (-)	E (-)
	β4	3	D (-)	E (-)	K (+)
	α5	1	N (0)	E (-)	E (-)
Net charge			- 4	- 5	+ 1

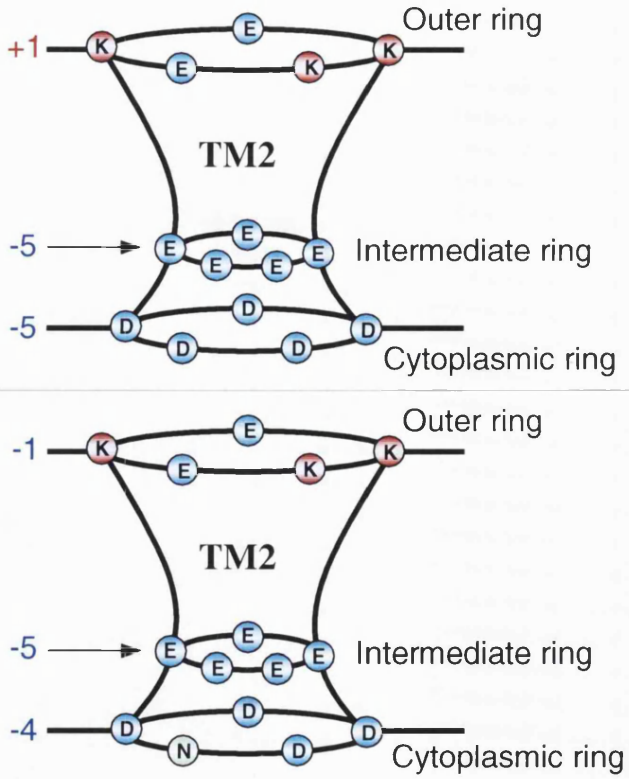

Table 5.9.1.b. Shown are the residues in the TM2 cytoplasmic (-4'), intermediate (-1') and outer (20') rings of charges for the α3, β4 and α5 subunits. The residues are indicated using the single letter amino acid code. The presumed stoichiometry for both α3β4 and α3β4α5 receptors is indicated by the subunit copy number. The net charge for each ring of charges is calculated on the basis of the subunit copy number. A graphical representation of the pore of the channel, with the residues lining the pore forming the cytoplasmic (-4'), intermediate (-1'), central (2') and outer (20') rings is shown for both α3β4 and α3β4α5 receptors, indicating the net charge on each ring. Note positively charged residues are indicated in red, negatively charged residues in blue and uncharged residues in white. Note that there is no increase in the net negative charge of the extracellular ring if α5 replaces α. Note that the subunit arrangement shown is based on that of the ACh binding protein.

5.9.2. 9' mutations in α5 do not affect the agonist sensitivity of α3β4α5 receptors

Mutating the 9' valine in the TM2 domain of α5 to a hydrophilic threonine did not change the agonist sensitivity of α3β4α5 receptors (see figure 5.2.2.). This is in contrast with the data from muscle nAChRs and from neuronal α3β4 and α3β4β3 receptors (see chapters 3 & 4), where such mutations consistently increase agonist potency. Mutations of 9' to threonine or serine are thought to act on channel gating by destabilising the closed state and/or by reducing desensitisation (possibly making the desensitised state of the channel conducting; Revah *et al.*, 1991; Labarca *et al.*, 1995; Filatov & White, 1995). These two microscopic effects should have opposite effects on the receptor macroscopic EC_{50}.

On the one hand, destabilisation of the closed state increases agonist efficacy and should therefore *decrease* agonist EC_{50} (shift the concentration-response curve to the left). Whether such a decrease will be detectable will depend on the magnitude of the microscopic effect of the mutation and on the actual value of agonist efficacy in the wild type receptor (Colquhoun, 1998).

On the other hand, a decrease in the extent of desensitisation should have the contrary effect of *increasing* the observed agonist EC_{50} (shifting the concentration response curve to the right). This is because desensitised states (by definition long-lived) contribute high affinity states to the receptor activation mechanism and therefore reduce EC_{50} values in functional assays and apparent affinity constants in binding assays.

The balance between these two contrasting effects of the mutation must tilt towards the latter if a receptor has particularly fast and extensive desensitisation under the recording

conditions used. This is clearly the case for the α3β4α5 receptor (see Figure 5.3.2.), in which responses to high ACh concentrations sag much more quickly and extensively that those of α3β4β3 receptors. It seems therefore likely that the reason we cannot detect an EC_{50} change upon V9'T mutation of α5 is that the gating effect of the mutation is counteracted by its effect on desensitisation.

The paucity of quantitative data on the microscopic activation and desensitisation mechanisms of neuronal nAChR makes it difficult to make this more than a qualitatively plausible explanation. A limitation in the sensitivity of our technique comes from the *Xenopus* oocyte expression system. On one hand, oocytes are a good choice for studying complex subunit combinations, such as our 'triplets', because they allow excellent cell-to-cell control of the constructs effectively injected. Nevertheless, the large size of the oocyte (approximately 1 mm in diameter) limits the effective rate of agonist application achievable: this is a considerable disadvantage when desensitisation is fast and extensive. Extending our work to transfected mammalian cell lines may achieve a better discrimination of the mutation effects on desensitisation vs. gating, especially since whole-cell recording also allows a better control of internal calcium concentrations, which are known to affect desensitisation processes (Khiroug et al., 1998).

It is interesting that L9'T mutation of α3 or β4 in α3β4α5 receptors did reduce ACh EC_{50}, but only by ten and six-fold, respectively. The corresponding mutations produced 17-20-fold decreases in EC_{50} in α3β4β3 receptors (see chapter 4). Even in the presence of a mutated α3 or β4 subunit, V9'T mutation in α5 still had no effect on agonist potency. This could be due to saturation in the effect of 9' hydrophilic mutations at high numbers of mutation copies, as seen for $GABA_A$ receptors (Chang & Weiss 1999),

although this is less marked for α3β4β3 nAChRs (see chapter 4). Conversely, the lack of effect of α5 V9'T may again be due to the cancelling out of the effects of the mutation on desensitisation and on gating, even though additional threonine mutations are present on the other receptor subunits. For this to be true, the 9' residue of α5 would have to have a much bigger impact on desensitisation than the same residue in the other subunits. Assessing which is the correct explanation will require experimental evidence from receptors expressed in a cell line plus an adequate model for desensitisation.

5.9.3. Stoichiometry of α3β4α5 receptors

The data presented in chapter 4 showed that α3β4β3 receptors have a stoichiometry of 2:2:1. This conclusion was reached because introducing the 9'T mutation in the different subunits produced a consistent and progressive increase in agonist potency. This was in agreement with a progressive increase in the effects of the mutation in parallel with the number of copies of the mutation incorporated, as is the case for muscle nAChRs (Labarca *et al.*, 1995) and for α3β4 receptors (see chapter 3). Because of the similarity between β3 and α5, it would seem reasonable to assumed that all triplet receptors containing these subunits may contain two copies of the typical α subunit and two copies of the typical β subunit together with only one copy of β3 or α5.

As previously discussed in chapters 3 and 4, for the data from reporter mutation experiments to be interpreted in terms of stoichiometry, the mutation must have a simple effect that is consistent and relatively independent of which subunit carries the mutation. Clearly, both assumptions failed in the case of α3β4α5 nAChRs. However, subunit stoichiometry in a pentameric receptor containing three different subunits can only be 2:2:1 or 3:1:1. A 2:2:1 stoichiometry is still the one that best accords with the data, particularly with the equivalence of mutating α3 or β4 and with α5 taking the

place of a β subunit. This stoichiometry could be checked (despite the lack of an independent and equivalent effect of the mutation) by expressing mixtures of wild type and mutant for each of the subunits and counting the different components of the dose response curve (Labarca *et al.*, 1995; Chang *et al.*, 1996). This however would only be possible if each mutation produces a substantial shift in EC_{50}, sufficient to allow the unequivocal determination of up to three components in the interval of the shift. In our case, the six- to ten-fold shifts observed when β4 or α3 are mutated are too small: maybe a different hydrophilic substitution (perhaps to serine) would produce a larger shift and make this approach possible.

In conclusion, our data indicate that α5 is incorporated in oocyte-expressed α3β4α5 nAChRs and contributes to this pentameric nAChR only one copy, which takes the place of a β subunit. Furthermore, α5 and its 9' TM2 residue had a profound effect on receptor desensitisation, possibly greater than the effect of other subunits. However, it remains to be seen whether α5 participates –directly or indirectly- to the agonist binding site or is a structural subunit (like β1 in muscle nAChRs).

5.9.4. The Hill slope of mutant receptors

The most likely explanation for the observation that the Hill slope decreases in oocytes expressing α3β4 + α5 wild-type or mutant, is an increase in desensitisation resulting from the incorporation of α5 (see figure 5.2.2.) in addition to an increase in the contribution of monoliganded openings in mutant receptors (see chapter 3).

5.9.5. The rundown of mutant receptors

Comparing the extent of rundown in mutant receptors with α3β4 or $\alpha3^{L9'T}\beta4$ in a two-tailed *t*-test assuming unequal variance, revealed a significant reduction in the extent of rundown when co-expressing α5 wildtype or mutant. The greatest effect was observed when co-expressing $\alpha3^{L9'T}\beta4$ with $\alpha5^{V9'T}$. The mean extent of rundown for $\alpha3^{L9'T}\beta4$ was 54.7 ± 8.6 % vs. 124.9 ± 8.5 % for oocytes expressing $\alpha3^{L9'T}\beta4\alpha5^{V9'T}$ (*p* 0.001; see table 5.7.4.), indicating a significant potentiation compared to $\alpha3^{L9'T}\beta4$. As discussed in chapter 4, the most likely explanation for this observation is use dependant unblocking of mutant receptors.

5.9.6. The I_{max} of mutant receptors

Comparing the I_{max} of mutant receptors with α3β4 in a two-tailed *t*-test assuming unequal variance, revealed a significant reduction only in $\alpha3^{L9'T}\beta4\alpha5^{V9'L}$. The mean I_{max} for α3β4 was 1430 ± 425 nA vs. 491 ± 104 nA for oocytes expressing $\alpha3^{L9'T}\beta4\alpha5^{V9'L}$ (*p* 0.02; see table 5.7.4.). A possible explanation for this observation is that $\alpha5^{V9'L}$ reduces the assembly and expression efficiency of $\alpha3^{L9'T}\beta4$, via the formation of non-functional receptors. This explanation seems unlikely, given the fact that no significant decrease in I_{max} is seen in oocytes expressing $\alpha3^{L9'T}\beta4\alpha5^{V9'T}$. Further, no such affect on assembly and expression efficiency has previously been reported for the 9' mutation. A more likely explanation, is that the cRNA concentration for the $\alpha3^{L9'T}\beta4\alpha5^{V9'L}$ was not equal to that of the other subunit combinations, possibly due to a 10-fold dilution error.

Chapter 6: Characterising 'triplet' α3β4β3 neuronal nicotinic acetylcholine receptors

Little is known about 'triplet' receptors containing the β3 subunit. It was only recently that Groot-Kormelink *et al.* (1998) showed that β3 could form a functional receptor. From the data presented in chapters 4 and 5 we know that the stoichiometry of 'triplet' receptors is 2:2:1. Thus one copy of β3 is incorporated, replacing a β, but the implications that this may have on the receptor is not clear, especially since we don't know whether β3 contributes to the ligand binding sites. As we have seen from chapter 5, it has been reported that α5 incorporation changes the properties of pair receptors (see Ramirez-Latorre *et al.*, 1996; Sivilotti *et al.*, 1997;Gerzanich *et al.*, 1998; Nelson & Lindstrom, 1999). We have also seen in the previous chapters that α5 and β3 have very similar amino acid sequences. If β3 does participate in the formation of the binding site, then it would be reasonable to expect that β3 incorporation may also have a similar effect on the properties of 'pair' receptors. Thus in the next set of experiments I characterised both the α3β4 'pair' and α3β4β3 'triplet' receptors in terms of agonist potency, the dissociation equilibrium constant for a competitive antagonist (*Kd*), single channel conductance and calcium permeability.

The potency of an agonist on the receptor depends on both binding and gating. Thus in principle, a non-α subunit may affect the potency of an agonist even if it does not contribute to the binding site (directly or indirectly). If β3 incorporation changes the relative potencies of a series of agonists on α3β4 receptors, then these agonists may be used to identify α3β4β3 receptor populations in native tissue.

As competitive antagonists bind to the receptor, but do not cause receptor activation, we can use a competitive antagonist to separate binding from gating. The dissociation equilibrium constant (*Kd*) of a competitive antagonist is a physical constant for the binding reaction, dependent on the nature of the binding site. Thus we could expect a

change in the residues forming the binding site to be revealed by a change in the antagonist *Kd*. However, given the comparatively larger size of antagonists it may not be possible to detect subtle changes in the binding of agonists caused by β3 incorporation. Obtaining the *Kd* for a competitive antagonist will allow me to determine if β3 incorporation affects the binding site of α3β4 receptors.

Imoto and colleagues have shown that the charge on the TM2 -4', -1' and 20' rings of residues affects single channel conductance, with the greatest increase in single channel conductance produced by an increase in the net negative charge on 20' (see chapter 1). Thus single channel conductance depends on the residues in the TM2 domain contributed by all 5 subunits in the pentamer. In principle, β3 incorporation could change the single channel conductance of α3β4 receptors. Obtaining a distinct single channel conductance for α3β4β3 may provide a useful pharmacological tool for identifying β3 containing receptor populations in native tissue.

Measuring the calcium permeability of α3β4 vs. α3β4β3 receptors provides more physiologically relevant characterisation data. If β3 incorporation increases calcium permeability, then the incorporation of β3 in native receptors may have physiological importance to the neuron. For example, an increase in the influx of calcium into the neuron through β3 containing nAChRs could trigger neurotransmitter release.

6.1. The agonist pharmacological profile of α3β4 versus α3β4β3 neuronal nicotinic acetylcholine receptors

Establishing a pharmacological profile or 'finger print' for 'triplet' receptors containing the β3 subunit is essential for investigating their possible role in native neuronal

nAChRs. If the incorporation of β3 changes the agonist rank order of a series of partial agonists, then this change may be used to distinguish native β3 containing 'triplet' receptors from 'pair' receptors in recordings from brain slices. The idea that β3 incorporation may affect the agonist potency profile of the α3β4 pair receptor is re-enforced by the data of Luetje & Patrick (1991). Luetje & Patrick (1991) used the nAChR agonists: ACh, Cyt, Nic and DMPP to construct agonist rank orders of potency. They found that the rank order of potency varied depending on the α or β subunit composition, indicating that both α and β subunits contribute to the agonist sensitivity of pair neuronal nAChRs (Luetje & Patrick, 1991). In order to improve the precision of the characterisation we choose to measure relative potency ratios (see Covernton *et al.*, 1994), instead of rank order of potencies.

The pharmacological profile of α3β4 and α3β4β3 receptors was obtained by bath-application of ACh or other agonists to oocytes expressing α3β4 or $\alpha3\beta4\beta3^{wt}$ receptors, using a protocol based on the method previously described by Covernton *et al.* (1994; see Chapter 2). Example responses from one oocyte expressing α3β4 'pair' or $\alpha3\beta4\beta3^{wt}$ 'triplet' receptors are shown in figure 6.1.1.

Initially a reference partial concentration response curve for ACh was obtained for each oocyte. Next a series of partial concentration response curves, parallel to the reference ACh curve, were obtained for the various agonists in the same oocyte (see table 6.3.3). Data were then plotted on log/log scale in order to produce linear plots and fitted to a power function derived from the Hill equation using David Colquhoun's CVfit programme (see Chapter 2). The partial concentration response curves for the range of agonists used in each oocyte were fitted simultaneously with equal weighting, with the constraint of equal Hill slopes in order to obtain parallel fits and allow estimates of the

horizontal distance between the partial concentration response curves - these can be expressed as potency ratios or relative potency values. Because almost all the agonists we used were more potent than ACh, it was more convenient to use relative potency, where numbers greater than 1 indicate the compound is more potent that ACh. Both potency ratios and relative potency values are shown in table 6.3.3.

Fitted potency ratios for each of the agonists on both α3β4 and α3β4β3 receptors were then tested for equal or non-equal potency using an unpaired *t*-test, assuming unequal variance in the two groups. Results of the *t*-test were expressed as *p* values (at a significance level of 0.05). Finally, all partial concentration response curves were re-fitted separately, in order to obtain their Hill slopes without the constraint of parallelism.

6.2. The agonist pharmacological profile of α3β4

The rank-order of agonist potencies for α3β4 was: epibatidine >> lobeline > Cyt ~ DMPP ~ Nic > ACh > CCh, where epibatidine is the most potent and CCh the least potent agonist (see table 6.3.3). This differs slightly from the rank order of potencies reported in the literature on the basis of agonist EC_{50} values, where DMPP is more potent than Cyt: DMPP > Cyt ~ Nic ~ ACh (Wang *et al.*, 1996; Chavez-Noriega *et al.*, 1997 and Gerzanich *et al.*, 1998). However, agonist EC_{50} values are not a robust method for describing agonist potencies as they are obtained at high agonist concentrations that may produce both agonist self block and desensitisation, distorting the apparent agonist potency (see Sivilotti *et al.*, 2000).

In terms of *rat* α3β4, data obtained from partial dose response curves results in a rank order of potencies of: Cyt > Nic ~ ACh > DMPP > CCh > Lob (Luetje & Patrick, 1991 and Covernton *et al.*, 1994). This suggests that the agonist rank order of potencies is species specific.

6.3. The relative potency of lobeline on α3β4 receptors is decreased by the co-expression of β3

Comparing the relative potencies of the agonists for α3β4 and α3β4β3 receptors revealed that lobeline is less potent on α3β4β3 than on α3β4 receptors, $p < 0.01$ (see table 6.3.3). However, the rank-order of potencies was unchanged: epibatidine >> lobeline > Cyt ~ DMPP ~ Nic > ACh > CCh (see figure 6.3.1 and 6.3.2.).

6.4. Lobeline is less potent on α3β4β3 than α3β4 receptors

The pharmacology of neuronal nAChRs can be affected by their subunit composition, allowing neuronal nAChRs to be characterised to some extent by their sensitivity to different agonists and antagonists (see for example Chavez-Noriega *et al.*, 1997).

The data presented above demonstrates that the only change in the agonist pharmacological profile of α3β4 receptors produced by β3 incorporation is a decrease in the relative potency of lobeline, with the agonist rank order unchanged. Because macroscopic recordings look at both binding and gating reactions, it is impossible to know which of these steps (if not both) mediate the effects of β3 incorporation on the relative potency. Thus, β3 may reduce the relative potency of lobeline either by affecting the ligand binding site and reducing the binding affinity of lobeline, and/or by

affecting the gating kinetics of the receptor and reducing efficacy. Single channel recordings would be required in order to clarify the effects of β3 incorporation.

While the change in lobeline relative potency is marked (approximately three-fold), there was no change in the rank order of agonist potencies. This means that the agonist profile approach would be useful for distinguishing native α3β4 receptors from α3β4β3 receptors only in the most favourable experimental conditions. i.e. if relatively pure populations were compared.

My data confirm and extend those of Groot-Kormelink *et al* (1998), showing that β3 incorporation does not change EC_{50} or nicotine potency and efficacy relative to ACh. This means that – in the first approximation - incorporation of β3 is unlikely to change the neurotransmitter sensitivity of α3β4 receptors or their role in responses to nicotine from tobacco smoke.

Interestingly, the greatest difference between our data and that reported in the literature is for the rank order of lobeline potency for human vs. *rat* α3β4. Further, lobeline is the only agonist for which the relative potency is significantly different between α3β4 and α3β4β3, with lobeline less potent on *rat* α3β4 and human α3β4β3 than human α3β4 receptors. In terms of the presumed agonist binding domain the amino acid sequence of human β3 and β4 only differ in loop E: β3 contains a lysine residue in position 106, compared to an arginine in β4; a valine in 112 in place of leucine in β4; and a threonine in 114 in place of a leucine in β4 (numbering of the AChBP, see table 6.4.1.). Both human and *rat* α3 are identical in the amino acid sequence of the presumed agonist binding domain. However, human β4, β3 and *rat* β4 all differ in residue 112 of loop E: leucine in human β4; valine in human β3 and glutamine in *rat* β4. This suggests that a

possible explanation of the difference in lobeline relative potency between human α3β4 and α3β4β3 receptors is due to the presence of different residues in the agonist binding domain contributed by β3 incorporation, specifically the nature of the residue in position 112. It would be interesting to co-express human β3 with *rat* α3β4 to see if the effect of β3 is species specific. Additionally mutating residue 112 would help to clarify this residues role in lobeline relative potency.

However, relative potency data alone is not enough to conclude whether β3 is involved in the agonist binding site or not. At low agonist concentrations the relative potency of an agonist depends on both the binding equilibrium constant (*Kd*) and the gating equilibrium constant (E). Obtaining the *Kd* for a competitive antagonist would provide conclusive evidence for the role of β3 in the binding site. Nevertheless, the change in lobeline relative potency is so small that it is unlikely to be a useful tool for identifying β3 containing receptors in native tissue.

If β3 does participate to the formation of one of the binding sites, the magnitude of its effects will depend on how much its binding residues differ from those of the β subunits that β3 replaces. It is however impossible to predict, without the appropriate experiments, what the effect of β3 incorporation will be on other 'pair' receptor combinations. Future experiments characterising different 'pair' receptor combinations with β3, for example α4β2β3, may reveal more striking differences in rank order and relative potencies of agonists.

Figure 6.1.1. Example responses from partial concentration response curves in α3β4 and α3β4β3 receptors

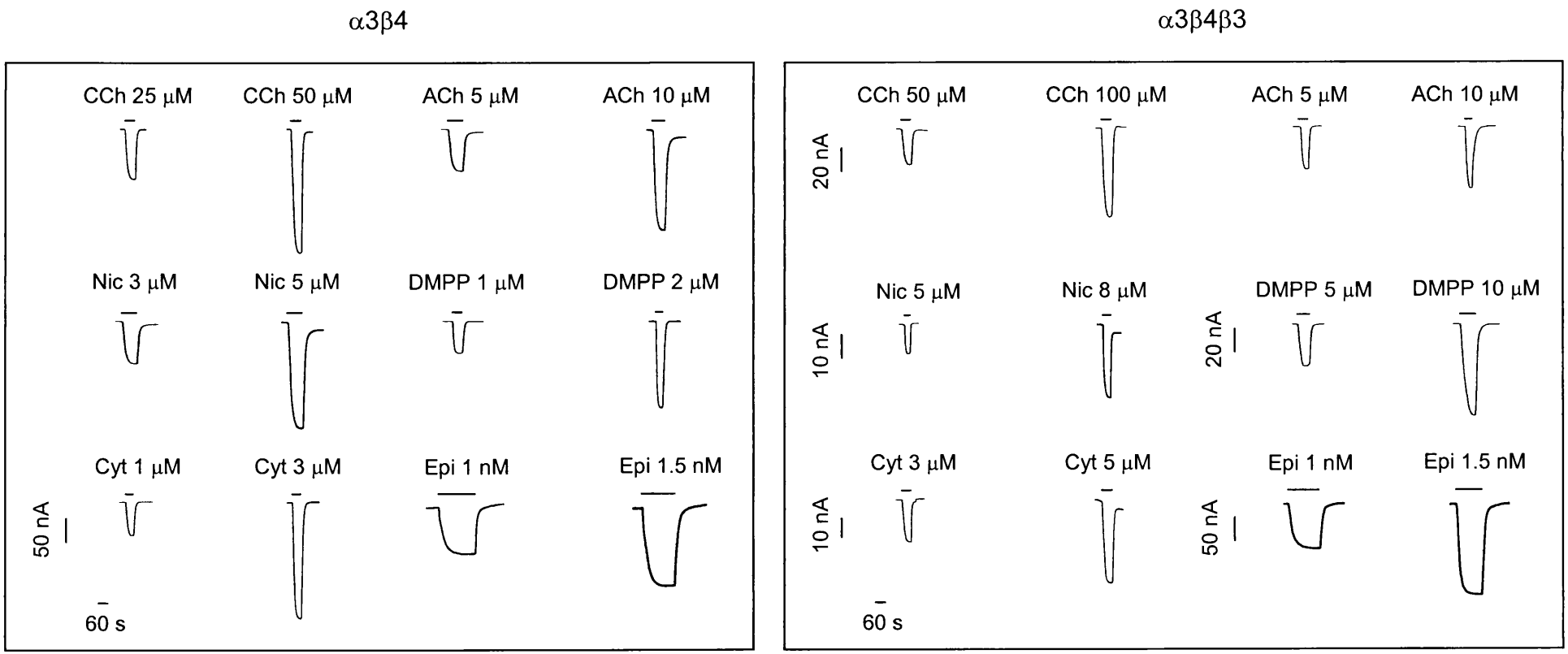

Figure 6.1.1 Shown are example inward currents elicited by bath applied application of agonists to oocytes expressing α3β4 or α3β4β3^{wt} receptors. The agonists used in theses examples were ACh, carbachol (CCh), Nicotine (Nic), DMPP, Cytisine (Cyt) and epibatidine (Epi). Agonist concentrations are indicated above each response along with application bars, indicating the duration of agonist application. Scale bars are shown for current amplitude and time.

Figure 6.3.1. The agonist rank order of potencies on α3β4 is unchanged by the co-expression of β3

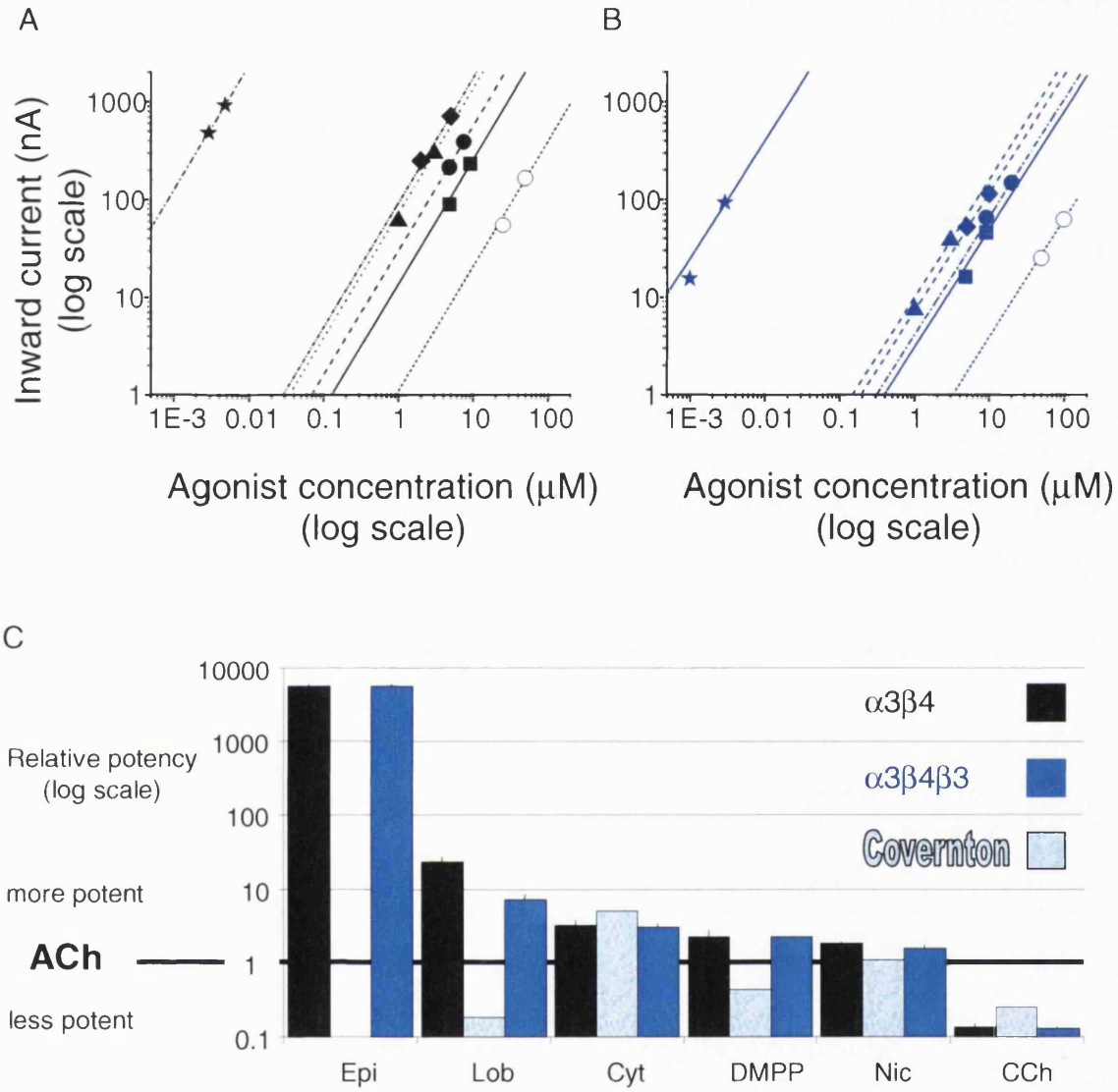

Figure 6.3.1. A and B show partial parallel concentration response curves for ACh (■), carbachol (❍), nicotine (●), cytosine (◆), DMPP (▲) and epibatidine (✳) for α3β4 (A) and ACh (■), carbachol (❍), nicotine (●), cytosine (◆), DMPP (▲) and epibatidine (✳) for α3β4β3 (B). Data were fitted simultaneously with a power function derived from the Hill equation in a constrained fit (with equal Hill slopes) in order to estimate the horizontal distance between curves, expressed as potency ratios (where ACh = 1). The ± S.D. of mean for the data is not shown where the errors fall within the plotted symbol. C shows a plot of the relative potency of agonists obtained from table 6.1.2. α3β4 receptors are indicated in black and α3β4β3 in blue and the data from Covernton *et al.* (1994) are shown for reference, represented by the light blue bars. Error bars show ± S.D. of mean (not shown where the errors fall within the plotted symbol). Agonist are labelled: Epi – Epibatidine; Lob – Lobeline; Cyt – Cytisine; DMPP; Nic- Nicotine; ACh – Acetylcholine; CCh – Carbachol. A reference red line indicates the potency of ACh (1), with agonists falling below the line being less potent and those above the line being the more potent.

Figure 6.3.2. The relative potency of Lobeline on α3β4 is decreased by the co-expression of β3

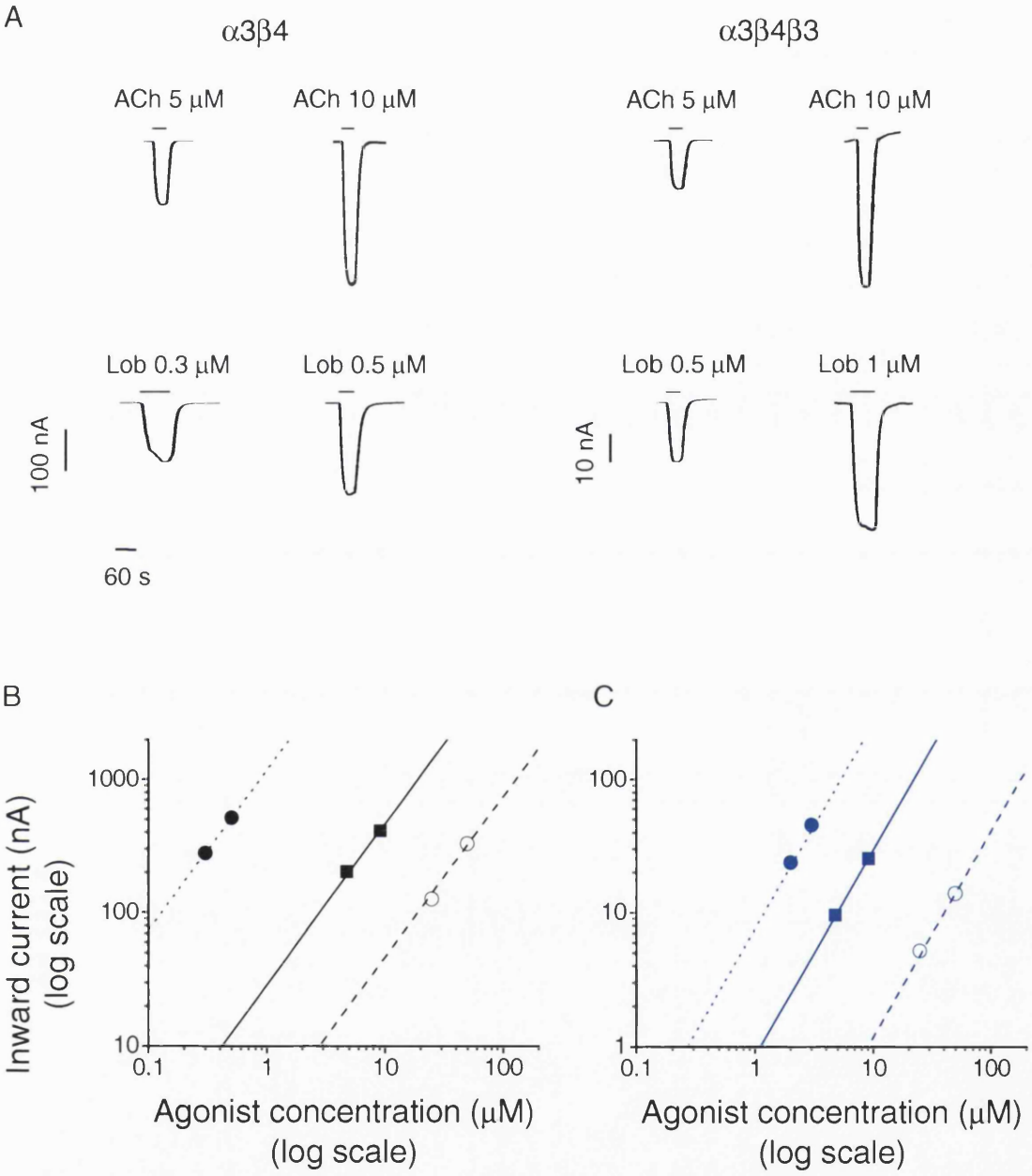

Figure 6.3.2. Shown are example inward currents elicited by bath applied application of agonists to oocytes expressing α3β4 or $\alpha3\beta4\beta3^{wt}$ receptors. The agonists used in theses examples were ACh or lobeline (Lob). Agonist concentrations are indicated above each response along with application bars, indicating the duration of agonist application. Scale bars are shown for current amplitude and time. B and C show partial parallel concentration response curves for ACh (■), carbachol (❍), lobeline (●) for α3β4 (A) and ACh (■), carbachol (❍), lobeline (●) for α3β4β3 (B). The ± S.D. of mean for the data is not shown where the errors fall within the plotted symbol. Data were fitted simultaneously with a power function derived from the Hill equation in a constrained fit (with equal Hill slopes) in order to estimate the horizontal distance between curves, expressed as potency ratios (where ACh = 1).

Table 6.3.3. Potency ratios for α3β4 and α3β4β3 human neuronal nAChRs expressed in *Xenopus* oocytes.

		α3β4			α3β4β3^{wt}			
	Fitted potency ratio from Covernton et al. (1994)	*Mean fitted potency ratio*	*Relative potency*	*n*	*Mean fitted potency ratio*	*Relative potency*	*n*	*p*
ACh		1	1		1	1		
Epibatidine	-	1.72 X 10^{-04} ± 4.23E-06	5828 ± 143.5	3	1.72 10^{-04} ± 7.71 X 10^{-06}	5831 ± 262.3	6	0.99
Lobeline	5.56	0.04 ± 0.01	23.0 ± 3.70	7	0.14 ± 0.02	7.14 ± 1.11	6	0.01
Cytisine	0.20	0.31 ± 0.04	3.23 ± 0.45	6	0.32 ± 0.02	3.10 ± 0.19	7	0.78
DMPP	2.33	0.44 ± 0.08	2.28 ± 0.41	7	0.45 ± 0.01	2.21 ± 0.06	9	0.86
Nicotine	0.91	0.55 ± 0.04	1.82 ± 0.12	8	0.62 ± 0.04	1.60 ± 0.10	13	0.16
Carbachol	4.00	7.53 ± 1.14	0.13 ± 0.02	6	7.71 ± 0.31	0.13 ± 0.01	6	0.88

Table. 6.3.3. The mean fitted potency ratio is the mean (± S.D. of mean) of parameter estimates obtained by fitting partial concentration response curve simultaneously with a power function. Relative potencies are expressed as reciprocals of the potency ratio (± Fieller S.D. of mean: expressed as S.D. of mean relative potency / mean relative potency^2). A relative potency greater than 1 indicates that the agonist is more potent than ACh.

Table 6.4.1. Summary of residues in the presumed ACh binding site of human α3, β3 and *rat* β4 subunits

Loop	D		A	E				B		F	C			
No.	53	55	89	104	106	112	114	143	145	164	185	187	188	192
α3 Human	-	-	Y					W	Y	-	Y	C	C	Y
α3 Rat	-	-	Y					W	Y	-	Y	C	C	Y
β4 Human	W	K	-	I	R	L	L	-	-	D	-	-	-	-
β4 Rat	W	K	-	I	R	Q	L	-	-	D	-	-	-	-
β3 Human	W	K	-	I	K	V	T	-	-	D	-	-	-	-

Table 6.4.1. Shows a sequence alignment of human α3, β4, β3 and rat α3 and β4 neuronal nAChR subunits to the amino acid residues (single letter code) involved in the AChBP model of the ligand binding site (loops indicated with numbering of the AChBP). The subunit type is indicated.

6.5. The antagonist profile of α3β4 and α3β4β3 receptors

From chapter 5 we have seen that α3β4β3 triplet receptors have a stoichiometry of 2:2:1, with β3 replacing one β4 subunit. However, these data only indicate the number of copies of β3 and not its position in the receptor complex. Knowing the arrangement of the triplet receptor is important to understand the function of β3.

For the muscle nAChR, two different models have been proposed for the nature of the agonist-binding site (see chapter 1): the α-δ, α-γ subunit interface (Karlin & Akabas, 1995) and the α subunits agonist binding pocket (Unwin, 1998). Both models agree that δ and γ subunits may influence the properties of the receptor by forming (for a review see Karlin & Akabas, 1995) or interacting (Unwin 1998) with the binding site. Thus it would follow that if β3 replaces a β4 subunit in the equivalent δ or γ position in the neuronal nAChR, then β3 may affect the properties of the receptor by interacting with the agonist-binding site.

The potency ratio data presented in the previous section show that β3 incorporation reduces the relative potency of lobeline, but the rank-order of agonist potencies is unchanged. However, potency ratio data alone is not sufficient to determine whether β3 interacts with the binding site or not. In an agonist potency ratio experiment we are measuring both the binding and the gating states of the reaction mechanism. In order to confirm whether β3 is involved in the binding site or not, we need to concentrate on the binding step of the reaction, separating binding and gating. We can get information on the binding site by using a competitive antagonist, because this binds to a site that overlaps with the agonist one (binding of agonist and competitive antagonist is mutually exclusive), but does not activate the receptor. Indeed, the sensitivity of competitive

antagonists on neuronal nAChRs has been shown to depend on the nature of both the α and β subunits (Cachelin & Rust 1995; Harvey & Luetje, 1996; Chavez-Noriega *et al.*, 1997). Note however that clearly the results reported are IC_{50}s (which depend on agonist concentration) and that the mechanism of action of the blocker has not been characterised.

A more robust approach is to use a competitive antagonist experimentally to calculate the equilibrium constant for the binding reaction (K_B) using the Schild method (Schild, 1949; Arunlakshana & Schild, 1959, see chapter 2). If β3 is involved in, or has an effect on the binding site of the receptor, then the K_B for a competitive antagonist could in principle differ between α3β4 and α3β4β3 receptors.

There are few true competitive antagonists of neuronal nAChR (Sivilotti *et al.*, 2000). Trimetaphan has been shown to act as a competitive antagonist on neuronal nAChRs in rat parasympathetic ganglion (Ascher *et al.*, 1979). Because often nAChR antagonists act as channel blockers, we reviewed the current literature for competitive antagonists for α3β4 receptors. One of the problems that we encountered was that often, complete Schild analysis was not carried out. We choose trimetaphan and DHβE because they have both been shown to act competitively on nAChRs (Ascher *et al.*, 1979; Bertrand *et al.*, 1992). Mecamylamine and +-tubocurarine were also chosen to expand the sensitivity of the characterisation, despite their known ability to act as open channel blockers. Mecamylamine and +-tubocurarine were used at low agonist concentrations (less than EC_{10}), to reduce channel block (given that this should be more effective at high p_{open}) and assess whether or not any competitive action was present. Despite these precautions, we failed to complete Schild analysis for mecamylamine and + tubocurarine, because channel block was apparent even at low concentrations.

As discussed in Chapter 1, the majority of ganglionic neuronal nAChRs consist of α3β4 'pair' and sometimes α3β4α5 'triplet' receptors (Conroy & Berg, 1995; Corriveau & Berg, 1993; Vernallis *et al.*, 1993). The reported competitive nature of trimetaphan on ganglionic nAChRs therefore makes it reasonable to expect it to behave as a competitive antagonist on recombinant α3β4 receptors. The next aim of the project was to estimate the K_B for α3β4 and α3β4β3 receptors, using trimetaphan in a Schild experiment. A difference in the K_B of the 'pair' vs. the 'triplet' would be a strong indication that the β3 subunit has changed the binding site.

6.6. The equilibrium constant for trimetaphan is similar for both α3β4 and α3β4β3 receptors

Initially a control, partial concentration-response curve for bath-applied ACh was obtained in oocytes expressing α3β4 and α3β4β3 receptors using the protocol described in Chapter 2. The oocytes were then superfused with Ringer containing the desired concentration of antagonist; ACh agonist responses were obtained by co-applying ACh (i.e. by making up the ACh concentration in trimetaphan solution), in order to maintain a constant antagonist concentration throughout the experiment (see solutions Chapter 2). Care was taken to make sure that equilibrium with the antagonist was reached. Example responses are shown in figures 6.6.1 and 6.6.2. Three concentrations of antagonist were tested to obtain a series of parallel, partial concentration-response curves for the construction of a Schild plot (see figures 6.6.3 – 6.6.6.). In order to reduce the potentially distorting effect of response rundown, we kept experiments short and each oocyte only provided one control and one antagonist concentration-response curve (i.e. one dose ratio value).

The partial concentration response curves for ACh in control conditions and in the presence of antagonist in each oocyte were then plotted on log/log scale in order to produce linear plots. Parallel ACh and ACh + antagonist curves for each oocyte were then fitted simultaneously with equal weighting and equal Hill slopes to a power function derived from the Hill equation using David Colquhoun's CVfit programme (see Chapter 2). Fitting produced estimates of the horizontal distance between the partial concentration response curves, expressed as dose ratios, where a dose ratio > 1 indicates a rightward shift in the concentration-response curve. Although each dose ratio was obtained from a separate experiment and thus a separate oocyte, the receptor expression levels were relatively constant (summarised in figure 6.6.6). Inspection of the dose response curves showed that the rightward shift produced by the antagonist appeared to be parallel, encouraging us to complete a Schild analysis.

The fitted dose ratios (termed *r*) from each oocyte were then pooled (see table 6.6.7.) and plotted on a log/log scale as *r*-1 against trimetaphan concentration, in order to construct Schild plots for both α3β4 and α3β4β3 receptors (the data points in figure 6.6.9.). The dose ratios were then fitted with weights given by the reciprocals of their variance, either in a free fit or in a Schild fit (with a fixed slope of 1) in order to obtain the K_B for the antagonist (see table 6.6.8. and figure 6.6.9.).

The free fit gave slopes of 0.8 and 1.07 for the α3β4 and the α3β4β3 combinations respectively. These values are not significantly different from 1, hence we proceeded with the Schild fit and obtained K_B values for trimetaphan of 75.5 ± 1.8 nM for α3β4 vs. 66.0 ± 1.7 nM for α3β4β3. The similarity in the K_B values suggests that β3 is not involved in the receptor binding site and that β3 may act as a structural subunit.

Figure 6.6.1. Example responses from partial concentration response curves in α3β4 receptors

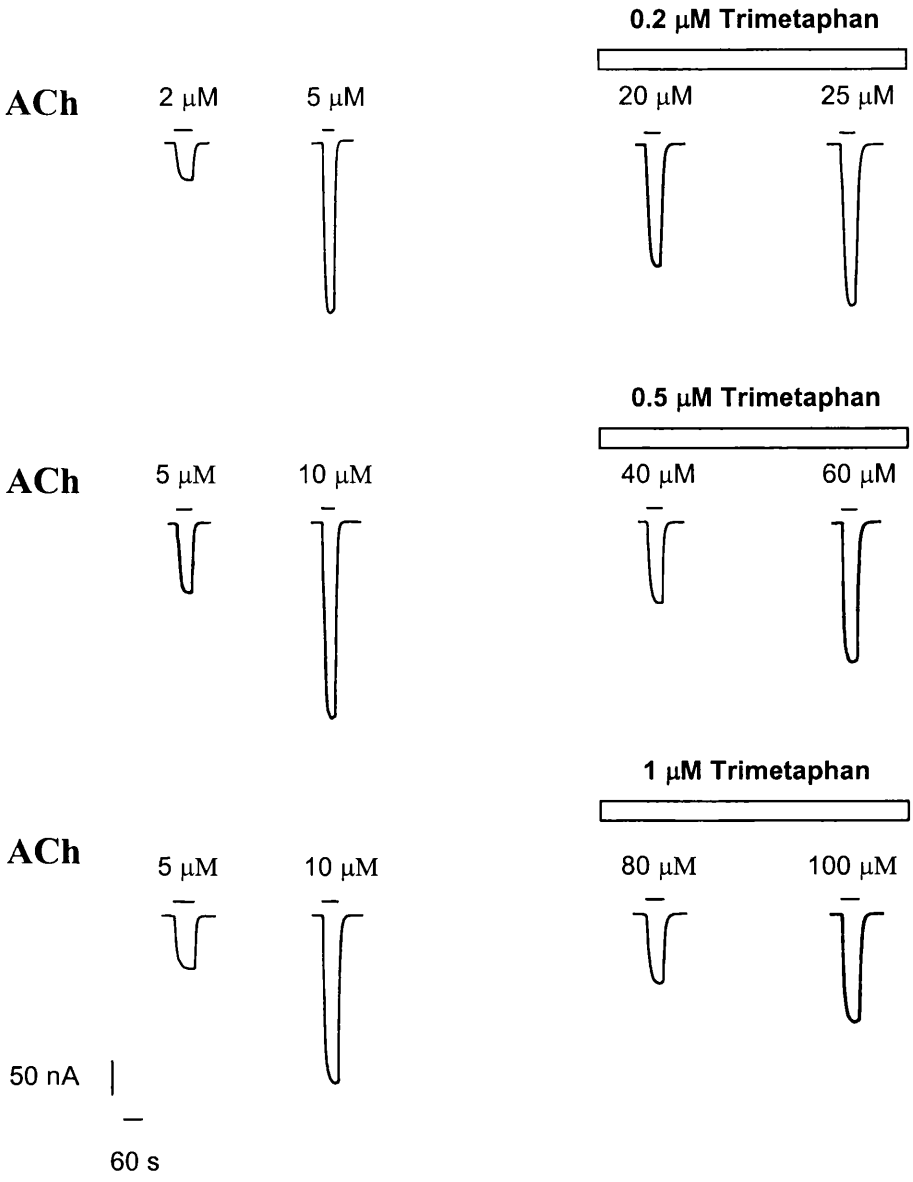

Figure 6.6.1. Shown are example inward currents elicited by bath applied application of ACh or ACh + trimetaphan (ACh + Tri) to oocytes expressing α3β4 receptors. ACh and trimetaphan concentrations are indicated above each response along with application bars, indicating the duration of agonist application. Scale bars are shown for current amplitude and time.

Figure 6.6.2. Example responses from partial concentration response curves in α3β4β3 receptors

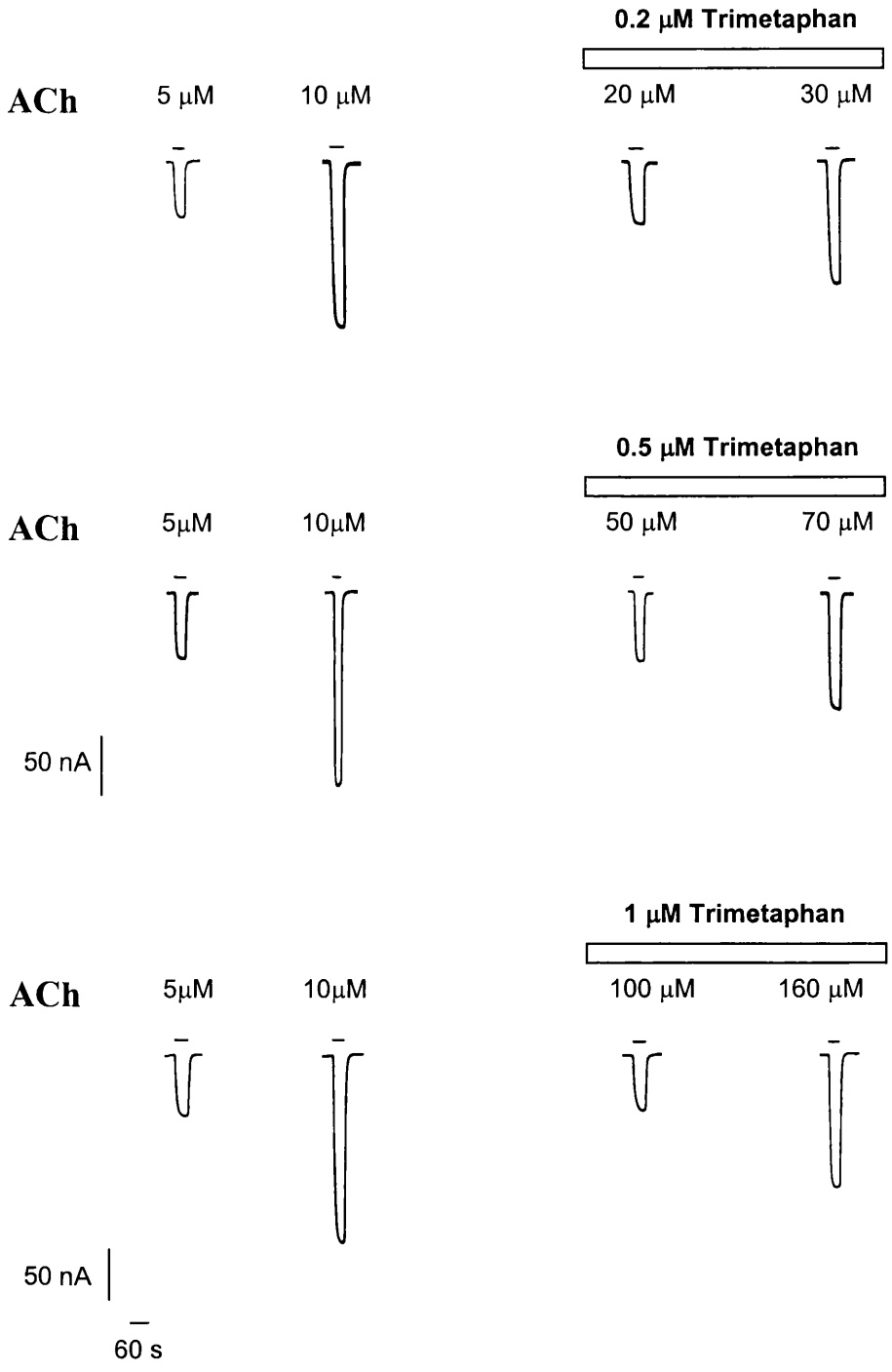

Figure 6.6.2. Shown are example inward currents elicited by bath applied application of ACh or ACh + trimetaphan (ACh + Tri) to oocytes expressing $\alpha 3\beta 4\beta 3^{wt}$ receptors. ACh and trimetaphan concentrations are indicated above each response along with application bars, indicating the duration of agonist application. Scale bars are shown for current amplitude and time.

Figure 6.6.3. Partial concentration response curves for 0.2 μM trimetaphan on oocytes expressing α3β4 or α3β4β3 receptors

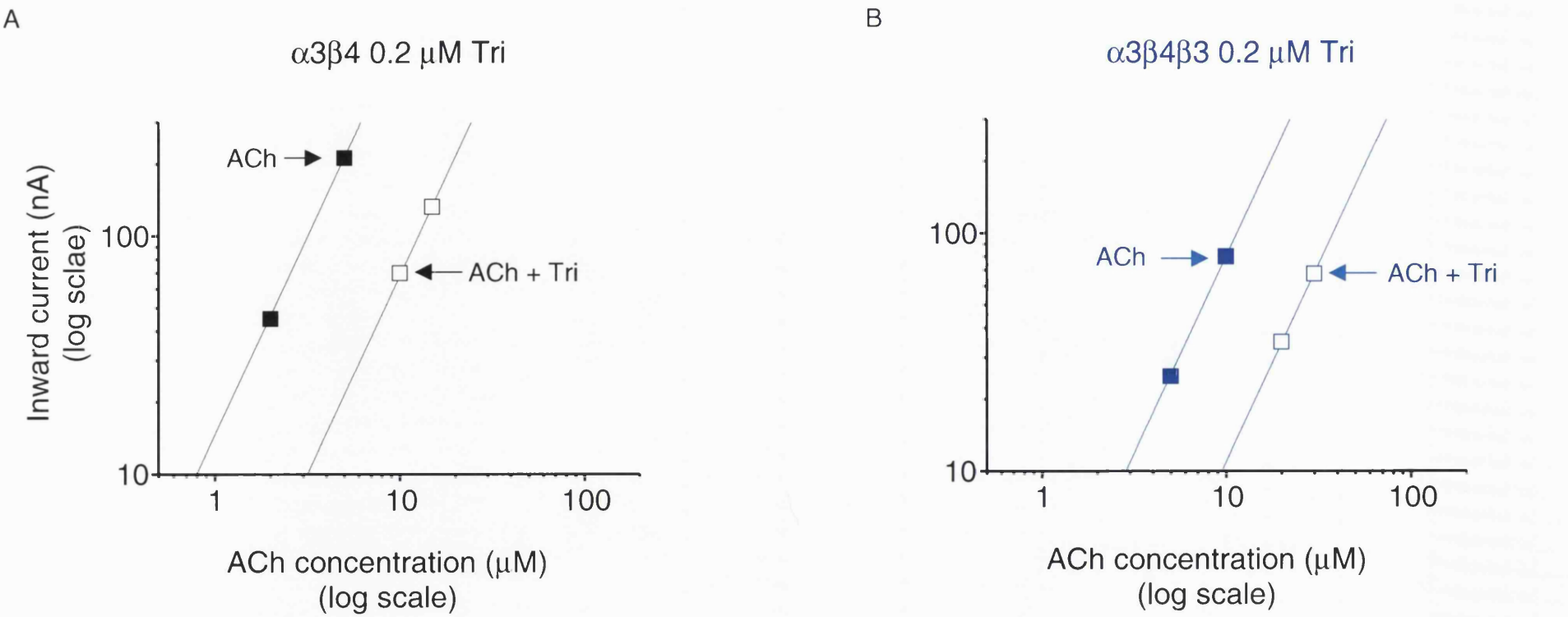

Figure 6.6.3. A and B show partial parallel concentration response curves for ACh (■) and ACh + trimetaphan (⊐) α3β4 and α3β4β3 ACh (■) and ACh + trimetaphan (❒).The ± S.D. of mean for the data is not shown where the errors fall within the plotted symbol. Data were fitted simultaneously with a power function derived from the Hill equation in a constrained fit (with equal Hill slopes) in order to estimate the horizontal distance between curves, expressed as dose ratios (where ACh = 1).

Figure 6.6.4. Partial concentration response curves for 0.5 μM trimetaphan on oocytes expressing α3β4 or α3β4β3 receptors

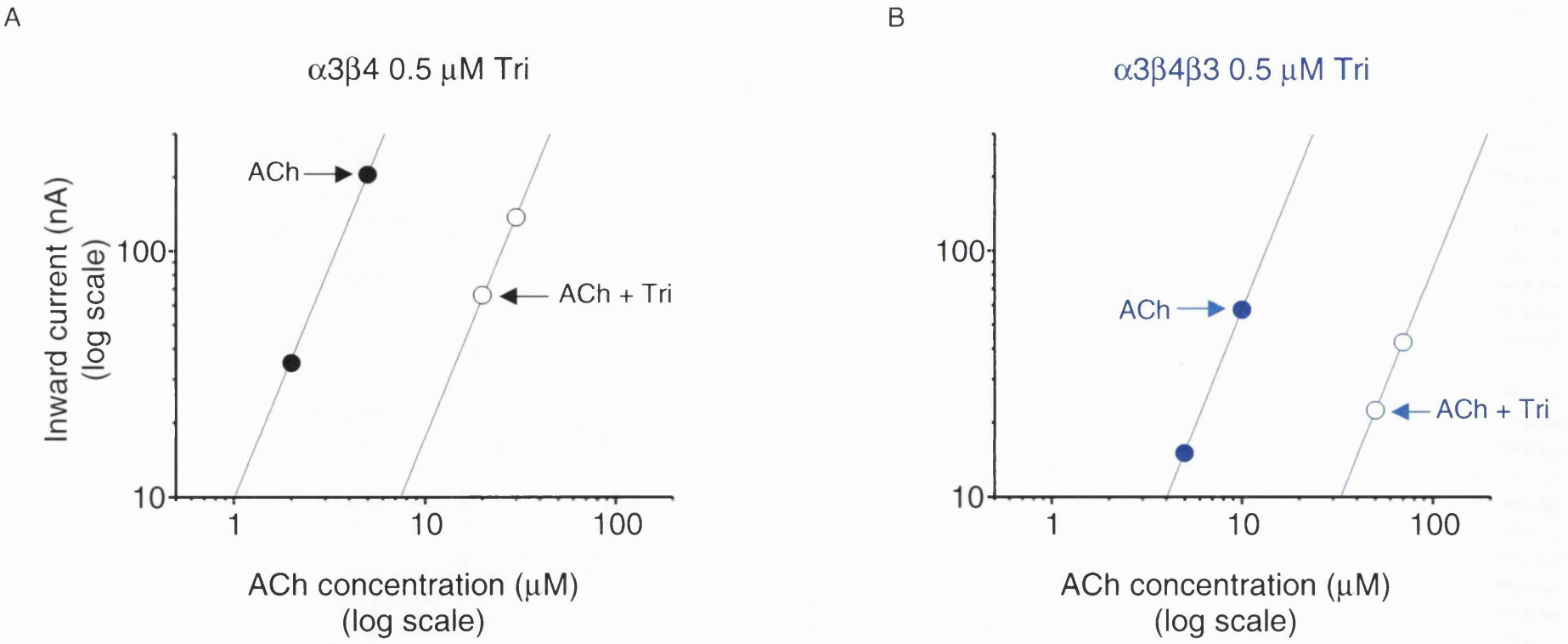

Figure 6.6.4. A and B show partial parallel concentration response curves for ACh (●) and ACh + trimetaphan (○) α3β4 and α3β4β3 ACh (●) and ACh + trimetaphan (○).The ± S.D. of mean for the data is not shown where the errors fall within the plotted symbol. Data were fitted simultaneously with a power function derived from the Hill equation in a constrained fit (with equal Hill slopes) in order to estimate the horizontal distance between curves, expressed as dose ratios (where ACh = 1).

Figure 6.6.5. Partial concentration response curves for 1 μM trimetaphan on oocytes expressing α3β4 or α3β4β3 receptors

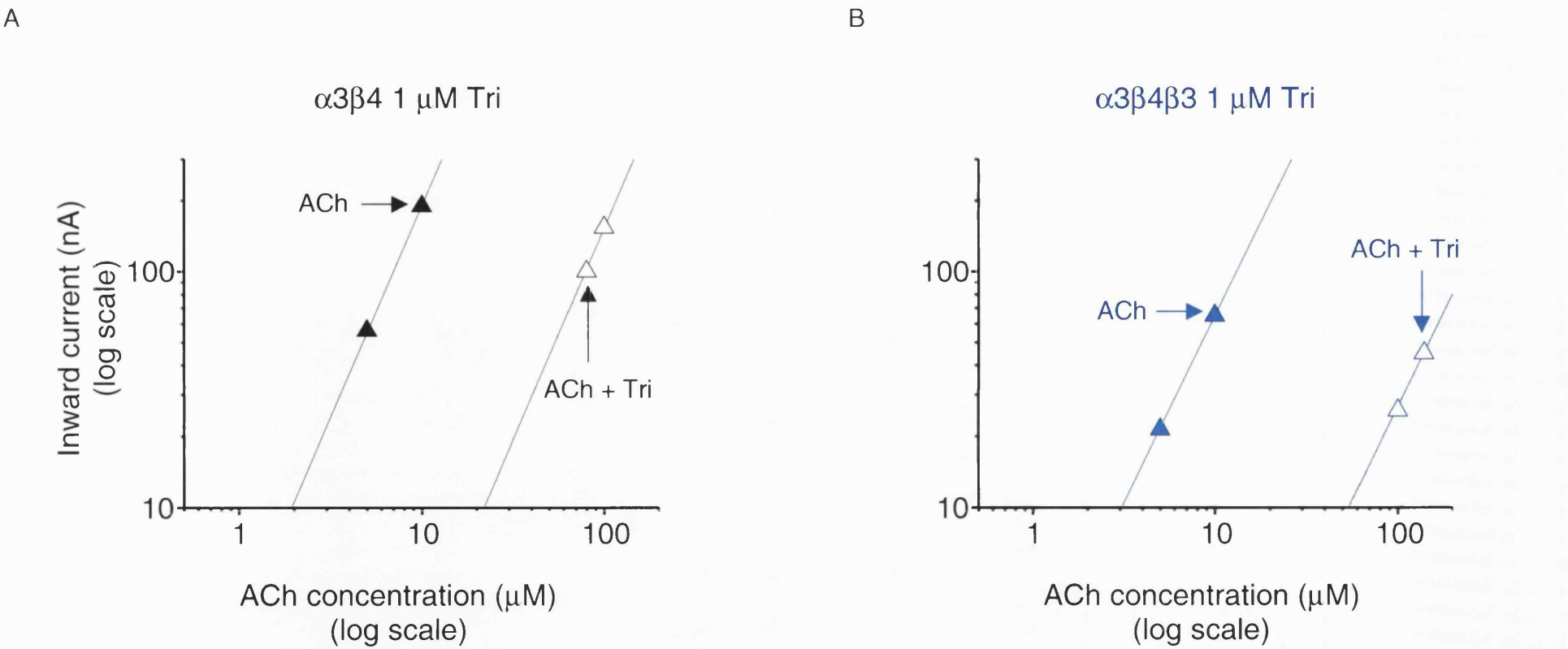

Figure 6.6.5. A and B show partial parallel concentration response curves for ACh (▲) and ACh + trimetaphan (△) α3β4 and α3β4β3 ACh (▲) and ACh + trimetaphan (△). The ± S.D. of mean for the data is not shown where the errors fall within the plotted symbol. Data were fitted simultaneously with a power function derived from the Hill equation in a constrained fit (with equal Hill slopes) in order to estimate the horizontal distance between curves, expressed as dose ratios (where ACh = 1).

Figure 6.6.6. Summary of partial concentration response curves for 0.2 - 1 μM trimetaphan on oocytes expressing α3β4 or α3β4β3 receptors

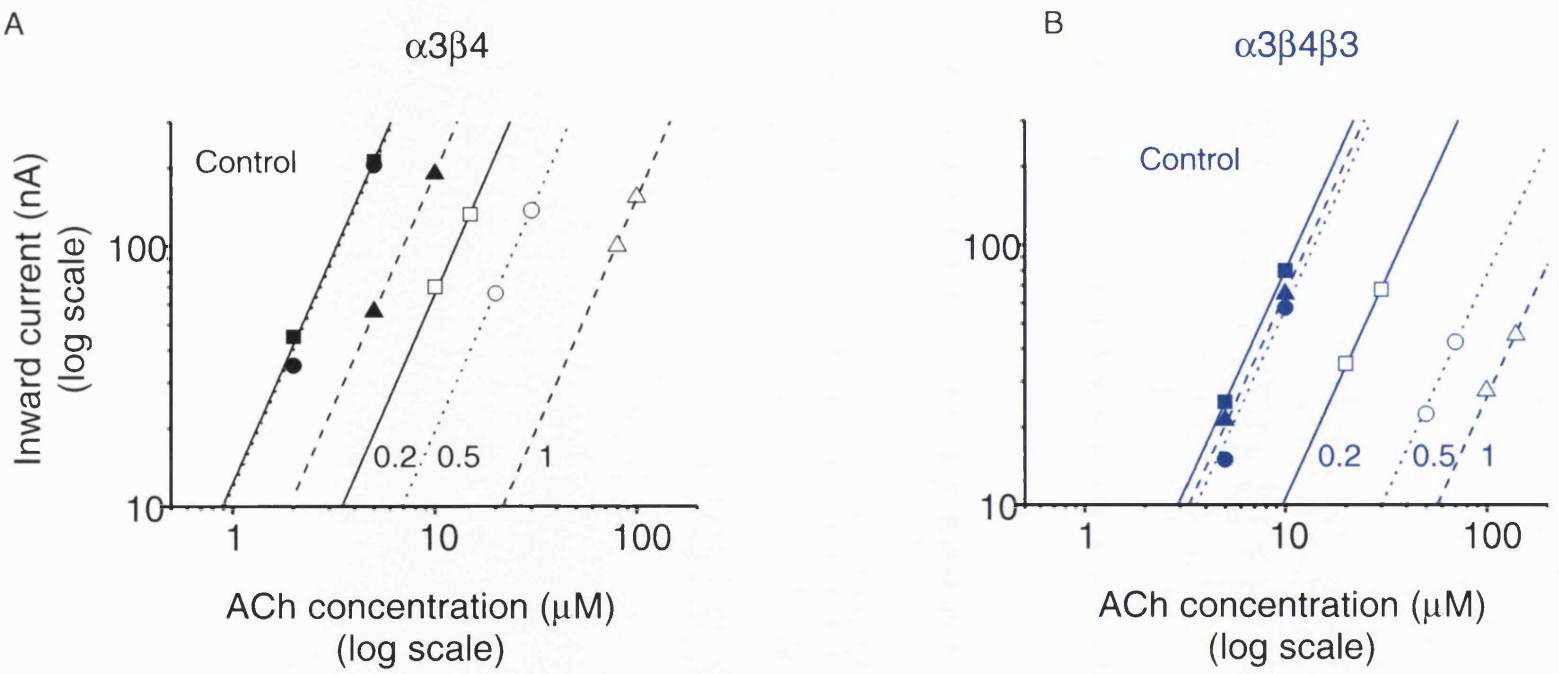

Figure 6.6.6. A and B show examples of partial parallel concentration response curves for α3β4 (black) and α3β4β3 (blue) receptors. ACh (solid lines) and ACh + trimetaphan (dotted lines) curves are indicated. Each set of ACh and ACh + trimetaphan curves were obtained from 1 oocyte experiment, with each experiment indicated as; control ACh (■) and ACh + 0.2 μM trimetaphan (❑), control ACh (●) and ACh + 0.5 μM trimetaphan (○), control ACh (▲) and ACh + 1 μM trimetaphan (△) for α3β4; control ACh (■) and ACh + 0.2 μM trimetaphan (❑), control ACh (●) and ACh + 0.5 μM trimetaphan (○), control ACh (▲) and ACh + 1 μM trimetaphan (△) for α3β4β3. The ± S.D. of mean for the data is not shown where the errors fall within the plotted symbol. Data were fitted simultaneously with a power function derived from the Hill equation in a constrained fit (with equal Hill slopes) in order to estimate the horizontal distance between curves, expressed as dose ratios (where ACh = 1).

Table 6.6.7. Fitted dose ratios for trimetaphan on α3β4 and α3β4β3 receptors

α3β4			α3β4β3			
Trimetaphan concentration (μM)	Dose ratio	*n*	Trimetaphan concentration (μM)	Dose ratio	*n*	*p*
0.2	4.35 ± 0.38	3	0.2	3.70 ± 0.15	6	0.22
0.5	7.62 ± 0.17	4	0.5	9.33 ± 0.48	6	**0.01**
1	13.02 ± 1.15	3	1	16.49 ± 0.52	3	**0.05**

Table 6.6.7. Shows the mean (± S.D. of mean) fitted dose ratios for trimetaphan on α3β4 and α3β4β3 receptors. Where *p* is the result of a 2 tail *t*-test assuming unequal variance. Here *p* values of 0.05 or less were taken to be significant. Note that the dose ratios for 0.5 and 1 μM trimetaphan differ significantly between α3β4 and α3β4β3.

Table 6.6.8. Schild fit of dose ratios for trimetaphan on α3β4 and α3β4β3 receptors

	Schild fit K_B (nM)	Free fit K_B (nM)	Slope	*n*
α3β4	75.5 ± 1.8	26.3	0.80	10
α3β4β3	66.0 ± 1.7 (*p* 0.67)	78.3	1.07	15
α3β4 (omitting 1 μM)	74.9 ± 1.9	19.0	0.74	10
α3β4β3 (omitting 1 μM)	68.0 ± 2.7 (*p* 0.48)	110.6	1.23	15

Table 6.6.8. Shows a summary of the mean (± S.D. of mean) binding equilibrium constant (K_B) for Trimetaphan on α3β4 and α3β4β3 neuronal nAChRs, obtained from a Schild plot where the slope is fixed to 1 (Schild fit) or a linear least squares fit (free slope) of the dose ratios in table 6.5.7. Here *p* is the result of a two-tailed *t*-test, comparing the mean K_B value for α3β4 with α3β4β3. Here *p* values of 0.05 or less were taken to be significant. Note that the constrained and free K_B values are similar for α3β4 and α3β4β3.

Figure 6.6.9. Schild plots for trimetaphan on α3β4 and α3β4β3 receptors

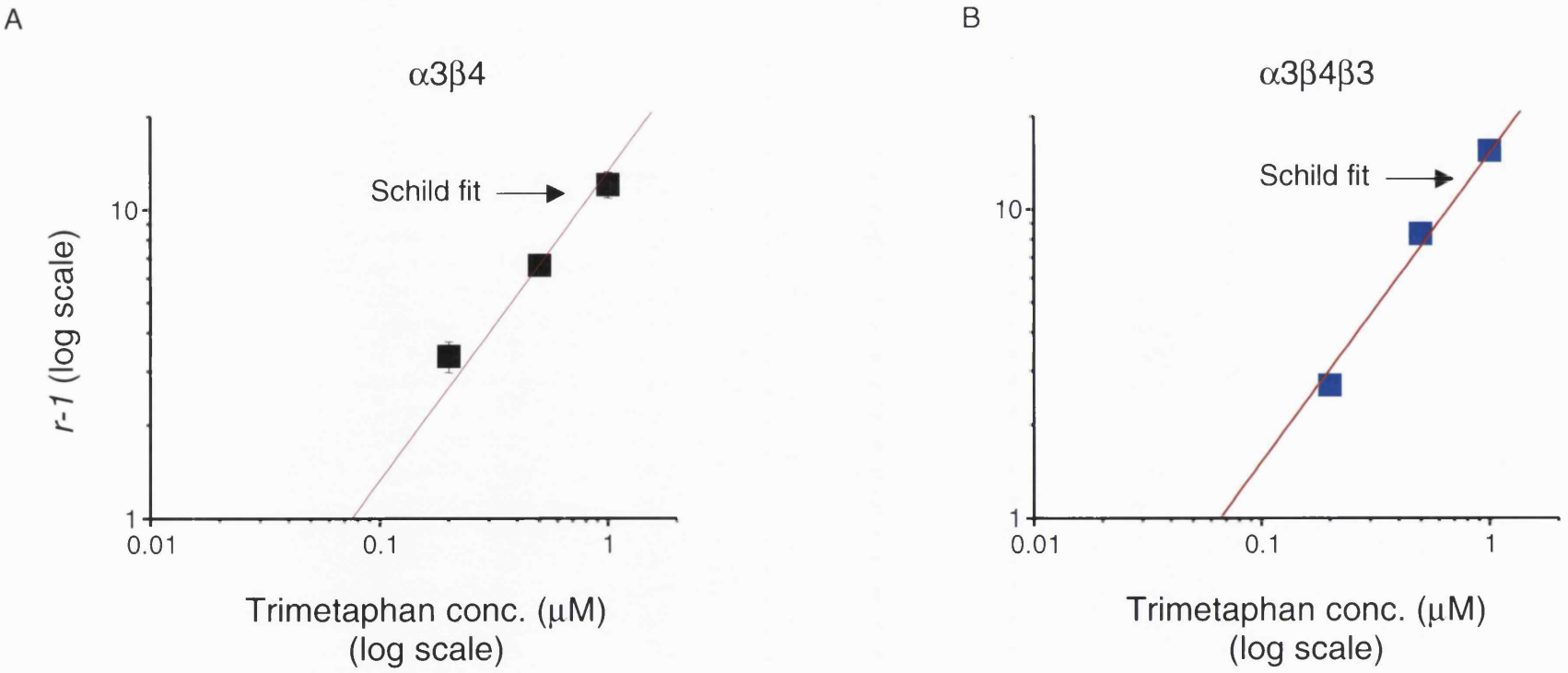

Figure 6.6.9. A and B show the Schild fits for trimetaphan on α3β4 and α3β4β3 receptors. Observed data points are shown for α3β4 (■) and α3β4β3 (■).The ± S.D. of mean for the data is not shown where the errors fall within the plotted symbol. Note that the α3β4β3 data provide a better Schild fit than α3β4.

6.7. Trimetaphan has a similar K_B for α3β4 and α3β4β3 receptors

Schild analysis with a competitive antagonist is the most robust method for characterising receptors as it measures a physical constant, the binding equilibrium constant of the agonist, unaffected by the nature of the agonist, the agonist concentration and the rate of agonist application (Sivilotti *et al.*, 2000).

Unfortunately for neuronal nAChRs, true competitive antagonists of neuronal nAChR are rare (Sivilotti *et al.*, 2000). Homomeric α7 receptors have a few competitive antagonists, such as α-conotoxin-ImI (selective for homomeric α7 over α2β2, α3β2, α4β2, α2β4, α3β4, α4β4 'pair' neuronal nAChRs expressed in *Xenopus* oocytes at concentrations of up to 5 μM; Johnson *et al.*, 1995) and acts competitively at α-Bgt sensitive (containing α7) neuronal nAChRs in rat hippocampal neurons (Pereira *et al.*, 1996). Methyllycaconitine (MLA) has been shown to act competitively on α7 homomeric receptors expressed in *Xenopus* oocytes (Palma *et al.*, 1996). Matsubayashi *et al.* (1998) have shown that strychnine acts competitively on α-Bgt sensitive neuronal nAChRs and as an open channel blocker on α-Bgt insensitive neuronal nAChRs (mostly α4β2) in rat hippocampal neurons. DHβE has been shown to act competitively on α7 (Bertrand *et al.*, 1992).

In terms of 'pair' receptors, α-conotoxin AuIB is selective for α3β4 over other 'pair' neuronal nAChRs expressed in *Xenopus* oocytes, but it has not been shown to act competitively (Luo *et al.*, 1998) and is currently not available. DHβE is potent at α4β2 and is thought to act competitively (Harvey & Luetje, 1996; Buisson *et al.*, 1996; Chavez-Noriega *et al.*, 1997), but has low potency on α3β4 (Harvey & Luetje, 1996; Chavez-Noriega *et al.*, 1997). Trimetaphan has been shown to act as a competitive

antagonist on neuronal nAChRs in rat parasympathetic ganglion (Ascher *et al.*, 1979). The reported competitive nature of Trimetaphan on ganglionic nAChRs therefore makes it reasonable to expect it to behave as a competitive antagonist on recombinant α3β4 receptors.

As we have seen in chapter 4, β3 replaces a β in the formation of the α3β4β3 triplet receptor. Thus it would follow that β3 incorporation may affect sensitivity and thus the K_B of trimetaphan on α3β4 'pair' receptors. Comparing α3β4 with α3β4β3 in a two-tailed *t*-test assuming unequal variance, revealed that the K_B values were similar for both receptors. Here α3β4 had mean K_B values of 75.5 ± 1.8 vs. 66.0 ± 1.7 (p 0.67). Thus β3 is incorporated, but does not significantly affect the binding site. Either β3 replaces a β4 in the binding site and is able to behave like β4, or β3 has a structural role replacing a β4 that is not involved in the binding site.

Data from the free fit of the trimetaphan dose ratios revealed a difference in the slopes between α3β4 and α3β4β3, with an increase in the slope from 0.8 for α3β4 to 1.07 for α3β4β3 (see table 6.6.8.). However, it is unlikely that the steep slope observed for a α3β4β3 is due to block, as omitting the 1 μM data point and refitting the data results in a steeping of the slope, yet retains similar mean K_B values for α3β4 and α3β4β3 (74.9 ± 1.9 vs. 68.0 ± 2.7, p 0.48, see table 6.6.8.). Further, no off responses (indicative of channel block washing off) were ever observed for any of the experiments. This would suggest that the shallower slope observed in α3β4 results from the rundown of responses.

Comparing the dose ratios for α3β4 with α3β4β3 in a two-tailed *t*-test, revealed a significant increase in the dose ratios for both 0.5 and 1 μM trimetaphan for α3β4β3. Here the mean dose ratio for 0.5 μM trimetaphan increased from 7.62 ± 0.17 for α3β4 to 9.33 ± 0.48 for α3β4β3 (p 0.01) and from 13.02 ± 1.15 for 1 μM for α3β4 to 16.49 ± 0.52 for α3β4β3 (p 0.05).

A possible explanation for this observed increase, is that the co-expression of β3 alters the binding site. However, the results of the Schild fit make this unlikely, as there is no significant difference in the resulting K_B values (see table 6.6.8.). A more likely explanation for this increase is that the extent of rundown is greater in α3β4 than α3β4β3.

6.8. Both α3β4 and α3β4β3 receptors are resistant to block by dihydro-β-erythroidine

Using the protocol described above for Trimetaphan, DHβE was applied to oocytes expressing α3β4 or α3β4β3 receptors. Initially a control, partial concentration-response curve for bath-applied ACh was obtained in oocytes expressing α3β4 and α3β4β3 receptors using the protocol described in Chapter 2. Next the oocytes were superfused with Ringer containing antagonist (see solutions Chapter 2); responses to ACh in the presence of DHβE were obtained by co-applying ACh and DHβE. Care was taken to make sure that equilibrium with the antagonist was reached. Example responses are shown in figures 6.8.2.

In order to reduce the potentially distorting effect of response rundown, we kept experiments short and each oocyte only provided one control and one antagonist concentration-response curve (i.e. one dose ratio value).

The partial concentration response curves for ACh in control conditions and in the presence of antagonist in each oocyte were then plotted on log/log scale in order to produce linear plots. Parallel ACh and ACh + antagonist curves for each oocyte were then fitted simultaneously with equal weighting and equal Hill slopes to a power function derived from the Hill equation using David Colquhoun's CVfit programme (see Chapter 2). Fitting produced estimates of the horizontal distance between the partial concentration response curves, expressed as dose ratios, where a dose ratio > 1 indicates a rightward shift in the concentration-response curve.

A concentration of 30 μM DHβE was required in both α3β4 and α3β4β3 receptors in order to produce a measurable rightward shift. Note from figure 6.8.2. that this rightward shift produced a partial concentration response curve which was parallel to the reference ACh partial concentration-response curve. Because the required concentration was so high and the dose ratios were similar for both α3β4 and α3β4β3 receptors, it was decided not to carry out a full Schild analysis.

The mean fitted dose ratios for the 30 μM concentration of DHβE were identical for α3β4 and α3β4β3 receptors: 3.66 ($n = 2$) for α3β4 vs. 3.83 for α3β4β3 ($n = 2$). If we make the assumption that DHβE is acting competitively, then a dose ratio of this magnitude at 30 μM would indicate an approximate K_B of 11 μM. This is in line with what is expected for DHβE on α3β4 receptors calculated from IC_{50} values using the Cheng-Prusoff correction (Wong *et al.*, 1995; Harvey & Luetje, 1996; Chavez-Noriega

et al., 1997 and Stauderman *et al.*, 1998). However, the Cheng-Prusoff correction is not valid for co-operative receptor activation (Lucia Sivilotti, personal communication).

Using chimeric subunits formed from combinations of rat β2 and β4, (Harvey & Luetje, 1996) identified the first 103 N-terminal residues of the β subunit as important for DHβE sensitivity in α3β2 and α3β4 receptors, with the major determinant located within residues 54 to 63 (rat β2 numbering). Mutating the residues between positions 54 and 63 further identified residues 55, 56 and 59 as important for DHβE sensitivity, with residue 59 having the greatest effect (Harvey & Luetje, 1996). Here mutating threonine in position 59 to lysine in the β2 subunit reduced the sensitivity of α3β2 to DHβE, shifting the DHβE inhibition curve 9-fold to the right, increasing the IC_{50} from 0.41 μM to 3.8 μM. Note residue 59 corresponds to the second residue of loop D of the complementary ligand binding site (residue 55 in the numbering of the AChBP).

Aligning the N-terminal domains of β2, β4 and β3 with rat β2, reveals that residues 54 to 63 are identical in β4 and β3 (see figure 6.8.1.). Thus it is possible that β3 would not affect the DHβE sensitivity even if it is incorporated in the binding site.

Figure 6.8.1. Sequence alignment of the N-terminal region conferring sensitivity to DHβE in human and rat neuronal nicotinic receptor β subunits

	54					59				63
Rat β2	T	N	V	W	L	T	Q	E	W	E
Human β2	T	N	V	W	L	T	Q	E	W	E
Human β4	T	N	V	W	L	K	Q	E	W	T
Human β3	T	N	V	W	L	K	Q	E	W	T

Figure 6.8.1. The residues conferring DHβE sensitivity in the N-terminal domain aligned with rat β2 (residues 54 to 63, rat β2 numbering). Residue 59, critical for DHβE sensitivity, is indicated in red. β subunit type and species of origin are indicated. All residues are shown according to the single letter amino acid code. Note there is no difference in the residues between human β4 and human β3.

Figure 6.8.2. Example responses from partial concentration response curves in α3β4 and α3β4β3 receptors

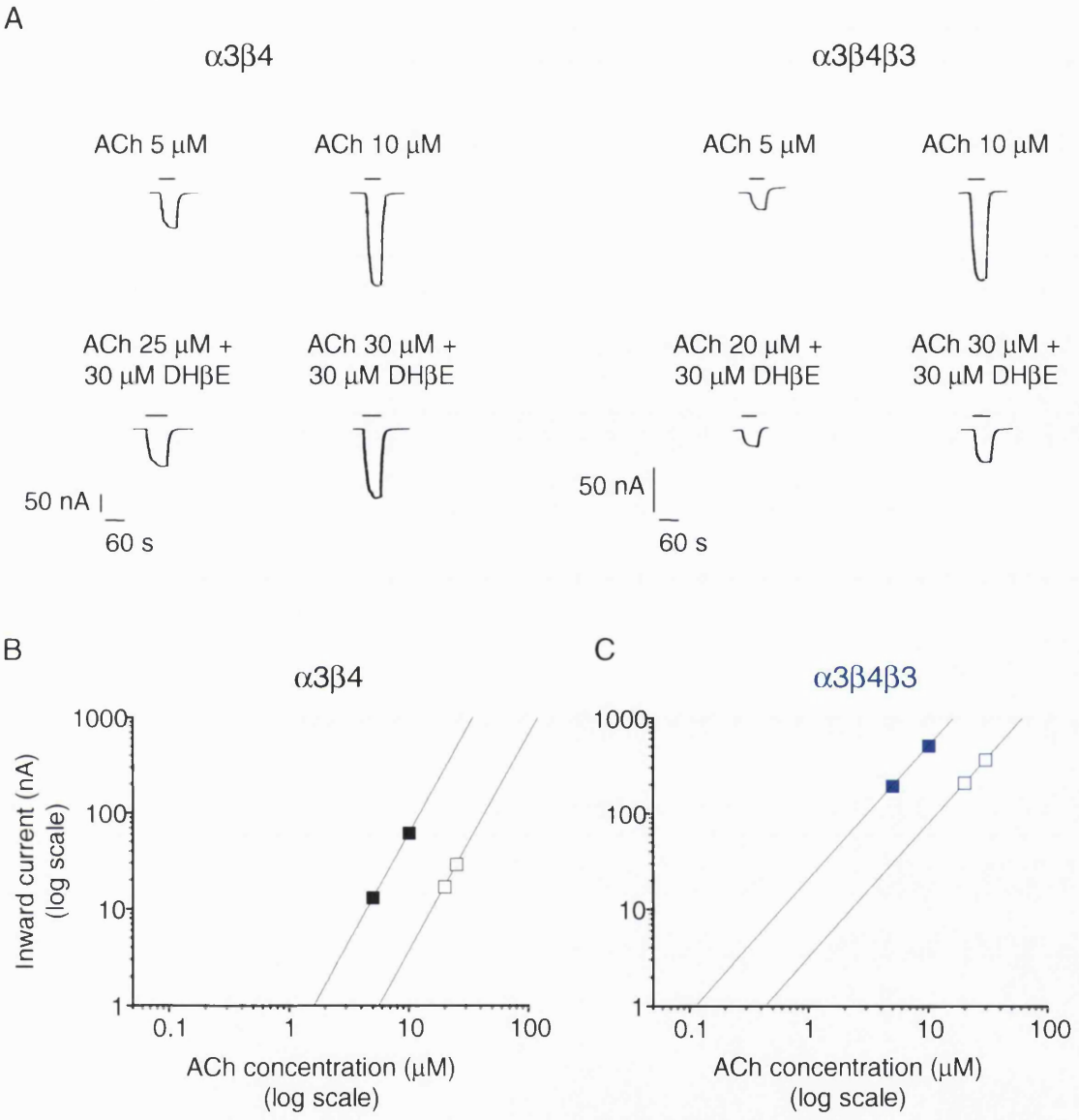

Figure 6.8.2. Shown are example inward currents elicited by bath applied application of ACh or ACh + DHβE to oocytes expressing α3β4 or $\alpha3\beta4\beta3^{wt}$ receptors. ACh and DHβE concentrations are indicated above each response along with application bars, indicating the duration of agonist application. Scale bars are shown for current amplitude and time. B and C show partial parallel concentration response curves for ACh (■) and ACh + DHβE (❑) α3β4 and α3β4β3 ACh (■) and ACh + DHβE (❑).The ± S.D. of mean for the data is not shown where the errors fall within the plotted symbol. Data were fitted simultaneously with a power function derived from the Hill equation in a constrained fit (with equal Hill slopes) in order to estimate the horizontal distance between curves, expressed as dose ratios (where ACh = 1).

6.9. +-tubocurarine and mecamylamine act non-competitively on α3β4β3 receptors

Using the same protocol as described for the antagonist experiments above, +-tubo or mecamylamine were applied to oocytes expressing α3β4β3 receptors. Initially a reference, partial concentration-response curve for bath-applied ACh was obtained in oocytes expressing α3β4 and α3β4β3 receptors using the protocol described in Chapter 2. Next the oocytes were continuously superfused with antagonist Ringer (see solutions Chapter 2) and ACh was co-applied until a stable partial concentration-response curve, parallel to the reference ACh curve, was obtained in the same oocyte.

The partial concentration response curves for ACh and ACh co-applied with antagonist in each oocyte were then plotted on log/log scale in order to produce linear plots. A concentration of 1 μM mecamylamine or 8 μM +-tubo was required in α3β4β3 receptors in order to produce measurable rightward shifts. Note from figures 6.9.1. and 6.9.2. that the rightward shift in the partial concentration response curve produced by either mecamylamine or +-tubo was not parallel to the reference ACh partial concentration-response curve, with slopes of 0.71 for mecamylamine compared to 2.07 for ACh (n = 1; see figures 6.9.1.) and 0.69 for +-tubo compared to 1.34 for ACh (*n* = 1; see figure 6.9.2.). The lack of parallel shifts in the partial concentration response curves for mecamylamine and +-tubo was taken to indicate that both antagonists were acting non-competitively and thus full Schild analysis was not carried out.

These findings are in good accord with the reported non-competitive action of mecamylamine and +-tubo on ganglionic nAChRs at micromolar concentrations (Ascher *et al.*, 1979; Fieber & Adams, 1991). However, we had hoped to obtain a

measurable effect of these antagonists at much lower concentrations, which may act competitively (as shown for mecamylamine 50 nM by Ascher *et al.*, 1979). Unfortunately this strategy failed, as micromolar concentrations were required in order to produce measurable shifts in the partial parallel concentration response curves.

Figure 6.9.1. Mecamylamine partial concentration response curves for α3β4β3 receptors

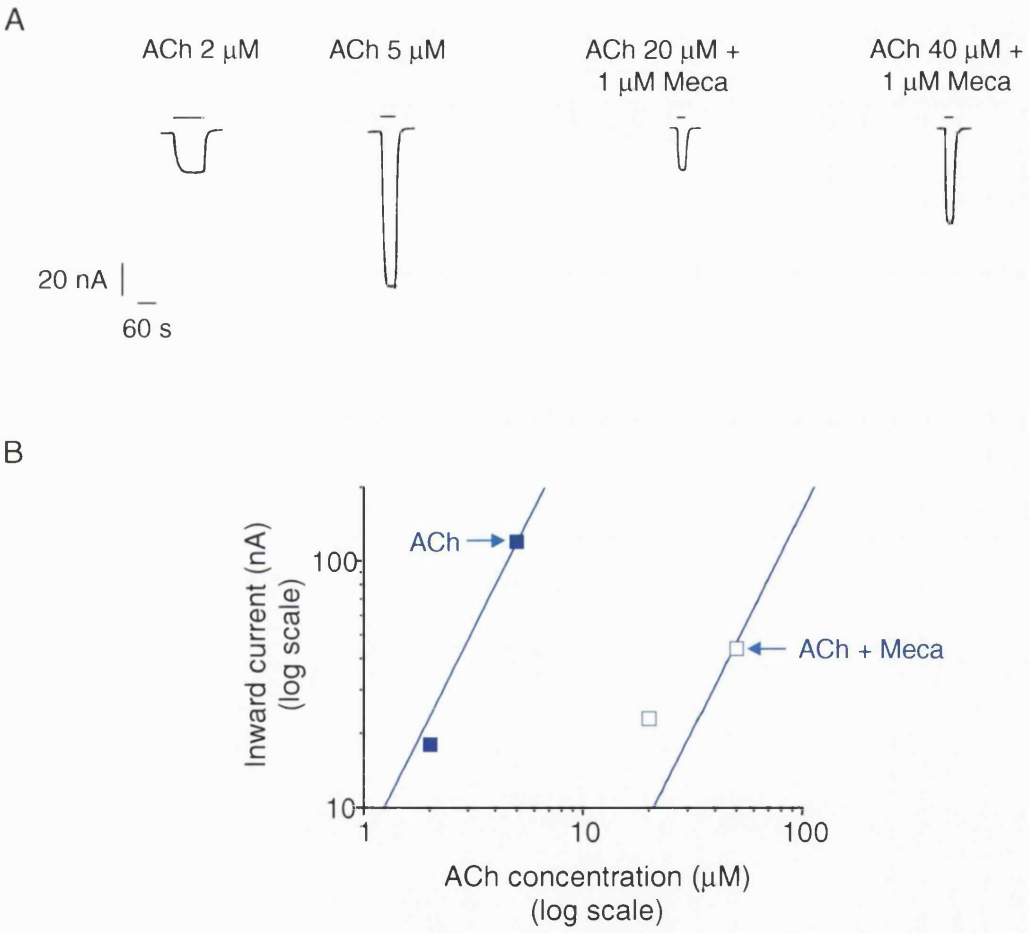

Figure 6.9.1 A. Shown are example inward currents elicited by bath applied application of ACh or ACh + mecamylamine (Meca) to oocytes expressing α3β4 or $\alpha3\beta4\beta3^{wt}$ receptors. ACh and mecamylamine concentrations are indicated above each response along with application bars, indicating the duration of agonist application. Scale bars are shown for current amplitude and time. B the partial concentration response curves for ACh (■) and ACh + mecamylamine (Meca; ❒) in oocytes expressing α3β4β3 receptors. The ± S.D. of mean for the data is not shown where the errors fall within the plotted symbol. Data were fitted with power functions derived from the Hill equation, constrained to be parallel.

Figure 6.9.2. +-tubocurarine partial concentration response curves for α3β4β3 receptors

A

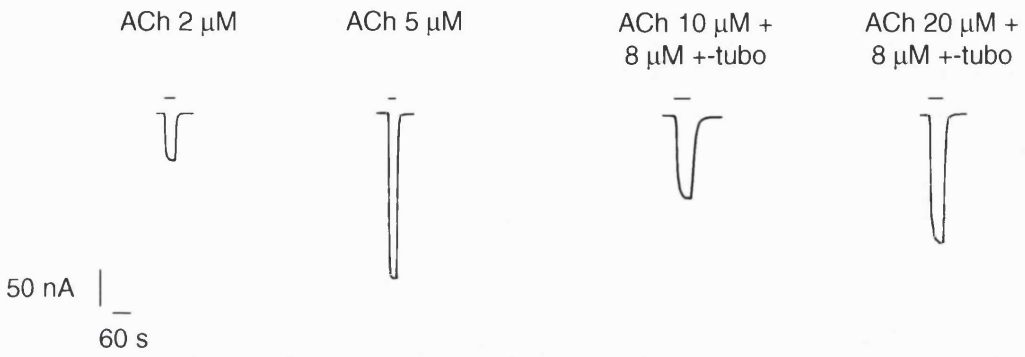

B

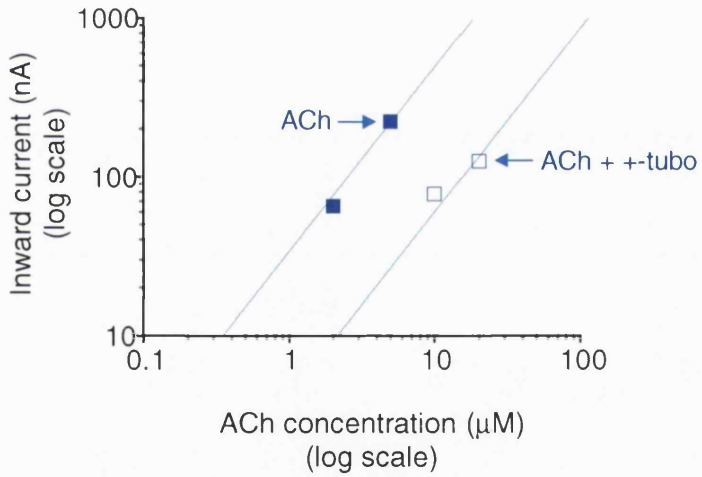

Figure 6.9.2. A shown are example inward currents elicited by bath applied application of ACh or ACh + +-tubo to oocytes expressing α3β4 or $\alpha3\beta4\beta3^{wt}$ receptors. ACh and +-tubo concentrations are indicated above each response along with application bars, indicating the duration of agonist application. Scale bars are shown for current amplitude and time. B shown above are the partial parallel concentration response curves for ACh (■) and ACh + +-tubo (❒) in oocytes expressing α3β4β3 receptors. The ± S.D. of mean for the data is not shown where the errors fall within the plotted symbol.

6.10. Calcium permeability of α3β4 'pair' versus α3β4β3^{wt} 'triplet' receptors

As we have seen in chapter 1, the TM2 domain of each receptor subunit contributes to the formation of the channel. Thus it would follow that residues in the TM2 domain are likely to affect the permeability of ions through the channel. Reducing the net charge on the cytoplasmic –1' ring in TM2 or increasing the side chain length of residues in –1' has been shown to reduce permeability of calcium and large monovalent cations (*Torpedo*, Konno *et al.*, 1991; α7, Bertrand *et al.*, 1993; Haghighi & Cooper, 2000). Further, Villarroel *et al.* (1991) report that the side chain length of the residue in the central (2') ring of TM2 affects large monovalent cation permeability, with permeability increasing as side chain length decreases.

As we have seen from chapter 5, α5 incorporation replaces one copy of β4. In terms of the TM2 domain this replaces the hydrophilic Thr residue in 2' with a hydrophobic Cys, with a shorter side chain (see figure 6.10.1.), whereas the Glu residues in –1' remains unchanged. The data of Villarroel *et al.* (1991) suggests that this will produce an increase in the permeability of the channel to large monovalent cations and possibly divalent cations, although divalent ions were not tested. In support of this hypothesis, Gerzanich *et al.* (1998) demonstrated that incorporation of α5 increases the calcium permeability of 'pair' receptors (α3β2 and α3β4) expressed in oocytes, as indicated by a rightward shift in the reversal potential obtained from I/V curves in different calcium concentrations.

As discussed in chapter 1, in terms of amino acid sequence, the TM2 domains of α5 and β3 are very similar (differing by only four amino acids see figure 6.10.1.). Further, we have seen from chapter 4 that β3 replaces one copy of β4 in the formation of the

α3β4β3 triplet receptor. This also reduces the side chain length in 2' and leaves the Glu residues in –1' unchanged, replacing the hydrophilic 2' Thr residue with a hydrophilic Ser (see figure 6.10.3.). Interestingly, if we compare the 3 rings of charges in the TM2 domain (reported to be involved in single channel conductance as discussed above) and the central ring in 2' with those of the highly calcium permeable α7 homomeric nAChR, β3 and α7 are more similar than β3 and α5. β3 and α7 both contain negatively charged Asp in the –4' position, negatively charged Glu in –1' and 20', hydrophilic Ser in 2', whereas α5 differs with neutral Asn in –4 and hydrophobic Cys in 2' (see figure 6.10.1. and tables 6.10.2. and 6.10.3.).

Given the similarity between β3 and α7, together with the data from Villarroel *et al.* (1991) and Gerzanich *et al.* (1998), it seems reasonable to predict that β3 incorporation might produce an increase in α3β4 calcium permeability; the nature of the TM2 residues in β3 suggests that – if the analysis of Villarroel *et al.* (1991) is correct - the magnitude of this increase will be equal to, or greater than that seen for α5.

Thus the next aim of the project was to investigate the effect of β3 incorporation on the calcium permeability of 'pair' receptors.

Figure 6.10.1. A comparison of the TM2 domains of α3, α5, α7, β4 and β3

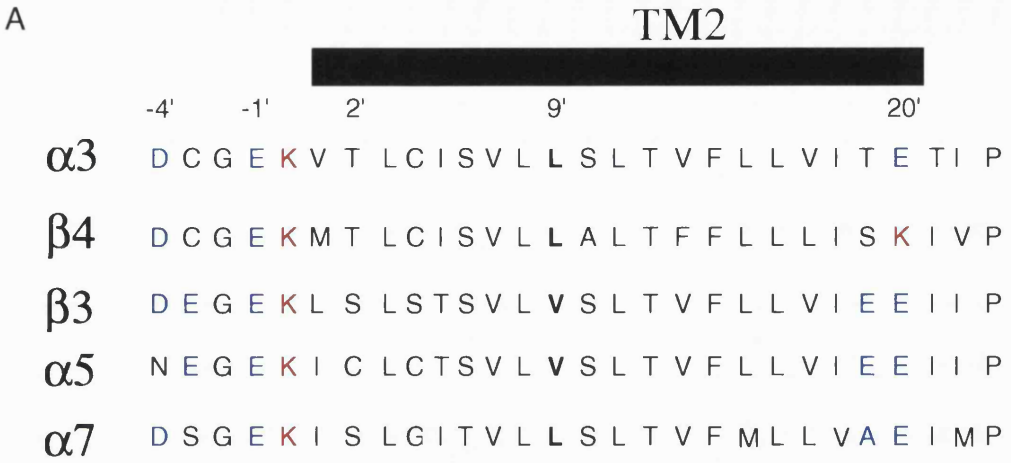

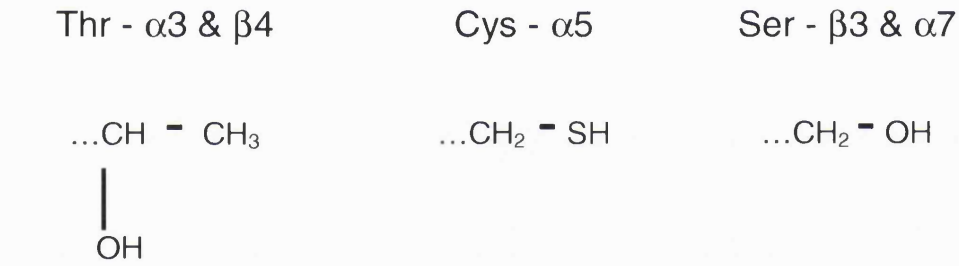

Figure 6.10.1. A shows the amino acid sequence for the TM2 domains of α3, α5, α7, β4 and β3, with the amino acids indicated with their single letter code. The residues thought to affect single channel conductance and large divalent cation permeability are indicated: the three rings of charges in –4', -1' and 20' and the uncharged residues in 2'. Note that β3 and α7 share identical residues in these regions. B shows the side chains of residues in 2' using the three letter amino acid code. Note that α5 or β3 incorporation reduces the side chain length of the residue in 2'.

Table 6.10.2. The 2' ring and the three rings of charges in the TM2 of α3, β4 and α5 subunits

Receptor	Subunit	Copy number	Cytoplasmic ring -4'	Intermediate ring -1'	2'	Outer ring 20'
α3β4	α3	2	D (-)	E (-)	T	E (-)
	β4	3	D (-)	E (-)	T	K (+)
Net charge			- 5	- 5	0	+ 1
α3β4α5	α3	2	D (-)	E (-)	T	E (-)
	β4	2	D (-)	E (-)	T	K (+)
	α5	1	N	E (-)	C	E (-)
Net charge			- 4	- 5	0	- 1

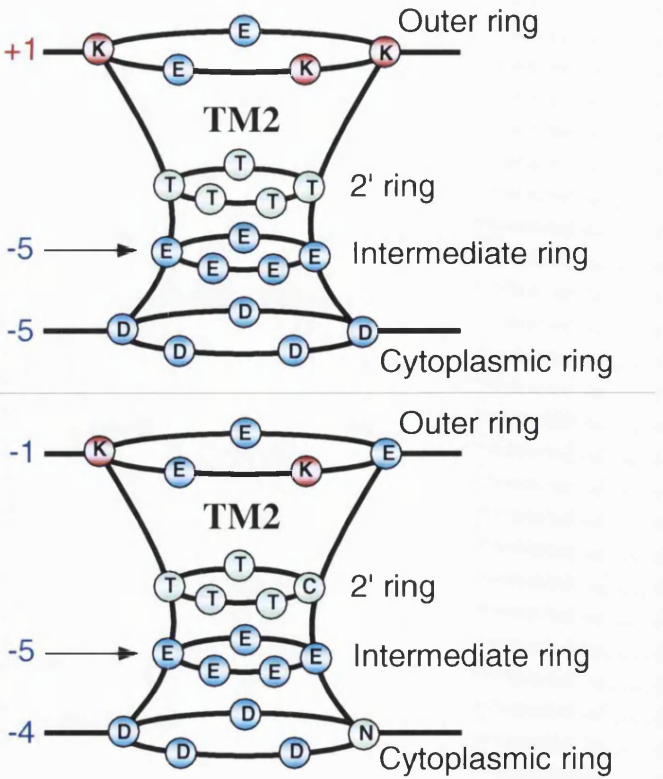

Table 6.10.2. Shown are the residues in the TM2 cytoplasmic (-4'), intermediate (-1'), the central (2') ring and outer (20') rings of charges for the α3, β4 and α5 subunits. The residues are indicated using the single letter amino acid code. The presumed stoichiometry for both α3β4 and α3β4α5 receptors is indicated by the subunit copy number. The net charge for each ring of charges is calculated on the basis of the subunit copy number. A graphical representation of the pore of the channel, with the residues lining the pore forming the cytoplasmic (-4'), intermediate (-1'), central (2') and outer (20') rings is shown for both α3β4 and α3β4α5 receptors, indicating the net charge on each ring. Note positively charged residues are indicated in red, negatively charged residues in blue and uncharged residues in green. The subunit arrangement shown is based on that of the ACh binding protein.

Table 6.10.3. The 2' ring and the three rings of charges in the TM2 of α3, β4 and β3 subunits

Receptor	Subunit	Copy number	Cytoplasmic ring -4'	Intermediate ring -1'	Central ring 2'	Outer ring 20'
α3β4	α3	2	D (-)	E (-)	T	E (-)
	β4	3	D (-)	E (-)	T	K (+)
Net charge			- 5	- 5	0	+ 1
α3β4β3	α3	2	D (-)	E (-)	T	E (-)
	β4	2	D (-)	E (-)	T	K (+)
	β3	1	D (-)	E (-)	S	E (-)
Net charge			- 5	- 5	0	- 1

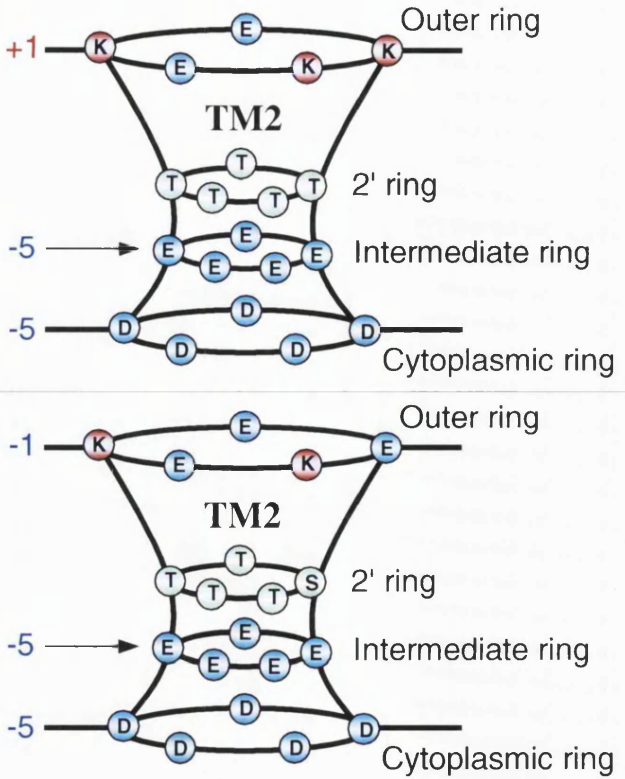

Table 6.10.3. Shown are the residues in the TM2 cytoplasmic (-4'), intermediate (-1'), the central (2') ring and outer (20') rings of charges for the α3, β4 and β3 subunits. The residues are indicated using the single letter amino acid code. The presumed stoichiometry for both α3β4 and α3β4β3 receptors is indicated by the subunit copy number. The net charge for each ring of charges is calculated on the basis of the subunit copy number. A graphical representation of the pore of the channel, with the residues lining the pore forming the cytoplasmic (-4'), intermediate (-1'), central (2') and outer (20') rings is shown for both α3β4 and α3β4β3 receptors, indicating the net charge on each ring. Note positively charged residues are indicated in red, negatively charged residues in blue and uncharged residues in green. The subunit arrangement shown is based on that of the ACh binding protein.

6.11. α3β4 and α3β4β3 receptors are equally permeable to calcium

Initially reference current/voltage relationship (I/V) curves were obtained during bath-applications of ACh in 1.8 mM calcium Ringer solution to oocytes expressing α3β4 and $\alpha3\beta4\beta3^{wt}$ receptors (see solutions, chapter 2), using the protocol described in chapter 2. The solutions used were chloride free and based on those of Gerzanich *et al.* (1998) in order to aid comparison of the data with that obtained for α5 (for solution composition, see chapter 2). The reversal potential was measured as the membrane holding potential at which current injection equalled zero. Reference I/V curves were then compared with I/V curves obtained in 18 mM calcium (see solutions, chapter 2) and the degree of shift, if any, determined from the change in reversal potential.

Comparison of the reversal potentials for 1.8 and 18 mM calcium Ringer revealed that both α3β4 and α3β4β3 receptors are somewhat permeable to calcium, but also that their permeability is similar (example I/V curves are shown in figure 6.11.2.). α3β4β3 receptors had mean reversal potentials of -15.1 ± 1.97 mV (n = 5) in 1.8 mM and -9.9 ± 1.40 mV (n = 5) in 18 mM calcium, compared to –18.7 ± 0.97 mV (n = 5) in 1.8 mM and –11.0 ± 1.91 mV (n = 5) in 18 mM calcium for α3β4 (see table 6.11.1). The resulting mean shift in the reversal potential was 5.20 ± 0.83 mV (n = 5) for α3β4β3 and 7.68 ± 1.47 mV (n = 5) for α3β4 (see table 6.11.1). The results of a 2 tail t-test assuming unequal variance revealed that the difference between the shift in reversal potential between α3β4β3 and α3β4 receptors was not statistically significant, p = 0.19 (see table 6.11.1).

Table 6.11.1. Calcium permeability of α3β4 vs α3β4β3 receptors

	Mean reversal potential (mV) 1.8 mM Ca^{2+}	Mean reversal potential (mV) 18 mM Ca^{2+}	Mean shift in reversal potential (mV)	Mean leak current at –40 mV (nA) 1.8 mM Ca^{2+}	Mean leak current at -40 mV (nA) 18 mM Ca^{2+}	Max total current (nA)	cRNA Injected (ng)	n	*p*
α3β4	-18.7 ± 1.0	-11.0 ± 1.9	7.7 ± 1.5	2.2 ± 6.1	24.2 ± 4.8	522	15	5	
α3β4β3	-15.1 ± 2.0	-9.9 ± 1.4	5.2 ± 0.8 (*p* 0.19)	-12.8 ± 7.0 (*p* 0.20)	-3.1 ± 7.0 (*p* 0.06)	302	25	5	0.19

Table 6.11.1. Mean (± S.D. mean) reversal potential is the mean of all potentials at which current injection was equal to zero. Mean (± S.D. mean) shift in reversal potential is the mean of the sum of all the reversal potentials in 18 mM calcium – all the reversal potentials in 1.8 mM calcium. Mean (± S.D. mean) leak current, is the mean of all leak currents recorded at a holding potential of –40 mV before the initiation of the voltage ramp in the external calcium concentration indicated. Where *p* is the result from a 2 tail *t*-test assuming equal variance.

Figure 6.11.2. I/V plots for α3β4 and α3β4β3 receptors in 1.8 and 18 mM external Calcium

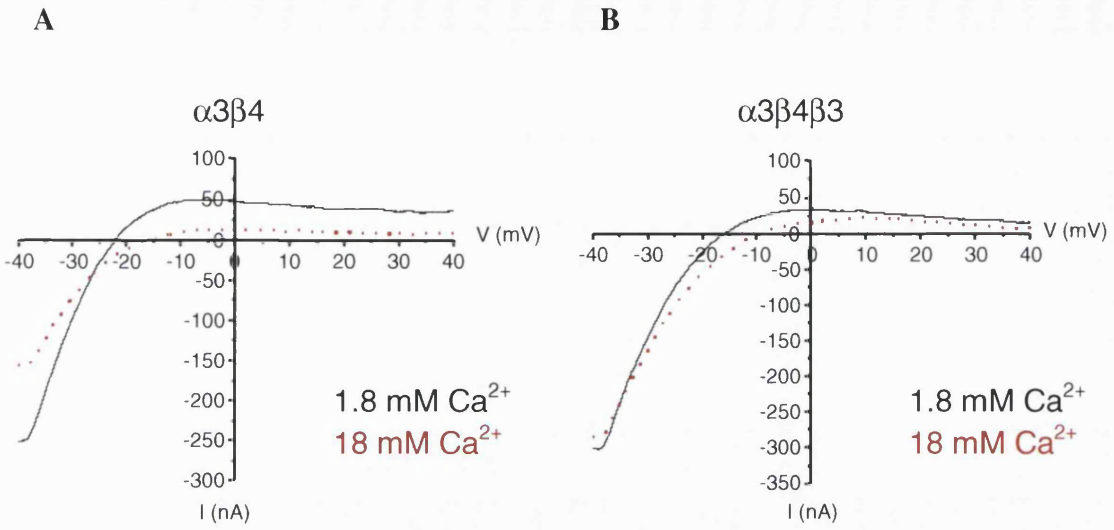

Figure 6.11.2. A and B show example I/V curves for α3β4 (A) and α3β4β3 (B) receptors in 1.8 (black) and 18 mM (red dotted curve) calcium Ringer. The curves plotted are the smoothed (100 point adjacent averaging) data points from mean leak subtracted curves from 4 ramps obtained in the same oocyte. Each 2 second ramp shifted the holding potential from -40 mV to + 40 mV. Note the shift in reversal potential from 1.8 to 18 mM calcium

All nAChRs are somewhat calcium permeable (see Sargent, 1993 and McGehee & Role, 1995 for reviews). Recombinant studies have also shown a variety of calcium permeabilities, depending on the α and β subunit composition of receptors (Sands & Barish, 1991; Adams & Nutter, 1992; Vernino *et al.*, 1992; Bertrand *et al.*, 1993; Gerzanich *et al.*, 1998; Haghighi & Cooper, 2000; for a review see McGehee & Role, 1995), with homomeric α7 receptors having the greatest permeability (Séguéla *et al.*, 1993; Delbono *et al.*, 1997; Gerzanich *et al.*, 1998; Fucile *et al.*, 2000; Haghighi & Cooper, 2000). In the native receptor, calcium entry through the nAChR may either directly evoke or modulate neurotransmitter release from the presynaptic neuron, by triggering exocytosis (for a review see MacDermott *et al.*, 1999). Thus any change in the calcium permeability of neuronal nAChRs could potentially have an important physiological impact on synaptic transmission.

In contrast to the predicted increase in calcium permeability, based on the similarity in the TM2 sequence between α5 and β3 and the presence of a Ser residue in the 2' position, the data presented above suggests that α3β4 and α3β4β3 receptors are equally permeable to calcium.

Under similar conditions, Gerzanich *et al.* (1998) report that increasing extracellular calcium by ten-fold from 1.8 to 18 mM produced a mean shift in the reversal potential of 6.1 mV for α3β4, a value similar to the one we observed (7.7 mV). This shift was much larger (11.7 mV) for α3β4α5 receptors.

It is possible that residual calcium activated chloride current (endogenous to the oocyte) is still present, even after incubation in chloride free solution and affected the sensitivity of our method. This would seem unlikely as the shift we observed for α3β4 was very similar to that reported by Gerzanich *et al.* (1998). It must be considered that the sensitivity of this method is limited, as an accurate measurement of the reversal potential is confounded by the strong inward rectification of the nAChR and by the relatively small signal to noise ratio for the current carried through nAChRs vs. the leak of the oocyte.

In order to clarify the question of calcium permeability for α3β4β3 receptors a more accurate method may be required. A future experiment could be carried out in cell lines, such as HEK293. The main advantages of using HEK293 cells are that they are small (improving the signal to noise ratio) and that we can control the intracellular solution using the whole cell patch clamp configuration. Such an experimental system would also allow a fura-2 ratiometric measurement of increases in calcium concentration produced by nAChR activation. The importance of this is that it would give us a value

which is more physiologically relevant. i.e. the proportion of current carried by calcium at the membrane resting potential.

Chapter 7: Summary

7.1. Summary

We have seen in the previous chapters that β3 can form a 'triplet' receptor when co-expressed with an α3β4 'pair' in *Xenopus* oocytes. Using a reporter mutation approach we have confirmed the known stoichiometry of 'pair' receptors as 2 α and 3 β and shown that 'triplet' receptors formed by co-expressing either β3 or α5 with an α/β 'pair' have a stoichiometry of 2:2:1.

Characterisation of α3β4β3 receptors revealed that the incorporation of β3 has relatively small effects on the pharmacology of the α3β4 receptors. The main change is a three-fold decrease in the potency of lobeline relative to ACh, but this does not affect agonist rank order of potencies. Incorporation of β3 has negligible effects on antagonist sensitivity assessed by the Schild *Kd* of the competitive antagonist trimetaphan and the dose ratio of 30 μM DHβE. Calcium permeability of the α3β4 'pair' was also unchanged (or the change is too small to be detected by reversal potential methods in oocytes). In addition to these data, unpublished data from Dr. Marco Beato demonstrates an increase in single channel conductance in β3-containing receptors, from 28.8 pS for α3β4 to 46.7 pS for α3β4β3. This increase in conductance is likely to be due to β3 replacing a β4 subunit (personal communication, Dr. Marco Beato).

It is tempting to interpret the relatively small effect of β3 on α3β4 agonist and antagonist sensitivity as an indication that β3 is not involved in the agonist binding site, assigning a purely structural role to β3. Note that substituting one β subunit for the other in 'pair' receptors has profound effects on the pharmacology of nAChRs (Luetje & Patrick, 1991; Harvey & Luetje, 1996). Here the most likely anticlockwise arrangement

of the α3β4β3 'triplet' receptor would be α3β4α3β4β3, with β3 in a structural position analogous the to the muscle nAChRs β subunit.

7.2. Relevance to native receptors

For our findings on recombinant β3-containing receptors to be relevant to native nAChR, two questions must be answered, *i.e.* whether we can extrapolate from the oocyte expression system to a mammalian neuron and, secondly, whether the β3 subunit is incorporated into native nAChR together with the α3 and β4 subunits.

Xenopus oocytes do express muscle-type nAChR with an accurate native stoichiometry (Anand *et al.*, 1991). No comparative data are available for neuronal nAChR. Nevertheless, the 2:3 stoichiometry observed in oocytes for α4β2 nAChR (Cooper *et al.*, 1991) is in good accord with the Hill slope values measured for native ganglionic nAChR (Covernton *et al.*, 1994). At the single-channel level, most oocyte-expressed α3β4 nAChRs differ in conductance and kinetics from native ganglionic receptors (which are likely to have a similar composition; Sivilotti *et al.*, 1997; Lewis *et al.*, 1997). It is assumed here that whatever it may be that causes discrepancies in conductances and kinetics does not have a major effect on relative potencies or stoichiometry. In support of this view, it has been found that, at whole-cell level, *Xenopus* oocytes do reproduce the relative agonist potencies seen for native ganglionic nAChRs with reasonable accuracy (Covernton *et al.*, 1994).

In terms of the effect of β3 incorporation on the α3β4 'pair', β3 produces only a small change in the potency of lobeline relative to ACh. This is unlikely to be useful for identifying β3 containing receptors. However, it is possible that β3 may produce a

greater effect on the pharmacology and biophysical properties of receptors with a different 'pair' background, for example, α4β2.

The reporter mutation approach can readily be extended to other new neuronal nAChR combinations to assess if β3 can form other 'triplet' receptors. If these do form, it must be tested if β3 incorporation affects the pharmacological and biophysical profile of 'pair' receptors. Given the widespread expression of α4β2, it would be of particular interest to look at α4β2 in combination with β3. For example, does α4β2 form an α4β2β3 'triplet' receptor ? What is its stoichiometry ? Does β3 incorporation affect the pharmacological and biophysical properties of the α4β2 'pair' ?

It is possible that β3 incorporation has a completely different effect for native receptors in a neuron. A possibility is that β3 is involved in receptor targeting. It is well known that neurons can regulate the composition of receptors in different domains and it could be that the presence of β3 targets the receptor complex to a different portion of the neuron (somatodendritic, pre or perisynaptic). It would be interesting to express epitope tagged α3β4 and α3β4β3 receptors in cultured neurons and see if β3 affects targeting of the receptor complex to different subdomains of the neuron.

Indeed chick ciliary ganglia have been shown to target different nAChR subtypes to specific subdomains of the neuron: the majority of receptors consist of α3β4α5 (sometimes with β2), which are mostly targeted to the postsynaptic membrane. However, some α7 receptors are also present, but excluded from the postsynaptic membrane and targeted to perisynaptic membranes of the dendrites (for a review see Temburni *et al.*, 2000). Further, data from chimeric subunits suggests that the

cytoplasmic loop between TM3 and TM4, whose amino acid sequence is highly variable between the neuronal nAChR subunits, may play a role in targeting (Williams *et al.*, 1998). Williams *et al.* (1998) report that over-expressing myc epitope-tagged α7 chimeras containing the cytoplasmic loop of α3 or α5 in chick ciliary ganglion targets the chimeric α7 receptors to different subdomains of the neuron: α7/α3 chimeras are targeted to postsynaptic areas, whereas $\alpha7^{wt}$ or α7/α5 chimeras are targeted to perisynaptic areas (Williams *et al.*, 1998).

Future work, extending our electrophysiological approach to determine and characterise which subunits can assemble, will undoubtedly help in the screening for specific compounds that discriminate between the different receptor subtypes. This work is essential for a better understanding of the function of neuronal nAChRs and the development of future drug therapies for nicotine addiction and pathological processes in neurological disorders, such as Alzheimer's disease, Parkinson's disease and Schizophrenia, in which a role for neuronal nAChRs has been proposed (for a review see Mihailescu & Drucker-Colin, 2000).

Bibliography

1. Adams, D. J. & Nutter, T. J. (1992). Calcium permeability and modulation of nicotinic acetylcholine receptor- channels in rat parasympathetic neurons. *J.Physiol Paris* **86**, 67-76.

2. Akabas, M. H., Kaufmann, C., Archdeacon, P., & Karlin, A. (1994). Identification of acetylcholine receptor channel-lining residues in the entire M2 segment of the α subunit. *Neuron* **13**, 919-927.

3. Akabas, M. H., Stauffer, D. A., Xu, M., & Karlin, A. (1992). Acetylcholine receptor channel structure probed in cysteine-substitution mutants. *Science* **258**, 307-310.

4. Albuquerque, E. X., Pereira, E. F. R., Alkondon, M., Eisenberg, H. M., & Maelicke, A. (2000). Neuronal nicotinic receptors and synaptic transmission in the mammalian central nervous system. In *Neuronal Nicotinic Receptors*, eds. Clementi, F., Fornasari, D., & Gotti, C., pp. 337-358. Springer Verlag, Berlin Heidelberg.

5. Alkondon, M., Braga, M. F., Pereira, E. F., Maelicke, A., & Albuquerque, E. X. (2000). alpha7 nicotinic acetylcholine receptors and modulation of gabaergic synaptic transmission in the hippocampus [In Process Citation]. *Eur.J.Pharmacol.* **393**, 59-67.

6. Alkondon, M., Pereira, E. F., & Albuquerque, E. X. (1998). alpha-bungarotoxin- and methyllycaconitine-sensitive nicotinic receptors mediate fast synaptic transmission in interneurons of rat hippocampal slices. *Brain Res.* **810**, 257-263.

7. Alkondon, M., Pereira, E. F., Barbosa, C. T., & Albuquerque, E. X. (1997). Neuronal nicotinic acetylcholine receptor activation modulates γ-aminobutyric acid release from CA1 neurons of rat hippocampal slices. *Journal of Pharmacology and Experimental Therapeutics* **283**, 1396-1411.

8. Alkondon, M., Pereira, E. F., Eisenberg, H. M., & Albuquerque, E. X. (1999). Choline and selective antagonists identify two subtypes of nicotinic acetylcholine receptors that modulate GABA release from CA1 interneurons in rat hippocampal slices. *Journal of Neuroscience* **19**, 2693-2705.

9. Anand, R., Conroy, W. G., Schoepfer, R., Whiting, P., & Lindstrom, J. (1991). Neuronal nicotinic acetylcholine receptors expressed in *Xenopus* oocytes have a pentameric quaternary structure. *Journal of Biological Chemistry* **266**, 11192-11198.

10. Anderson, A. D., Troyanovskaya, M., & Wackym, P. A. (1997). Differential expression of α2-7, α9 and β2-4 nicotinic acetylcholine receptor subunit mRNA in the vestibular end-organs and Scarpa's ganglia of the rat. *Brain Research* **778**, 409-413.

11. Aramakis, V. B. & Metherate, R. (1998). Nicotine selectively enhances NMDA receptor-mediated synaptic transmission during postnatal development in sensory neocortex. *J.Neurosci.* **18**, 8485-8495.

12. Arias, H. R. (1997). Topology of ligand binding sites on the nicotinic acetylcholine receptor. *Brain Research Reviews* **25**, 133-191.

13. Arunlakshana, O. & Schild, H. O. (1959). Some quantitative uses of drug antagonists (Reprinted from Brit J Pharmacol, vol 14, pg 48, 1959). *British Journal of Pharmacology* **120**, 151-161.

14. Ascher, P., Large, W. A., & Rang, H. P. (1979). Studies on the mechanism of action of acetylcholine antagonists on rat parasympathetic ganglion cells. *J.Physiol* **295** , 139-170.

15. Aubert, I., Araujo, D. M., Cecyre, D., Robitaille, Y., Gauthier, S., & Quirion, R. (1992). Comparative alterations of nicotinic and muscarinic binding sites in Alzheimer's and Parkinson's diseases. *J.Neurochem.* **58**, 529-541.

16. Azam, L., Winzer-Serhan, U. H., Chen, Y., & Leslie, F. M. (2002). Expression of neuronal nicotinic acetylcholine receptor subunit mRNAs within midbrain dopamine neurons. *J.Comp Neurol.* **444**, 260-274.

17. Balestra, B., Vailati, S., Moretti, M., Hanke, W., Clementi, F., & Gotti, C. (2000). Chick optic lobe contains a developmentally regulated alpha2alpha5beta2 nicotinic receptor subtype. *Molecular Pharmacology* **58**, 300-311.

18. Benwell, M. E. & Balfour, D. J. (1997). Regional variation in the effects of nicotine on catecholamine overflow in rat brain. *Eur.J.Pharmacol.* **325**, 13-20.

19. Berne R. B. & Levy M. N. (1993) In: *Physiology*, 3rd edition. Mosby-Year Book, Inc, St. Louis, Missouri, USA.

20. Bertrand, D., Ballivet, M., & Rungger, D. (1990). Activation and blocking of neuronal nicotinic acetylcholine receptor reconstituted in *Xenopus* oocytes. *Proceedings of the National Academy of Sciences U.S.A.* **87**, 1993-1997.

21. Bertrand, D., Bertrand, S., & Ballivet, M. (1992). Pharmacological properties of the homomeric α7 receptor. *Neurosci.Lett.* **146**, 87-90.

22. Bertrand, D., Galzi, J.-L., Devillers-Thiéry, A., Bertrand, S., & Changeux, J.-P. (1993). Mutations at two distinct sites within the channel domain M2 alter calcium permeability of neuronal α7 nicotinic receptors. *Proceedings of the National Academy of Sciences U.S.A.* **90**, 6971-6975.

23. Blount, P. & Merlie, J. P. (1989). Molecular basis of the two nonequivalent ligand binding sites of the muscle nicotinic acetylcholine receptor. *Neuron* **3**, 349-357.

24. Blount, P. & Merlie, J. P. (1990). Mutational analysis of muscle nicotinic acetylcholine receptor subunit assembly. *J. Cell Biol.* **111**, 2613-2622. *Journal of Cell Biology* **111**, 2613-2622.

25. Blount, P., Smith, M. M., & Merlie, J. P. (1990). Assembly intermediates of the mouse muscle nicotinic acetylcholine receptor in stably transfected fibroblasts. *Journal of Cell Biology* **111**, 2601-2611.

26. Bonner, T. I. New Subtypes of muscarinic acetylcholine receptors. Trends in Pharmacological Sciences supplement, 11-15. 1989.

27. Boulter, J., Connolly, J., Deneris, E., Goldman, D., Heinemann, S., & Patrick, J. (1987). Functional expression of two neuronal nicotinic acetylcholine receptors from cDNA clones identifies a gene family. *Proceedings of the National Academy of Sciences U.S.A.* **84**, 7763-7767.

28. Boulter, J., Evans, K., Goldman, D., Martin, G., Treco, D., Heinemann, S., & Patrick, J. (1986). Isolation of a cDNA clone coding for a possible neural nicotinic acetylcholine receptor alpha-subunit. *Nature* **319**, 368-374.

29. Brejc, K., van Dijk, W. J., Klaassen, R. V., Schuurmans, M., van der Oost, J., Smit, A. B., & Sixma, T. K. (2001). Crystal structure of an ACh-binding protein reveals the ligand-binding domain of nicotinic receptors. *Nature* **411**, 269-276.

30. Brennan, P. A. & Keverne, E. B. (1997). Neural mechanisms of mammalian olfactory learning. *Progress in Neurobiology* **51**, 457-481.

31. Buisson, B., Gopalakrishnan, M., Arneric, S. P., Sullivan, J. P., & Bertrand, D. (1996). Human α4α2 neuronal nicotinic acetylcholine receptor in HEK 293 cells: A patch-clamp study. *Journal of Neuroscience* **16**, 7880-7891.

32. Cachelin, A. B. & Rust, G. (1995). β-subunits co-determine the sensitivity of rat neuronal nicotinic receptors to antagonists. *Pflügers Archiv-European J.Physiol* **429**, 449-451.

33. Caulfield, M. P. (1993). Muscarinic receptors-characterization, coupling and function. *Pharmacology and Therapeutics* **58**, 319-379.

34. Champtiaux, N., Han, Z. Y., Bessis, A., Rossi, F. M., Zoli, M., Marubio, L., McIntosh, J. M., & Changeux, J. P. (2002). Distribution and pharmacology of alpha 6-containing nicotinic acetylcholine receptors analyzed with mutant mice. *J.Neurosci.* **22**, 1208-1217.

35. Chang, Y., Wang, R., Barot, S., & Weiss, D. S. (1996). Stoichiometry of a recombinant $GABA_A$ receptor. *Journal of Neuroscience* **16**, 5415-5424.

36. Chang, Y. & Weiss, D. S. (1998). Substitutions of the highly conserved M2 leucine create spontaneously opening rho1 gamma-aminobutyric acid receptors. *Molecular Pharmacology* **53**, 511-523.

37. Chang, Y. C. & Weiss, D. S. (1999). Allosteric activation mechanism of the α1 β2 γ2 γ-aminobutyric acid type A receptor revealed by mutation of the conserved M2 leucine. *Biophysical Journal* **77**, 2542-2551.

38. Charnet, P., Labarca, C., Leonard, R. J., Vogelaar, N. J., Czyzyk, L., Gouin, A., Davidson, N., & Lester, H. A. (1990). An open-channel blocker interacts with adjacent turns of alpha-helices in the nicotinic acetylcholine receptor. *Neuron* **4**, 87-95

39. Charpantier, E., Barneoud, P., Moser, P., Besnard, F., & Sgard, F. (1998). Nicotinic acetylcholine subunit mRNA expression in dopaminergic neurons of the rat substantia nigra and ventral tegmental area. *Neuroreport.* **9**, 3097-3101.

40. Chatrenet, B., Tremeau, O., Bontems, F., Goeldner, M. P., Hirth, C. G., & Menez, A. (1990). Topography of toxin-acetylcholine receptor complexes by using photoactivatable toxin derivatives. *Proc.Natl.Acad.Sci.U.S.A* **87**, 3378-3382.

41. Chavez-Noriega, L. E., Crona, J. H., Washburn, M. S., Urrutia, A., Elliott, K. J., & Johnson, E. C. (1997). Pharmacological characterization of recombinant human neuronal nicotinic acetylcholine receptors hα2β2, hα2β4, hα3β2, hα3β4, hα4β2, hα4β4 and hα7 expressed in *Xenopus* oocytes. *Journal of Pharmacology and Experimental Therapeutics* **280**, 346-356.

42. Clarke, P. B. & Pert, A. (1985). Autoradiographic evidence for nicotine receptors on nigrostriatal and mesolimbic dopaminergic neurons. *Brain Res.* **348**, 355-358.

43. Claudio, T., Paulson, H. L., Green, W. N., Ross, A. F., Hartman, D. S., & Hayden, D. (1989). Fibroblasts transfected with *Torpedo* acetylcholine receptor β-, γ-, and δ-subunit cDNAs express functional receptors when infected with a retroviral α recombinant. *Journal of Cell Biology* **108**, 2277-2290.

44. Clementi, F., Fornasari, D., & Gotti, C. (2000). Neuronal nicotinic receptors, important new players in brain function. *Eur.J.Pharmacol.* **393**, 3-10.

45. Coggan, J. S., Paysan, J., Conroy, W. G., & Berg, D. K. (1997). Direct recording of nicotinic responses in presynaptic nerve terminals. *Journal of Neuroscience* **17**, 5798-5806.

46. Colquhoun, D. (1998). Binding, gating, affinity and efficacy: The interpretation of structure-activity relationships for agonists and of the effects of mutating receptors. *British Journal of Pharmacology* **125**, 923-947.

47. Colquhoun, D. & Sakmann, B. (1985). Fast events in single-channel currents activated by acetylcholine and its analogues at the frog muscle end-plate. *J.Physiol (Lond)* **369**, 501-557.

48. Conroy, W. G. & Berg, D. K. (1995). Neurons can maintain multiple classes of nicotinic receptors distinguished by different subunit compositions. *Journal of Biological Chemistry* **270**, 4424-4431.

49. Conroy, W. G. & Berg, D. K. (1998). Nicotinic receptor subtypes in the developing chick brain: appearance of a species containing the α4, β2, and α 5 gene products. *Molecular Pharmacology* **53**, 392-401.

50. Cooper, E., Couturier, S., & Ballivet, M. (1991). Pentameric structure and subunit stoichiometry of a neuronal nicotinic acetylcholine receptor. *Nature* **350**, 235-238.

51. Coronas, V., Durand, M., Chabot, J. G., Jourdan, F., & Quirion, R. (2000). Acetylcholine induces neuritic outgrowth in rat primary olfactory bulb cultures [In Process Citation]. *Neuroscience* **98**, 213-219.

52. Corringer, P. J., Le Novère, N., & Changeux, J. P. (2000). Nicotinic receptors at the amino acid level. *Annu.Rev.Pharmacol.Toxicol.* **40**, 431-458.

53. Corriveau, R. A. & Berg, D. K. (1993). Coexpression of multiple acetylcholine receptor genes in neurons: quantification of transcripts during development. *Journal of Neuroscience* **13**, 2662-2671.

54. Covernton, P. J. O., Kojima, H., Sivilotti, L. G., Gibb, A. J., & Colquhoun, D. (1994). Comparison of neuronal nicotinic receptors in rat sympathetic neurons with subunit pairs expressed in *Xenopus* oocytes. *J.Physiol.(Lond.)* **481**, 27-34.

55. Czajkowski, C., Kaufmann, C., & Karlin, A. (1993). Negatively charged amino acid residues in the nicotinic receptor delta subunit that contribute to the binding of acetylcholine. *Proceedings of the National Academy of Sciences, USA* **90**, 6285-6289.

56. Dale, H. H. (1914). *J. Pharmacol. Exp. Ther.* **6**, 147-190.

57. Dale, H. H., Feldberg, W., & Vogt, M. (1936). Release of acetylcholine at voluntary motor nerve endings. *J.Physiol* **86**, 353-380.

58. Davidson, A., Mengod, G., Matus-Leibovitch, N., & Oron, Y. (1991). Native *Xenopus* oocytes express two types of muscarinic receptors. *FEBS Lett.* **284**, 252-256.

59. Delbono, O., Gopalakrishnan, M., Renganathan, M., Monteggia, L. M., Messi, M. L., & Sullivan, J. P. (1997). Activation of the recombinant human α_7 nicotinic acetylcholine receptor significantly raises intracellular free calcium. *Journal of Pharmacology and Experimental Therapeutics* **280**, 428-438.

60. Deneris, E. S., Boulter, J., Swanson, L. W., Patrick, J., & Heinemann, S. (1989). β3: a new member of nicotinic acetylcholine receptor gene family is expressed in brain. *Journal of Biological Chemistry* **264**, 6268-6272.

61. Drescher, D. G., Khan, K. M., Green, G. E., Morley, B. J., Beisel, K. W., Kaul, H., Gordon, D., Gupta, A. K., Drescher, M. J., & Barretto, R. L. (1995). Analysis of nicotinic acetylcholine receptor subunits in the cochlea of the mouse. *Comp.Biochem.Physiol.* **112C**, 267-273.

62. Eccles, J. C., Fatt, P., Landgren, S., & Winsbury, G. J. (1954). Spinal cord potentials generated by volleys in the large muscle afferents. *J.Physiol* **125**, 590-606.

63. Edmonds, B., Gibb, A. J., & Colquhoun, D. (1995). Mechanisms of activation of muscle nicotinic acetylcholine receptors, and the time course of endplate currents. *Annual Review of Physiology* **57**, 469-493.

64. Eertmoed, A. L. & Green, W. N. (1999). Nicotinic receptor assembly requires multiple regions throughout the gamma subunit. *Journal of Neuroscience* **19**, 6298-6308.

65. el Bizri, H. & Clarke, P. B. (1994). Blockade of nicotinic receptor-mediated release of dopamine from striatal synaptosomes by chlorisondamine and other nicotinic antagonists administered in vitro. *Br.J.Pharmacol.* **111**, 406-413.

66. Elgoyhen, A. B., Vetter, D. E., Katz, E., Rothlin, C. V., Heinemann, S. F., & Boulter, J. (2001). α10: A determinant of nicotinic cholinergic receptor function in mammalian vestibular and cochlear mechanosensory hair cells. *Proceedings of the National Academy of Sciences U.S.A.* **98**, 3501-3506.

67. Elliott, K. J., Jones, J. M., Sacaan, A. I., Lloyd, G. K., & Corey-Naeve, J. (1998). 6-hydroxydopamine lesion of rat nigrostriatal dopaminergic neurons differentially affects nicotinic acetylcholine receptor subunit mRNA expression. *Journal of Molecular Neuroscience* **10**, 251-260.

68. Fabian-Fine, R., Skehel, P., Errington, M. L., Davies, H. A., Sher, E., Stewart, M. G., & Fine, A. (2001). Ultrastructural distribution of the alpha7 nicotinic acetylcholine receptor subunit in rat hippocampus. *J.Neurosci.* **21**, 7993-8003.

69. Farrar, S. J., Whiting, P. J., Bonnert, T. P., & McKernan, R. M. (1999). Stoichiometry of a ligand-gated ion channel determined by fluorescence energy transfer. *Journal of Biological Chemistry* **274**, 10100-10104.

70. Feller, M. B., Wellis, D. P., Stellwagen, D., Werblin, F. S., & Shatz, C. J. (1996). Requirement for cholinergic synaptic transmission in the propagation of spontaneous retinal waves. *Science* **272**, 1182-1187.

71. Fieber, L. A. & Adams, D. J. (1991). Acetylcholine-evoked currents in cultured neurons dissociated from rat parasympathetic cardiac ganglia. *J.Physiol* **434**, 215-237.

72. Figl, A., Viseshakul, N., Shafaee, N., Forsayeth, J., & Cohen, B. N. (1998). Two mutations linked to nocturnal frontal lobe epilepsy cause use-dependent potentiation of the nicotinic ACh response. *Journal of Physiology* **513**, 655-670.

73. Filatov, G. N. & White, M. M. (1995). The role of conserved leucines in the M2 domain of the acetylcholine receptor in channel gating. *Molecular Pharmacology* **48**, 379-384.

74. Fischbach, G. D. & Schuetze, S. M. (1980). A post-natal decrease in acetylcholine channel open time at rat end- plates. *J.Physiol (Lond)* **303**, 125-137.

75. Fisher, J. L., Pidoplichko, V. I., & Dani, J. A. (1998). Nicotine modifies the activity of ventral tegmental area dopaminergic neurons and hippocampal GABAergic neurons. *J.Physiol Paris* **92**, 209-213.

76. Forsayeth, J. R. & Kobrin, E. (1997). Formation of oligomers containing the β3 and β4 subunits of the rat nicotinic receptor. *Journal of Neuroscience* **17**, 1531-1538.

77. Frazier, C. J., Buhler, A. V., Weiner, J. L., & Dunwiddie, T. V. (1998). Synaptic potentials mediated via α-bungarotoxin sensitive acetylcholine receptors in rat hippocampal interneurons. *Journal of Neuroscience* **18**, 8228-8235.

78. Fucile, S., Barabino, B., Palma, E., Grassi, F., Limatola, C., Mileo, A. M., Alemà, S., Ballivet, M., & Eusebi, F. (1997). α_5 subunit forms functional $\alpha_3\beta_4\alpha_5$ nAChRs in transfected human cells. *NeuroReport* **8**, 2433-2436.

79. Fucile, S., Palma, E., Mileo, A. M., Miledi, R., & Eusebi, F. (2000). Human neuronal threonine-for-leucine-248 α7 mutant nicotinic acetylcholine receptors are highly Ca^{2+} permeable. *Proceedings of the National Academy of Sciences U.S.A.* **97**, 3643-3648.

80. Galzi, J.-L. & Changeux, J.-P. (1995). Neuronal nicotinic receptors: Molecular organization and regulations. *Neuropharmacol.* **34**, 563-582.

81. Gerzanich, V., Peng, F., Wang, F., Wells, G., Anand, R., Fletcher, S., & Lindstrom, J. (1995). Comparative pharmacology of epibatidine: A potent agonist for neuronal nicotinic acetylcholine receptors. *Molecular Pharmacology* **48**, 774-782.

82. Gerzanich, V., Wang, F., Kuryatov, A., & Lindstrom, J. (1998). α5 subunit alters desensitization, pharmacology, Ca^{++} permeability and Ca^{++} modulation of human neuronal α3 nicotinic receptors. *Journal of Pharmacology and Experimental Therapeutics* **286**, 311-320.

83. Giraudat, J., Dennis, M., Heidmann, T., Chang, J. Y., & Changeux, J. P. (1986). Structure of the high-affinity binding site for noncompetitive blockers of the acetylcholine receptor: serine-262 of the delta subunit is labeled by [3H]chlorpromazine. *Proc.Natl.Acad.Sci.U.S.A* **83**, 2719-2723.

84. Giraudat, J., Dennis, M., Heidmann, T., Haumont, P. Y., Lederer, F., & Changeux, J. P. (1987). Structure of the high-affinity binding site for noncompetitive blockers of the acetylcholine receptor: [3H]chlorpromazine labels homologous residues in the beta and delta chains. *Biochemistry* **26**, 2410-2418.

85. Goodman, C. S. & Shatz, C. J. (1993). Developmental mechanisms that generate precise patterns of neuronal connectivity. *Cell* **72 Suppl**, 77-98.

86. Gotti, C., Fornasari, D., & Clementi, F. (1997). Human neuronal nicotinic receptors. *Progress in Neurobiology* **53**, 199-237.

87. Grady, S., Marks, M. J., Wonnacott, S., & Collins, A. C. (1992). Characterization of nicotinic receptor-mediated [3H]dopamine release from synaptosomes prepared from mouse striatum. *J.Neurochem.* **59**, 848-856.

88. Gray, R., Rajan, A. S., Radcliffe, K. A., Yakehiro, M., & Dani, J. A. (1996). Hippocampal synaptic transmission enhanced by low concentrations of nicotine. *Nature* **383**, 713-716.

89. Green, W. N. (1999). Ion channel assembly: creating structures that function. *Journal of General Physiology* **113**, 163-169.

90. Green, W. N. & Claudio, T. (1993). Acetylcholine receptor assembly: subunit folding and oligomerization occur sequentially. *Cell* **74**, 57-69.

91. Green, W. N. & Millar, N. S. (1995). Ion-channel assembly. *Trends in Neurosciences* **18**, 280-287.

92. Green, W. N. & Wanamaker, C. P. (1997). The role of the cystine loop in acetylcholine receptor assembly. *Journal of Biological Chemistry* **272**, 20945-20953.

93. Green, W. N. & Wanamaker, C. P. (1998). Formation of the nicotinic acetylcholine receptor binding sites. *Journal of Neuroscience* **18**, 5555-5564.

94. Groot-Kormelink, P. J., Luyten, W. H. M. L., Colquhoun, D., & Sivilotti, L. G. (1998). A reporter mutation approach shows incorporation of the "orphan" subunit β3 into a functional nicotinic receptor. *Journal of Biological Chemistry* **273**, 15317-15320.

95. Groot Kormelink, P. J. & Luyten, W. H. (1997). Cloning and sequence of full-length cDNAs encoding the human neuronal nicotinic acetylcholine receptor (nAChR) subunits beta3 and beta4 and expression of seven nAChR subunits in the human neuroblastoma cell line SH-SY5Y and/or IMR-32. *FEBS Letters* **400**, 309-314.

96. Gu, Y., Camacho, P., Gardner, P., & Hall, Z. W. (1991a). Identification of two amino acid residues in the epsilon subunit that promote mammalian muscle acetylcholine receptor assembly in COS cells. *Neuron* **6**, 879-887.

97. Gu, Y., Forsayeth, J., Verrall, S., Yu, X.-M., & Hall, Z. W. (1991b). Assembly of the mammalian muscle acetylcholine receptor in transfected COS cells. *Journal of Cell Biology* **114**, 799-807.

98. Gurdon, J. B., Lane, C. D., Woodland, H. R., & Marbaix, G. (1971). Use of frog eggs and oocytes for the study of messenger RNA and its translation in living cells. *Nature* **233**, 177-182.

99. Haghighi, A. P. & Cooper, E. (2000). A molecular link between inward rectification and calcium permeability of neuronal nicotinic acetylcholine alpha3beta4 and alpha4beta2 receptors. *J.Neurosci.* **20**, 529-541.

100. Han, Z. Y., le Novère, N., Zoli, M., Hill, J. A., Jr., Champtiaux, N., & Changeux, J. P. (2000). Localization of nAChR subunit mRNAs in the brain of Macaca mulatta. *Eur.J.Neurosci.* **12**, 3664-3674.

101. Harvey, S. C. & Luetje, C. W. (1996). Determinants of competitive antagonist sensitivity of neuronal nicotinic receptor α subunits. *Journal of Neuroscience* **16**, 3798-3806.

102. Hefft, S., Hulo, S., Bertrand, D., & Muller, D. (1999). Synaptic transmission at nicotinic acetylcholine receptors in rat hippocampal organotypic cultures and slices. *J.Physiol* **515**, 769-776.

103. Hernandez, M.-C., Erkman, L., Matter-Sadzinski, L., Roztocil, T., Ballivet, M., & Matter, J.-M. (1995). Characterization of the nicotinic acetylcholine receptor β3 gene. Its regulation within the avian nervous system is effected by a promoter 143 base pairs in length. *Journal of Biological Chemistry* **270**, 3224-3233.

104. Hille, B. (1992). *Ionic Channels of Excitable Membranes*, Sinauer Associates Inc., Sunderland, Mass, USA.

105. Hucho, F., Oberthur, W., & Lottspeich, F. (1986). The ion channel of the nicotinic acetylcholine receptor is formed by the homologous helices M II of the receptor subunits. *FEBS Lett.* **205**, 137-142.

106. Hucho, F., Tsetlin, V. I., & Machold, J. (1996). The emerging three-dimensional structure of a receptor. The nicotinic acetylcholine receptor. *Eur.J.Biochem.* **239**, 539-557.

107. Hunt, R. (1900). Further observations on the blood-pressure-lowering bodies in extracts of the suprarenal gland. *In American Journal of Physiology V (1901)* Proceedings of the American Physiological Society, 13th annual meeting, vi-vii.

108. Imoto, K., Busch, C., Sakmann, B., Mishina, M., Konno, T., Nakai, J., Bujo, H., Mori, Y., Fukuda, K., & Numa, S. (1988). Rings of negatively charged amino acids determine the acetylcholine receptor channel conductance. *Nature* **335**, 645-648.

109. Imoto, K., Konno, T., Nakai, J., Wang, F., Mishina, M., & Numa, S. (1991). A ring of uncharged polar amino acids as a component of channel constriction in the nicotinic acetylcholine receptor. *FEBS Lett.* **289**, 193-200.

110. Imperato, A. & Di Chiara, G. (1986). Preferential stimulation of dopamine release in the nucleus accumbens of freely moving rats by ethanol. *J.Pharmacol.Exp.Ther.* **239**, 219-228.

111. Jackson, M. B. (1988). Dependence of acetylcholine receptor channel kinetics on agonist concentration in cultured mouse muscle fibres. *J.Physiol (London)* **397**, 555-583.

112. Janson, A. M., Fuxe, K., Sundstrom, E., Agnati, L. F., & Goldstein, M. (1988). Chronic nicotine treatment partly protects against the 1-methyl-4- phenyl-2,3,6-tetrahydropyridine-induced degeneration of nigrostriatal dopamine neurons in the black mouse. *Acta Physiol Scand.* **132**, 589-591.

113. Jeyarasasingam, G., Tompkins, L., & Quik, M. (2002). Stimulation of non-alpha7 nicotinic receptors partially protects dopaminergic neurons from 1-methyl-4-phenylpyridinium-induced toxicity in culture. *Neuroscience* **109**, 275-285.

114. Ji, D., Lape, R., & Dani, J. A. (2001). Timing and location of nicotinic activity enhances or depresses hippocampal synaptic plasticity. *Neuron* **31**, 131-141.

115. Johnson, D. S., Martinez, J., Elgoyhen, A. B., Heinemann, S. F., & McIntosh, J. M. (1995). α-conotoxin Iml exhibits subtype-specific nicotinic acetylcholine receptor blockade: Preferential inhibition of homomeric α7 and α9 receptors. *Molecular Pharmacology* **48**, 194-199.

116. Jones, I. W., Bolam, J. P., & Wonnacott, S. (2001). Presynaptic localisation of the nicotinic acetylcholine receptor beta2 subunit immunoreactivity in rat nigrostriatal dopaminergic neurons. *J.Comp Neurol.* **439**, 235-247.

117. Jones, S., Sudweeks, S., & Yakel, J. L. (1999). Nicotinic receptors in the brain: correlating physiology with function. *Trends in Neurosciences* **22**, 555-561.

118. Jones, S. & Yakel, J. L. (1997). Functional nicotinic ACh receptors on interneurons in the rat hippocampus. *J.Physiol* **504**, 603-610.

119. Kakinuma, A., Chazenbalk, G., Filetti, S., McLachlan, S. M., & Rapoport, B. (1996). Both the 5' and 3' noncoding regions of the thyrotropin receptor messenger ribonucleic acid influence the level of receptor protein expression in transfected mammalian cells. *Endocrinology* **137**, 2664-2669.

120. Kandel, E. R. and Schwartz, J. H. (1985). *Principles of neural science*, 2nd edition, Elsevier, Amsterdam, NL.

121. Karlin, A. (1993). Structure of nicotinic acetylcholine receptors. *Current Opinion in Neurobiology* **3**, 299-309.

122. Karlin, A. & Akabas, M. H. (1995). Towards a structural basis for the function of nicotinic acetylcholine receptors and their cousins. *Neuron* **15**, 1231-1244.

123. Katz, B. & Miledi, R. (1971). Further observations on acetylcholine noise. *Nat.New Biol.* **232**, 124-126.

124. Kearney, P. C., Zhang, H., Zhong, W., Dougherty, D. A., & Lester, H. A. (1996). Determinants of nicotinic receptor gating in natural and unnatural side chain structures at the M2 9' position. *Neuron* **17**, 1221-1229.

125. Keller, S. H., Lindstrom, J., & Taylor, P. (1996). Involvement of the chaperone protein calnexin and the acetylcholine receptor beta-subunit in the assembly and cell surface expression of the receptor. *Journal of Biological Chemistry* **271**, 22871-22877.

126. Keller, S. H., Lindstrom, J., & Taylor, P. (1998). Inhibition of glucose trimming with castanospermine reduces calnexin association and promotes proteasome degradation of the α-subunit of the nicotinic acetylcholine receptor. *Journal of Biological Chemistry* **273**, 17064-17072.

127. Klink, R., de Kerchove, d. A., Zoli, M., & Changeux, J. P. (2001). Molecular and physiological diversity of nicotinic acetylcholine receptors in the midbrain dopaminergic nuclei. *Journal of Neuroscience* **21**, 1452-1463.

128. Konno, T., Busch, C., von Kitzing, E., Imoto, K., Wang, F., Nakai, J., Mishina, M., Numa, S., & Sakmann, B. (1991). Rings of anionic amino acids as structural determinants of ion selectivity in the acetylcholine receptor channel. *Proceedings of the Royal Society of London Series B-Biological Sciences* **244**, 69-79.

129. Kozak, M. (1991). An analysis of vertebrate mRNA sequences: intimations of translational control. *Journal of Cell Biology* **115**, 887-903.

130. Kreienkamp, H. J., Maeda, R. K., Sine, S. M., & Taylor, P. (1995a). Intersubunit contacts governing assembly of the mammalian nicotinic acetylcholine receptor. *Neuron* **14**, 635-644.

131. Kuryatov, A., Gerzanich, V., Nelson, M., Olale, F., & Lindstrom, J. (1997). Mutation causing autosomal dominant nocturnal frontal lobe epilepsy alters Ca^{2+} permeability, conductance, and gating of human α4β2 nicotinic acetylcholine receptors. *Journal of Neuroscience* **17**, 9035-9047.

132. Labarca, C., Nowak, M. W., Zhang, H., Tang, L., Deshpande, P., & Lester, H. A. (1995). Channel gating governed symmetrically by conserved leucine residues in the M2 domain of nicotinic receptors. *Nature* **376**, 514-516.

133. Langley, J. N. (1878). On the physiology of the salivary secretion. Part II. On the mutual antagonism of atropin and pilocarpin, having especial reference to their relations in the sub-maxillary gland of the cat. *J.Physiol* **1**, 339-369.

134. Langley, J. N. (1905). On the reaction of cells and of nerve-endings to certain poisons, chiefly as regards the reaction of striated muscle to nicotine and curari. *J.Physiol* **33**, 374-413.

135. Le Jeune, H., Aubert, I., Jourdan, F., & Quirion, R. (1996). Developmental profiles of various cholinergic markers in the rat main olfactory bulb using quantitative autoradiography. *J.Comp Neurol.* **373**, 433-450.

136. Le Novère, N., Zoli, M., & Changeux, J. P. (1996). Neuronal nicotinic receptor alpha 6 subunit mRNA is selectively concentrated in catecholaminergic nuclei of the rat brain. *Eur.J.Neurosci.* **8**, 2428-2439.

137. Le Novère, N. & Changeux, J.-P. (1995). Molecular evolution of the nicotinic acetylcholine-receptor: an example of multigene family in excitable cells. *Journal Of Molecular Evolution* **40**, 155-172.

138. Leonard, R. J., Labarca, C. G., Charnet, P., Davidson, N., & Lester, H. A. (1988). Evidence that the M2 membrane-spanning region lines the ion channel pore of the nicotinic receptor. *Science* **242**, 1578-1581.

139. Levy, F., Guevara-Guzman, R., Hinton, M. R., Kendrick, K. M., & Keverne, E. B. (1993). Effects of parturition and maternal experience on noradrenaline and acetylcholine release in the olfactory bulb of sheep. *Behav.Neurosci.* **107**, 662-668.

140. Li, X., Rainnie, D. G., McCarley, R. W., & Greene, R. W. (1998). Presynaptic nicotinic receptors facilitate monoaminergic transmission. *Journal of Neuroscience* **18**, 1904-1912.

141. Listerud, M., Brussaard, A. B., Devay, P., Colman, D. R., & Role, L. W. (1991). Functional contribution of neuronal AChR subunits revealed by antisense oligonucleotides [published erratum appears in Science 1992 Jan 3;255(5040): 12]. *Science* **254**, 1518-1521.

142. Loewi, O. (1921). *Pflügers Arch,* **189**, 239-242.

143. Luetje, C. W. & Patrick, J. (1991). Both α- and β-subunits contribute to the agonist sensitivity of neuronal nicotinic acetylcholine receptors. *J.Neurosci.* **11**, 837-845.

144. Luetje, C. W., Piattoni, M., & Patrick, J. (1993). Mapping of ligand-binding sites of neuronal nicotinic acetylcholine receptors using chimeric α subunits. *Molecular Pharmacology* **44**, 657-666.

145. Luo, S., Kulak, J. M., Cartier, G. E., Jacobsen, R. B., Yoshikami, D., Olivera, B. M., & McIntosh, J. M. (1998). α-Conotoxin AuIB selectively blocks α3β4 nicotinic acetylcholine receptors and nicotine-evoked norepinephrine release. *J.Neurosci.* **18**, 8571-8579.

146. MacDermott, A. B., Role, L. W., & Siegelbaum, S. A. (1999). Presynaptic ionotropic receptors and the control of transmitter release. *Annu.Rev.Neurosci.* **22**, 443-485.

147. Maggi, L., Sher, E., & Cherubini, E. (2001). Regulation of GABA release by nicotinic acetylcholine receptors in the neonatal rat hippocampus. *J.Physiol* **536**, 89-100.

148. Matsubayashi, H., Alkondon, M., Pereira, E. F., Swanson, K. L., & Albuquerque, E. X. (1998). Strychnine: a potent competitive antagonist of α-bungarotoxin-sensitive nicotinic acetylcholine receptors in rat hippocampal neurons. *Journal of Pharmacology and Experimental Therapeutics* **284**, 904-913.

149. McGehee, D. S., Heath, M. J. S., Gelber, S., Devay, P., & Role, L. W. (1995). Nicotine enhancement of fast excitatory synaptic transmission in CNS by presynaptic receptors. *Science* **269**, 1692-1696.

150. McGehee, D. S. & Role, L. W. (1995). Physiological diversity of nicotinic acetylcholine receptors expressed by vertebrate neurons. *Annual Review of Physiology* **57**, 521-546.

151. McQuiston, A. R. & Madison, D. V. (1999). Nicotinic receptor activation excites distinct subtypes of interneurons in the rat hippocampus. *Journal of Neuroscience* **19**, 2887-2896.

152. Mereu, G., Yoon, K. W., Boi, V., Gessa, G. L., Naes, L., & Westfall, T. C. (1987). Preferential stimulation of ventral tegmental area dopaminergic neurons by nicotine. *Eur.J.Pharmacol.* **141**, 395-399.

153. Merlie, J. P. & Lindstrom, J. (1983). Assembly in vivo of mouse muscle acetylcholine receptor: identification of an α subunit species that may be an assembly intermediate. *Cell* **34**, 747-757.

154. Mihailescu, S. & Drucker-Colin, R. (2000). Nicotine, Brain Nicotinic Receptors, and Neuropsychiatric Disorders. *Arch.Med.Res.* **31**, 131-144.

155. Miller, C. (1989). Genetic manipulation of ion channels: a new approach to structure and mechanism. *Neuron* **2**, 1195-1205.

156. Mishina, M., Takai, T., Imoto, K., Noda, M., Takahashi, T., Numa, S., Methfessel, C., & Sakmann, B. (1986). Molecular distinction between fetal and adult forms of muscle acetylcholine receptor. *Nature* **321**, 406-411.

157. Mitra, M., Wanamaker, C. P., & Green, W. N. (2001). Rearrangement of nicotinic receptor alpha subunits during formation of the ligand binding sites. *J.Neurosci.* **21** , 3000-3008.

158. Miyazawa, A., Fujiyoshi, Y., Stowell, M., & Unwin, N. (1999). Nicotinic acetylcholine receptor at 4.6 A resolution: transverse tunnels in the channel wall. *Journal of Molecular Biology* **288**, 765-786.

159. Morley, B. J., Li, H.-S., Hiel, H., Drescher, D. G., & Elgoyhen, A. B. (1998). Identification of the subunits of the nicotinic cholinergic receptors in the rat cochlea using RT-PCR and in situ hybridization. *Molecular Brain Research* **53**, 78-87.

160. Moss, S. J., McDonald, B. J., Rudhard, Y., & Schoepfer, R. (1996). Phosphorylation of the predicted major intracellular domains of the rat and chick neuronal nicotinic acetylcholine receptor α 7 subunit by cAMP-dependent protein kinase. *Neuropharmacology* **35**, 1023-1028.

161. Nathanson, N. M. (1987). Molecular properties of the muscarinic acetylcholine receptor. *Annu.Rev.Neurosci.* **10**, 195-236.

162. Nelson, M. E. & Lindstrom, J. (1999). Single channel properties of human α3 AChRs: impact of β2, β4 and α5 subunits. *J.Physiol* **516**, 657-678.

163. Ogden, D. (1994). *Microelectrode techniques, The Plymouth workshop handbook*, 2nd edition, The company of biologists Ltd, Cambridge, UK.

164. Orr-Urtreger, A., Göldner, F. M., Saeki, M., Lorenzo, I., Goldberg, L., De Biasi, M., Dani, J. A., Patrick, J. W., & Beaudet, A. L. (1997). Mice deficient in the α7 neuronal nicotinic acetylcholine receptor lack α-bungarotoxin binding sites and hippocampal fast nicotinic currents. *Journal of Neuroscience* **17**, 9165-9171.

165. Ortells, M. O. & Lunt, G. G. (1995). Evolutionary history of the ligand-gated ion-channel superfamily of receptors. *Trends in Neurosciences* **18**, 121-127.

166. Palma, E., Bertrand, S., Binzoni, T., & Bertrand, D. (1996). Neuronal nicotinic α7 receptor expressed in *Xenopus* oocytes presents five putative binding sites for methyllycaconitine. *J.Physiol* **491**, 151-161.

167. Palma, E., Maggi, L., Barabino, B., Eusebi, F., & Ballivet, M. (1999). Nicotinic acetylcholine receptors assembled from the alpha7 and beta3 subunits. *Journal of Biological Chemistry* **274**, 18335-18340.

168. Papke, R. L., Craig, A. G., & Heinemann, S. F. (1994). Inhibition of nicotinic acetylcholine receptors by Bis (2,2,6,6-tetramethyl-4-piperidinyl) sebacate (Tinuvin 770), an additive to medical plastics. *Journal of Pharmacology and Experimental Therapeutics* **268**, 718-726.

169. Papke, R. L., Duvoisin, R. M., & Heinemann, S. F. (1993). The amino terminal half of the nicotinic β–subunit extracellular domain regulates the kinetics of inhibition by neuronal bungarotoxin. *Proceedings of the Royal Society of London Series B-Biological Sciences* **252**, 141-148.

170. Pedersen, S. E., Bridgman, P. C., Sharp, S. D., & Cohen, J. B. (1990). Identification of a cytoplasmic region of the Torpedo nicotinic acetylcholine receptor alpha-subunit by epitope mapping. *Journal of Biological Chemistry* **265**, 569-581.

171. Pedersen, S. E. & Cohen, J. B. (1990). d-Tubocurarine binding sites are located at alpha-gamma and alpha-delta subunit interfaces of the nicotinic acetylcholine receptor. *Proc.Natl.Acad.Sci.U.S.A* **87**, 2785-2789.

172. Pereira, E. F. R., Alkondon, M., McIntosh, J. M., & Albuquerque, E. X. (1996). α-conotoxin-ImI: A competitive antagonist at α-bungarotoxin-sensitive neuronal nicotinic receptors in hippocampal neurons. *Journal of Pharmacology and Experimental Therapeutics* **278**, 1472-1483.

173. Perry, E. K., Morris, C. M., Court JA, Cheng, A., Fairbairn, A. F., McKeith, I. G., Irving, D., Brown, A., & Perry, R. H. (1995). Alteration in nicotine binding sites in Parkinson's disease, Lewy body dementia and Alzheimer's disease: possible index of early neuropathology. *Neuroscience* **64**, 385-395.

174. Picciotto, M. R., Zoli, M., Rimondini, R., Léna, C., Marubio, L. M., Merlo Pich, E., Fuxe, K., & Changeux, J.-P. (1998). Acetylcholine receptors containing the β2 subunit are involved in the reinforcing properties of nicotine. *Nature* **391**, 173-177.

175. Pidoplichko, V. I., DeBiasi, M., Williams, J. T., & Dani, J. A. (1997). Nicotine activates and desensitizes midbrain dopamine neurons. *Nature* **390**, 401-404.

176. Quick, M. W., Naeve, J., Davidson, N., & Lester, H. A. (1992). Incubation with horse serum increases viability and decreases background neurotransmitter uptake in Xenopus oocytes. *Biotechniques* **13**, 357-361.

177. Quik, M., Polonskaya, Y., Gillespie, A., Lloyd, K., & Langston, J. W. (2000). Differential alterations in nicotinic receptor alpha6 and beta3 subunit messenger RNAs in monkey substantia nigra after nigrostriatal degeneration. *Neuroscience* **100**, 63-72.

178. Ramirez-Latorre, J., Yu, C. R., Qu, X., Perin, F., Karlin, A., & Role, L. (1996). Functional contributions of α 5 subunit to neuronal acetylcholine receptor channels. *Nature* **380**, 347-351.

179. Rang, H. P., Dale, M. M. (1991). *Pharmacology*, 2nd edition, Churchill Livingstone, London, UK.

180. Rapier, C., Lunt, G. G., & Wonnacott, S. (1990). Nicotinic modulation of [3H]dopamine release from striatal synaptosomes: pharmacological characterisation. *J.Neurochem.* **54**, 937-945.

181. Ravel, N., Elaagouby, A., & Gervais, R. (1994). Scopolamine injection into the olfactory bulb impairs short-term olfactory memory in rats. *Behav.Neurosci.* **108**, 317-324.

182. Ravel, N., Vigouroux, M., Elaagouby, A., & Gervais, R. (1992). Scopolamine impairs delayed matching in an olfactory task in rats. *Psychopharmacology (Berl)* **109**, 439-443.

183. Revah, F., Bertrand, D., Galzi, J.-L., Devillers-Thiéry, A., Mulle, C., Hussy, N., Bertrand, S., Ballivet, M., & Changeux, J.-P. (1991). Mutations in the channel domain alter desensitization of a neuronal nicotinic receptor. *Nature* **353**, 846-849.

184. Rinne, J. O., Myllykyla, T., Lonnberg, P., & Marjamaki, P. (1991). A postmortem study of brain nicotinic receptors in Parkinson's and Alzheimer's disease. *Brain Res.* **547**, 167-170.

185. Rivera, C., Voipio, J., Payne, J. A., Ruusuvuori, E., Lahtinen, H., Lamsa, K., Pirvola, U., Saarma, M., & Kaila, K. (1999). The K+/Cl- co-transporter KCC2 renders GABA hyperpolarizing during neuronal maturation. *Nature* **397**, 251-255.

186. Roerig, B., Nelson, D. A., & Katz, L. C. (1997). Fast synaptic signaling by nicotinic acetylcholine and serotonin 5-HT3 receptors in developing visual cortex. *Journal of Neuroscience* **17**, 8353-8362.

187. Ryan, R. E., Ross, S. A., Drago, J., & Loiacono, R. E. (2001). Dose-related neuroprotective effects of chronic nicotine in 6-hydroxydopamine treated rats, and loss of neuroprotection in alpha4 nicotinic receptor subunit knockout mice. *Br.J.Pharmacol.* **132**, 1650-1656.

188. Saedi, M. S., Anand, R., Conroy, W. G., & Lindstrom, J. (1990). Determination of amino acids critical to the main immunogenic region of intact acetylcholine receptors by in vitro mutagenesis. *Federation of European Biochemical Societies* **267**, 55-59.

189. Saedi, M. S., Conroy, W. G., & Lindstrom, J. (1991). Assembly of Torpedo acetylcholine receptors in Xenopus oocytes. *Journal of Cell Biology* **112**, 1007-1015.

190. Sakmann, B. & Brenner, H. R. (1978). Change in synaptic channel gating during neuromuscular development. *Nature* **276**, 401-402.

191. Sands, S. B. & Barish, M. E. (1991). Calcium permeability of neuronal nicotinic acetylcholine receptor channels in PC12 cells. *Brain Res.* **560**, 38-42.

192. Sands, S. B., Costa, A. C. S., & Patrick, J. W. (1993). Barium permeability of neuronal nicotinic receptor α7 expressed in *Xenopus* oocytes. *Biophysical Journal* **65**, 2614-2621.

193. Sargent, P. B. (1993). The diversity of neuronal nicotinic acetylcholine receptors. *Annual Review of Neuroscience* **16**, 403-443.

194. Schild, H. O. (1949). pA_x and competitive drug antagonism. *British Journal of Pharmacology* **4**, 277-280.

195. Seguela, P., Wadiche, J., Dineley-Miller, K., Dani, J. A., & Patrick, J. W. (1993). Molecular cloning, functional properties, and distribution of rat brain alpha 7: a nicotinic cation channel highly permeable to calcium. *Journal of Neuroscience* **13**, 596-604.

196. Sgard, F., Charpantier, E., Bertrand, S., Walker, N., Caput, D., Graham, D., Bertrand, D., & Besnard, F. (2002). A novel human nicotinic receptor subunit, alpha10, that confers functionality to the alpha9-subunit. *Molecular Pharmacology* **61**, 150-159.

197. Sheffield, E. B., Quick, M. W., & Lester, R. A. J. (2000). Nicotinic acetylcholine receptor subunit mRNA expression and channel function in medial habenula neurons. *Neuropharmacology* **39**, 2591-2603.

198. Sherman-Gold, R. (1993). *The Axon guide for electrophysiology and biophysics laboratory techniques*. Axon Instruments Inc, Foster City, CA, USA.

199. Sigel, E. (1990). Use of Xenopus oocytes for the functional expression of plasma membrane proteins. *J.Membr.Biol.* **117**, 201-221.

200. Sine, S. M. (1993). Molecular dissection of subunit interfaces in the acetylcholine receptor: identification of residues that determine curare selectivity. *Proc.Natl.Acad.Sci.U.S.A* **90**, 9436-9440.

201. Sine, S. M. & Claudio, T. (1991a). Gamma- and delta-subunits regulate the affinity and the cooperativity of ligand binding to the acetylcholine receptor. *Journal of Biological Chemistry* **266**, 19369-19377.

202. Sine, S. M. & Claudio, T. (1991b). Stable expression of the mouse nicotinic acetylcholine receptor in mouse fibroblasts. Comparison of receptors in native and transfected cells. *Journal of Biological Chemistry* **266**, 13679-13689.

203. Sine, S. M., Claudio, T., & Sigworth, F. J. (1990). Activation of *Torpedo* acetylcholine receptors expressed in mouse fibroblasts. Single channel current kinetics reveal distinct agonist binding affinities. *Journal of General Physiology* **96**, 395-437.

204. Sivilotti, L. G., Colquhoun, D., & Millar, N. (2000). Comparison of native and recombinant neuronal nicotinic receptors: problems of measurement and expression. In *Neuronal Nicotinic Receptors*, eds. Clementi, F., Fornasari, D., & Gotti, C., pp. 379-416. Springer Verlag, Berlin Heidelberg.

205. Sivilotti, L. G., McNeil, D. K., Lewis, T. M., Nassar, M. A., Schoepfer, R., & Colquhoun, D. (1997). Recombinant nicotinic receptors, expressed in *Xenopus* oocytes, do not resemble native rat sympathetic ganglion receptors in single-channel behaviour. *J.Physiol* **500**, 123-138.

206. Smit, A. B., Syed, N. I., Schaap, D., van Minnen, J., Klumperman, J., Kits, K. S., Lodder, H., Der Schors, R. C., van Elk, R., Sorgedrager, B., Brejc, K., Sixma, T. K., & Geraerts, W. P. (2001). A glia-derived acetylcholine-binding protein that modulates synaptic transmission. *Nature* **411**, 261-268.

207. Soliakov, L. & Wonnacott, S. (1996). Voltage-sensitive Ca2+ channels involved in nicotinic receptor-mediated [3H]dopamine release from rat striatal synaptosomes. *J.Neurochem.* **67**, 163-170.

208. Soliakov, L. & Wonnacott, S. (2001). Involvement of protein kinase C in the presynaptic nicotinic modulation of [(3)H]-dopamine release from rat striatal synaptosomes. *Br.J.Pharmacol.* **132**, 785-791.

209. Stauderman, K. A., Mahaffy, L. S., Akong, M., Veliçelebi, G., Chavez-Noriega, L. E., Crona, J. H., Johnson, E. C., Elliott, K. J., Gillespie, A., Reid, R. T., Adams, P., Harpold, M. M., & Corey-Naeve, J. (1998). Characterization of human recombinant neuronal nicotinic acetylcholine receptor subunit combinations $\alpha2\beta4$, $\alpha3\beta4$ and $\alpha4\beta4$ stably expressed in HEK293 cells. *J.Pharmacol.Exp.Therap.* **284**, 777-789.

210. Stroud, R. M., McCarthy, M. P., & Shuster, M. (1990). Nicotinic acetylcholine receptor superfamily of ligand-gated ion channels. *Biochemistry* **29**, 11009-11023.

211. Sumikawa, K., Houghton, M., Emtage, J. S., Richards, B. M., & Barnard, E. A. (1981). Active multi-subunit ACh receptor assembled by translation of heterologous mRNA in Xenopus oocytes. *Nature* **292**, 862-864.

212. Sussman, J. L., Harel, M., Frolow, F., Oefner, C., Goldman, A., Toker, L., & Silman, I. (1991). Atomic structure of acetylcholinesterase from Torpedo californica: a prototypic acetylcholine-binding protein. *Science* **253**, 872-879.

213. Tsunoyama, K. & Gojobori, T. (1998). Evolution of nicotinic acetylcholine receptor subunits. *Molecular Biology and Evolution* **15**, 518-527.

214. Unwin, N. (1993). Nicotinic acetylcholine receptor at 9 Å resolution. *Journal of Molecular Biology* **229**, 1101-1124.

215. Unwin, N. (1995). Acetylcholine receptor channel imaged in the open state. *Nature* **373**, 37-43.

216. Unwin, N. (1998). The nicotinic acetylcholine receptor of the *Torpedo* electric ray. *Journal of Structural Biology* **121**, 181-190.

217. Unwin, N. (2000). The Croonian Lecture 2000. Nicotinic acetylcholine receptor and the structural basis of fast synaptic transmission. *Phil.Trans.R.Soc.Lond.B* **355**, 1813-1829.

218. Unwin, N. (2001). Nicotinic acetylcholine receptor and the structural basis of fast synaptic transmission. *Phil.Trans.R.Soc.Lond.B* **355**, 1813-1829.

219. Vailati, S., Moretti, M., Balestra, B., McIntosh, J. M., Clementi, F., & Gotti, C. (2000). $\beta3$ subunit is present in different nicotinic receptor subtypes in chick retina. *Eur.J.Pharmacol.* **393**, 23-30.

220. Vernallis, A. B., Conroy, W. G., & Berg, D. K. (1993). Neurons assemble acetylcholine receptors with as many as three kinds of subunits while maintaining subunit segregation among receptor subtypes. *Neuron* **10**, 451-464.

221. Vernino, S., Amador, M., Luetje, C. W., Patrick, J., & Dani, J. A. (1992). Calcium modulation and high calcium permeability of neuronal nicotinic acetylcholine receptors. *Neuron* **8**, 127-134.

222. Vidal, C. & Changeux, J. P. (1993). Nicotinic and muscarinic modulations of excitatory synaptic transmission in the rat prefrontal cortex in vitro. *Neuroscience* **56** , 23-32.

223. Villarroel, A., Herlitze, S., Koenen, M., & Sakmann, B. (1991). Location of a threonine residue in the α-subunit M2 transmembrane segment that determines the ion flow through the acetylcholine receptor channel. *Proceedings of the Royal Society of London Series B-Biological Sciences* **243**, 69-74.

224. Wang, F., Gerzanich, V., Wells, G. B., Anand, R., Peng, X., Keyser, K., & Lindstrom, J. (1996a). Assembly of human neuronal nicotinic receptor $\alpha5$ subunits with $\alpha3$, $\beta2$, and $\beta4$ subunits. *Journal of Biological Chemistry* **271**, 17656-17665.

225. Wang, F., Nelson, M. E., Kuryatov, A., Olale, F., Cooper, J., Keyser, K., & Lindstrom, J. (1998). Chronic nicotine treatment up-regulates human α3β2 but not α3β4 acetylcholine receptors stably transfected in human embryonic kidney cells. *Journal of Biological Chemistry* **273**, 28721-28732.

226. Wess, J. (1996). Molecular biology of muscarinic acetylcholine receptors. *Crit Rev.Neurobiol.* **10**, 69-99.

227. Wheeler, S. V., Chad, J. E., & Foreman, R. (1993). Residues 1 to 80 of the N-terminal domain of the β subunit confer neuronal bungarotoxin sensitivity and agonist selectivity on neuronal nicotinic receptors. *FEBS Letters* **332**, 139-142.

228. White, B. H. & Cohen, J. B. (1992). Agonist-induced changes in the structure of the acetylcholine receptor M2 regions revealed by photoincorporation of an uncharged nicotinic noncompetitive antagonist. *Journal of Biological Chemistry* **267**, 15770-15783.

229. Whiteaker, P., Peterson, C. G., Xu, W., McIntosh, J. M., Paylor, R., Beaudet, A. L., Collins, A. C., & Marks, M. J. (2002). Involvement of the alpha3 subunit in central nicotinic binding populations. *J.Neurosci.* **22**, 2522-2529.

230. Williams, B. W., Temburni, M. K., Schwartz Levey, M., Bertrand, S., Bertrand, D., & Jacob, M. H. (1998). The long internal loop of the α3 subunit targets nAChRs to subdomains within individual synapses on neurons *in vivo*. *Nature Neuroscience* **1**, 557-562.

231. Wong, E. T., Holstad, S. G., Mennerick, S. J., Hong, S. E., Zorumski, C. F., & Isenberg, K. E. (1995). Pharmacological and physiological properties of a putative ganglionic nicotinic receptor, $\alpha_3\beta_4$, expressed in transfected eucaryotic cells. *Molecular Brain Research* **28**, 101-109.

232. Wonnacott, S. (1997). Presynaptic nicotinic ACh receptors. *Trends in Neurosciences* **20**, 92-98.

233. Wonnacott, S., Kaiser, S., Mogg, A., Soliakov, L., & Jones, I. W. (2000). Presynaptic nicotinic receptors modulating dopamine release in the rat striatum [In Process Citation]. *Eur.J.Pharmacol.* **393**, 51-58.

234. Yakel, J. L., Lagrutta, A., Adelman, J. P., & North, R. A. (1993). Single amino acid substitution affects desensitization of the 5-hydroxytryptamine type 3 receptor expressed in *Xenopus* oocytes. *Proceedings of the National Academy of Sciences U.S.A.* **90**, 5030-5033.

235. Yu, C. R. & Role, L. W. (1998a). Functional contribution of the α5 subunit to neuronal nicotinic channels expressed by chick sympathetic ganglion neurons. *J.Physiol* **509**, 667-681.

236. Yu, C. R. & Role, L. W. (1998b). Functional contribution of the α7 subunit to multiple subtypes of nicotinic receptors in embryonic chick sympathetic neurons. *J.Physiol* **509**, 651-665.

237. Zarei, M. M., Radcliffe, K. A., Chen, D., Patrick, J. W., & Dani, J. A. (1999). Distributions of nicotinic acetylcholine receptor alpha7 and beta2 subunits on cultured hippocampal neurons. *Neuroscience* **88**, 755-764.

238. Zhang, Y., Chen, J., & Auerbach, A. (1995). Activation of recombinant mouse acetylcholine receptors by acetylcholine, carbamylcholine and tetramethylammonium. *J.Physiol* **486 (Pt 1)**, 189-206.

239. Zwart, R. & Vijverberg, H. P. (1998). Four pharmacologically distinct subtypes of α4β2 nicotinic acetylcholine receptor expressed in *Xenopus laevis* oocytes. *Molecular Pharmacology* **54**, 1124-1131.